JOURNAL OF FLUID MECHANICS

VOLUME 6 PART 4

NOVEMBER 1959

THE UNIVERSITY OF MICHIGAN
DEC 15 1959
ENGINEERING LIBRARY

PUBLISHED BY

CAMBRIDGE UNIVERSITY PRESS

BENTLEY HOUSE, 200 EUSTON ROAD, LONDON, N.W. 1

AMERICAN BRANCH: 32 EAST 57TH STREET, NEW YORK 22, N.Y.

Price 30*s.* (*U.S.A.* $5.00)

The JOURNAL OF FLUID MECHANICS exists for the publication of theoretical and experimental investigations of all aspects of the mechanics of fluids, and is issued in four parts per volume.

EDITOR

DR G. K. BATCHELOR

Department of Applied Mathematics and Theoretical Physics, University of Cambridge, Free School Lane, Cambridge, England

ASSISTANT EDITORS

DR T. B. BENJAMIN, DR I. PROUDMAN, DR P. G. SAFFMAN

Department of Applied Mathematics and Theoretical Physics, University of Cambridge, Free School Lane, Cambridge, England

ASSOCIATE EDITORS

PROF. G. F. CARRIER

Pierce Hall, Harvard University, Cambridge 38, *Massachusetts, U.S.A.*

DR W. C. GRIFFITH

Research and Development Laboratory, Missile Systems Division, Lockheed Aircraft Corporation, Palo Alto, California, U.S.A.

M. J. LIGHTHILL

Royal Aircraft Establishment, Farnborough, Hampshire, England

PROF. R. R. LONG

School of Engineering, The Johns Hopkins University, Baltimore 18, *Maryland, U.S.A.*

Authors wishing to have papers published in the JOURNAL should communicate them to any one of the persons named above, choosing one in their own country where possible.

Authors are urged to ensure that their papers are written clearly and attractively, in order that their work will be readily accessible to readers.

Manuscripts should be typed in double spacing on one side of the paper only, with references listed at the end in alphabetical order of authors. Drawings should be done on a large scale in Indian ink on tracing cloth or drawing paper, the lettering being shown clearly in pencil for reproduction by the printer; the list of captions should be typed at the end of the manuscript. Proofs of papers from overseas will usually be despatched to authors by airmail. There is no charge for publication. Authors are entitled to receive 50 offprints of a paper in the JOURNAL free of charge, and additional offprints can be purchased if ordered in advance.

SUBSCRIPTIONS

The subscription price for a volume of four parts is £5. 10*s*. net, post free, payable in advance; separate parts 30*s*. net, plus postage. Subscriptions may be sent to any bookseller, or to the Cambridge University Press, Bentley House, 200 Euston Road, London, N.W. 1.

Subscribers in the United States should send their orders to the Cambridge University Press, American Branch, 32 East 57th Street, New York 22. The subscription price per volume is $18.50, post free, payable in advance; separate parts $5.00, plus postage.

n of
es of

lge,

lge,

S.A.

com-
their

d at-

only,
vings
aper,
nter;
ofs of
There
of a
nased

pay-
ay be
ouse,

ridge
The
arate

Non-equilibrium flow over a wavy wall

By WALTER G. VINCENTI
Department of Aeronautical Engineering, Stanford University, Stanford, California

(Received 27 March, 1959)

A small-disturbance solution is obtained for the steady two-dimensional flow over a sinusoidal wall of an inviscid gas in vibrational or chemical non-equilibrium. The results are based on a single, linear, third-order partial differential equation, which plays the same role here as does the Prandtl–Glauert equation in equilibrium flow. The solution is valid throughout the range from subsonic to supersonic speeds and for all values of the rate parameter from equilibrium to frozen flow (in both of which limits it reduces to Ackeret's classical solution of the Prandtl–Glauert equation). The results illustrate in simple fashion some of the properties of non-equilibrium flow, such as the occurrence of pressure drag at subsonic speeds and the absence of the discontinuous phenomena that characterize the Prandtl–Glauert theory when the flow changes from subsonic to supersonic.

1. Introduction

This work was motivated by the desire to obtain an analytical solution—preferably a simple one—to some problem in the two-dimensional flow of a gas in vibrational or chemical non-equilibrium. It appeared at the outset that the most likely possibility for such a solution would be the small-disturbance problem of the steady flow over an infinite sinusoidal wall. Thirty years ago, Ackeret (1928) showed that this problem of the 'wavy wall' admits of a particularly simple solution when the gas is in thermodynamic equilibrium. As it turns out, interesting and instructive results can again be obtained in the non-equilibrium case, still on the basis of relatively simple mathematics.

The material that follows is a logical supplement to the work of Chu (1957), Wood & Kirkwood (1957*a*), Moore (1958), and Broer (1958), all of whom have studied the phenomena of wave propagation under non-equilibrium conditions. As a result of this work, the roles played by the so-called 'frozen' and 'equilibrium' speeds of sound in problems of wave propagation are now well understood. (The equilibrium speed of sound is the speed of sound calculated on the assumption that the vibrational and chemical states of the fluid change so as to maintain their equilibrium relationship with the other state variables at every instant; the frozen speed of sound is calculated on the assumption that vibrational and chemical states are fixed—that is, do not change at all.) It is clear, in particular, that for any finite reaction rate in the fluid the front of an infinitesimal wave propagates relative to the fluid at the frozen speed of sound, which is invariably the greater of the two. This is true no matter how large the reaction rate, so long as it is not

infinite. Only when the rate becomes infinitely large does the wave-front velocity drop back to the lower equilibrium speed of sound. This discontinuous change in wave-front velocity in the limit of an infinite reaction rate is related to a reduction in the order of the governing differential equation with a resulting abrupt change in the identity of the characteristic surfaces. Despite this discontinuous change in wave-front velocity, however, the flow field is found to depend on the reaction rate in a continuous and uniform manner. This has been demonstrated by Chu (1957), who showed how a solution calculated for a large but finite reaction rate tends in the limit of infinite rate to the same solution as would be obtained by making the rate infinite at the outset. For the details the reader is referred to Chu's paper. We need only note here that, despite the discontinuous change in wave-front speeds, the flow calculated on the physically unrealistic basis of infinite rates (i.e. complete equilibrium) does have meaning with reference to a real flow with large but finite rates.

The foregoing, in brief, is the state of affairs in one-dimensional unsteady flow. A similar situation prevails in the two-dimensional steady case. Again there is a discontinuous change in the order of the governing differential equation, and hence in the characteristics of the equation, when the reaction rate becomes infinite. Despite this, Ackeret's solution for identically infinite rates (i.e. complete equilibrium) reappears as the natural limit of the non-equilibrium solution when the rate tends to infinity. This is true both in supersonic flow, where the characteristics are real and the problem is again essentially one in wave propagation, as well as in subsonic flow, where the characteristics are imaginary.

As in the note by Moore (1958), the results will be obtained by solution of a single third-order partial differential equation, which is here derived directly on the assumption of steady flow. This equation, which appears as equation (27), plays the same role in non-equilibrium theory as does the classical Prandtl–Glauert equation in equilibrium flow. It might therefore be useful as the basis for a theory of thin airfoils in a reactive fluid. The equation also provides one more example of a type of linear equation that arises in a number of problems in which there is a time lag between different state properties of the medium.

Subsequent to the completion of the present work, the author received a report by Gibson & Moore (1958) that does in fact consider the problem of the thin airfoil in supersonic flow on the basis of the same differential equation used here, derived by these writers via the corresponding acoustic equation. This was followed by a further paper by the same authors (Moore & Gibson, 1959) that also includes results for the wavy wall. The methods of the present paper are, however, formally different from those of Gibson & Moore.

The methods and results that follow can be applied equally well to vibrational non-equilibrium of a single-component gas or to chemical non-equilibrium of a mixture in which a single reaction occurs. Since understanding rather than application is the aim, no attempt is made to extend the treatment to multiple processes. All effects of viscosity, heat conduction, and diffusion are neglected.

2. Basic equations

We begin by setting down the equations of gas dynamics for three-dimensional time dependent flow. If ρ is the mass density and u_i ($i = 1, 2, 3$) are the velocity components, the continuity equation can be written

$$\frac{D\rho}{Dt} + \rho \frac{\partial u_j}{\partial x_j} = 0, \tag{1}$$

where the repeated dummy subscripts denote the summation convention and the substantial derivative is given as usual by $D(\ )/Dt \equiv \partial(\ )/\partial t + u_k \partial(\ )/\partial x_k$. If p is the pressure, the Eulerian equations of motion under the present assumptions are

$$\frac{Du_i}{Dt} + \frac{1}{\rho}\frac{\partial p}{\partial x_i} = 0 \quad (i = 1, 2, 3). \tag{2}$$

The adiabatic energy equation can be written in several equivalent forms. If h is the enthalpy per unit mass, two of these are

$$\frac{D}{Dt}\left(\frac{u^2}{2} + h\right) - \frac{1}{\rho}\frac{\partial p}{\partial t} = 0, \tag{3a}$$

$$\frac{Dh}{Dt} - \frac{1}{\rho}\frac{Dp}{Dt} = 0. \tag{3b}$$

The equivalence of these equations can be shown with the aid of equation (2).

The above equations (1), (2) and (3) constitute five equations for the six unknowns ρ, u_i, p, and h. To complete the set we must introduce equations specifying the thermo-chemical properties of the gas.

For present purposes we consider the non-equilibrium thermo-chemical state to be described by the usual thermodynamic variables p, ρ, T, h, e, s, etc., plus an additional quantity q that specifies the vibrational or chemical state of the gas. (For vibrational non-equilibrium, q is taken as T_i, the internal vibrational temperature; for chemical non-equilibrium of a dissociating diatomic gas, it would be taken as α, the degree of dissociation.) For the assumed non-equilibrium situation, the specification of any three of these variables fixes the thermo-chemical state—that is, all of the other variables are then determined.

Following Broer (1958), we shall find it convenient to use p, ρ, and q as the primary state variables. The enthalpy h is thus assumed to be given by a state equation of the form

$$h = h(p, \rho, q). \tag{4a}$$

This may also be written in differential form as

$$dh = h_p dp + h_\rho d\rho + h_q dq, \tag{4b}$$

where the subscript indicates differentiation with respect to the noted variable, the other two state variables being held fixed.

The variable q is governed in a gas at rest by a rate equation which gives dq/dt as a function of the state of the gas and which can be written in the form

$$\frac{dq}{dt} = \frac{L(p, \rho, q)}{\theta}, \tag{5}$$

where L is a function of the thermo-chemical state and θ is a positive quantity which is related to the specific rate constant. (The smaller is θ, the faster is the reaction rate, and vice versa.) The quantity θ is also, in general, a function of the thermo-chemical state, but that need not concern us here. When the gas is in equilibrium, then dq/dt is zero, and equation (5) defines an equilibrium value of q—say $\bar{q}$—given by

$$L(p,\rho,\bar{q}) = 0, \tag{6a}$$

from which

$$\bar{q} = \bar{q}(p,\rho). \tag{6b}$$

There are, correspondingly, equilibrium values of the other state variables, such as (cf. equation (4a))

$$\bar{h} = h[p,\rho,\bar{q}(p,\rho)] = \bar{h}(p,\rho). \tag{7}$$

For the gas in motion, we assume that the rate equation following a fluid element has the same form as equation (5), that is

$$\frac{Dq}{Dt} = \frac{L(p,\rho,q)}{\theta}. \tag{8}$$

In general, Dq/Dt for the gas in motion has a finite value in regions between shock waves.

The case of infinitely fast reaction rates corresponds to letting $\theta \to 0$ in the rate equation. In this limit, since Dq/Dt is finite, equation (8) reduces simply to $L(p,\rho,q) = 0$. This means (cf. equation (6a)) that the state of the gas in this case is determined everywhere by the equilibrium relation $q = \bar{q}$. We thus see that the flow in the limit of infinitely fast reaction rates is the classical equilibrium flow. (For a more complete discussion of this limiting process, see Chu (1957).) The case of infinitely slow reaction rates is found by letting $\theta \to \infty$ in equation (8), which gives $q =$ constant. The resulting flow is the so-called frozen flow.

Equations (1), (2), (3), (4) and (8) now constitute a set of seven equations for the seven unknowns ρ, u_i, p, h, and q. They are thus sufficient for a solution of the problem.

If we wish to consider the entropy s of the non-equilibrium gas, this can be done by means of a state relation of the form

$$dh = T\,ds + \frac{1}{\rho}dp + Q\,dq, \tag{9}$$

where T is the absolute temperature and h is now considered as a function of s, p, and q. For chemical non-equilibrium, the quantity $Q \equiv (\partial h/\partial q)_{s,p}$ is related to the chemical potentials; for vibrational non-equilibrium it is equal to $c_i(T_i - T)\,dT_i/T_i$, where c_i is the vibrational specific heat (see, for example, Wood & Kirkwood (1957b)). For a system in equilibrium, it is known from chemical thermodynamics that h must be a minimum with respect to any virtual change in q for fixed s and p. The equilibrium value of $\bar{q} = \bar{q}(p,\rho)$ can therefore be found also from the equation

$$Q(p,\rho,\bar{q}) = 0. \tag{10}$$

The result must, of course, be the same as that found from equation (6a).

If equation (9) is applied following a fluid element, we have, in view of the energy equation (3b),

$$\frac{Ds}{Dt} = -\frac{Q}{T}\frac{Dq}{Dt}. \tag{11}$$

It is thus seen that for the limiting cases of equilibrium flow ($q = \bar{q}$ and hence $Q = 0$) and frozen flow ($Dq/Dt = 0$), the changes of state of a fluid element are isentropic. For any intermediate case ($Q \neq 0$ and $Dq/Dt \neq 0$), it follows from the second law of thermodynamics as applied to the present adiabatic situation that

$$\frac{Ds}{Dt} > 0,$$

that is, the flow process must be irreversible.

3. Linearized equations

Since our ultimate concern is with the small-disturbance flow over a wavy wall, we shall linearize the equations at this point. This step could be deferred until later, but it will simplify the manipulation of the equations to introduce it here. We shall also restrict ourselves to steady flow.

We assume as usual that the flow field is described by a perturbation on a uniform parallel flow with velocity U_∞ in the x_1 direction. If the perturbation quantities are denoted by primes, the velocity components are then given by $u_1 = U_\infty + u_1'$, $u_2 = u_2'$, $u_3 = u_3'$. The thermodynamic variables are given correspondingly by $p = p_\infty + p'$, $h = h_\infty + h'$, etc. The undisturbed stream is assumed to be in equilibrium—that is, $q_\infty = \bar{q}_\infty$.

The linearized form of the substantial derivative in the case of steady flow is $D(\ )/Dt = U_\infty \partial(\ )/\partial x_1$. With this expression the conservation equations (1), (2) and (3a) can be linearized at once to obtain

$$\rho_\infty \frac{\partial u_j'}{\partial x_j} + U_\infty \frac{\partial \rho'}{\partial x_1} = 0, \tag{12}$$

$$\rho_\infty U_\infty \frac{\partial u_i'}{\partial x_1} + \frac{\partial p'}{\partial x_i} = 0 \quad (i = 1, 2, 3), \tag{13}$$

$$U_\infty \frac{\partial u_1'}{\partial x_1} + \frac{\partial h'}{\partial x_1} = 0. \tag{14}$$

The linearized form of the differential state relation (4b) is

$$dh' = h_{p_\infty} dp' + h_{\rho_\infty} d\rho' + h_{q_\infty} dq', \tag{15}$$

where the partial derivatives are now evaluated at the conditions of the undisturbed stream.

The linearization of the rate equation requires somewhat more attention. By expanding the function $L(p, \rho, q)$ about the free-stream condition, equation (8) can be approximated first by

$$U_\infty \frac{\partial q'}{\partial x_1} = \frac{L(p_\infty, \rho_\infty, q_\infty) + L_{p_\infty} p' + L_{\rho_\infty} \rho' + L_{q_\infty} q'}{\theta_\infty + \theta'}.$$

Since the free-stream is in equilibrium, we have $L(p_\infty, \rho_\infty, q_\infty) = L(p_\infty, \rho_\infty, q_\infty) = 0$ (cf. equation (6a)), and the equation can be simplified further to

$$U_\infty \frac{\partial q'}{\partial x_1} = \frac{1}{\theta_\infty} (L_{p_\infty} p' + L_{\rho_\infty} \rho' + L_{q_\infty} q'). \tag{16}$$

We now introduce the concept of a fictitious, *local* equilibrium value of q given by $\bar{q}(p,\rho)$. This is the equilibrium value of q corresponding to the actual (non-equilibrium) values of p and ρ at a local point in the field. It is *not* the same as the value of q that would exist at that point if the entire field were in equilibrium—that is, in the limit of infinitely fast reaction rates. This fictitious equilibrium value $\bar{q}$ can be related to the actual values of p and ρ by equation (6*a*). Expanding the left-hand side of this equation about the free-stream condition and writing $\bar{q} = \bar{q}_\infty + \bar{q}' = q_\infty + \bar{q}'$ (where $\bar{q}_\infty = q_\infty$, as before, since the free stream is in equilibrium), equation (6*a*) can be linearized as

$$L_{p_\infty} p' + L_{\rho_\infty} \rho' + L_{q_\infty} \bar{q}' = 0.$$

With the aid of this relation, equation (16) can be written finally as

$$U_\infty \frac{\partial q'}{\partial x_1} = \frac{\bar{q}' - q'}{\tau_\infty}, \tag{17}$$

where $\tau_\infty \equiv -\theta_\infty / L_{q_\infty}$ is the relaxation time of the non-equilibrium process evaluated at free-stream conditions. Equation (17) could have been obtained by assuming a linearized rate equation at the outset on the plausible grounds that the flow over a slightly wavy wall could never be far out of equilibrium. The present approach has the advantage of showing that this simplified rate equation is a formal consequence of the other approximations in the linearized analysis.

The linearized rate equation (17) introduces the new unknown $\bar{q}'$ into the analysis. We must therefore add an additional equation. This is given by equation (6*b*), which can be written in linearized differential form as

$$d\bar{q}' = \bar{q}_{p_\infty} dp' + \bar{q}_{\rho_\infty} d\rho'. \tag{18}$$

Equations (12), (13), (14), (15), (17) and (18) now constitute eight linearized equations in eight unknowns.

The foregoing equations will now be combined to obtain a single equation with the velocity components as the unknowns. We begin by using the state equation (15) to rewrite the energy equation (14) as

$$U_\infty \frac{\partial u_1'}{\partial x_1} + h_{p_\infty} \frac{\partial p'}{\partial x_1} + h_{\rho_\infty} \frac{\partial \rho'}{\partial x_1} + h_{q_\infty} \frac{\partial q'}{\partial x_1} = 0.$$

The derivatives $\partial\rho'/\partial x_1$ and $\partial p'/\partial x_1$ are next eliminated from this equation by means of the continuity equation (12) and the first of the Eulerian equations (13). The result can be written

$$U_\infty h_{q_\infty} \frac{\partial q'}{\partial x_1} = (\rho_\infty h_{p_\infty} - 1)\, U_\infty^2 \frac{\partial u_1'}{\partial x_1} + \rho_\infty h_{\rho_\infty} \frac{\partial u_j'}{\partial x_j}. \tag{19}$$

Now, turning to the linearized rate equation (17), we differentiate this with respect to x_1 and write with the aid of equation (18)

$$\tau_\infty U_\infty \frac{\partial^2 q'}{\partial x_1^2} = \bar{q}_{p_\infty} \frac{\partial p'}{\partial x_1} + \bar{q}_{\rho_\infty} \frac{\partial \rho'}{\partial x_1} - \frac{\partial q'}{\partial x_1}.$$

This can be further rewritten with the aid of equations (12) and (13) as

$$\tau_\infty U_\infty \frac{\partial^2 q'}{\partial x_1^2} + \frac{\partial q'}{\partial x_1} + \rho_\infty U_\infty \bar{q}_{p_\infty} \frac{\partial u_1'}{\partial x_1} + \frac{\rho_\infty}{U_\infty} \bar{q}_{\rho_\infty} \frac{\partial u_j'}{\partial x_j} = 0. \tag{20}$$

All that need be done now to obtain an equation in the u_i is to differentiate equation (19) with respect to x_1 and use the result and the original equation (19) to eliminate the derivatives of q' from equation (20). This gives finally, after some rearrangement of terms,

$$\frac{h_{\rho\infty}U_\infty\tau_\infty}{h_{\rho\infty}+h_{q\infty}\bar{q}_{\rho\infty}}\frac{\partial}{\partial x_1}\left[\frac{h_{p\infty}-1/\rho_\infty}{h_{\rho\infty}}U_\infty^2\frac{\partial u_1'}{\partial x_1}+\frac{\partial u_j'}{\partial x_j}\right]+\left[\frac{h_{p\infty}+h_{q\infty}\bar{q}_{p\infty}-1/\rho_\infty}{h_{\rho\infty}+h_{q\infty}\bar{q}_{\rho\infty}}U_\infty^2\frac{\partial u_1'}{\partial x_1}+\frac{\partial u_j'}{\partial x_j}\right]=0. \tag{21}$$

As in the work of Broer (1958), the coefficients of the first terms inside the brackets can be related to the frozen and equilibrium speeds of sound. To this end we use the general thermodynamic relation

$$\left(\frac{\partial p}{\partial\rho}\right)_s=-\frac{(\partial h/\partial\rho)_p}{(\partial h/\partial p)_\rho-1/\rho}. \tag{22}$$

The square of the frozen speed of sound a_f^2 is obtained by taking $\partial p/\partial\rho$ with both s and q fixed. We thus obtain, in view of the relation (22),

$$a_f^2\equiv\left(\frac{\partial p}{\partial\rho}\right)_{s,q}=-\frac{(\partial h/\partial\rho)_{p,q}}{(\partial h/\partial p)_{\rho,q}-1/\rho}=-\frac{h_\rho}{h_p-1/\rho}. \tag{23}$$

The square of the equilibrium speed of sound a_e^2 is obtained by taking $\partial p/\partial\rho$ with s fixed and equilibrium maintained. This last condition means that we hold $q=\bar{q}(p,\rho)$, or equivalently $h=h[p,\rho,\bar{q}(p,\rho)]=\bar{h}(p,\rho)$. We thus obtain from equation (22)

$$a_e^2\equiv\left[\left(\frac{\partial p}{\partial\rho}\right)_s\right]_{h=\bar{h}}=-\frac{(\partial\bar{h}/\partial\rho)_p}{(\partial\bar{h}/\partial p)_\rho-1/\rho}=-\frac{h_\rho+h_q\bar{q}_\rho}{h_p+h_q\bar{q}_p-1/\rho}. \tag{24}$$

With the aid of these last two relations, equation (21) can be written finally as

$$K\frac{\partial}{\partial x_1}\left[(1-M_{f\infty}^2)\frac{\partial u_1'}{\partial x_1}+\frac{\partial u_2'}{\partial x_2}+\frac{\partial u_3'}{\partial x_3}\right]+\left[(1-M_{e\infty}^2)\frac{\partial u_1'}{\partial x_1}+\frac{\partial u_2'}{\partial x_2}+\frac{\partial u_3'}{\partial x_3}\right]=0, \tag{25}$$

where $M_{f\infty}=U_\infty/a_{f\infty}$, $M_{e\infty}=U_\infty/a_{e\infty}$, and

$$K=\frac{h_{\rho\infty}U_\infty\tau_\infty}{h_{\rho\infty}+h_{q\infty}\bar{q}_{\rho\infty}}. \tag{26}$$

Equation (25) is the desired single equation for the velocity components.

To show that a velocity potential may be introduced, we rewrite the three linearized Euler equations (13) as the single vector equation

$$\rho_\infty U_\infty\frac{\partial\mathbf{u}'}{\partial x_1}+\operatorname{grad}p'=0,$$

and take the curl of this equation. This gives

$$\frac{\partial}{\partial x_1}\operatorname{curl}\mathbf{u}'=0.$$

In view of the linearized relation $D(\ )/Dt=U_\infty\partial(\ )/\partial x_1$, this result means that the vorticity of a fluid element remains constant. Since we are concerned with perturbations on an initially uniform flow in which the vorticity is zero, it follows

that the perturbed flow will remain irrotational. We may therefore introduce a perturbation potential ϕ such that $u_i' = \partial\phi/\partial x_i$. Equation (25) then becomes

$$K\frac{\partial}{\partial x_1}\left[(1-M_{f_\infty}^2)\frac{\partial^2\phi}{\partial x_1^2}+\frac{\partial^2\phi}{\partial x_2^2}+\frac{\partial^2\phi}{\partial x_3^2}\right]+\left[(1-M_{e_\infty}^2)\frac{\partial^2\phi}{\partial x_1^2}+\frac{\partial^2\phi}{\partial x_2^2}+\frac{\partial^2\phi}{\partial x_3^2}\right]=0. \qquad (27)$$

The foregoing is the governing differential equation for non-equilibrium flows that are a small departure from a uniform parallel stream. Its relationship to the classical Prandtl–Glauert equation is apparent. If we set $K = 0$—that is, if the relaxation time τ_∞ is zero—the equation reduces to the Prandtl–Glauert equation for equilibrium flow as one would expect. At the opposite limit of frozen flow (τ_∞ and $K \to \infty$), it goes over into essentially the Prandtl–Glauert equation with the Mach number now based on the frozen rather than the equilibrium speed of sound. For any non-zero value of K, the characteristics of the equation, which are indicative of the character of the solution, are determined by the third-order terms. For example, in two-dimensional flow ($\partial^2\phi/\partial x_3^2 = 0$) there are three characteristics given by the lines $y =$ constant and $dy/dx = \pm 1/\sqrt{(M_{f_\infty}^2 - 1)}$. The existence of the characteristics $y =$ constant, which are the streamlines to the present approximation, is a reflexion of the possibility of differences in entropy from one streamline to the next when non-equilibrium processes are present. The characteristics $dy/dx = \pm 1/\sqrt{(M_{f_\infty}^2 - 1)}$ play essentially the same role as do the corresponding characteristics that are well known in equilibrium flow. They may be real or imaginary depending on whether M_{f_∞} is greater or less than one, and are thus indicative of the hyperbolic or elliptic nature of the flow. This is the situation no matter how small the value of K, so long as it is not zero. When K is identically zero, however, the characteristics change discontinuously, being now determined by the second-order terms. The characteristics $y =$ constant now cease to exist and the remaining characteristics are replaced discontinuously by the lines $dy/dx = \pm 1/\sqrt{(M_{e_\infty}^2 - 1)}$. The equation is therefore now hyperbolic or elliptic depending on whether M_{e_∞} is greater or less than one. We thus see that when K goes from a positive value to zero, the equation will retain a hyperbolic character if both M_{f_∞} and M_{e_∞} are greater than one and an elliptic character if both are less than one. Since a_{f_∞} must always be greater than a_{e_∞}, however, there must also exist a range of U_∞ in which $M_{f_\infty} < 1$ and $M_{e_\infty} > 1$. In this range the equation will change its character discontinuously from elliptic to hyperbolic when $K = 0$. This entire situation is typical of singular perturbation problems as discussed by Lagerstrom, Cole & Trilling (1949). The number of different cases here, however, is greater than one usually finds in a single equation, owing to the possibility of a change in type of both of the linear operators that make up the equation.

Equation (27) for $M_{f_\infty} > 1$ is similar to the acoustic equation given by Moore (1958). As pointed out by Moore, an equation of the same general type has also been been derived by Morrison (1956) for the propagation of elastic waves in a material in which there is a lag between stress and strain. For $M_{f_\infty} < 1$, equation (27) is also formally equivalent to the equation obtained by Lagerstrom *et al.* in their linearized treatment of stationary waves in a viscous compressible fluid. A third-order equation of this type would thus appear to be representative

of a number of small-disturbance processes in which non-equilibrium phenomena are involved.

Equation (27) can be applied to any gas involving a single vibrational or chemical process provided we know $h = h(p, \rho, q)$, $\bar{q} = \bar{q}(p, \rho)$, and τ. For example, in the case of vibrational non-equilibrium of an otherwise perfect diatomic gas, where q is to be identified with the vibrational temperature T_i, the enthalpy is given, in view of the state equation $p/\rho = RT$, by

$$h = \tfrac{7}{2}RT + \int c_i dT_i = \frac{7}{2}\frac{p}{\rho} + \int c_i dT_i,$$

where c_i is the vibrational specific heat. The equilibrium value of $\bar{q}$ is given by $\bar{T}_i = T = p/R\rho$. The relaxation time is defined by the linearized rate equation $DT_i/Dt = (T - T_i)/\tau$ and would usually be taken from experimental measurements as a function of T and ρ. Substitution of these quantities into equations (23) and (24) gives

$$a_{f_\infty}^2 = \tfrac{7}{5}RT_\infty \quad \text{and} \quad a_{e_\infty}^2 = \frac{\frac{7}{2}R + c_{i_\infty}}{\frac{5}{2}R + c_{i_\infty}} RT_\infty,$$

while equation (26) gives

$$K = \frac{\frac{7}{2}RU_\infty \tau_\infty}{\frac{7}{2}R + c_{i_\infty}}.$$

Owing to the neglect of non-linear effects, equation (27) may be expected to suffer from the same shortcomings as does the Prandtl–Glauert equation—that is, it will provide a relatively poor approximation at transonic and hypersonic speeds. As will be seen, however, the discontinuous behaviour that obviously invalidates the solutions of the Prandtl–Glauert equation at transonic speeds disappears with the inclusion of the non-equilibrium process.

Equation (27), like the Prandtl–Glauert equation, could be used as the basis for a theory of thin airfoils. Here, however, we shall examine only the original problem of the wavy wall.

4. Solution for wavy wall

We consider the two-dimensional flow in the half plane above the infinite sinusoidal wall

$$X_2 = \epsilon \sin 2\pi \frac{x_1}{l}, \tag{28}$$

where ϵ denotes the amplitude of the waves and l their wavelength. The boundary condition at the wall is taken in the usual linearized form

$$\left(\frac{\partial \phi}{\partial x_2}\right)_{x_2=0} = u_2'(x_1, 0) = U_\infty \frac{dX_2}{dx_1} = 2\pi U_\infty \frac{\epsilon}{l} \cos 2\pi \frac{x_1}{l}. \tag{29}$$

The boundary conditions at infinity are that $u_1' = \partial\phi/\partial x_1$ and $u_2' = \partial\phi/\partial x_2$ remain finite as $x_2 \to \infty$. Since the boundary conditions are unchanged by shifting the origin an integral number of wavelengths in the x_1-direction, it follows at once that ϕ must be periodic in x_1 with period l.

It is convenient to begin by transforming to the new variables $x = 2\pi x_1/l$ and $y = 2\pi x_2/l$. With this transformation and the notation $k = 2\pi K/l$, $a = 1 - M_{f_\infty}^2$,

$b = 1 - M_{e_\infty}^2$, the differential equation (27) as applied to two-dimensional flow can be written

$$ka\frac{\partial^3\phi}{\partial x^3} + k\frac{\partial^3\phi}{\partial x\,\partial y^2} + b\frac{\partial^2\phi}{\partial x^2} + \frac{\partial^2\phi}{\partial y^2} = 0, \tag{30}$$

and the boundary condition (29) becomes

$$\left(\frac{\partial\phi}{\partial y}\right)_{y=0} = U_\infty \epsilon \cos x. \tag{31}$$

The new parameter k in equation (30) is a dimensionless measure of the importance of the non-equilibrium process (cf. equation (26)).

Equation (30) is a linear equation with constant coefficients. One possible solution is given by the exponential form

$$\phi(x, y) = e^{\alpha x - \beta y}, \tag{32}$$

provided α and β are related by the following equation found by substituting the expression (32) into the differential equation (30):

$$\beta^2 = -a^2\frac{b + ka\alpha}{1 + k\alpha}. \tag{33}$$

Here α and β are, in general, complex numbers. The negative sign is taken with β in anticipation of the boundary condition at infinity.

The fact that the solution must be real and periodic suggests that it be taken in the form

$$\phi(x, y) = A\,e^{\alpha x - \beta y} + B\,e^{\alpha^* x - \beta^* y}, \tag{34}$$

where A and B are complex constants and α^* and β^* are the complex conjugates of α and β. In particular, since ϕ is to be periodic in x, we take $\alpha = i$ and $\alpha^* = -i$. With the notation $\beta = \delta + i\lambda$ and $\beta^* = \delta - i\lambda$, where δ and λ are real quantities, the solution (34) can then be written in the purely real form

$$\phi(x, y) = e^{-\delta y}\left[C\cos(x - \lambda y) + D\sin(x - \lambda y)\right], \tag{35}$$

where C and D are real constants related to A and B by $C = A + B$ and $D = i(A - B)$.

To find δ and λ, we return to equation (33) and substitute $\beta = \delta + i\lambda$ and $\alpha = i$. (The same result would be obtained by use of the complex conjugates.) By equating the real and imaginary parts of the resulting equation, we find the following simultaneous equations for δ and λ:

$$\delta^2 - \lambda^2 = \frac{b + k^2 a}{1 + k^2} = P\,(\text{say}), \tag{36a}$$

$$2\delta\lambda = \frac{k(a - b)}{1 + k^2} = Q\,(\text{say}). \tag{36b}$$

Note that P can be positive or negative depending on the values of a and b. Q will always be positive, however, since $a_{f_\infty} > a_{e_\infty}$ with the result that $M_{f_\infty} < M_{e_\infty}$ and $a > b$. The formal solution of equations (36) is given by

$$\delta = \pm\left[\tfrac{1}{2}(P \pm \sqrt{[P^2 + Q^2]})\right]^{\frac{1}{2}}, \quad \lambda = \pm\left[\tfrac{1}{2}(-P \pm \sqrt{[P^2 + Q^2]})\right]^{\frac{1}{2}}.$$

Obviously, the absolute value of the radical in these expressions will always be greater than P. The plus sign must therefore be used with the radical to insure that δ and λ will be real. To satisfy the boundary condition at infinity, the sign of δ itself must also be taken as plus. Since Q is always positive in equation (36*b*), it then follows that λ likewise must be plus. With this choice of signs and substitution of P and Q from equations (36), δ and λ are given finally by

$$\left.\begin{matrix}\delta\\ \lambda\end{matrix}\right\} = \left\{\frac{1}{2(1+k^2)}\left[\pm(b+k^2a)+\sqrt{\{(1+k^2)(b^2+k^2a^2)\}}\right]\right\}^{\frac{1}{2}}, \tag{37}$$

where the upper sign goes with δ and the lower with λ.

It remains to satisfy the boundary condition at the wall and thus determine the constants C and D in solution (35). To this end equation (35) is substituted into condition (31) to obtain the following simultaneous equations:

$$\lambda C - \delta D = 0,$$
$$\delta C + \lambda D = -U_\infty \epsilon.$$

These have the solution

$$C = -\frac{\delta}{\delta^2+\lambda^2}U_\infty\epsilon, \quad D = -\frac{\lambda}{\delta^2+\lambda^2}U_\infty\epsilon.$$

The potential (35) can thus be written finally as

$$\phi(x,y) = -\frac{U_\infty\epsilon}{\delta^2+\lambda^2}e^{-\delta y}\left[\delta\cos(x-\lambda y)+\lambda\sin(x-\lambda y)\right], \tag{38}$$

where δ and λ are given by equation (37). In obtaining this solution no distinction has been necessary between subsonic and supersonic flow.

5. Discussion of solution

A. *Flow field*

The potential function (38), when expressed in terms of the original variables x_1 and x_2, yields the following expressions for the disturbance velocies:

$$\frac{u_1'}{U_\infty} = \frac{1}{U_\infty}\frac{\partial\phi}{\partial x_1} = \frac{2\pi(\epsilon/l)}{\delta^2+\lambda^2}e^{-2\pi\delta(x_2/l)}\left(\delta\sin 2\pi\frac{x_1-\lambda x_2}{l}-\lambda\cos 2\pi\frac{x_1-\lambda x_2}{l}\right), \tag{39}$$

$$\frac{u_2'}{U_\infty} = \frac{1}{U_\infty}\frac{\partial\phi}{\partial x_2} = 2\pi\frac{\epsilon}{l}e^{-2\pi\delta(x_2/l)}\cos 2\pi\frac{x_1-\lambda x_2}{l}. \tag{40}$$

The horizontal disturbance velocity can also be written

$$\frac{u_1'}{U_\infty} = \frac{2\pi(\epsilon/l)}{\sqrt{(\delta^2+\lambda^2)}}e^{-2\pi\delta(x_2/l)}\sin 2\pi\frac{(x_1-\Delta x_1)-\lambda x_2}{l}, \tag{39*a*}$$

where $\Delta x_1/l = (1/2\pi)\tan^{-1}(\lambda/\delta)$.

Before examining the detailed nature of the functions δ and λ, some general results can be stated. Under all conditions the disturbance velocities decay exponentially with x_2 along the lines $x_1 - \lambda x_2 =$ constant, which are straight lines with slope (measured from the vertical)

$$\frac{dx_1}{dx_2} = \lambda. \tag{41}$$

The rate of decay is proportional to the value of δ. Along the straight lines (41) the vertical disturbance velocity is in phase with the slope of the wall. The horizontal disturbance velocity, however, is out of phase with the wall. For a given value of x_2, it lags behind the ordinate of the wall by the horizontal distance Δx_1 as given in equation (39a).

To see what the foregoing results mean in terms of Mach number, we must examine the dependence of δ and λ on M_{f_∞} and M_{e_∞}. In terms of these variables, equation (37) gives

$$\left.\begin{matrix}\delta\\ \lambda\end{matrix}\right\} = \left[\frac{1}{2(1+k^2)}\left\{\pm(1-M_{e_\infty}^2)\pm k^2(1-M_{f_\infty}^2)+\sqrt{[(1+k^2)\{(1-M_{e_\infty}^2)^2+k^2(1-M_{f_\infty}^2)^2\}]}\right\}\right]^{\frac{1}{2}}. \tag{42}$$

For the limiting cases of $k = 0$ (equilibrium flow) and $k = \infty$ (frozen flow), equation (42) reduces to the simple results of the following table:

	$k=0$. Equilibrium flow		$k=\infty$. Frozen flow	
	Subsonic $M_{e_\infty} < 1$	Supersonic $M_{e_\infty} > 1$	Subsonic $M_{f_\infty} < 1$	Supersonic $M_{f_\infty} > 1$
δ	$\sqrt{(1-M_{e_\infty}^2)}$	0	$\sqrt{(1-M_{f_\infty}^2)}$	0
λ	0	$\sqrt{(M_{e_\infty}^2-1)}$	0	$\sqrt{(M_{f_\infty}^2-1)}$

In both limiting cases therefore, the disturbance velocities are given by equations of the following form:

For subsonic flow,

$$\frac{u_1'}{U_\infty} = \frac{2\pi(\epsilon/l)}{\sqrt{(1-M_\infty^2)}}\exp\left[-2\pi\sqrt{(1-M_\infty^2)}\,\frac{x_2}{l}\right]\sin 2\pi\frac{x_1}{l},$$

$$\frac{u_2'}{U_\infty} = 2\pi\frac{\epsilon}{l}\exp\left[-2\pi\sqrt{(1-M_\infty^2)}\,\frac{x_2}{l}\right]\cos 2\pi\frac{x_1}{l}.$$

For supersonic flow,

$$\frac{u_1'}{U_\infty} = -\frac{2\pi(\epsilon/l)}{\sqrt{(M_\infty^2-1)}}\cos 2\pi\frac{x_1-\sqrt{(M_\infty^2-1)}\,x_2}{l},$$

$$\frac{u_2'}{U_\infty} = 2\pi\frac{\epsilon}{l}\cos 2\pi\frac{x_1-\sqrt{(M_\infty^2-1)}\,x_2}{l}.$$

These are of the same form as the classical results obtained by Ackeret on the basis of the Prandtl–Glauert equation (see, for example, Liepmann & Roshko (1957)). The decay of the velocity field is zero for supersonic flow, and the rearward rotation of the lines along which the decay takes place is zero for subsonic flow. As one would expect, the only difference between the results for equilibrium and frozen flow is in the speed of sound on which the Mach number is based.

The variation of δ and λ for an intermediate value of k is shown in figure 1, together with curves for the two limiting cases. The results are plotted as functions of M_{e_∞} for a value of the ratio $a_{f_\infty}/a_{e_\infty}$ of 11/10, which is a convenient value, though perhaps slightly larger than one would actually find for a single non-equilibrium

process in a diatomic gas. It follows that $M_{f_\infty} = (a_{e_\infty}/a_{f_\infty})\, M_{e_\infty} = (10/11)\, M_{e_\infty}$. The intermediate value of $k = 1$ was chosen as giving very nearly the maximum value of the variables in the regions in which the variation with k is not monotonic.

Figure 1 shows that the existence of a finite relaxation time removes certain of the qualitative differences that distinguish subsonic flow from supersonic flow in the two limiting cases. (The transition from one type of flow to the other, in fact, is no longer clearly defined.) The exponential decay of the velocity field, as measured by the value of δ, now persists throughout the Mach-number range. As before, it decreases rapidly in the near-sonic region. It never disappears entirely,

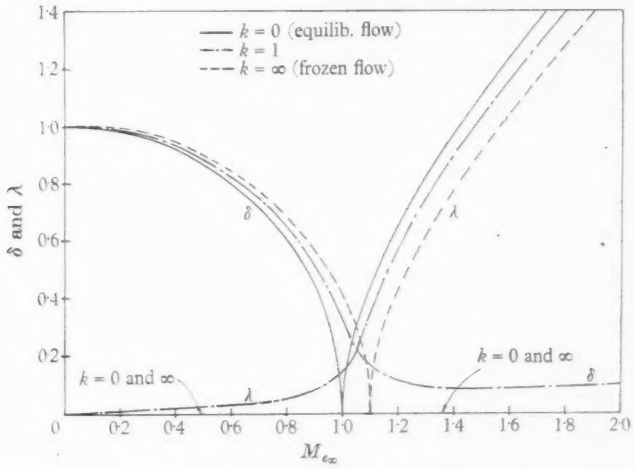

FIGURE 1. Values of δ and λ as functions of M_{e_∞} for $a_{f_\infty}/a_{e_\infty} = 11/10$.

however, as it does for both equilibrium and frozen flow at supersonic speed. The rearward rotation of the lines of exponential decay, which is measured by the value of λ, is now zero for incompressible flow only ($M_{e_\infty} = 0$). As in the two limiting cases, it grows rapidly in the near-sonic region. It is evident to a slight extent, however, even at lower speeds.

Other things being equal, the effect of differences in relaxation time is shown by the variation of δ and λ with k for fixed M_{e_∞}. For a value of $M_{e_\infty} < 1$ (see figure 1), δ increases monotonically with increasing k, whereas λ rises to a maximum and then declines. In the limits of $k = 0$ and ∞ the disturbance field is of the classical subsonic type with marked exponential decay along vertical lines. For a value of $M_{e_\infty} > a_{f_\infty}/a_{e_\infty}$, the situation is reversed: λ varies monotonically and δ exhibits a maximum. In the two limiting cases the field is now of the classical linearized supersonic type with the velocities propagating undiminished along rearward sloping lines. For $1 < M_{e_\infty} < a_{f_\infty}/a_{e_\infty}$, the variation of δ and λ with k is rather complicated. In the limit of $k = 0$ (equilibrium flow), the disturbance field is of the classical supersonic type; for $k = \infty$ (frozen flow), it is of the classical subsonic type.

The entire situation with regard to variations in both M_{e_∞} and k is exemplified in figure 2, which shows typical streamline patterns for three values each of both

of these parameters. The behaviour observed here is related, of course, to the various possibilities as regards the elliptic or hyperbolic character of the two parts of the differential equation as previously discussed.

It is worth noting that the classical supersonic flow with propagation along outgoing (i.e. rearward sloping) Mach lines appears here as the natural limit of the non-equilibrium solution. In the classical analysis, which sets $k = 0$ in the

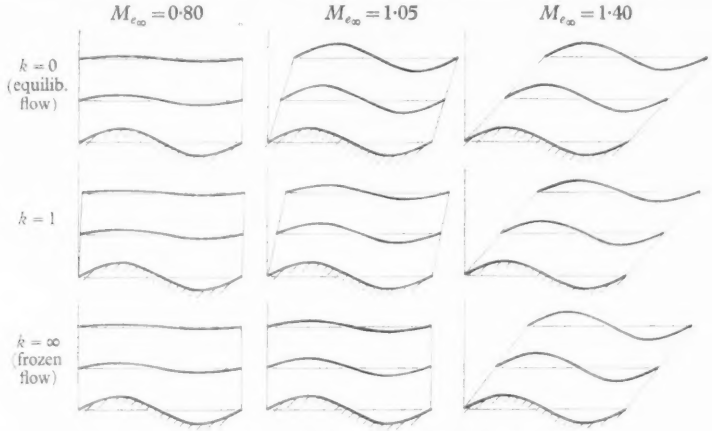

FIGURE 2. Typical streamline patterns for $\epsilon/l = \frac{1}{12}$.

differential equation at the outset, there exists in addition a mathematical solution representing propagation along the incoming Mach lines, and this solution must be discarded on physical grounds. In the present analysis, the non-equilibrium (i.e. irreversible) process determines a unique direction of propagation, and this automatically picks out the physically correct result in the limit.

B. *Pressure distribution and drag coefficient*

To the accuracy required in the two-dimensional small-disturbance case, the pressure coefficient $C_p \equiv (p - p_\infty)/\frac{1}{2}\rho_\infty U_\infty^2$ can be found from equation (13) as

$$C_p = -2\frac{u_1'}{U_\infty}.$$

Substitution from equation (39a) gives for the pressure coefficient on the wall

$$(C_p)_{x_2=0} = -\frac{4\pi(\epsilon/l)}{\sqrt{(\delta^2+\lambda^2)}}\sin 2\pi\frac{x_1 - \Delta x_1}{l}. \tag{43}$$

A plot of $\Delta x_1/l = (1/2\pi)\tan^{-1}(\lambda/\delta)$ for the conditions of figure 1 is shown in figure 3. For $k = 1$ the point of minimum pressure on the wall is seen to shift continuously backward from the crest toward the point of maximum negative slope as the Mach number increases. This is in contrast to the situation in the Ackeret solution ($k = 0$ and ∞), where a shift of one-quarter wavelength takes place discontinuously as the flow changes from subsonic to supersonic. The results of equation (43) and figure 1 also show that the pressure coefficient in

non-equilibrium flow always remains finite. This is again in contrast to both limiting cases, where C_p becomes indeterminately large at the sonic speed.

The drag coefficient per wavelength of wall can be calculated from

$$c_d = \int_0^1 (C_p)_{x_2=0} \frac{dX_2}{dx_1} d\left(\frac{x_1}{l}\right).$$

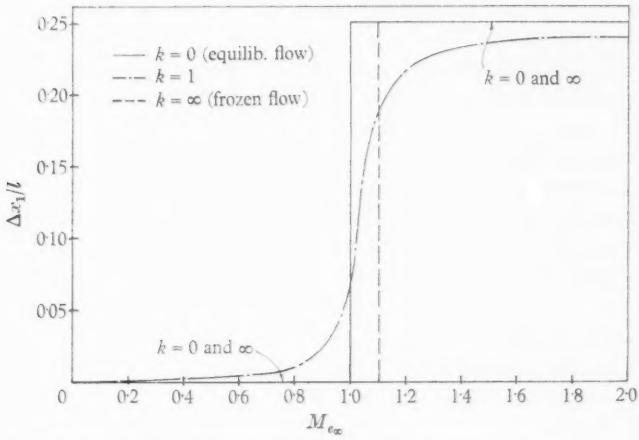

FIGURE 3. Relative shift of pressure distribution as a function of $M_{e\infty}$ for $a_{f\infty}/a_{e\infty} = \frac{11}{10}$.

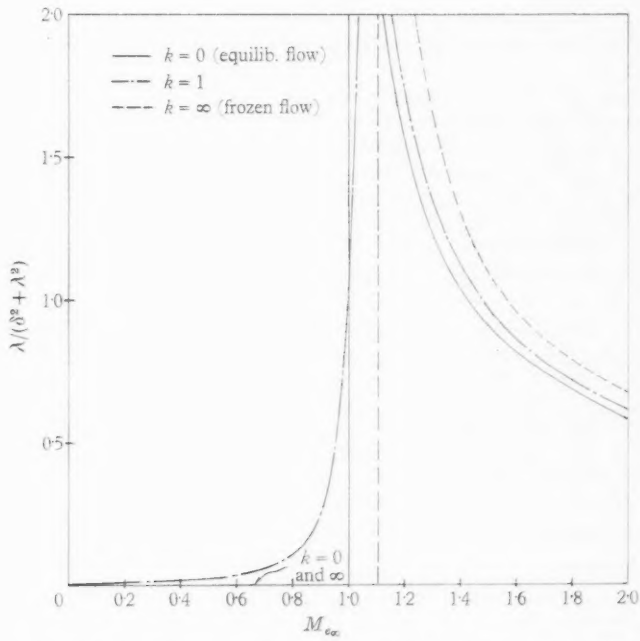

FIGURE 4. Drag parameter as a function of $M_{e\infty}$ for $a_{f\infty}/a_{e\infty} = \frac{11}{10}$.

Substitution from equations (28) and (43) gives

$$c_d = 4\pi^2 \left(\frac{\epsilon}{l}\right)^2 \frac{\lambda}{\delta^2+\lambda^2}. \tag{44}$$

The factor $\lambda/(\delta^2+\lambda^2)$ is plotted as a function of $M_{e\infty}$ in figure 4. As would be expected from the previous results, the non-equilibrium effects eliminate the discontinuous behaviour in drag coefficient that is a characteristic feature of the classical Ackeret solution. The maximum in the near-sonic range is still sharp—so much so that the labour required to find it precisely did not seem worthwhile. It is, nevertheless, not infinite. The non-zero drag that is now evident for $M_{e\infty} < 1$ is due to the presence of a mechanism for entropy increase even at subsonic speeds (cf. equation (11)). At supersonic speeds there are now two sources of entropy rise: shock waves, whose action is well known from classical gas dynamics, and non-equilibrium effects, which now act in the regions between shock waves. The net effect is apparently to cause the drag for $M_{e\infty} > a_{f\infty}/a_{e\infty}$ to lie between the limiting values calculated for equilibrium and frozen flow.

The author is indebted to his colleagues Drs Krishnamurty Karamcheti and Chi-chang Chao for suggesting the method of solution of the differential equation, and to Mr J. Howard Drake for numerical calculations.

REFERENCES

Ackeret, J. 1928 Über Luftkräfte bei sehr grossen Geschwindigkeiten insbesondere bei ebenen Strömungen. *Helv. phys. acta*, **1**, 301.

Broer, L. J. F. 1958 Characteristics of the equations of motion of a reacting gas. *J. Fluid Mech.* **4**, 276.

Chu, Boa-Teh 1957 Wave propagation and the method of characteristics in reacting gas mixtures with applications to hypersonic flow. *WADC* TN-57-213, May 1957.

Gibson, W. E. & Moore, F. K. 1958 Acoustic propagation in a diatomic gas subject to thermal or chemical relaxation. *Cornell Aero. Lab. Rep.* no. HF–1056–A–2.

Lagerstrom, P. A., Cole, J. D. & Trilling, L. 1949 Problems in the theory of viscous compressible fluids. *Calif. Inst. Tech.*, Report on Contract N6onr-Task Order VII, Office of Naval Research.

Liepmann, H. W. & Roshko, A. 1957 *Elements of Gas Dynamics*. New York: John Wiley and Sons.

Moore, F. K. 1958 Propagation of weak waves in a dissociated gas. *J. Aero Sci.* **25**, 279.

Moore, F. K. & Gibson, W. E. 1959 Propagation of weak disturbances in a gas subject to relaxation effects. *Inst. Aero. Sci. Rep.* no. 59–64.

Morrison, J. A. 1956 Wave propagation in rods of Voigt material and visco-elastic materials with three-parameter models. *Quart. Appl. Math.* **14**, 1953.

Wood, W. W. & Kirkwood, J. G. 1957*a* Characteristic equations for reactive flow. *J. Chem. Phys.* **27**, 596.

Wood, W. W. & Kirkwood, J. G. 1957*b* Hydrodynamics of a reacting and relaxing fluid. *J. Appl. Phys.* **28**, 395.

Pressure and velocity measurements on detonation waves in hydrogen-oxygen mixtures

By D. H. EDWARDS, G. T. WILLIAMS* AND J. C. BREEZE†
Department of Physics, University College of Wales, Aberystwyth

(Received 23 December 1958 and in revised form 16 April 1959)

Measurements are described of the static pressures and velocities of detonation waves in hydrogen-oxygen mixtures, together with the pressures arising on their normal reflexion at the closed end of the explosion tube. Two explosion tubes, of diameter 10 and 1·6 cm, were employed to study the diameter effect on the wave pressures. The experimental results are compared with calculated values of the wave properties for a range of hydrogen-oxygen mixtures initially at atmospheric pressure. In the 10 cm tube the static pressures and velocities are found to agree well with theory for mixtures with hydrogen content in the approximate range 50–75 %; the evidence from pressure profiles and wave velocities indicates that mixtures outside this range may not be able to support ideal C–J waves. Detonation waves in all the mixtures studied in the 1·6 cm tube are found to be subideal. A possible explanation, in terms of energy loss to the tube wall, of the discrepancy between experiment and theory is discussed. Spinning occurs in mixtures near the limits of detonation in the smaller tube; the measured frequencies are found to be in reasonable agreement with the values predicted by the theories of Manson (1947) and Fay (1952).

1. Introduction

Of the various properties of gaseous detonation waves, the velocities have been studied experimentally far more extensively than any other. Early investigators in this field were able to obtain tolerably good values for the wave velocities by means of chronoelectric methods (e.g. Berthelot & Vieille 1882) or from the records of the waves on moving photographic plates or film (e.g. Mallard & Le Chatelier 1900). Since then, the considerable advancements which have been made in high-speed photography and in the application of electronic techniques to the measurement of time intervals enable wave velocities to be measured to a high degree of precision. An example of such measurements is the study of the wave velocities in hydrogen-oxygen mixtures made by Berets, Greene & Kistiakowsky (1950).

In contrast to wave-velocity measurements, pressure measurements have received far less attention; this fact is understandable since it is a more difficult quantity to measure with accuracy. Early work gave no more than a crude and

* Now at M.O.S. Arm. Res. Dev. Estab., Fort Halstead.
† Now at Department of Physics, University of Western Ontario, London, Ontario.

uncertain measure of the peak pressures generated in detonation waves. Thus Dixon & Cain (1894) attempted to estimate the pressures generated from the known strengths of glass tubes which were just fractured by the impact of the wave, whilst Campbell, Littler & Whitworth (1932) noted how metal foils of various thickness, placed across the end of an explosion tube, were ruptured. The results of both investigations were very approximate in view of the uncertainties in the mechanisms of fracture or rupture. Similarly, the results of the crusher gauge experiments of Rimarski & Konschak (1934) and Henderson (1941) must be regarded as unreliable.

The most significant measurements reported of detonation pressures in hydrogen-oxygen mixtures appear to be those of Gordon (1949) and Davies, Edwards & Thomas (1950). Gordon employed tourmaline gauges, in which oil or soft wax was used to damp the crystal vibrations, and although the results he presents are few and some of the gauge records are marred by oscillations, quite good agreement is observed between the measured and the theoretical values of pressure for a few compositions. Davies *et al.* used both quartz crystal gauges and the Hopkinson pressure bar method in the electrical form devised by Davies (1948), and in a preliminary investigation obtained results which were promising. It was apparent, however, that a more satisfactory gauge design was required before completely reliable pressure measurement could be achieved.

The need for a study of the pressure distribution in the detonation wave, in addition to a measure of its velocity, may be appreciated from the following considerations. (Contrary to strict usage the term detonation wave will frequently be employed in the present paper to denote the shock front, the reaction zone together with the non-steady regime of the rarefaction wave.) In the case of the ideal detonation wave the Chapman–Jouguet (C–J) plane is identified in the hydrodynamic theory with the plane of complete chemical and thermal equilibrium. Kirkwood & Wood (1954), however, have shown that thermodynamic equilibrium at the C–J plane is not an essential requirement in the generalized theory. Deviations from complete equilibrium at the C–J plane would be expected to give rise to differences between the observed detonation wave parameters and those computed on the assumption of equilibrium. Thus if the rate of release of chemical energy within the reaction zone is lowered, for example by cooling of the reacting gases at the walls of the confining vessel, then the rate of evolution of useful energy may drop below the level required for the propagation of the ideal C–J wave. In this case, the velocity of the wave will be less than the ideal value and the C–J condition, $U_1 = u_1 + c_1$, will now hold for the plane in which the energy required to propagate the wave (i.e. useful energy) is just balanced by the evolution of chemical energy. Berets *et al.* (1950) suggest that the excellent agreement which is usually observed between theoretical and experimental velocities may be due to the stabilizing action on the detonation velocity of the largely dissociated reaction systems, in which exothermic and endothermic reactions, involving both mole increment and decrement, are proceeding simultaneously. This interpretation appears to have been rejected later by Kistiakowsky & Zinman (1955), and agreement between experiment and equilibrium calculations is taken as proof of the attainment of

thermodynamic equilibrium in the C–J plane. In the view of the present authors, the original hypothesis of the buffering effect of the reactants on the wave velocity is of some importance, and consequently an examination of the velocity alone does not provide a sufficiently strong criterion to establish whether equilibrium has been achieved in the C–J plane. Moreover, the measurement of any other parameter, such as pressure, density or temperature, for the same reason, would equally be insensitive to small departures from strict equilibrium at the C–J plane. If, however, the pressure-time or density distribution (Kistiakowsky & Kydd 1955) in the wave are known in conjunction with the velocity, then the two parameters give a more complete description of the wave than is obtained from the measurement of the wave velocity alone. Furthermore, a comparison of the detonation pressure with the theoretical value should provide a far more sensitive criterion of the validity of the C–J hypothesis itself than a measure of the velocity. This fact can be verified from an examination of theoretical data (e.g. Manson 1947); for if it is assumed that the end-point of the detonation moves away from the C–J point along the Rankine–Hugoniot curve for complete reaction, the corresponding changes in pressure are, for small deviations, several times as large as the resulting changes in velocity.

In this paper, results are presented of measurements of the static and reflexion pressures in detonation waves in various hydrogen-oxygen mixtures confined in tubes; measurements of the wave velocities were made simultaneously with the pressure measurements. Since no systematic investigation appears to have been carried out previously on the effect of explosion tube diameter on the wave pressures, comparable to the work of Berets *et al.* (1950) on the wave velocity, pressure measurements have been obtained for two explosion tubes of different diameter.

2. The numerical calculations

The best results available of the theoretical properties of detonation waves in hydrogen–oxygen mixtures are those of Berets *et al.* (1950), who employed the most recent thermochemical data given by the National Bureau of Standards (1949). Their calculations were made for an initial gas pressure of 1 atm. at a standard temperature of 25 °C. The ambient temperatures normally found in our laboratories are, however, nearer 18 °C, and whereas wave velocities are comparatively insensitive to small changes in initial gas temperatures, a significant dependence on such changes is found for the values of the wave pressures. Furthermore, to the authors' knowledge, no results have been reported of the properties of the shock wave arising on normal reflexion of a plane detonation wave at a rigid surface. For these reasons, a new series of calculations have been made of the properties of both the detonation wave and normally reflected shock wave.

2.1. *The detonation wave*

In the computation of the properties of the detonation wave, it is assumed that the burnt gases obey the ideal gas law (see Schmidt 1941; Kistiakowsky, Knight & Malin 1952), and the C–J plane is defined as the plane of thermodynamic

equilibrium over which the condition $U_1 = u_1 + c_1$ obtains, where U_1, u_1 and c_1 are the wave, mass and sound velocities, respectively. Moreover, Brinkley & Richardson (1953) and Kirkwood & Wood (1954) have shown that the sound velocity, c_1, at the C–J plane must be evaluated at the instantaneous frozen composition (i.e. the total mole number being regarded as independent of pressure and temperature) and not, as had been previously assumed, for mobile equilibrium. Following Berets *et al.* (1950) allowance has been made in the calculations for the following equilibria:

$$\tfrac{1}{2}H_2 \rightleftharpoons H,$$
$$\tfrac{1}{2}O_2 \rightleftharpoons O,$$
$$H_2 + \tfrac{1}{2}O_2 \rightleftharpoons H_2O,$$
$$\tfrac{1}{2}H_2 + \tfrac{1}{2}O_2 \rightleftharpoons OH.$$

Initial composition	Temp. T_1 (°K.)	Pressure (C–J) (atm.)	Density ratio (ρ_1/ρ_0)	Velocity U_1 (m/s)	Velocity c_1 (m/s)	Mass velocity u_1 (m/s)	Final Composition (%)						Total mole number n
							H_2O	H_2	O_2	OH	H	O	
$8H_2+O_2$	2717	14·53	1·74	3802	2186	1615	24·70	73·82	0·00	0·11	1·36	0·00	8·00
$4H_2+O_2$	3439	17·79	1·76	3425	1942	1483	42·74	45·16	0·15	3·37	8·16	0·41	4·27
$3H_2+O_2$	3607	18·44	1·77	3197	1807	1390	48·97	31·68	0·89	7·20	9·78	1·48	3·36
$2H_2+O_2$	3675	18·59	1·77	2853	1610	1243	53·00	16·72	5·13	12·85	8·17	4·13	2·40
H_2+O_2	3467	17·63	1·77	2333	1318	1015	47·59	4·14	26·34	13·45	2·65	5·83	1·67
H_2+2O_2	3029	15·79	1·76	1941	1103	838	34·76	0·62	55·57	6·22	0·34	2·49	2·58
H_2+3O_2	2662	14·14	1·75	1759	1006	752	26·92	0·11	69·77	2·43	0·04	0·72	3·33

TABLE 1. The detonation wave. Initial pressure, 1 atm.; initial temperature, 18 °C.

The method adopted for the solution of the detonation wave and reflected shock wave equations closely follows that used by Huff, Gordon & Morrell (1951) for the computation of the equilibrium composition and temperature of chemical reactions. This method, when applied to the detonation and reflected shock wave equations arranged in a suitable form, gives a rapidly convergent solution and has been found suitable for use with a desk calculator and for programming on an electronic digital computer. The calculated values of the parameters at the C–J plane and their values behind the leading shock of the detonation wave, termed the 'von Neumann' peak, are given in tables 1 and 2. In addition to the symbols already defined, p, ρ and T denote the pressure, density and temperature respectively, and the subscripts 0, 1 and 2 are used to define their values in the unburnt gases, behind the incident detonation front, and behind the reflected shock front, respectively; the peak values of the parameters are designated by a circumflex accent.

2.2. *The reflected shock wave*

The computation of the reflected shock wave properties has been divided into two parts:

(*a*) The computation of the properties of the shock wave obtained on reflexion of the von Neumann peak, in which it is assumed that, immediately on reflexion,

the shock wave moves into a medium which is at the conditions prevailing at the von Neumann peak of the incident detonation wave, and for which the boundary condition at the reflecting wall is $\hat{u}_2 = 0$.

(*b*) A similar computation to the above has been made for the C–J plane in which it is assumed that the boundary condition for the reflexion is $u_2 = 0$.

Initial composition	Temp. $\hat{T}_1$ (°K.)	Pressure $\hat{p}_1$ (atm.)	Density ratio ρ_1/ρ_0	Velocity U_1 (m/s)	Mass velocity $\hat{u}_1$ (m/s)
$8H_2+O_2$	1505	26·68	5·16	3802	3065
$4H_2+O_2$	1739	32·69	5·47	3425	2799
$3H_2+O_2$	1778	33·89	5·55	3197	2621
$2H_2+O_2$	1774	34·16	5·61	2853	2344
H_2+O_2	1678	32·43	5·63	2333	1919
H_2+2O_2	1521	29·10	5·57	1941	1593
H_2+3O_2	1391	26·06	5·45	1759	1437

TABLE 2. The von Neumann peak in the detonation wave.
Initial pressure, 1 atm.; initial temperature, 18 °C.

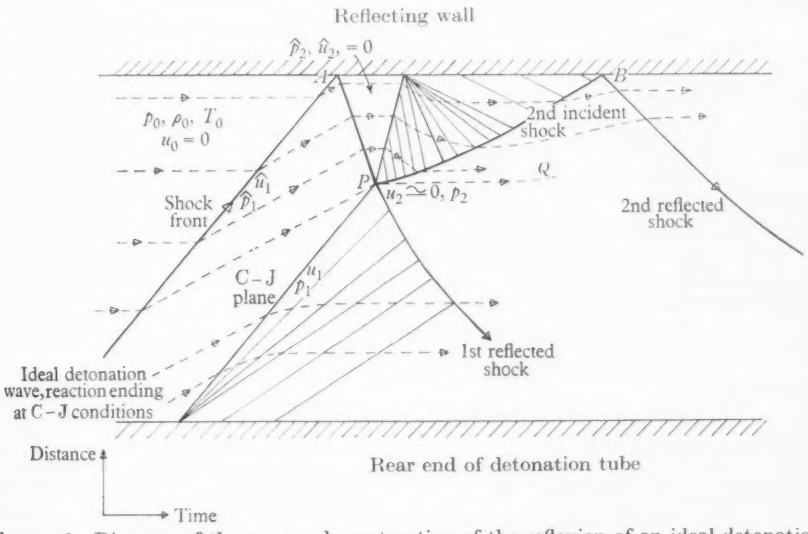

FIGURE 1. Diagram of the proposed construction of the reflexion of an ideal detonation wave at a rigid surface. Particle paths, — ▷ —.

A possible construction of the reflexion process of an ideal detonation wave at a rigid surface has been suggested to the authors by Mr C. K. Thornhill. In order to simplify the geometry the device is adopted of compressing the reaction into an instantaneous event, a short finite time after the passage of the causal shock; i.e. the detonation wave is replaced by an initial shock followed by a short period of steady state at peak conditions and ending in a 'reaction shock' running into the C–J state. This construction is shown, in a qualitative fashion, in the diagram of figure 1.

From the diagram it is seen that the present computation refers to conditions at the point P, on the dividing particle-path PQ, which represents the point of intersection of the reflected shock and incident C–J plane, assuming that the mass flow u_2 is reduced almost to rest at this point. The point P is at a distance of the order of the width of the reaction zone of the incident detonation wave away from the reflecting wall; for gaseous mixtures initially at atmospheric pressure, the reaction time is of the order of 1 μs and the thickness of the reaction

Initial composition	Temp. T_2 (°K)	Pressure p_2 (atm.)	Density ratio ρ_2/ρ_1	Velocity U_2 (m/s)	Final composition (%)						Total mole number, n
					H_2O	H_2	O_2	OH	H	O	
$8H_2+O_2$	3136	34·31	2·02	1581	24·10	72·08	0·00	0·40	3·40	0·01	8·16
$4H_2+O_2$	3773	42·22	2·10	1343	39·28	44·01	0·27	4·95	10·70	0·78	4·39
$3H_2+O_2$	3915	43·79	2·12	1239	44·20	31·86	1·14	9·00	11·68	2·12	3·47
$2H_2+O_2$	3971	44·18	2·13	1100	47·64	17·89	5·18	14·63	9·63	5·02	2·58
H_2+O_2	3763	41·83	2·12	902	43·37	5·01	24·79	15·91	3·56	7·37	1·72
H_2+2O_2	3345	37·29	2·10	747	32·14	0·98	53·21	8·88	0·66	4·12	2·64
H_2+3O_2	3016	33·31	2·05	715	25·33	0·27	67·94	4·50	0·15	1·81	3·58

TABLE 3. The reflected shock wave. Initial pressure, 1 atm.; initial temperature, 18 °C.

Initial composition	Temp. $\hat{T}_2$ (°K)	Pressure $\hat{p}_2$ (atm.)	Density ratio $\hat{\rho}_2/\hat{\rho}_1$	Velocity $\hat{U}_2$ (m/s)
$8H_2+O_2$	2783	175·4	3·55	1200
$4H_2+O_2$	3243	226·6	3·72	1030
$3H_2+O_2$	3322	237·8	3·76	951
$2H_2+O_2$	3315	241·7	3·79	841
H_2+O_2	3128	229·9	3·80	685
H_2+2O_2	2819	203·7	3·78	573
H_2+3O_2	2559	178·6	3·73	527

TABLE 4. The peak values in the reflected shock wave. Initial pressure, 1 atm.; initial temperature, 18 °C.

zone is $\sim$ 1 mm (Kistiakowsky & Kydd 1956). An important feature of the construction is the hypothesis that a pressure and velocity balance is achieved at the dividing particle-path PQ by the existence of a second shock front which is reflected at the point B in the diagram a finite time after the arrival of the first shock at the reflecting wall; experimental evidence in support of this proposition is discussed later. Calculated values of the parameters at the point P are given in table 3 and their peak values at the wall in table 4.

2.3. *The effect of initial temperature*

Several calculations were carried out for the stoichiometric mixture assuming different values of initial temperature. In figure 2 graphs are shown of the percentage deviation of the detonation velocities and pressures, from their

values calculated for an initial temperature of 18 °C, plotted against temperature. Over the range of temperatures which is likely to occur under laboratory conditions, the variation of the detonation, von Neumann peak, reflected shock and peak reflected shock pressures is sufficiently linear to permit a general correction factor of $-0{\cdot}34\,\%$ per °C rise in temperature to be applied to the values of p_1, $\hat{p}_1$ and p_2, and $-0{\cdot}40\,\%$ per °C to the values of $\hat{p}_2$, given in tables 1–4. The variation of detonation velocity with temperature, shown in the same diagram, is seen to be sufficiently small so as to be negligible for most purposes over moderate ranges of temperature.

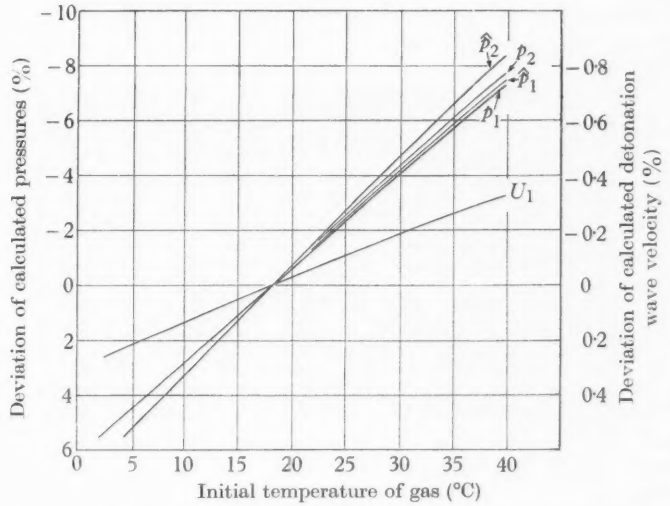

FIGURE 2. Graphs showing the variation with initial gas temperature of the percentage deviation of detonation and shock wave parameters in $2H_2 + O_2$ from their values calculated for an initial temperature of 18 °C. Initial gas pressure 1 atm.

3. Experimental work

3.1. *The explosion tubes*

The two explosion tubes are of circular cross-section, the larger tube is made of mild steel with $\frac{1}{2}$ in. thick wall and internal diameter 10 cm, whilst the smaller tube is of brass of internal diameter 1·6 cm and $\frac{1}{8}$ in. wall. Both tubes consist of two sections, termed the 'driving' and 'test' sections, each of the same diameter, which are approximately 1 and 4 m long, respectively. Heavy flanges are welded to the ends of both sections of the 10 cm diameter tube enabling them to be bolted together; by placing a cellophane diaphragm between the flanges the two sections can be isolated from each other. The ends of the tube are closed by means of two steel plates. All the flanges are grooved to accommodate rubber O-rings to ensure vacuum-tight connexions. The smaller tube is similarly designed. The internal wall of the large tube has a slight roughness, whereas the wall of the brass tube is reasonably smooth; no measures were taken to improve these surfaces, the tubes being used as supplied by the manufacturers.

3·2. *The pressure gauges and ionization probes*

A pressure gauge has been developed in this Laboratory which employs an X-cut quartz disk to measure the average stress over the cross-section of a duralumin rod. The construction and behaviour of this gauge is described by Edwards (1958) who has shown that it gives satisfactory records of the pressure profile in gaseous detonation waves. Pressure bars of $\frac{1}{4}$ and $\frac{1}{2}$ in. diameter have been used in the present investigation, the former for the measurement of the reflexion pressures and the latter for the static pressures in the waves. The time interval over which the gauge will record is determined by the length of bar used; in most instances a gauge capable of recording over an interval of 220 μs was adequate, but when recordings were required over longer intervals a gauge

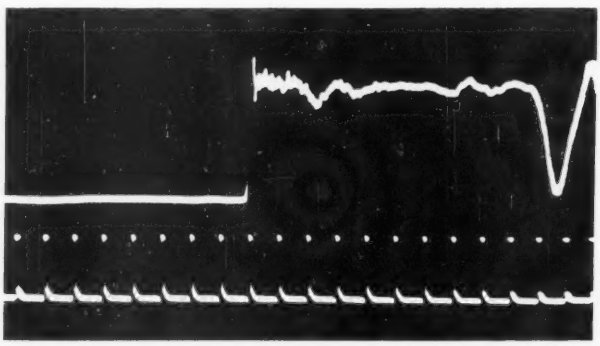

FIGURE 3. Oscillogram obtained with $\frac{1}{4}$ in. gauge when set to measure the reflexion pressure due to a shock wave in air. Shock Mach number: 1·75. Timing marks: 20 μs.

of greater length was employed which responded to pressure pulses of approximately 1·1 ms duration. The pressure gauges could be set to measure the static and reflexion pressures by screwing the gauge head into bushes, one is placed in the cylindrical wall of the tube at a distance of 30 cm from the end of the tube and another is placed centrally in the end-plate. In order to reduce the transmission of stress waves propagated in the explosion tube wall to the gauge, these bushes are constructed of polythene. The measuring end of the static pressure gauge is machined to the same radius as the internal wall of the tube so that when the gauge is mounted in position this face is flush with the internal wall surface. Similar care is taken to ensure that the reflexion pressure gauge is flush with the end-plate.

The manner in which the gauges are calibrated by a ball impact method has been described by Edwards (1958). In addition to this method, the gauges were calibrated by the impact of shock waves in air, generated in a 5 cm diameter shock tube. A typical record obtained when a $\frac{1}{4}$ in. diameter gauge is set to measure the reflected shock pressure is shown in figure 3. It is seen that oscillations due to dispersion of the stress waves in the gauge bar occur immediately after the initial rise. The average voltage level, however, remains constant over an interval of $\sim$ 220 μs before the return of the pulse of tension

from the free end of the pressure bar. Values of the gauge constant can be determined from these records to an accuracy of within 1 %.

Velocity measurements on the detonation waves are made by the ionization probe technique. The design of the probes and of the associated electrical circuitry used in the 10 cm diameter tube closely resemble those described by Knight & Duff (1955). Twelve probes are fitted into the tube wall in two groups of six, the probes in each group being placed at intervals of 10 and 20 cm, respectively. In the 1·6 cm tube 10 mm sparking plugs are used as probes, their ends having been slightly modified so that no part protrudes into the tube and interferes with the gas flow.

3.3. *The recording apparatus*

Any circuit external to the pressure gauge must possess a sufficiently high input impedance if leakage of charge from the gauge is to be kept low during the time in which the gauge signal is being recorded. For this purpose, a cathode-follower is used which has an input impedance of 20 MΩ and whose frequency characteristics are constant up to 2 Mc/s. The signal from the cathode-follower is fed by a coaxial cable into a recording room where it is amplified and displayed on a c.r.o., a Solarscope Type CD 513, and recorded on a stationary plate camera. The time-base of the c.r.o. is initiated at a predetermined interval before the arrival of the pressure gauge signal by a pulse from an ionization probe.

Two methods are available for recording the ionization probe signals. In the first, when it is desired to follow the variation of the wave velocity along the length of the tube, the voltage pulses, after appropriate shaping, are displayed on a c.r.o. and recorded photographically. Alternatively, if only the average velocity over a particular length of tube is desired, the pulses from two selected probes are employed to trigger a 'Cintel' microsecond chronometer. The accuracy obtainable by these methods in the measurement of velocity is generally $\sim \frac{1}{2}$ %.

3.4. *Preparation of the gas mixtures*

The driving and test sections of the explosion tube are evacuated simultaneously, the pressure in the tube being measured by a mercury manometer and a 'Vacustat' gauge; a residual pressure of 0·1 mm of mercury is considered satisfactory. After evacuation the tube is isolated from the vacuum pump and each section is filled in turn, the constituent gases being obtained from commercial cylinders. The partial pressure of each component gas is measured by means of the mercury manometer, which can be read to the nearest 0·05 cm. The test section of each tube is filled first and in the case of the 10 cm diameter tube a coarse grid, fixed near the end of the driving section, provides support for the diaphragm during this operation. A minimum time of 12 h is allowed for the gases to mix. Facilities are available for pre-mixing the gases in large cylinders before admitting them into the 1·6 cm tube; in this way errors in metering small volumes of gas are avoided.

4. Results

4.1. *The 10 cm diameter tube*

In all the experiments performed in this tube, the gaseous mixture was initially at atmospheric pressure and at room temperature which was within a degree or two of 18 °C. In the preliminary work, the cellophane diaphragm separating the driving and test sections was absent, the detonation being initiated by electrically firing copper acetylide matchheads. The pressures obtained, however, even with the more strongly detonating mixtures, were substantially higher than the theoretical values and the measured velocities in all mixtures were between 3 and 4% below those calculated. After carefully checking the recording apparatus it was concluded that even after a run of approximately 5 m in mixtures near the stoichiometric composition, a stable wave was not established by this method of initiation. It was, therefore, abandoned in favour of the shock wave method of initiation, the shock waves being generated by detonating a stoichiometric acetylene-oxygen mixture, at an initial pressure of 1 atm., contained in the driving section.

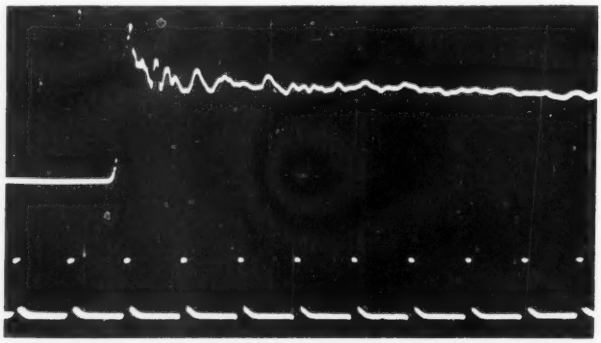

FIGURE 4. Oscillogram of the response of the $\frac{1}{2}$ in. gauge to the static pressure in a detonation wave in $2H_2+O_2$ in the 10 cm diameter tube. Timing marks: 20 μs.

A typical oscillogram, obtained with the $\frac{1}{2}$ in. pressure gauge, of the static pressure in $2H_2+O_2$ is shown in figure 4 and the pressure-time distributions derived from three such records are given in figure 5. The oscillations appearing have been smoothed out so that the general trend of the profile can be appreciated more readily. It will be observed that the rise time of the pressure to the peak value is 7·0 μs, which exceeds the time of traverse of the wave across the end of the pressure gauge of 4·45 μs. This discrepancy in the two values arises from the distortion of the pulse due to the dispersion of the stress pulse as it travels along the pressure-bar; this has the effect of rounding-off sharp pressure variations and lengthening the rise-times (see Davies 1948). The peak pressure observed in the records is attributed to the partial response of the gauge to the von Neumann peak pressure within the detonation wave. That this peak is not due to a gauge effect may be verified by comparing the records with the record of figure 3 obtained for the shock waves in air, in which the characteristic overshoot of the pressure bar signal due to dispersion is seen to be markedly different

to the response for the detonation wave. The average value obtained from four records for this peak pressure is 27·1 atm. compared with the theoretical value of 34·16 atm. An exact response to the peak pressure is not to be expected since the reaction zone of the wave is extremely narrow and is obviously outside the limit of resolution obtainable with the gauge; the significance of this peak will be discussed later. Following the peak value the pressure on the records falls rapidly, until after an interval of $\sim 5\,\mu s$ the pressure begins to level out and

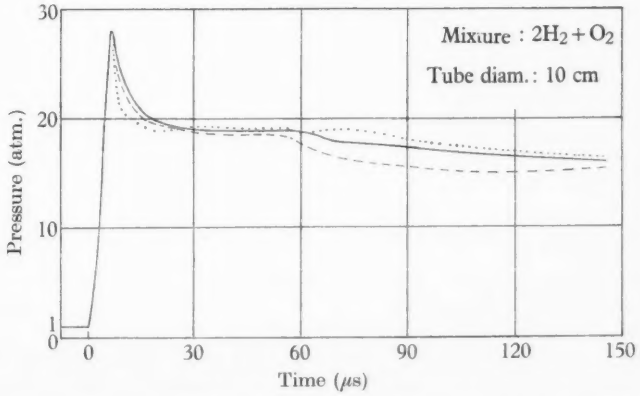

FIGURE 5. Pressure-time distributions obtained from three recordings with a $\frac{1}{2}$ in. gauge set to measure the static pressure in $2H_2 + O_2$. Tube diameter: 10 cm.

Peak pressure (obs.) (atm.)	Average pressure 20–80 μs (obs.) (atm.)	Average pressure 100–200 μs (atm.)	Rise time (obs.) (μs)
26·8	19·0	16·7	7·2
26·7	18·4	15·2	7·2
27·9	18·6	16·7	6·8
27·1	18·6	17·5	7·1

TABLE 5. Reproducibility of the static pressures in $2H_2 + O_2$ in 10 cm diameter tube. Peak pressure (theor.), 34·16 atm.; C–J pressure (theor.), 18·59 atm.

remains sensibly constant for the next 80–90 μs, and thereafter it begins to decay slowly under the influence of the following rarefaction wave. The average pressure over the period 20–80 μs has been measured for comparison with the theoretical value, and the mean value found from four records for this mixture is 18·6 atm. which is in excellent agreement with the computed C–J value of 18·59 atm. To illustrate the reproducibility of the static pressure records, values for the four records obtained with the stoichiometric mixture are given in table 5.

Pressure–time curves for the non-stoichiometric mixtures investigated are shown in figure 6. As before, the small amplitude irregular oscillations appearing on the records have been smoothed out. The general shapes of the curves for all

the mixtures are very similar except for $H_2 + 3O_2$ which does not exhibit the sharp initial rise found in the others. The values of the observed and theoretical peak and C–J pressures are given for each mixture in table 6, and the corresponding wave velocities in Table 7.

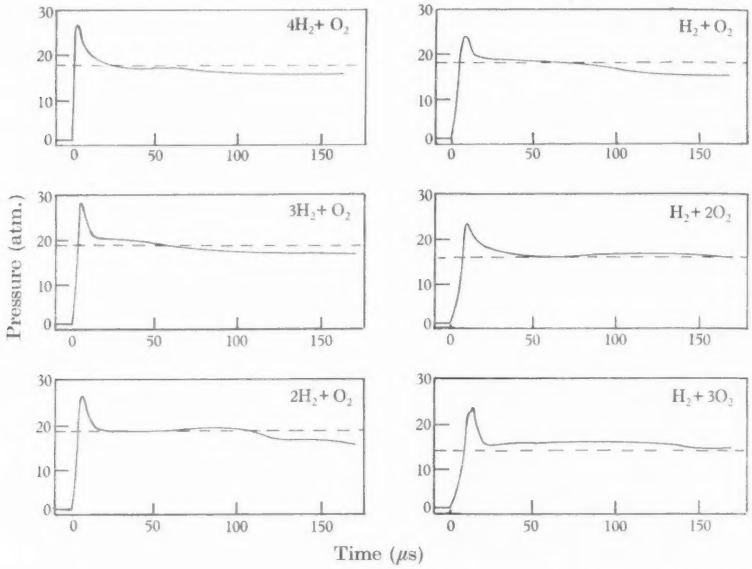

FIGURE 6. Static pressure–time curves for various mixture compositions in the 10 cm diameter tube. Broken lines represent the calculated C–J pressures.

Mixture	Peak pressure (obs.) (atm.)	Peak pressure (theor.) (atm.)	Average pressure 20–80 μs (obs.) (atm.)	C–J pressure (theor.) (atm.)
$4H_2+O_2$	27·3	32·69	18·0	17·78
$3H_2+O_2$	28·1	33·89	18·4	18·44
$2H_2+O_2$	27·1	34·16	18·6	18·59
H_2+O_2	26·1	32·43	18·3	17·63
H_2+2O_2	25·0	29·10	16·7	15·79
H_2+3O_2	24·9	26·06	15·1	14·14

TABLE 6. Static pressures in the 10 cm diameter tube.

The pressure-time relationship obtained when the $\frac{1}{4}$ in. gauge is set to measure the pressure due to the normal reflexion of a detonation wave in $2H_2 + O_2$ at the plate closing the end of the tube is shown in figure 7. As would be expected the initial rise-time of 3·2 μs is shorter than the corresponding times on the static records. Following the initial peak, the pressure drops rapidly and after a further interval, ranging between 11 and 19 μs, depending on the composition of the

mixture, a second very sharp peak occurs which again rapidly decays; thereafter, the pressure remains reasonably constant for the next 100 μs or so before beginning to rise slowly. Similar features are observed for the reflexion records in all the mixtures and consequently they are not reproduced; numerical values are given in table 8.

Mixture	Velocity (obs.) (m/s)	Velocity (theor.) (m/s)	Standard deviation (%)	Deviation from theory (%)
$4H_2+O_2$	3344	3425	0·7	−2·3
$3H_2+O_2$	3156	3197	0·2	−1·3
$2H_2+O_2$	2825	2853	0·5	−1·0
H_2+O_2	2320	2333	0·5	−0·6
H_2+2O_2	1909	1941	0·3	−1·6
H_2+3O_2	1691	1759	0·3	−3·8

TABLE 7. Detonation velocities in the 10 cm diameter tube

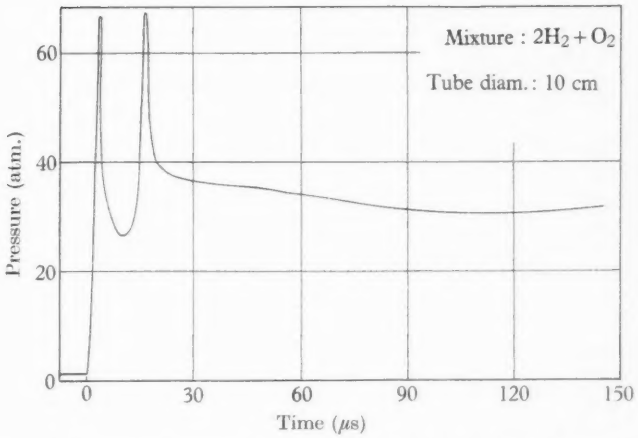

FIGURE 7. Pressure–time curves of the reflexion pressure for a detonation wave in $2H_2+O_2$ in the 10 cm diameter tube.

Mixture	Peak pressure (obs.) (atm.)	Peak pressure (theor.) (atm.)	Average pressure 20–100 μs (atm.)	C–J reflexion pressure (theor.) (atm.)
$4H_2+O_2$	59·4	226·6	37·0	42·22
$3H_2+O_2$	59·7	237·8	37·5	43·79
$2H_2+O_2$	62·5	241·7	33·8	44·18
H_2+O_2	60·6	229·9	38·0	41·82
H_2+2O_2	—	203·7	34·3	37·29
H_2+3O_2	75·4	178·5	37·9	33·31

TABLE 8. Reflexion pressures in the 10 cm diameter tube.

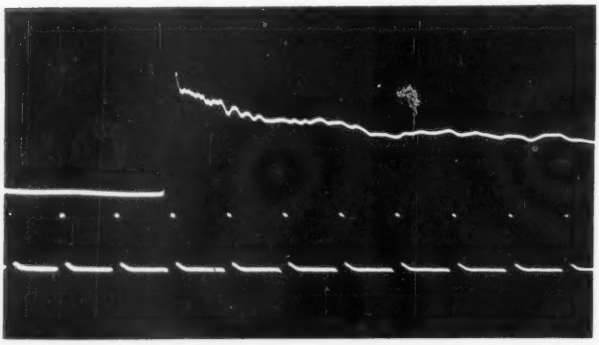

FIGURE 8. Oscillogram of static pressure in $2H_2 + O_2$ in the 1·6 cm diameter tube. Timing marks: 20 μs.

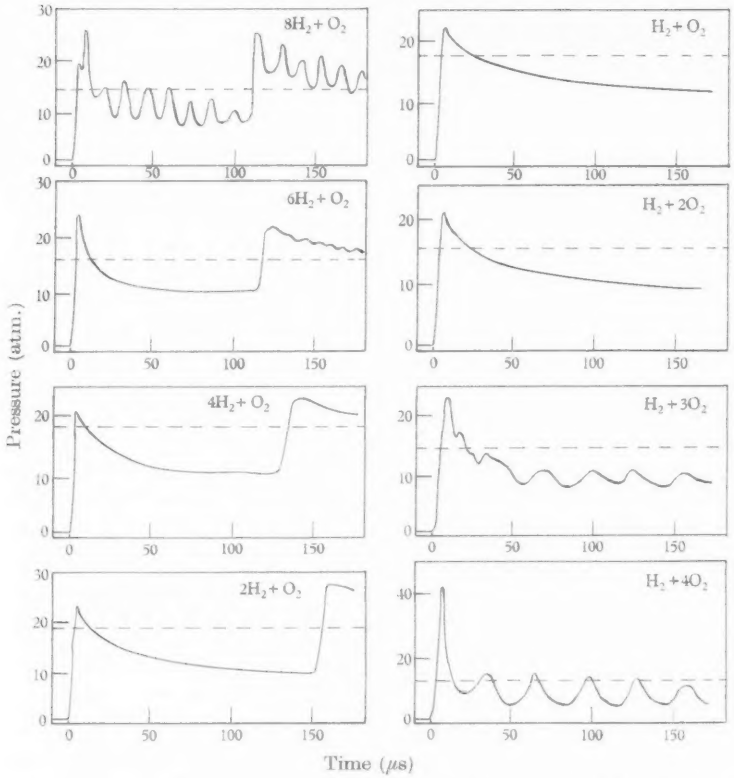

FIGURE 9. Static pressure–time curves for various mixture compositions in the 1·6 cm diameter tube. Broken lines represent the calculated C–J pressures.

4.2. *The 1·6 cm diameter explosion tube*

An oscillogram obtained in the 1·6 cm diameter tube for the detonation wave in $2H_2+O_2$ is shown in figure 8; the initiating mixture again is $C_2H_2+O_2$ at an initial pressure of 1 atm. Pressure–time curves for each of the mixtures examined in this tube are given in figure 10; on the first four of these records the shock wave reflected from the closed end of the tube has been recorded. The compositions

Mixture	Peak pressure (obs.) (atm.)	Peak pressure (theor.) (atm.)	Average pressure 20–80 μs (obs.) (atm.)	C–J pressure (theor.) (atm.)
$8H_2+O_2$	33·2	26·7	11·6	14·53
$6H_2+O_2$	24·2	29·4	12·3	15·85
$4H_2+O_2$	23·3	32·7	13·5	17·78
$2H_2+O_2$	24·3	34·2	14·6	18·59
H_2+O_2	21·7	32·4	14·4	17·63
H_2+2O_2	21·3	29·1	13·4	15·79
H_2+3O_2	23·4	26·1	11·2	14·14
H_2+4O_2	43·4	24·2	10·2	12·60

TABLE 9. Static pressure in the 1·6 cm diameter tube.

Mixture	Velocity (obs.) (m/s)	Velocity (theor.) (m/s)	Standard deviation (%)	Deviation from theory (%)
$8H_2+O_2$	3542	3802	0·5	−6·8
$6H_2+O_2$	3550	3750	0·4	−5·3
$4H_2+O_2$	3268	3425	0·3	−4·6
$2H_2+O_2$	2769	2853	1·0	−3·0
H_2+O_2	2315	2333	0·2	−0·8
H_2+2O_2	1901	1941	0·2	−2·1
H_2+3O_2	1683	1759	0·2	−4·3
H_2+4O_2	1522	1680	0·2	−9·4

TABLE 10. Detonation velocities in the 1·6 cm diameter tube.

Mixture	Peak pressure (obs.) (atm.)	Peak pressure (theor.) (atm.)	Average pressure 20–100 μs (obs.) (atm.)	C–J reflexion pressure (theor.) (atm.)
$8H_2+O_2$	81·4	175·4	21·9	34·31
$6H_2+O_2$	67·0	201·0	22·8	38·26
$4H_2+O_2$	66·9	226·6	28·5	42·22
$2H_2+O_2$	60·5	241·7	30·9	44·18
H_2+O_2	51·5	229·9	30·4	41·83
H_2+2O_2	56·6	203·7	26·6	37·29
H_2+3O_2	104·9	178·5	28·2	33·31
H_2+4O_2	118·0	153·3	23·3	29·33

TABLE 11. Reflexion pressures in the 1·6 cm diameter tube.

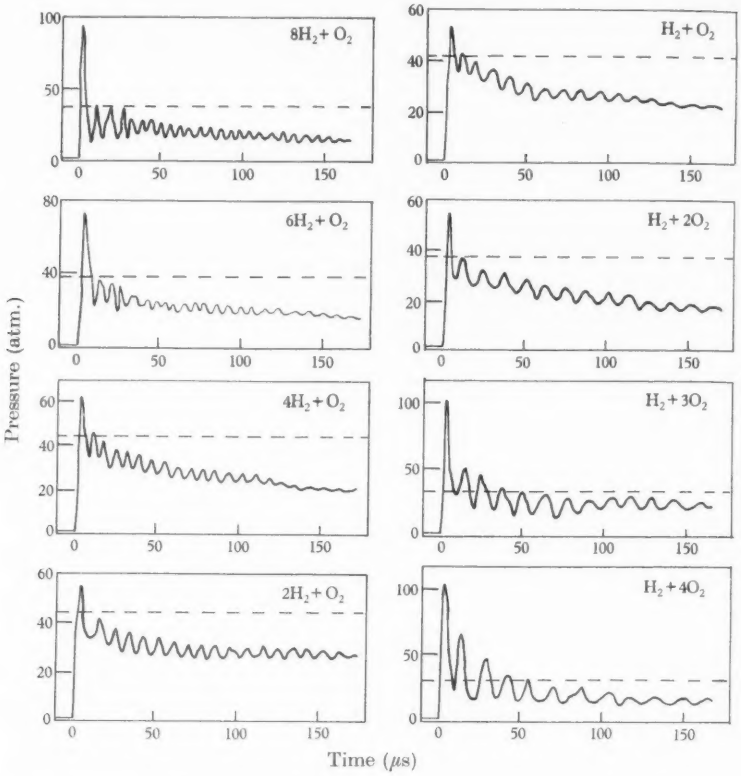

FIGURE 10. Pressure–time curves of the reflexion pressures for various mixture compositions in the 1·6 cm diameter tube. Broken lines represent the calculated reflexion pressures.

Mixture	Fundamental mode spin frequency (Kc/s)	Frequency observed on static gauge (Kc/s)	Frequency observed behind reflected shock on static gauge (Kc/s)	Frequency observed on reflexion gauge (Kc/s)
$8H_2+O_2$	80·7	76	79·9	154·9
$6H_2+O_2$	76·2	—	138·0	143·5
$4H_2+O_2$	71·7	—	—	129·8
$2H_2+O_2$	59·4	—	—	110·2
H_2+O_2	48·6	—	—	93·3
H_2+2O_2	40·7	—	—	76·5
H_2+3O_3	37·1	36·3	—	74·3
H_2+4O_2	33·6	32·9	—	66·3

TABLE 12. Frequencies of vibrations observed on the static and reflexion pressure records in 1·6 cm diameter tube.

$8H_2+O_2$, H_2+3O_2 and H_2+4O_2 show pronounced regular oscillations; the periods of these oscillations have been measured and they will be discussed later in connexion with the theory of spinning detonation. In all the records no pressure plateau occurs after the initial peak; the pressure drops relatively rapidly after the peak value and continues to do so throughout the duration of the record. However, since it is useful to compare the pressures of the detonation waves in the two tubes, the mean pressures over the interval 20–80 μs on the records are quoted in Table 9. Values of the velocities for the various mixtures are given in table 10.

Pronounced oscillations are found on all the reflexion pressure–time curves in the 1·6 cm tube which are given in figure 10. The curves show an initial sharp pressure peak followed by a slow decay in pressure, but after approximately 80 μs the pressure remains fairly constant for the remainder of the record. Observed and calculated values for the reflexion pressures are given in table 11, and the frequencies of the oscillations in both the static and reflexion records in table 12.

5. Discussion

5.1. *The 10 cm diameter tube*

The static pressures observed in this tube (table 6) are in general agreement with the theoretical C–J pressures and for some of the mixtures the agreement is well within the experimental error. Most of the observed values, however, are somewhat higher than the theoretical values; the discrepancies, which are more pronounced for mixtures containing excess oxygen, cannot be accounted for by systematic errors in measurement. Furthermore, the observed detonation velocities are all lower than the calculated values, the lack of agreement becoming more serious the further the gas composition is removed from stoichiometric. Berets *et al.* (1950), in their investigation of the velocities of detonation waves in hydrogen-oxygen in a 10 cm tube, obtained good agreement with theory in the middle composition range, lower velocities in mixtures with excess hydrogen, and higher velocities in mixtures with excess oxygen. During the course of later investigations Kistiakowsky & Zinman (1955) report that the high velocities observed in the excess oxygen mixtures were due entirely to overdriving of the mixture by the initiator. This interpretation would seem to imply that the low velocities, when excess hydrogen is present, are genuine and since in these mixtures the effects of overdrive would presumably have been present, it can only be inferred that the effect of its removal would be to yield even lower values than were originally observed. Even after allowing for the spread in the present measurements the conclusion cannot be escaped that, for the extreme composition, the velocities are significantly lower than those computed. At first it was thought that these low values could be attributed to the imperfections in the explosion tube wall; in view of the work of Kistiakowsky & Zinman on acetylene-oxygen mixtures however, this hypothesis would appear to be untenable since the 'wall-effect' is independent of the mixture composition.

Berets *et al.* (1950) attribute the differences between experimental and theoretical velocities to energy losses to the explosion tube wall. Such losses

could arise in two ways: (1) by the instantaneous cooling of a layer of gas in contact with the wall, and (2) by friction at the wall causing a reduction in mass velocity in the proximity of the wall. Both effects would give rise to a rarefaction wave which is propagated into the interior of the tube. If this occurs within the reaction zone, the resulting lowering of the temperature reduces the rate of chemical reaction thereby causing a lowering of the detonation velocity. At the same time, this hypothesis necessarily implies a lowering of the pressure which is contrary to the experimental evidence. Thus although cooling and frictional effects are almost certainly present, they are alone insufficient to explain the observed deviations of pressure, so that some further mechanism must be present which maintains the pressure at a higher value. On close examination of the pressure profiles of figure 6, it is seen that the further the mixture composition is removed from the stoichiometric, the longer the pressure takes to decay from its peak to the C–J equilibrium value. Even though the gauge is incapable of reproducing faithfully the pressure variations which occur in times of a few microseconds, a comparison of the width of the peak in various mixtures provides a relative measure of the duration of the reaction zone. It appears reasonable to assume that although the greater part of the chemical reaction is completed within the first few microseconds, complete equilibrium is not attained in some mixtures until $\sim 80\ \mu$s after the onset of the detonation wave. This effect is more marked in mixtures away from stoichiometric composition where the rate of chemical reaction is much lower owing to the lower temperature. Thus mixtures away from stoichiometric may not be able to support an ideal C–J wave at all; the detonation waves in these mixtures corresponding to the subideal waves of Brinkley & Richardson (1953). These waves have been shown to propagate with velocities which are less than the ideal C–J values and since the rate of chemical reaction is low the pressure in the wave will not decay as quickly as in the ideal wave. From the present pressure and velocity measurements it may be concluded that the hydrodynamic theory gives a correct description of the detonation wave in hydrogen-oxygen mixtures having a hydrogen content in the range of approximately 50–75 %. The agreement between experiment and theory, however, does not imply that the assumption of chemical equilibrium at the C–J plane has been rigorously established.

The first peak on the reflexion pressure records corresponds to the reflexion of the von Neumann peak of the incident wave; the magnitude of the peak pressures recorded bears no resemblance to the calculated values due to the inadequacy of the gauge response. The interesting feature of these records is the second sharp peak, which occurs in all the mixtures studied in this tube, and which appears to present strong evidence for the second reflected shock front predicted by the construction shown in figure 1 for the normal reflexion of a detonation wave. It is certain that the second peak is not attributable to a property of the gauge, and the time interval between its occurrence and the first peak shows a corresponding variation with the acoustic velocity of the burnt gases of the mixtures. Further elucidation of the reflexion process, however, must await a photographic investigation of waves in this tube. Moreover, the values of the properties calculated on the assumption stated in

§ 2.2(*b*) are essentially the values obtaining at a plane a distance of the order of the width of the reaction zone in front of the reflecting wall; consequently there is no strict basis for comparison between the calculated pressures and the pressures measured at the wall. It is to be expected, however, that they would be of the same order of magnitude as the comparison, given in table 8, between the calculated and observed average pressures in the interval 20–100 μs shows.

5.2. *The 1·6 cm diameter tube*

The main features of the static pressure records obtained in this tube are the relatively rapid decay of the pressure following the initial peak and the pronounced oscillations occurring in the mixtures $H_2 + 3O_2$, $H_2 + 4O_2$ and $8H_2 + O_2$. Furthermore, the measured velocities are all less than the ideal values, the deviations being greater for extreme compositions. To account for these low velocities and the observed pressure profiles it must be assumed that all the waves in the 1·6 cm tube are subideal. It has been noted above that the effect of the rarefaction wave, which originates at the wall of the tube due to cooling of the gas, is to lower the pressure and the rate of chemical reaction which in turn tends to maintain the pressure at a higher value. Whereas it was concluded that in the 10 cm tube the latter effect is dominant, in the small diameter tube it is reasonable to expect the lowering of the pressure due to cooling of the burnt gas to have the greater effect on the pressure profile of the wave. Consequently, the low values of pressure found in the 1·6 cm tube are probably due to the encroachment of the rarefaction wave into the reaction zone. If this were so, a large part of the energy released by the chemical reaction is lost to the walls of the tube since the reaction zone is spread out down the tube; this would lead to wave velocities less than the theoretical values, which is borne out by experiment.

The large amplitude oscillations occurring on the records of three of the mixtures are attributed to spinning of the wave. Measured values of the spin frequencies are compared in table 12 with values derived from the theories of Manson (1947) and Fay (1952), in which the frequency ν of the fundamental mode of transverse vibration is related to the acoustic velocity in the burnt gas c_1 and the tube radius r_0 by $\nu = c_1\, 1{\cdot}841/2\pi r_0$. The agreement between the observed and calculated frequencies leaves no doubt as to the nature of these vibrations; the observed values are, however, slightly lower due to the value of c_1 being lower than the ideal value assumed. It is seen that these vibrations persist behind the reflected shock wave in $8H_2 + O_2$ (figure 9), but their frequency has increased slightly compared with the detonation wave. A similar effect has been observed by Knight & Duff (1952), by means of light emission photographs, where the frequency of the transverse vibrations increased as the burnt gas flowed through the reflected shock front. This fact may be accounted for by the higher temperature behind the reflected wave giving a higher sound velocity.

The reflexion pressure records for all the mixtures examined in this tube exhibit very regular non-sinusoidal pressure undulations whose recurrence frequency given in table 12 are approximately twice the measured spin frequencies on the static pressure records. However, no evidence of a second mode spin frequency is found on any of the static pressure records of the detonation

wave. In the record obtained with $6H_2 + O_2$ (figure 10), where the reflected shock wave has also been recorded by the static pressure gauge, the higher frequency oscillations are present although their amplitude is small. Schlieren streak photographs taken in this Laboratory of the reflexion of spinning waves at a rigid wall reveal that the pressure undulations recorded on the end pressure gauge are caused by the reflexion of longitudinal compression waves behind the detonation front. The recurrence frequency of the pressure crests of the longitudinal mode of vibration measured from these photographs agrees very well with the results obtained from the pressure records. The pressures set up by this mode of vibration are very small, but after reflexion they are sufficiently great to be detected not only on the end gauge but also on the side gauge. These vibrations probably correspond to the passage of pressure pulses upstream due to the chemical reaction proceeding in the rarefaction wave; this mechanism is essentially the same as that proposed by Brinkley & Richardson (1953) to explain the build up of an ideal C–J wave.

6. Conclusions

The low velocities observed in mixtures near the limits of detonation and with decreasing tube diameter are in general agreement with the results of previous investigators. Decreasing the tube diameter also decreases the wave pressures; the pressure profile is found to be much more dependent on tube diameter than velocity. The hypothesis that energy is abstracted from the wave through the formation of a rarefaction wave at the wall of the tube is capable not only of explaining the low velocities observed but also the slightly high pressures in the 10 cm tube and the rapid decay of the pressure in the 1·6 cm tube. From a consideration of the pressure and velocity data in the 10 cm tube together it is concluded that mixtures with hydrogen content in approximately the range 50–75 % are able to support ideal waves; waves in mixtures outside these limits are subideal in the sense the term is defined by Brinkley & Richardson (1953). All the detonation waves examined in the 1·6 cm diameter tube are subideal and energy losses to the wall are sufficiently great to cause certain mixtures near the detonation limits to spin; these same mixtures showed no evidence of spin in the 10 cm tube. Further support for the subideal nature of the waves in the 1·6 cm tube is deduced from the vibrations, whose frequency is about twice the fundamental mode spin frequency, recorded on the reflexion gauge in all mixtures; these are attributed to the reflexion of pressure pulses which are delivered upstream by the chemical reaction taking place in the rarefaction wave.

The authors are greatly indebted to Dr J. W. Maccoll, head of the Applied Mathematics Division, M.O.S. Arm. Res. Dev. Estab., Fort Halstead, for his interest in the numerical work and the use of the digital computer, to Mr H. J. Gawlik and Mr F. J. Berry for their assistance during the programming of the problem, and to Mr C. K. Thornhill for his valuable suggestions.

REFERENCES

Berets, D. J., Greene, E. F. & Kistiakowsky, G. B. 1950 *J. Amer. Chem. Soc.* **72**, 1080.

Berthelot, M. & Vieille, P. 1882 *C.R. Acad. Sci., Paris*, **94**, 101, 149, 822; **95**, 151, 199.

Brinkley, S. R. Jr. & Richardson, J. M. 1953 *Fourth Symposium on Combustion*, p. 450. Baltimore: Williams and Wilkins.

Campbell, C., Littler, W. B. & Whitworth, C. 1932 *Proc. Roy. Soc.* A, **137**, 380.

Davies, R. M. 1948 *Phil. Trans.* A, **240**, 375.

Davies, R. M., Edwards, D. H. & Thomas, D. E. 1950 *Proc. Roy. Soc.* A, **204**, 17.

Dixon, H. B. & Cain, R. S. 1894 *Mem. Manchester Lit. Phil. Soc.* p. 174.

Edwards, D. H. 1958 *J. Sci. Instrum.* **35**, 346.

Fay, J. A. 1952 *J. Chem. Phys.* **20**, 942.

Gordon, W. E. 1949 *Third Symposium on Combustion Flame and Explosion Phenomena*, p. 579. Baltimore: Williams and Wilkins.

Henderson, J. 1941 *Proc. Pacific Coast Gas Ass.* p. 32.

Huff, V. N., Gordon, S. & Morrell, V. E. 1951 *N.A.C.A. Rep.* no. 1037. Washington: National Advisory Committee for Aeronautics.

Kirkwood, J. G. & Wood, W. W. 1954 *J. Chem. Phys.* **22**, 1915.

Kistiakowsky, G. B., Knight, H. T. & Malin, M. E. 1952 *J. Chem. Phys.* **20**, 884.

Kistiakowsky, G. B. & Kydd, P. H. 1955 *J. Chem. Phys.* **23**, 271.

Kistiakowsky, G. B. & Kydd, P. H. 1956 *J. Chem. Phys.* **25**, 824.

Kistiakowsky, G. B. & Zinman, W. G. 1955 *J. Chem. Phys.* **23**, 1889.

Knight, H. T. & Duff, R. E. 1952 *J. Chem. Phys.* **20**, 1493.

Knight, H. T. & Duff, R. E. 1955 *Rev. Sci. Instrum.*, **263**, 257.

Mallard, E. & Le Chatelier, H. L. 1900 *C.R. Acad. Sci., Paris*, **130**, 1755; **131**, 30.

Manson, N. 1947 *Propagation des Détonations et des Déflagrations dans les Melanges Gazeux*. Paris: L'Office National d'Etudes et de Recherches Aeronautique et de l'Institut Français des Pétroles.

National Bureau of Standards 1949 *Selected Values of the Properties of Hydrocarbons and Related Compounds*. American Petroleum Institute.

Rimarski, S. & Konschak, L. 1934 *Autogene Metallbearb.* **27**, 209.

Schmidt, A. 1941 *Z. phys. Chem.* A, **189**, 88.

On the stability of a shear layer

By J. MENKES
California Institute of Technology, Jet Propulsion Laboratory

(Received 25 February 1959)

The effects of density variation in the absence of gravity on the stability of a horizontal shear layer between two streams of uniform velocities is investigated. The density is assumed to decrease exponentially with height and the velocity is represented by $U(y) = \tanh y$.

The method of small disturbances is employed to obtain the neutral stability curve. It is demonstrated that disturbances with wave-numbers larger than the width of the transition layer are attenuated.

Qualitative agreement with experimental evidence is obtained.

1. Introduction

The mixing zone between two parallel streams, each of which has initially uniform velocity and density, may be represented for the purpose of stability analysis by an inviscid shear layer. The general problem of stability of an inviscid fluid with continuously varying velocity and density distribution in a direction normal to the mean flow was first attacked by Taylor (1931) and Goldstein (1931). Employing the method of small disturbances, they obtained an equation of the Orr–Sommerfeld type. While the equation is linear, its coefficients depend on the velocity and density distribution in the unperturbed shear layer. In order to render the problem mathematically tractable, they considered simple flows in which the velocity or velocity gradient is constant, and the density is constant or varies exponentially. The properties of the more general layer were to be deduced from a superposition of the simple flows. Drazin (1958) observed that a velocity distribution that varies as the hyperbolic tangent of the transverse co-ordinate can be handled analytically; such a profile does represent the transition of velocity rather well. Blackshear (1957) recognized the connexion between the stability of a flame downstream of a bluff body flame stabilizer and the investigations of Taylor and Goldstein. Another interesting application of the theory is concerned with the stability of a liquid film on the ablating body of a vehicle re-entering the atmosphere. Here we investigate the stability of a free, heterogeneous shear layer, neglecting the influence of gravity.

2. Derivation of the stability equation

The equations of motion governing the behaviour of an inviscid fluid under the action of gravity (which is included initially to make the comparison with the work of Taylor, Goldstein and Drazin more convenient) are Euler's equation

$$\frac{\mathbf{D}\mathbf{u}}{Dt} = -\frac{\nabla p}{\rho} - g\nabla y, \tag{1}$$

the condition of incompressibility $$\frac{D\rho}{Dt} = 0, \tag{2}$$

and the equation of continuity $$\nabla . \mathbf{u} = 0. \tag{3}$$

The velocity components, the pressure and the density are assumed to consist of a time-independent part and a perturbation, i.e.

$$u = V[U(y) + \psi'_y(x, y, t)], \quad v = -V\psi'_x(x, y, t), \tag{4a}$$

$$p = P(y) + p'(x, y, t), \quad \rho = \rho_0[\bar{\rho}(y) + \rho'(x, y, t)], \tag{4b}$$

$$\psi' = \psi(y) \exp[ik(x - ct)], \quad c = c_r + ic_i. \tag{4c}$$

Here, $V = U(\infty) = -U(-\infty)$, and ψ' is a perturbation stream function. $U(y)$, $P(y)$ and $\bar{\rho}(y)$ describe the ambient state whose stability is to be investigated. $x = x_1/d$, $y = y_1/d$, where x_1, y_1 are the physical co-ordinates and d is so chosen that $dU/dy = 1$ at $y = 0$; thus d characterizes the width of the transition layer. Denoting the Froude number V^2/gd by F and eliminating ρ' and p' from equations (1), (2) and (3) we obtain

$$(U - c)(\psi'' - k^2\psi) - U''\psi + (\ln \bar{\rho})'[(U - c)\psi' - (U - c)'\psi] - \frac{(\ln \bar{\rho})'\psi}{F(U - c)} = 0, \tag{5}$$

where primes denote differentiation with respect to y. We now set $\bar{\rho} = \exp(-2Ly)$ and obtain:

$$(U - c)(\psi'' - k^2\psi) - U''\psi - 2L[(U - c)\psi' - (U - c)'\psi] + \frac{2L}{F}\frac{\psi}{U - c} = 0. \tag{6}$$

It is well known that $J = 2L/F$ (the Richardson number) measures the ratio of the buoyancy forces to the inertia forces. In meteorological applications, where the characteristic length associated with the phenomena is usually large, buoyancy forces are very important. In the kind of small-scale aerodynamic application that is under consideration here, the effect of gravity is usually negligible. The parameter L measures the degree of heterogeneity of inertia of the fluid. The density gradient through a flame is very sharp, and it is expected that this will have a considerable effect on the stability of the flow system. It is thus proposed to neglect the term in the equation that is multiplied by the Richardson number and keep the one that has L as its coefficient. The present investigation consequently endeavours to deal with the limiting case $J = 0$, and $L \neq 0$.

3. Analysis

Drazin (1958) recognized that a velocity distribution of the form $U = \tanh y$ can be studied analytically if the independent variable y is changed to $U(y)$. With the aid of this transformation (which is essentially a hodograph transformation), the stability equation is cast into a special form of the Lamé equation. By a transformation of the dependent variable suggested by the method of Papperitz as applied to the hypergeometric equation (e.g. see Morse & Feshbach 1953, p. 539), equation (6) is cast into a form which under certain circumstances permits

one to obtain a trivial integral, namely, a constant. Only the degenerate case $c = 0$ is treated by Drazin.

As the primary velocity distribution we take $U(y) = \tanh y$, and we introduce U as the independent variable. Noting that

$$dU/dy = \operatorname{sech}^2 y = 1 - U^2, \quad d^2U/dy^2 = -2U(1-U^2),$$

denoting now by primes differentiation with respect to U, and setting

$$\psi(y) = \phi(U),$$

one obtains: $$\phi'' - 2\frac{(L+U)}{1-U^2}\phi' + \left[\frac{2(U+L)}{(U-c)(1-U^2)} - \frac{k^2}{(1-U^2)^2}\right]\phi = 0 \tag{7}$$

with the boundary conditions $k\phi(U) = 0$ at $U = \pm 1$.

It is instructive at this point to set $L = c = 0$, thereby obtaining

$$(1-U^2)\phi'' - 2U\phi' + \left[2 - \frac{k^2}{1-U^2}\right]\phi = 0. \tag{8}$$

The solution of equation (8), consistent with our boundary conditions, is the Legendre function $P_1^k(U)$, where

$$P_1^0 \equiv P_1 = U \quad \text{and} \quad P_1^1 = (1-U^2)^{\frac{1}{2}}.$$

These are the *only* two solutions, since $k \leqslant 1$ when $L = 0$.

Equation (7) is of a rather simple type. Its singularities which are located at ± 1 and c are regular singularities. It can be demonstrated that the point at infinity is also a regular singularity. The substitution into equation (7) of

$$Z = (U-1)^{-\alpha_1}(U-c)^{-\alpha_2}(U+1)^{-\alpha_3}\phi,$$

where the α's are each one of the exponents relative to the singularity and are given by

$$\alpha_1 = \frac{L}{2}(\lambda - 1), \quad \alpha_2 = 0, \quad \alpha_3 = \frac{L}{2}(\lambda + 1); \quad \lambda = +\sqrt{\left(1 + \frac{k^2}{L^2}\right)},$$

leads to the equation

$$Z'' + \left(\frac{1+\lambda L}{U-1} + \frac{1+\lambda L}{U+1}\right)Z' + \frac{1}{(U+1)(U-1)(U-c)} \times [(L^2\lambda^2 + L\lambda - 2)U - (L^2\lambda^2 c + L\lambda c + 2L)]Z = 0,$$

with the boundary conditions that Z be *regular* at $U = c$ and ± 1.

The most general solution of equation (9) can be written in the symbolic form of the Riemann P-function:

$$Z = P\begin{bmatrix} +1 & c & -1 & \infty & \\ 0 & 0 & 0 & \sigma & U \\ a_1 & a_2 & a_3 & \tau & \end{bmatrix}.$$

The fact that one each of the exponents relative to the singularities at $+1$, -1, and c vanishes implies that *one* of the solutions is regular there. For the case in which

$$L^2\lambda^2 + L\lambda - 2 = 0$$

and

$$(L^2\lambda^2 c + L\lambda c + 2L) = 0 \quad (L \neq 0),$$

one of the exponents at infinity vanishes as well, thereby assuring a solution that is regular everywhere. The only such function is, of course, a constant. A sufficient condition for the existence of the solution, $Z = \text{const.}$, is

$$L\lambda = 1 \text{ or } -2 \quad \text{and} \quad c = -L.$$

The negative root for $L\lambda$ must be discarded because the exponent at $U = -1$ must be positive in order to satisfy the boundary conditions there. The fact that c is negative means that the waves propagate in phase with the heavier and lower ($y < 0$) fluid rather than in the upper and lighter layers. The neutral stability boundary is thus given by $L\lambda = 1$, i.e. by

$$L^2 + k^2 = 1.$$

4. Results and discussion

The form of the neutral stability curve warrants a few words of explanation. The circle $L^2 + k^2 = 1$ corresponds to the *upper* branch of the stability boundary; the origin represents the degenerate *lower* branch of the stability boundary. The two 'branches' do actually join up in the complex domain. Thus the area contained between the two 'branches' represents unstable disturbances.

Disturbances having a wavelength less than the characteristic length d are stable. The effect of the density gradient is stabilizing. The latter conclusion is in qualitative agreement with the known fact that a cooled wall has a stabilizing effect on a boundary layer. A simple illustration of the effect of the density gradient may be had by the following considerations. Let us consider the case of self-excited disturbances. This corresponds to $c_i \neq 0$ and consequently $U - c$ does not vanish in the real domain. Neglect the Froude number in (7) and multiply it by the complex conjugate $\tilde{\psi}$ of ψ. If one now subtracts from the resultant equation *its* complex conjugate one obtains (the method is essentially the same as Lin's (1955)):

$$\frac{d}{dy}[\psi'\tilde{\psi} - \tilde{\psi}'\psi] = \frac{c - \tilde{c}}{|U-c|^2}(U'' + U'\bar{\rho}'/\bar{\rho})\,|\psi|^2,$$

or

$$\frac{d}{dy}[\psi'\tilde{\psi} - \tilde{\psi}'\psi] = \frac{2ic_i\,|\psi|^2}{\bar{\rho}|U-c|^2}\frac{d}{dy}[\bar{\rho}U'].$$

When both sides are integrated from $-\infty$ to $+\infty$ the left-hand side vanishes on account of the boundary conditions and we are left with the following generalization of Rayleigh's criterion:

$$2ic_i \int_{-\infty}^{+\infty} \frac{|\psi|^2}{\bar{\rho}\,|U-c|^2}[\bar{\rho}U']'\,dy = 0.$$

This integral illustrates what we have set out to show, namely, that for an inhomogeneous fluid the fact that U'' vanishes somewhere is *not* the proper criterion for the existence of amplified disturbances. The integral also shows that the quantity $d(\rho dU/dy)/dy$ which was shown by Lees & Lin (1946) to dominate the behaviour of the inertial forces in the compressible (i.e. non-homogeneous) boundary layer arises naturally in the present criterion. There is, however, an essential difference between the free shear layer and a boundary layer-type shear flow. The free shear

layer is unstable for a band of disturbances even in the inviscid case (corresponding to infinite Reynolds number), whereas the 'inviscid' boundary layer is absolutely stable.

The fact that only disturbances within a certain band of wavelengths are amplified has been demonstrated experimentally by Blackshear. While it must be borne in mind that his experimental configuration is not the best approximation to the mathematical model investigated here, it is of interest to note that he found that disturbances with a non-dimensional wave-number of order unity or larger are stable. The effect of the density gradient is also qualitatively confirmed by his experiment.

This paper presents the results of one phase of research carried out at the Jet Propulsion Laboratory, California Institute of Technology, under Contract No. DA-04-495-Ord 18, sponsored by the Department of the Army, Ordnance Corps.

REFERENCES

Blackshear, P. 1957 *NACA TN* 3830.

Drazin, P. G. 1958 *J. Fluid Mech.* **4**, 214.

Goldstein, S. 1931 *Proc. Roy. Soc.* A, **132**, 524.

Lees, L. & Lin, C. C. 1946 *NACA TN* 1115.

Lin, C. C. 1955 *The Theory of Hydrodynamic Stability.* Cambridge University Press.

Morse, P. & Feshbach, H. 1953 *Methods of Theoretical Physics.* New York: McGraw-Hill.

Taylor, G. I. 1931 *Proc. Roy. Soc.* A, **132**, 499.

Continuum equations in the dynamics of rarefied gases

By MAX KROOK
Harvard University and Smithsonian Astrophysical Observatory

(Received 16 April 1959)

A procedure is given for translating boundary-value problems of gas dynamics from microscopic form into approximately equivalent continuum form. The continuum formulations involve state-variables that are either half-space moments, or complete moments of the molecular distribution functions. Moment equations derived from the kinetic equations are reduced to a determinate set by representing the distribution functions as sums of 'modified Maxwellian functions based on various characteristic temperatures and velocities'. The particular choice of such a representation depends on the Knudsen number and on the nature of the microscopic boundary conditions.

1. Introduction

Considerable progress has been made in the study of gaseous systems whose behaviour is governed by the Navier–Stokes equations. These equations are, however, valid only in cases where departures from local thermodynamic equilibrium are uniformly small at all positions and times. There are many systems of interest that involve considerable departures from states of local thermodynamic equilibrium. Such systems can be treated only within the framework of a more general formalism than the Navier–Stokes formalism.

Kinetic theory provides a microscopic, and therefore rather general, formulation of gas dynamics. However, very few problems of the theory can be handled completely and explicitly in microscopic form. Instead, we usually proceed by first translating a microscopically formulated problem into an 'approximately equivalent' macroscopic (i.e. continuum) form. We then attempt to solve the mathematically simpler continuum problem. From a practical standpoint, the microscopic theory is general for just the reason that it constitutes the basis for generating an unlimited number of distinct types of continuum theory. In this paper we shall discuss procedures for translating microscopically formulated boundary-value problems of gas dynamics into approximately equivalent continuum problems.

The microscopic state of a system is specified by molecular distribution functions, one for each species of molecule in the system. The microscopic equations of motion then have the form of non-linear integro-differential equations which can be solved only approximately, if at all. As indicated above, we usually begin by deriving from the kinetic equations a system of differential equations for a finite set of macroscopic variables. The macroscopic variables may be interpreted formally as state-variables that specify the state of some continuum; the

differential equations are then interpreted as the equations of motion for that continuum. Different types of continua are distinguished one from another by the number of independent state-variables, by the physical significance of those state-variables, and by the particular form of the equations of motion.

For any gaseous system the quantities of direct physical interest are various macroscopic fields such as density, flow velocity, stress, etc. These variables can be expressed as simple functions of low-order moments of the molecular velocity distributions. An approximation method may then be counted as adequate if it leads to an accurate prediction for the behaviour of the lower-order moments, even when it determines high-order moments with poor accuracy.

When the physical interaction of gas molecules with boundaries of the system has been specified, we can formulate the (microscopic) boundary conditions to be satisfied by the distribution functions. In the translation of a specific microscopic problem into an approximately equivalent continuum problem, our choice of a suitable continuum formalism will depend intimately on the nature of the microscopic boundary data, and on the values of certain dimensionless parameters (Knudsen number K, Mach number M, etc.) that characterize the system of interest. In particular, it is important that we use a continuum formalism which permits an adequate (approximate) representation of the physical boundary data in terms of the state-variables of the theory.

The methods to be presented in this paper will be formulated with specific reference to one-dimensional problems for a simple gas in the absence of external fields (the extension to more complex cases is quite straightforward in principle). The microscopic state of a system is then specified by a single distribution function $f(\mathbf{v}, x, t)$, which is a function of the velocity variables $\mathbf{v} \equiv (v_1, v_2, v_3)$, of a position co-ordinate x, and of the time t.

The number density $n(x,t)$, the flow velocity $\mathbf{q}(x,t)$, and the kinetic temperature $T(x,t)$ are defined by the usual relations (see Chapman & Cowling 1939)

$$\left.\begin{aligned} n = \int f\,d\mathbf{v}, \quad n\mathbf{q} = \int \mathbf{v} f\,d\mathbf{v}, \\ \frac{3nkT}{m} = \int (\mathbf{v}-\mathbf{q})^2 f\,d\mathbf{v}, \end{aligned}\right\} \tag{1.1}$$

where m is the molecular mass, k is Boltzmann's constant, and the integrations extend over the whole velocity space. It is convenient to introduce also a stress tensor $p_{i,j}(x,t)$ and a heat flux vector $\mathbf{h}(x,t)$ defined by

$$p_{i,j} = \int m(v_i - q_i)(v_j - q_j) f\,d\mathbf{v} \quad (i,j = 1,2,3), \tag{1.2}$$

$$\mathbf{h} = \int \tfrac{1}{2} m(\mathbf{v}-\mathbf{q})^2 (\mathbf{v}-\mathbf{q}) f\,d\mathbf{v}. \tag{1.3}$$

The behaviour of the system is governed by the kinetic equation

$$\frac{\partial f}{\partial t} + v_1 \frac{\partial f}{\partial x} = \frac{\delta f}{\delta t}. \tag{1.4}$$

$\delta f/\delta t$ denotes a non-linear functional of f, whose explicit form depends on the model used to represent the molecular interactions, e.g. the Maxwell–Boltzmann

model, the Fokker–Planck model (for ionized gases), and various types of 'statistical model'. In the Maxwell–Boltzmann model, the interaction term has the form of a collision integral (see Chapman & Cowling 1939):

$$\frac{\delta f}{\delta t} = \iiint \{-f(\mathbf{v})\, f(\mathbf{w}) + f(\mathbf{v}')\, f(\mathbf{w}')\}\, gb\, db\, d\epsilon\, d\mathbf{w}, \tag{1.5}$$

where $g = |g| = |\mathbf{w} - \mathbf{v}|$, and $\mathbf{v}', \mathbf{w}'$ are the final velocities of two molecules in a binary collision with initial velocities $\mathbf{v}$, $\mathbf{w}$, with impact parameter b, and with orientation of the plane of the relative orbit specified by the angle ϵ. For conciseness, the arguments x, t of the distribution functions have not been exhibited explicitly in the integrand of equation (2.3). Statistical models will be discussed in § 12.

2. Moments as state-variables

Let us ignore, for the moment, any limitations that might be imposed by the nature of the boundary data. Multiplying the kinetic equation (1.1) in turn by 1, $\mathbf{v}$ and $\frac{1}{2}m\mathbf{v}^2$, and integrating over velocity space, we can derive five continuum equations* in which $\rho = nm$, $\mathbf{q}$ and T appear as independent state-variables (see Chapman & Cowling 1939) thus:

$$\left.\begin{aligned} \frac{\partial \rho}{\partial t} + q_1 \frac{\partial \rho}{\partial x} + \rho \frac{\partial q_1}{\partial x} &= 0, \\ \rho \frac{\partial q_i}{\partial t} + \rho q_1 \frac{\partial q_i}{\partial x} + \frac{\partial p_{1,i}}{\partial x} &= 0, \\ \frac{\partial T}{\partial t} + q_1 \frac{\partial T}{\partial x} + \frac{2}{3nk}\left[p_{1,j} \frac{\partial q_j}{\partial x} + \frac{\partial h_1}{\partial x}\right] &= 0. \end{aligned}\right\} \tag{2.1}$$

These equations are *formally* independent of the microscopic state of the gas, and of the special law of force between molecules. This is a consequence of the conservation of mass, momentum, and energy in molecular collisions. The conservation laws guarantee the elimination of all collision terms from the equations; in fact, the set of equations (2.1) makes maximum use of the simplifying consequences of the conservation theorems.

The equations (2.1) do not, however, constitute a determinate set. In addition to the basic state-variables ρ, $\mathbf{q}$ and T, they also involve the stress tensor $p_{i,j}$ and the heat flux vector $\mathbf{h}$. To make up a determinate set of continuum equations from the equations (2.1), we may proceed in either of two main ways.

On the one hand, we may elect to regard the quantities $p_{i,j}$ and $\mathbf{h}$ as *dependent* state-variables, and therefore expressible in terms of the basic state-variables ρ, $\mathbf{q}$, and T (and possibly also in terms of space gradients of ρ, $\mathbf{q}$, T). For cases in which departures from local thermodynamic equilibrium are uniformly small, the above equations can now be reduced to the Navier–Stokes equations by applying the Chapman–Enskog procedure to the kinetic equations. This derivation supplies not only the form of the Navier–Stokes equations, but also explicit formulae for the coefficients of viscosity, heat conduction, etc., as functionals of the laws of

* The same set of equations is valid also for composite systems and for molecules with internal degrees of freedom, provided $\mathbf{q}$, T, $p_{i,j}$ and $\mathbf{h}$ are defined appropriately.

force between molecules. For cases in which appreciable departures from local thermodynamic equilibrium do occur, we might try to relate the variables $p_{i,j}$ and $\mathbf{h}$ to the basic state-variables in an entirely different manner. We would thereby obtain continua specified by exactly the same basic state-variables as the 'Navier–Stokes continuum', but obeying different equations of motion; such continua have, of course, to be counted as different from the Navier–Stokes continuum.

On the other hand, we may elect to assign to the stress components $p_{i,j}$, and possibly also to some velocity moments of still higher order, the status of basic state-variables on the same footing as ρ, $\mathbf{q}$, and T. We can construct *formal* equations of motion for the new basic state-variables by multiplying through the kinetic equations with suitable functions of velocity, and then integrating over velocity space. The equations obtained in this way are again not a determinate set, and for two reasons.

In the first place, the new equations contain velocity moments which are not themselves basic state-variables, and which have therefore ultimately to be expressed as functions of the basic variables. In the second place, the equations contain non-vanishing moments of the collision integrals. These collision moments cannot be eliminated by invoking the conservation theorems, since those theorems have already been 'used up' in eliminating collision moments from equations (2.1). All the non-vanishing collision moments must ultimately also be expressed in terms of the basic state-variables.

Continuum theories of the above type are capable of representing the behaviour of gases which depart considerably from local thermodynamic equilibrium, provided only that the distribution functions at the system boundaries are not 'seriously' singular on surfaces in velocity space. This condition is usually satisfied in systems with very small Knudsen number.

In other cases, however, the distribution functions at the boundaries will generally be discontinuous on a plane in velocity space, e.g. when gas molecules that impinge on a wall are 'processed' by the wall before being returned to the gas. It is then necessary to use a continuum formalism that is adapted to the form of the microscopic boundary conditions (Krook 1955*a*, *b*). An appropriate formalism of this kind can be based on the use of half-space velocity moments as state-variables instead of complete moments.

For systems with small Knudsen number in which departures from local thermodynamic equilibrium are uniformly small, we would of course use the Navier–Stokes equations. In this paper, however, we shall be concerned primarily with problems in which the distribution functions exhibit steep gradients (or discontinuities), in the interior of the gas, or at boundaries, or both. (For cases in which linearization of the collision terms is permissible, the theory admits considerable simplification.)

3. Use of approximating forms

In any scheme for constructing a determinate set of macroscopic equations from the kinetic equation, an essential ingredient is the assignment of a specific form to the distribution function f in its dependence on certain of the independent variables $\mathbf{v}$, x, and t. This form contains arbitrary parameters that are treated as

unspecified functions of the remaining independent variables. In the Chapman–Enskog method, the arbitrary parameters appear as functions of the velocity **v**. In Grad's method (Grad 1949), and also in the method of this paper, the unspecified parameters are interpreted as functions of position and time. An approximate solution of the problem is then known when the parameters have been determined as functions of x and t. In practice, however, it is generally more convenient to select particular moments of the velocity distributions to serve as state-variables, and to construct equations of motion for those moments.

We have noted that the formal properties of the distribution function depend markedly on the values of various dimensionless parameters that characterize the system. Of special importance for our consideration is the Knudsen number $K = l/|x_2 - x_1|$, where l is some typical value of the molecular mean free path, and $x = x_1$, $x = x_2$ are the boundaries of the system. For systems with boundaries at infinity (and sometimes also for systems with x_1 and x_2 finite), K has to be replaced (or supplemented) by a 'local Knudsen number' which is a measure of the steepness of local gradients in the gas. The most general type of approximating functions contemplated in this paper may reasonably be expected to provide representations that are, in a sense, uniformly valid over the whole range of Knudsen number, or of local Knudsen number.

In an approximation of order N, the distribution function is approximated by a function that involves N arbitrary parameters. The corresponding continuum equations are then a set of N differential equations for N state-variables (i.e. moments). The derivation of the continuum equations is of course only an intermediate step in the solution of any problem. These equations have still to be solved subject to appropriate initial and boundary conditions. The solution will be feasible only when the order of approximation N is not too large. It is therefore desirable that the approximating forms be chosen so as to yield optimum accuracy for given order N.

In this paper, the approximating functions will have the form of sums of 'modified Maxwellian functions based on various characteristic velocities and temperatures'. As we shall see, such representations can be motivated on physical grounds, and have the advantage that all (or most) of the mathematical manipulations involved in the construction of continuum equations can often be carried out analytically.

4. Auxiliary functions

The kinetic equation (1.4) has to be solved subject to conditions imposed at the boundaries of the system at $x = x_1$ and $x = x_2$ ($x_1 < x_2$). In general, the physical interaction of gas molecules with a solid wall introduces a fundamental distinction between the velocity distributions of incoming and outgoing molecules at the wall. In fact, the distribution function is then singular on the plane $v_1 = 0$ in velocity space.

It is advantageous to recognize the singularity explicitly in the mathematical formalism by using different approximating forms for f in the two regions $v_1 > 0$ and $v_1 < 0$ of **v**-space. To this end we introduce two auxiliary functions $f_+(\mathbf{v}, x, t)$ and $f_-(\mathbf{v}, x, t)$ defined only in the half-spaces $v_1 > 0$ and $v_1 < 0$ respectively (see

Krook 1955*a*, *b*; Gross, Jackson & Ziering 1957). Within their respective domains of definition, the values of f_+ and f_- are specified by the relation

$$f(\mathbf{v}, x, t) = \begin{cases} f_+(\mathbf{v}, x, t) & (v_1 > 0), \\ f_-(\mathbf{v}, x, t) & (v_1 < 0). \end{cases} \tag{4.1}$$

Depending on the type of physical interaction at the walls, the mathematical boundary conditions may take the form of a specification of $f_+(\mathbf{v}, x_1, t)$ and $f_-(\mathbf{v}, x_2, t)$, or a specification of relations between f_+ and f_- at $x = x_1$ and $x = x_2$, or etc.

It is sometimes convenient, especially when the velocity distribution exhibits special symmetry, to refer velocity space to co-ordinates other than rectangular Cartesian. Thus, for the case of axial symmetry, we may use polar co-ordinates (v, θ, ϕ), and write $f = f(v, \mu, x, t)$ where $\mu \equiv \cos\theta$. The function $f_+(v, \mu, x, t)$ is defined only for $0 < \mu \leqslant 1$ and $f_-(v, \mu, x, t)$ is defined only for $-1 \leqslant \mu < 0$, so that

$$f(v, \mu, x, t) = \begin{cases} f_+(v, \mu, x, t) & (\mu > 0), \\ f_-(v, \mu, x, t) & (\mu < 0). \end{cases} \tag{4.2}$$

For systems with boundaries at finite values of x_1 and x_2, we shall generally have to use different representations for f_+ and f_-. In an approximation of order $N = N_+ + N_-$, f_+ and f_- are approximated by functional forms that involve N_+ and N_- arbitrary parameters, respectively.

In certain limiting situations (e.g. Knudsen number $K \ll 1$), it is sufficient to use a single approximating form for the complete distribution f. For systems with boundaries at infinity, f is generally not singular on the plane $v_1 = 0$, and a unified representation of f_+ and f_- is again admissible though not necessarily expedient.

5. Moments

With any function of velocity $\phi(\mathbf{v})$, we associate functionals $\mathscr{M}_+[\phi]$, $\mathscr{M}_-[\phi]$ and $\mathscr{M}[\phi]$, defined as functions of x and t by the relations

$$\mathscr{M}_\pm[\phi] \equiv \int_\pm \phi f \, d\mathbf{v} \equiv \int_\pm \phi f_\pm \, d\mathbf{v}, \tag{5.1a,b}$$

$$\mathscr{M}[\phi] \equiv \int \phi f \, d\mathbf{v} = \mathscr{M}_+[\phi] + \mathscr{M}_-[\phi], \tag{5.1c}$$

where $\int_+$ and $\int_-$ denote integration over the velocity half-spaces $v_1 > 0$ and $v_1 < 0$, respectively. The functions ϕ to be considered here generally have the form of a product of powers of the velocity components, (e.g. $v_1^{m_1} v_2^{m_2} v_3^{m_3}$ or $v^p \mu^q$), and sometimes the form of a sum of such terms (e.g. $v_1^p \mathbf{v}^2 \equiv v_1^p (v_1^2 + v_2^2 + v_3^2)$). The functionals (5.1) will be termed 'moments' of the distribution function; $\mathscr{M}_\pm[\phi]$ are half-space moments, and $\mathscr{M}[\phi]$ is a complete moment. Our continuum theories will involve either half-space moments or complete moments as basic state-variables.

With the function $\phi(\mathbf{v})$ we also associate half-space interaction moments $\mathscr{P}_+[\phi]$, $\mathscr{P}_-[\phi]$, and a complete interaction moment $\mathscr{P}[\phi]$, defined as functions of x and t by the relations

$$\mathscr{P}_\pm[\phi] \equiv \int_\pm \phi \frac{\delta f}{\delta t} d\mathbf{v}, \tag{5.2a, b}$$

$$\mathscr{P}[\phi] \equiv \int \phi \frac{\delta f}{\delta t} d\mathbf{v} = \mathscr{P}_+[\phi] + \mathscr{P}_-[\phi]. \tag{5.2c}$$

From the definitions (1.1) and (5.1), it then follows that

$$n = \mathscr{M}[1] = \mathscr{M}_+[1] + \mathscr{M}_-[1], \tag{5.3}$$

$$nq_i = \mathscr{M}[v_i] = \mathscr{M}_+[v_i] + \mathscr{M}_-[v_i] \quad (i = 1, 2, 3), \tag{5.4}$$

$$n\frac{3kT}{m} = \mathscr{M}[(\mathbf{v}-\mathbf{q})^2] = \mathscr{M}_+[(\mathbf{v}-\mathbf{q})^2] + \mathscr{M}_-[(\mathbf{v}-\mathbf{q})^2]. \tag{5.5}$$

The conservation laws for particle number, momentum and energy in molecular interactions imply the relations

$$\mathscr{P}[1] = 0, \quad \mathscr{P}[v_i] = 0, \quad \mathscr{P}[\mathbf{v}^2] = 0. \tag{5.6}$$

6. Moment equations

Let $\phi_1(\mathbf{v})$, $\phi_2(\mathbf{v}), \ldots, \phi_N(\mathbf{v})$ be any particular set of N simple functions, i.e. products of powers of velocity components or sums of such products. Multiplying the kinetic equation (1.4) by $\phi_j(\mathbf{v})$ and integrating (a) over the half-space $v_1 > 0$, (b) over the half-space $v_1 < 0$, we obtain two sets of half-space moment equations:

$$\frac{\partial}{\partial t}\mathscr{M}_+[\phi_j] + \frac{\partial}{\partial x}\mathscr{M}_+[v_1\phi_j] = \mathscr{P}_+[\phi_j] \quad (j = 1, 2 \ldots N), \tag{6.1a}$$

$$\frac{\partial}{\partial t}\mathscr{M}_-[\phi_j] + \frac{\partial}{\partial x}\mathscr{M}_-[v_1\phi_j] = \mathscr{P}_-[\phi_j] \quad (j = 1, 2 \ldots N). \tag{6.1b}$$

Integration over the whole velocity space, instead of the half-spaces, yields a single set of complete-moment equations

$$\frac{\partial}{\partial t}\mathscr{M}[\phi_j] + \frac{\partial}{\partial x}\mathscr{M}[v_1\phi_j] = \mathscr{P}[\phi_j] \quad (j = 1, 2 \ldots N) \tag{6.1c}$$

Considering for the present only the $2N$ half-moment equations (6.1a, b), we next define a set of $2N$ basic (independent) *state-variables* $M_j^{(+)}(x, t)$, $M_j^{(-)}(x, t)$, $(j = 1, 2 \ldots N)$, as the half-space moments that correspond to N particular simple functions $\psi_1(\mathbf{v}), \ldots, \psi_N(\mathbf{v})$, i.e.

$$M_j^{(+)} \equiv \mathscr{M}_+[\psi_j], \quad M_j^{(-)} \equiv \mathscr{M}_-[\psi_j] \quad (j = 1, 2 \ldots N). \tag{6.2a, b}$$

Moments $\mathscr{M}_\pm[\psi]$ that are not basic state-variables will be termed 'extraneous moments'. Our aim will be to construct, from the $2N$ formal equations (6.1a, b), a determinate set of equations of motion for the $2N$ independent state-variables $M_j^{(\pm)}$.

The choice of N functions ϕ_j in the equations (6.1), and of N functions ψ_j for the definitions (6.2), is largely arbitrary. In practice, the functions ϕ_j are usually

selected to comprise simple functions of lowest degree. It is then convenient to select the N functions ψ_j in such a way that, in the formal equations (6.1a, b), as many moments as possible are basic state-variables. For time-independent problems, the identification $\psi_j = v_1 \phi_j$ ($j = 1, 2 \ldots N$), would result in the exclusive occurrence of basic state-variables on the left-hand sides of equations (6.1a, b). However, certain moments will appear naturally in our approximating formulae, through definitions of characteristic local velocities and temperatures (see § 9). It is then convenient to include those moments among the basic state-variables.

In general the formal equations will involve some extraneous moments. Furthermore (except with the simpler types of statistical model), the interaction moments $\mathscr{P}_{\pm}[\phi_j]$ have purely formal significance, and are not directly expressible in terms of moments of f. In order to reduce the basic equations (6.1a, b) to a determinate system, we have to express all extraneous moments and the $2N$ interaction moments in terms of the basic state-variables.

Similar considerations apply to the N complete-moment equations (6.1c), with basic state-variables $\mathscr{M}_j(x, t)$ defined by the relations

$$M_j \equiv \mathscr{M}[\psi_j] = M_j^{(+)} + M_j^{(-)} \quad (j = 1, 2 \ldots N). \tag{6.2c}$$

7. Reduction procedure

The $2N$ formal equations (6.1a, b) can be reduced to a determinate set by representing f_+ and f_- as specific functions of $\mathbf{v}$, involving $2N$ parameters $A_j^{(+)}$ and $A_j^{(-)}$ ($j = 1, 2 \ldots N$); the parameters are interpreted as unknown functions of x and t. The more general types of approximating function to be considered here will depend on the state-variables $M_k^{(\pm)}$ as well as on the parameters $A_k^{(\pm)}$, thus

$$f_+(\mathbf{v}, x, t) = g_+(\mathbf{v}; A_k^{(+)}, M_k^{(+)}, M_k^{(-)}), \tag{7.1a}$$

$$f_-(\mathbf{v}, x, t) = g_-(\mathbf{v}; A_k^{(-)}, M_k^{(+)}, M_k^{(-)}), \tag{7.1b}$$

where g_+ and g_- are prescribed functions of the indicated arguments.

Using the approximations (7.1), we may evaluate the moments $M_j^{(\pm)} = \mathscr{M}_{\pm}[\psi_j]$ in the form

$$M_j^{(+)} = G_j^{(+)}(A_k^{(+)}; M_k^{(+)}, M_k^{(-)}) \quad (j = 1, 2 \ldots N), \tag{7.2a}$$

$$M_j^{(-)} = G_j^{(-)}(A_k^{(-)}; M_k^{(+)}, M_k^{(-)}) \quad (j = 1, 2 \ldots N), \tag{7.2b}$$

where the $G_j^{(+)}$ and $G_j^{(-)}$ are known functions of their arguments. For the approximating functions contemplated in this paper, $G_j^{(\pm)}$ will be linear functions of the parameters $A_k^{(\pm)}$, with coefficients that may depend on the state-variables.

Solving the two sets of (linear) equations (7.2), we obtain formulae for the parameters $A_j^{(\pm)}$ as functions of the state-variables:

$$A_j^{(+)} = H_j^{(+)}(M_k^{(+)}, M_k^{(-)}), \tag{7.3a}$$

$$A_j^{(-)} = H_j^{(-)}(M_k^{(+)}, M_k^{(-)}), \tag{7.3b}$$

where the $H_j^{(\pm)}$ are again known functions of their arguments. In the important special case that the functions (7.1a, b) do not involve the state-variables explicitly, the functions $H_j^{(+)}$ and $H_j^{(-)}$ are simply linear functions of the state-variables $M_k^{(+)}$ and $M_k^{(-)}$, respectively.

Substitution of the formulae (7.3) for $A_j^{(\pm)}$ on the right-hand sides of equations (7.1) now provides representations for $f_\pm$ that contain only the state-variables, and not the parameters thus:

$$f_\pm = h_\pm(\mathbf{v};\, M_k^{(+)}, M_k^{(-)}), \tag{7.4a, b}$$

where h_+ and h_- are known functions of their arguments. Any functionals of f_+ and f_- can now be evaluated, at least in principle, as explicit functions of the $2N$ state-variables $M_k^{(\pm)}$. In particular, extraneous moments $\mathscr{M}_\pm[\psi]$, and interaction moments $\mathscr{P}_\pm[\phi_j]$, can thus be determined as functions of the state-variables. When these functions are substituted in the formal equations (6.1a, b), we obtain a determinate set of equations of motion for the state-variables.

An analogous process with complete moments M_j as state-variables, leads from the formal equations (6.1c) to a determinate set of N equations for the M_j.

The macroscopic boundary conditions satisfied by the state-variables $M_j^{(\pm)}$ are readily derived from the microscopic boundary conditions on f_+ and f_-. If, for example, the boundary values $f_+(\mathbf{v}, x_1)$ and $f_-(\mathbf{v}, x_2)$ are specified, direct integration provides the boundary values $M_j^{(+)}(x_1)$ and $M_j^{(-)}(x_2)$ for the state-variable.

The formulae for the interaction moments $\mathscr{P}_\pm[\phi_j]$ as functions of the state-variables involve coefficients that appear in the form of multiple integrals. Since the derivation of continuum equations is merely a preliminary step in the solution of a problem of gas dynamics, the usefulness of the procedure outlined above will depend crucially on the extent to which these multiple integrals can be evaluated in closed form. (The elimination of extraneous moments in closed form presents no difficulty.) This circumstance places severe restrictions on the types of approximating forms that can reasonably be used to represent the velocity distributions. Sums of modified Maxwellian functions provide satisfactory representations from this point of view, especially when used in conjunction with statistical models.

8. Modified Maxwellian functions

The normalized Maxwell distribution function corresponding to average velocity $\mathbf{Q}$ and temperature $\Theta \equiv m\alpha^2/k$ will be denoted by $\Psi(\mathbf{v};\mathbf{Q},\Theta)$ or $\Phi(\mathbf{v};\mathbf{Q},\alpha)$:

$$\begin{aligned}\Psi(\mathbf{v};\,\mathbf{Q},\Theta) &\equiv \left(\frac{m}{2\pi k\Theta}\right)^{\frac{3}{2}} \exp\left[-m(\mathbf{v}-\mathbf{Q})^2/2k\Theta\right] \\ &= \Phi(\mathbf{v};\,\mathbf{Q},\alpha) \equiv \left(\frac{1}{2\pi\alpha^2}\right)^{\frac{3}{2}} \exp\left[-(\mathbf{v}-\mathbf{Q})^2/2\alpha^2\right].\end{aligned} \tag{8.1}$$

A function $F(\mathbf{v};\mathbf{Q},\alpha)$ will be termed a 'modified Maxwellian function (MM function), based on $(\mathbf{Q},\Theta)$ or on $(\mathbf{Q},\alpha)$', when it has the form

$$F = \Psi(\mathbf{v};\,\mathbf{Q},\Theta)\,P\left(\frac{\mathbf{v}}{\alpha}\right) = \Phi(\mathbf{v};\,\mathbf{Q},\alpha)\,P\left(\frac{\mathbf{v}}{\alpha}\right), \tag{8.2}$$

where P represents a polynomial in the components of $\mathbf{v}/\alpha$, with coefficients that may be functions of x and t. The velocity $\mathbf{Q}$, and the temperature Θ or associated speed $\alpha = (k\Theta/m)^{\frac{1}{2}}$, may be prescribed constants or they may be functions of the basic state-variables. The modifying polynomial P in the formula (8.2) represents a distortion of the basic Maxwellian distribution $\Psi(\mathbf{v};\,\mathbf{Q},\Theta)$.

9. Characteristic velocities and temperatures

For any particular system, we can define a number of characteristic macroscopic velocities $\mathbf{V}_\lambda$ and associated temperatures Θ_λ ($\lambda = 1, 2 \ldots s$). Among such velocity-temperature pairs, we note in particular the following:

(*a*) Constant pairs $(\mathbf{Q}_1, T_1)$ and $(\mathbf{Q}_2, T_2)$ which generally appear in the specification of microscopic boundary conditions at $x = x_1$ and $x = x_2$, respectively.

(*b*) The pair $(\mathbf{q}, T)$ consisting of the local macroscopic velocity $\mathbf{q}(x,t)$ and kinetic temperature $T(x,t)$.

(*c*) Two pairs $(\mathbf{q}, T_+)$ and $(\mathbf{q}, T_-)$ where $T_+(x,t)$ and $T_-(x,t)$ are local kinetic temperatures associated with the half-space velocity distributions $v_1 > 0$ and $v_1 < 0$, respectively, thus

$$\frac{kT_\pm}{m} \equiv \beta_\pm^{-2} = \frac{\mathscr{M}_\pm[(\mathbf{v}-q)^2]}{3\mathscr{M}_\pm[1]}. \tag{9.1a,b}$$

(*d*) Two pairs $(\mathbf{q}_+, T'_+)$ and $(\mathbf{q}_-, T'_-)$ which provide a 'purer' characterization than (*c*) for the half-space velocity distributions. The velocities $\mathbf{q}_\pm(x,t)$ and temperatures $T'_\pm(x,t)$ are defined by the relations

$$(\mathbf{q}_\pm)_1 = q_1; \quad (\mathbf{q}_\pm)_j = \frac{\mathscr{M}_\pm[v_j]}{\mathscr{M}_\pm[1]} \quad (j = 2, 3), \tag{9.2a,b}$$

$$\frac{kT'_\pm}{m} \equiv (\beta'_\pm)^2 = \frac{\mathscr{M}_+[(\mathbf{v}-\mathbf{q}_\pm)^2]}{3\mathscr{M}_\pm[1]}. \tag{9.3a,b}$$

We note that the velocities and temperatures of (*b*), (*c*) and (*d*) are all expressible directly in terms of complete moments or half-space moments of the velocity distributions. A different type of characteristic local velocity and temperature will be introduced in § 11.

Instead of the velocity-temperature pairs $(\mathbf{V}_\lambda, \Theta_\lambda)$, it is often convenient to use the corresponding velocity-speed pairs $(\mathbf{V}_\lambda, \alpha_\lambda)$ with

$$\alpha_\lambda = (k\Theta_\lambda/m). \tag{9.4}$$

10. Approximating functions

The approximating functions that we propose to use, in conjunction with the procedure outlined in § 7, have the general form of sums of modified Maxwellian functions based on the characteristic velocity-temperature pairs $(\mathbf{V}_\lambda, \Theta_\lambda)$ or associated velocity-speed pairs $(\mathbf{V}_\lambda, \alpha_\lambda)$ ($\lambda = 1, 2 \ldots s$). We thus assign to f_+ and f_- or to f, the general approximate representations

$$f_\pm = \sum_{\lambda=1}^{s} \Phi(\mathbf{v}; \mathbf{V}_\lambda, \alpha_\lambda) P_\lambda^{(\pm)}\left(\frac{\mathbf{v}}{\alpha_\lambda}\right), \tag{10.1a,b}$$

$$f = \sum_{\lambda=1}^{s} \Phi(\mathbf{v}; \mathbf{V}_\lambda, \alpha_\lambda) P_\lambda\left(\frac{\mathbf{v}}{\alpha_\lambda}\right). \tag{10.1c}$$

The modifying polynomials $P_\lambda^{(+)}$, $P_\lambda^{(-)}$ and P_λ contain $N_\lambda^{(+)}$, $N_\lambda^{(-)}$ and N_λ terms, respectively, with coefficients that are regarded as unknown functions of x and t.

The approximation provided by the formulae (10.1 a, b) is of order $\sum_\lambda (N_\lambda^{(+)} + N_\lambda^{(-)})$, and that provided by (10.1 c) is of order $\sum_\lambda N_\lambda$.

In practice, of course, we would not generally include in the sums (10.1) components corresponding to *all* available velocity-temperature pairs $(\mathbf{V}_\lambda, \Theta_\lambda)$ $(\lambda = 1, 2 \ldots s)$. In most cases, physical considerations suggest that certain components may reasonably be omitted from the representations. Some arguments to justify the representation of distribution functions in terms of MM functions will be given in § 14.

We have already noted the desirability of using representations that permit the expression of interaction moments, in sufficiently simple form, as functions of the basic state-variables. This requirement is most stringent when the interaction term $\delta f/\delta t$ has the Maxwell–Boltzmann form (1.5). Complete interaction moments $\mathscr{P}[\phi_j]$ can generally be reduced in a straightforward manner for representations of the form (10.1 c). The reduction of the half-space moments $\mathscr{P}_\pm[\phi_j]$ with approximating forms (10.1 a, b) is much more troublesome when $\delta f/\delta t$ has the Maxwell–Boltzmann form.

The reduction of the interaction moments is simpler when the interaction terms have the Fokker–Planck form, as for ionized gases (see Rosenbluth, MacDonald & Judd, 1957). For the class of 'statistical models' discussed in § 11, the reduction of the interaction moments $\mathscr{P}[\phi_j]$, $\mathscr{P}_\pm[\phi_j]$ can usually be effected without difficulty.

The use of approximating forms (8.5 a, b, c) may be regarded as constituting a natural generalization of Mott–Smith's method of solution of the Boltzmann equation for a stationary plane shock wave in a simple gas (Mott-Smith 1951). Mott-Smith represents the distribution function f as a sum of two (unmodified) Maxwellian functions

$$f(\mathbf{v}, x) = A(x)\Psi(\mathbf{v}; Q_1\mathbf{i}, T_1) + B(x)\Psi(\mathbf{v}; Q_2\mathbf{i}, T_2), \tag{10.2}$$

where $(Q_1\mathbf{i}, T_1)$ and $(Q_2\mathbf{i}, T_2)$ are the (constant) velocity-temperature pairs that correspond to the equilibrium conditions at $x = -\infty$ and $x = +\infty$, respectively. The application of the generalized approximations for this problem will be discussed in § 15.

From another point of view, the approximating forms (10.1 a, b, c) may also be regarded as providing a generalization of Grad's method which is based on a representation of f as a single MM function based on the local velocity and temperature, i.e. on $(\mathbf{q}, T)$.

11. Collisional temperatures

The velocities $\mathbf{q}$, $\mathbf{q}_\pm$ and temperatures T, $T_\pm$, $T'_\pm$ defined in § 9, serve to characterize the local velocity distributions f and $f_\pm$. We may introduce another type of characteristic velocity $\mathbf{Q}_c(x, t)$ and temperature $T_c(x, t)$ to characterize the velocity distribution of those molecules that have suffered collisions locally.

Let $\sigma(\mathbf{v}, x, t)$ denote the local collision frequency for molecules of velocity $\mathbf{v}$. In the Maxwell–Boltzmann model (for example), we would have

$$\sigma(\mathbf{v}, x, t) = \iiint f(\mathbf{w}, x, t)\,|\mathbf{v} - \mathbf{w}|\,b\,db\,d\epsilon\,d\mathbf{w}. \tag{11.1}$$

A possible, but not unique, definition of $\mathbf{Q}_c(x,t)$ and $T_c(x,t)$ is contained in the following five equations:

$$\left.\begin{aligned} &\nu\int\phi(\mathbf{v})\,\sigma(\mathbf{v},x,t)\Psi(\mathbf{v};\mathbf{Q}_c,T_c)\,d\mathbf{v}=\int\phi\sigma f(\mathbf{v},x,t)\,d\mathbf{v},\\ &\phi=1,v_1,v_2,v_3,\mathbf{v}^2. \end{aligned}\right\} \tag{11.2}$$

(A number density $\nu(x,t)$ is also defined automatically by these equations.)

The basis for the definitions (11.2) is provided by the property that those molecules which have suffered collision at x will, after collision, have an approximately Maxwellian velocity distribution corresponding to an average velocity and a temperature determined by the total momentum and energy of the colliding molecules. Since the collision frequency σ generally depends on $\mathbf{v}$, the 'collisional velocity' $\mathbf{Q}_c(x,t)$ and 'collisional temperature' $T_c(x,t)$ will differ from the local velocity $\mathbf{q}(x,t)$ and local kinetic temperature $T(x,t)$ of the gas.

12. Interaction models

The formal complexity of the Maxwell–Boltzmann collision integrals is a consequence of the fact that they take into account the detailed geometry of all individual kinds of binary collision. In the Fokker–Planck model (for ionized gases), the collision geometry is treated statistically to a certain extent.

In the class of 'statistical' models, the velocity distribution of those molecules that have locally suffered a collision is related purely statistically to their pre-collision velocity distribution. Two characteristic features of these models are: (*a*) the formal simplicity of their interaction terms as compared to those of the Maxwell–Boltzmann and Fokker–Planck models, and (*b*) their flexibility in permitting a representation of many detailed aspects of molecular interactions. A general account of statistical models will be published elsewhere.

In one of the simpler types of statistical model, the interaction term is assumed to have the form

$$\frac{\delta f}{\delta t}=\sigma(\mathbf{v},x,t)\{-f+\nu\Psi(\mathbf{v},\mathbf{Q},\mathscr{T})\}, \tag{12.1}$$

where the collision frequency $\sigma(\mathbf{v},x,t)$ may be prescribed, or may be a functional of f as, for example, in equation (11.1). The macroscopic variables $\nu(x,t)$, $\mathbf{Q}(x,t)$ and $\mathscr{T}(x,t)$ are determined uniquely by the conditions that particle-number, momentum, and energy be conserved in molecular interactions. The defining relations for ν, $\mathbf{Q}$ and $\mathscr{T}$ are then just the five equations (11.2).

For the special case that $\sigma=n.\kappa(x,t)$ is independent of $\mathbf{v}$, the interaction term (12.1) is particularly simple. Here $\nu\equiv n$, $\mathbf{Q}\equiv\mathbf{q}$ and $\mathscr{T}\equiv T$, where $n,\mathbf{q},T$ are, respectively, the local number density, average velocity, and kinetic temperature (see Bhatnagar, Gross & Krook, 1954). We then have

$$\frac{\delta f}{\delta t}=-n\kappa f+n^2\kappa\Psi(\mathbf{v};\mathbf{q},T). \tag{12.2}$$

We note that, with the model (12.2), the interaction moments are obtained directly in terms of moments of f.

Apart from its great intrinsic simplicity, this constant collision-time model is of special formal interest for the reason that numerically exact solutions can be obtained without excessive difficulty for a number of one-dimensional boundary-value problems (Krook 1955*b*). Some insight may then be gained into the accuracy of the present and other approximation methods by comparing approximate solutions with the exact solutions for the same problem. The results of such a comparison in the case of Couette flow with boundary walls at different temperatures, and for various values of Mach numbers, Knudsen number and ratio of wall temperatures, will be reported as soon as exact solutions become available from calculations now in progress on an IBM 704 computer.

13. Integral equations

For one-dimensional, time-independent problems, the kinetic equation (1.5) can be written in the general form

$$v_1 \frac{\partial f(\mathbf{v}, x)}{\partial x} = \sigma(\mathbf{v}, x)\{-f(\mathbf{v}, x) + \mathscr{E}(\mathbf{v}, x)\}, \tag{13.1}$$

where σ and $\sigma\mathscr{E}$ are prescribed functionals of f. The function $\sigma(\mathbf{v}, x)$ may be interpreted formally as a '(collisional) absorption coefficient' for molecules of velocity $\mathbf{v}$ at x. The function $\sigma(\mathbf{v}, x)\,\mathscr{E}(\mathbf{v}, x)$ may then be interpreted as the 'rate of generation' of molecules of velocity $\mathbf{v}$, by collisions at x.

Any boundary-value problem for the equation (13.1) is readily transformable to an integral-equation problem. To this end, we define a function

$$\lambda(\mathbf{v}, x) = \int_{x_1}^{x} \sigma(\mathbf{v}, x')\, dx' \tag{13.2}$$

which will, in general, be a functional of f. Equation (13.1) may then be written in the form:

$$\frac{\partial}{\partial x}\{f \exp[\lambda(\mathbf{v}, x)]\} = \frac{1}{v_1}\sigma(\mathbf{v}, x)\,\mathscr{E}(\mathbf{v}, x) \exp[\lambda(\mathbf{v}, x)]. \tag{13.3}$$

Integrating equation (13.3) over (x_1, x) for $v_1 > 0$, and over (x, x_2) for $v_1 < 0$, we obtain the non-linear integral equations:

$$f_+(\mathbf{v}, x) = f_+(\mathbf{v}, x_1) \exp[-\lambda(\mathbf{v}, x)/v_1] + \frac{1}{v_1}\int_{x_1}^{x} \mathscr{E}(\mathbf{v}, x) \exp[-\{\lambda(\mathbf{v}, x) - \lambda(\mathbf{v}, x')\}/v_1]\, d\lambda', \tag{13.4a}$$

$$f_-(\mathbf{v}, x) = f_-(\mathbf{v}, x_2) \exp[-\{\lambda(\mathbf{v}, x_2) - \lambda(\mathbf{v}, x)\}/|v_1|] + \frac{1}{|v_1|}\int_{x}^{x_2} \mathscr{E}(\mathbf{v}, x') \exp[-\{\lambda(\mathbf{v}, x') - \lambda(\mathbf{v}, x)\}/|v_1|]\, d\lambda', \tag{13.4b}$$

where we have written $d\lambda' \equiv \sigma(\mathbf{v}, x')\, dx'$. The form of these equations is instructive when considered in connexion with the approximation procedures presented in this paper.

We note first that, for a fixed x, the emission function $\sigma(\mathbf{v}, x)\,\mathscr{E}(\mathbf{v}, x)$ is the velocity distribution (after collision) of just those molecules that have suffered collision at x. On general grounds, we may expect $\mathscr{E}(\mathbf{v}, x)$ to be approximately

Maxwellian in $\mathbf{v}$; the average velocity and the temperature appropriate to $\mathscr{E}(\mathbf{v}, x)$ are the collisional velocity $\mathbf{Q}_c(x)$ and the collisional temperature $T_c(x)$ defined in § 11. Further, the function $[\lambda(\mathbf{v}, x) - \lambda(\mathbf{v}, x')]/|v_1|$ is the number of mean free paths between planes perpendicular to $\mathbf{i}$ at x and x', for molecules of velocity $\mathbf{v}$.

Equations (13.4) show that, in general, each of $f_+(\mathbf{v}, x)$ and $f_-(\mathbf{v}, x)$ can be regarded as a superposition of two essentially different types of distribution:

A. A partially-attenuated boundary distribution represented by the first term on the right-hand side of each equation (13.4). The degree of attenuation depends on the position of x relative to the boundary, and depends on the magnitude and direction of the molecular velocity $\mathbf{v}$.

B. A more complex distribution represented by the second term on the right-hand sides of equations (13.4), and made up of weighted contributions from the collisional emission of $\mathbf{v}$-molecules at all points $x' < x$ for $f_+(\mathbf{v}, x)$, and at all points $x' > x$ for $f_-(\mathbf{v}, x)$. In this component, the emission $\sigma\mathscr{E}(\mathbf{v}, x')$ at x' is weighted by the negative exponential of the number of mean free paths of a $\mathbf{v}$-molecule between x' and x.

In subsequent sections, we will refer to these two types of partial distribution as component *A* and component *B*, respectively.

One negative conclusion can be drawn immediately from the structure of equations (13.4) and, in particular, from the structure of the terms corresponding to component *B*: any representation of $f_+(\mathbf{v}, x)$ (or of $f_-(\mathbf{v}, x)$), as a modified Maxwellian function based on a *single* velocity-temperature pair, is liable to have poor accuracy except in certain special limiting cases.

Proceeding rather heuristically, we could approximate the component *B* by a sum of *MM* functions based on the collisional velocity-temperature pairs $(\mathbf{Q}_c(x'_j), T_c(x'_j))$ at a number of points $x'_1, x'_2 \ldots$ in the interval (x_1, x_2). Such an approximation procedure would itself be rather formidable, and we would of course prefer to use *local* velocity-temperature pairs for the field point x rather than pairs for a sequence of source-points x'_j. By defining a sufficiently wide variety of characteristic local velocity-temperature pairs, and by using *MM* functions based on such local pairs, we may hope to mimic the representation provided by *MM* functions based on collisional pairs in the above way. This argument can in no way be regarded as *justifying* the approximation procedures of the previous sections; it serves only to lend some plausibility to those procedures.

In the subsequent sections of this paper, we shall discuss in a formal way two particular time-independent boundary-value problems: (*a*) a problem of non-linear heat conduction, and (*b*) the problem of shock-wave structure.

14. Non-linear heat conduction

We consider a system composed of a simple gas in a steady state between parallel plates $x = x_1$ and $x = x_2$ ($x_2 > x_1$). The plates are maintained at constant temperatures T_1 and T_2, respectively ($T_1 > T_2$). We shall suppose that molecules which strike a wall are adsorbed and are subsequently re-emitted into the gas with a Maxwellian distribution appropriate to the wall temperature.

The boundary conditions then have the form

$$f_+(\mathbf{v}, x_1) = a_1\Psi(\mathbf{v}; 0, T_1), \quad f_-(\mathbf{v}, x_2) = a_2\Psi(\mathbf{v}; 0, T_2), \qquad (14.1\,a, b)$$

where at most one of the positive constants a_1, a_2 may be specified arbitrarily. In the integral equations (13.4a, b) we have now to substitute the formulae (14.1a, b) for $f_+(\mathbf{v}, x_1)$ and $f_-(\mathbf{v}, x_2)$. (For the simplest statistical models, the exact numerical solution of these equations is then feasible (Krook 1955b).)

The system is characterized by two dimensionless ratios, the Knudsen number K and the temperature ratio of the plates, $r = T_2/T_1$. We shall suppose that r is appreciably less than unity, so that the gradients in the gas are steep, unless $K \ll 1$. The Knudsen number can be defined as the reciprocal of some average value of the function $\lambda(v, \mathbf{i}, x)/|v_1|$.

Since the velocity distribution has axial symmetry about a direction parallel to $\mathbf{i}$, we may refer velocity space to the co-ordinates (v, μ, ϕ). The distribution functions $f_\pm(v, \mu, x)$ could be represented generally by a sum of MM functions based on T_1, T_2, and on an extensive set of local characteristic velocity-temperature pairs. In the interests of mathematical tractability, we would of course economize as far as possible in the number of MM functions to be used in a representation of $f_\pm$. This would generally require the use of different kinds of approximation in different ranges of Knudsen number.

To discuss the formal dependence of the velocity distribution on the value of the Knudsen number, we subdivide the range $(0, \infty)$ of K roughly into five subintervals:

(I) $K \ll 1$;

(II) K an order of magnitude less than unity, say $K \sim 0{\cdot}2$;

(III) $K \sim 1$;

(IV) K an order of magnitude greater than unity, say $K \sim 5$;

(V) $K \gg 1$.

Only in ranges I and V can we make a reasonably unambiguous choice of approximate representations for $f_\pm$. We shall discuss the five ranges of K separately, and shall indicate possible, but by no means unique, approximations for each range.

Range I. ($K \ll 1$)

The distance $x_2 - x_1$ comprises many mean free paths. Equations (13.4) then show that the wall distributions (14.1) are completely attenuated in comparatively thin layers in the immediate vicinity of the respective plates. Further, the component B for the point x is made up of (attenuated) collisional emissions at points x' for which $\mathscr{E}(\mathbf{v}, x')$ differs only slightly from $\mathscr{E}(\mathbf{v}, x)$. The local velocity distribution at x thus differs only slightly from a Maxwellian velocity distribution for a single velocity and temperature, which may therefore be taken to be the local velocity $\mathbf{q}(x)$, and the local kinetic temperature $T(x)$. Moreover, the velocity distribution $f(\mathbf{v}, x)$ at a boundary has only a slight discontinuity on the plane $v_1 = 0$. In this case, departures from local thermodynamic equilibrium are everywhere small, and so the problem for $K \ll 1$ can be treated by the Navier–Stokes formalism.

Range V. ($K \gg 1$)

The distance $(x_2 - x_1)$ is a very small fraction of a mean free path. Nearly all the molecules emitted by a plate (except those emitted practically tangentially) strike the opposite plate before they can collide with another gas molecule. In the

formulae (13.4a, b) for $f_{\pm}(\mathbf{v}, x)$, component A predominates everywhere and component B is comparatively small everywhere.

In this range, the primary requirement is that we should provide representations for the non-uniformly attenuating wall distributions. We could thus use the approximating forms

$$f_{+}(\mathbf{v}, x) = \Psi(\mathbf{v};\, 0, T_1) \sum_{m,n} A^{(+)}_{m,n}(x)\, \mu^m v^n, \tag{14.2a}$$

$$f_{-}(\mathbf{v}, x) = \Psi(\mathbf{v};\, 0, T_2) \sum_{m,n} A^{(-)}_{m,n}(x)\, \mu^m v^n. \tag{14.2b}$$

Component B in f_{+} or f_{-} would by itself be represented rather inaccurately by an MM function based on T_1 or T_2. In the derivation of continuum equations from the relations (14.2), the presence of component B gives rise to a slight modification of the coefficients $A^{(\pm)}_{m,n}$ from what would be their pure component A values.

Range IV. ($K \sim 5$)

In this case, most of the molecules emitted from a wall reach the opposite wall before they can collide with other gas molecules. Component A, i.e. the attenuating wall distribution, is still, as in range V, the dominant term in equations (13.4). Component B, however, is by no means negligible and should receive explicit recognition in our approximations for $f_{\pm}$.

In formula (13.4a) for $f_{+}(\mathbf{v}, x)$, component B includes significant contributions from the collisional emission $\mathscr{E}(\mathbf{v}, x')$ at all points x' in (x_1, x). Similarly, component B in $f_{-}(\mathbf{v}, x)$ includes significant contributions from the collisional emission at all points in (x, x_2). Roughly speaking, the emission $\mathscr{E}(\mathbf{v}, x')$ at any point results from the interaction of two distributions with temperatures T_1 and T_2. We therefore approximate component B as a sum of MM functions based on the boundary temperatures T_1 and T_2. We would then represent the complete distributions $f_{\pm}(\mathbf{v}, x)$ (component A + component B) in the form

$$f_{\pm}(\mathbf{v}, x) = \sum_{\lambda=1}^{2} \Psi(\mathbf{v};\, 0, T_\lambda) \sum_{m,n} A^{(\lambda,\pm)}_{m,n}(x)\, \mu^m v^n, \tag{14.3a}$$

$$A^{(\lambda,+)}_{m,n}(x_1) = a_1 \delta_{\lambda,1} \delta_{m,0} \delta_{n,0}, \quad A^{(\lambda,-)}_{m,n}(x_2) = a_2 \delta_{\lambda,2} \delta_{m,0} \delta_{n,0}. \tag{14.4a, b}$$

Range II. ($K \sim 0{\cdot}2$)

Most of the molecules emitted from a plate collide in the gas before they can strike the opposite plate. Component B of equation (13.4) thus predominates, but component A is by no means negligible.

For $v_1 > 0$, the contributions to component B of $f_{+}(v, \mu, x)$ come from collisional emission $\mathscr{E}(\mathbf{v}, x')$ at points $x' < x$ and within about one mean free path of x. In this case we may approximate $f_{\pm}(v, \mu, x)$ by the forms

$$f_{\pm} = \Psi(\mathbf{v};\, 0, T(x)) \sum_{m,n} A^{(\pm)}_{m,n} \mu^m v^n + \Psi(\mathbf{v};\, 0, T_{\pm}(x)) \sum_{m,n} B^{(\pm)}_{m,n} \mu^m v^n, \tag{14.5a, b}$$

where $T(x)$ is the local kinetic temperature and $T_{+}(x)$, $T_{-}(x)$ are the temperatures associated with molecules that have $v_1 > 0$, $v_1 < 0$, respectively.

We note that $T_+(x_1) = T_1$, $T_-(x_2) = T_2$, so that

$$A^{(+)}_{m,n}(x_1) = 0, \quad B^{(+)}_{m,n}(x_1) = a_1 \delta_{m,0}\delta_{n,0};$$

and

$$A^{(-)}_{m,n}(x_2) = 0, \quad B^{(-)}_{m,n}(x_2) = a_2 \delta_{m,0}\delta_{n,0}.$$

Range III. ($K \sim 1$)

In this range, component A and component B of equation (13.4) are of comparable importance. The collisional temperature $T_c(x)$ also varies appreciably with x between x_1 and x_2. It would appear to be desirable to use sums of at least three MM functions for this case, e.g.

$$f_\pm = \sum_{\lambda=1}^{2} \Psi(\mathbf{v}; 0, T_\lambda) \sum_{m,n} A^{(\lambda,\pm)}_{m,n} \mu^m v^n + \Psi(\mathbf{v}; 0, T_\pm) \sum_{m,n} B^{(\pm)}_{m,n} \mu^m v^n, \quad (14.6a, b)$$

(or the form with $T(x)$ instead of $T_\pm(x)$).

The types of approximation quoted above for various ranges of K are of course not the only, or even necessarily the best, approximating forms. When MM functions based on local characteristic temperatures appear in the representation, the resulting continuum equations are formally complex (see § 15). It may sometimes be desirable to exploit the formal simplicity that results from the use of *constant* velocity-temperature pairs, by using only MM functions based on the boundary temperatures T_1, T_2 and on a sequence of constant temperatures intermediate between T_1 and T_2.

15. Choice of basic state-variables

In cases where the approximate representation of the distribution function involves only constant velocity-temperature pairs, the derivation of continuum equations is completely straightforward. The formalism is somewhat more complicated when the approximations include MM functions based on local characteristic velocity-temperature pairs. We shall illustrate this point by considering the approximation (14.5) (range II) for the heat transfer problem of the previous section.

Let us define the half-space moments $R^{(\pm)}_{j,l}(x)$ by the equations

$$R^{(\pm)}_{j,l} = \frac{1}{\beta_1^{l+3}} \int_\pm \mu^j v^l f_\pm(v, \mu, x)\, d\mathbf{v} \quad (j, l = 0, 1, 2\ldots), \quad (15.1)$$

where $\beta_1^2 = kT_1/m$. The local temperatures $T(x)$, $T_+(x)$, $T_-(x)$ and the corresponding speeds $\beta(x)$, $\beta_+(x)$, $\beta_-(x)$, are defined by the relations

$$\beta^2 = \frac{kT}{m} = \frac{R^{(+)}_{0,2} + R^{(-)}_{0,2}}{3(R^{(+)}_{0,0} + R^{(-)}_{0,0})}, \quad (15.2)$$

$$\beta_\pm^2 = \frac{kT_\pm}{m} = \frac{R^{(\pm)}_{0,2}}{3R^{(\pm)}_{0,0}}. \quad (15.3a, b)$$

If we use the approximating forms

$$f_\pm = \Phi(\mathbf{v}; 0, \beta) \sum_{m,n} A^{(\pm)}_{mn} \mu^m \left(\frac{v}{\beta}\right)^n + \Phi(\mathbf{v}; 0, \beta_\pm) \sum_{m,n} B^{(\pm)}_{mn} \mu^m \left(\frac{v}{\beta_\pm}\right)^n, \quad (15.4a, b)$$

we obtain, for the moments, the approximations

$$R^{(\pm)}_{j,l} = \sum_{m,n} A^{(\pm)}_{mn} \frac{(\pm 1)^{j+m}\, 2^{\frac{1}{2}(l+n)}\, \Gamma\{\frac{1}{2}(l+n+3)\}}{(j+m+1)\sqrt{\pi}} \left(\frac{\beta}{\beta_1}\right)^l \Bigg\} + \sum_{m,n} B^{(\pm)}_{mn} \frac{(\pm 1)^{j+m}\, 2^{\frac{1}{2}(l+n)}\, \Gamma\{\frac{1}{2}(l+n+3)\}}{(j+m+1)\sqrt{\pi}} \left(\frac{\beta_\pm}{\beta_1}\right)^l \Bigg\} \tag{15.5a,b}$$

The local speeds $\beta(x)$, $\beta_\pm(x)$ that appear in the coefficients on the right-hand side of equations (15.5a, b) are themselves given in terms of the moments $R^{(\pm)}_{0,0}(x)$, $R^{(\pm)}_{0,2}(x)$ by the relations (15.3). It is then convenient to include these four moments $R^{(\pm)}_{0,0}$ and $R^{(\pm)}_{0,2}$ in the set of basic state-variables. The coefficients $A^{(\pm)}_{m,n}$, $B^{(\pm)}_{m,n}$ are then non-linear in $R^{(\pm)}_{0,0}$ and $R^{(\pm)}_{0,2}$, but are linear functions of the remaining basic state-variables.

Examples of continuum equations for such cases will be given in a subsequent paper where the methods of this paper are used, in conjunction with statistical models, to discuss the problem of Couette flow with heat transfer.

16. Structure of shock waves

We consider a plane stationary shock wave in a simple gas. The boundary conditions are

$$\left.\begin{aligned} f(\mathbf{v}, -\infty) &= n_1 \Psi(\mathbf{v}; Q_1\mathbf{i}, T_1), \\ f(\mathbf{v}, +\infty) &= n_2 \Psi(\mathbf{v}; Q_2\mathbf{i}, T_2). \end{aligned}\right\} \tag{16.1a,b}$$

The number density $n_2 = n(+\infty)$, average velocity $Q_2\mathbf{i} = \mathbf{q}(+\infty)$, and temperature $T_2 = T(+\infty)$ are determined uniquely by n_1, Q_1, T_1, and the Mach number $M = Q_1/(5kT_1/3m)^{\frac{1}{2}}$.

Since the boundaries are at infinity, the integral equations (13.4) reduce to the form

$$f_+(\mathbf{v}, x) = \frac{1}{v_1} \int_{-\infty}^{x} \mathscr{E}(\mathbf{v}, x) \exp\left[-\{\lambda(\mathbf{v}, x) - \lambda(\mathbf{v}, x')\}/v_1\right] d\lambda', \tag{16.2a}$$

$$f_-(\mathbf{v}, x) = \frac{1}{|v_1|} \int_{x}^{\infty} \mathscr{E}(\mathbf{v}, x) \exp\left[-\{\lambda(\mathbf{v}, x') - \lambda(\mathbf{v}, x)\}/|v_1|\right] d\lambda'. \tag{16.2b}$$

The Knudsen number $K = 0$, and the distribution function $f(\mathbf{v}, x)$ is continuous in $\mathbf{v}$-space. However, the transition from the supersonic régime to the subsonic régime is practically confined to a layer whose thickness is of the order of a few mean free paths. In this layer, the distribution function exhibits steep gradients (the local Knudsen number is of order unity). In this case

$$\mathscr{E}(\mathbf{v}, x) \to \left\{\begin{aligned} &\text{const.} \times f(\mathbf{v}, -\infty) \quad \text{as} \quad x \to -\infty, \\ &\text{const.} \times f(\mathbf{v}, +\infty) \quad \text{as} \quad x \to +\infty. \end{aligned}\right\} \tag{16.3}$$

The velocity distribution is axially symmetric about the direction $\mathbf{i}$. We obtain formally simple continuum equations if we represent the complete distribution as the sum of MM functions based on the constant pairs $(Q_1\mathbf{i}, T_1)$ $(Q_2\mathbf{i}, T_2)$, in the form

$$f = \sum_{\lambda=1}^{2} \Psi(\mathbf{v}; Q_\lambda\mathbf{i}, T_\lambda) \sum_{m,n} A^{(\lambda)}_{m,n} v_1^m v^{2n}. \tag{16.4}$$

Formally more complicated equations are obtained with the unsymmetrical approximation

$$f = \Psi(\mathbf{v}; Q_1\mathbf{i}, T_1) \sum_{m,n} A_{mn} v_1^m v^{2n} + \Psi(\mathbf{v}; \mathbf{q}, T) \sum_{m,n} B_{mn} v_1^m v^{2n}. \tag{16.5}$$

Even with the Maxwell–Boltzmann model, the representations (15.4) and (15.5) permit the multiple integrals involved in the interaction moments to be evaluated in terms of error functions. Approximations of the form (16.4) have been used to analyse the structure of shock fronts in ionized gases (Krook 1959).

If we use the simpler forms of statistical model for the molecular interactions, it is feasible to use separate representations for $f_+(\mathbf{v}, x)$ and $f_-(\mathbf{v}, x)$, e.g.

$$f_+ = \Psi(\mathbf{v}, Q_1\mathbf{i}, T_1) \sum_{m,n} A^{(+)}_{mn} v_1^m v^{2n} + \Psi(\mathbf{v}, \mathbf{q}, T) \sum_{m,n} B^{(+)}_{mn} v_1^m v^{2n}, \tag{16.6a}$$

$$f_- = \Psi(\mathbf{v}, Q_2\mathbf{i}, T_2) \sum_{m,n} A^{(-)}_{mn} v_1^m v^{2n} + \Psi(\mathbf{v}, \mathbf{q}, T) \sum_{m,n} B^{(-)}_{mn} v_1^m v^{2n}. \tag{16.6b}$$

The forms (16.5) and (16.6*a*, *b*) contain a more explicit representation of the collisional emission than does the form (16.4).

17. Conclusion

When the methods of this paper are used to construct continuum equations, the only place in which we may encounter difficulty is in the expression of the interaction moments as functions of the basic state-variables. This process generally involves the evaluation of multiple integrals with products of two *MM* functions as integrands.

If the law of force between molecules is given in analytic form, and if f is not singular on the plane $v_1 = 0$, these integrals can usually be evaluated explicitly, even when the interaction term has the Maxwell–Boltzmann form. If f is singular on the plane $v_1 = 0$, and we therefore use different representations for f_+ and f_-, the evaluation of the relevant integrals for the half-space interaction moments in the Maxwell–Boltzmann model is troublesome. It is for just such cases that the statistical models prove particularly useful; the evaluation of the half-space interaction moments is generally quite straightforward with these models.

In subsequent papers, the methods presented in this paper will be applied to obtain approximate solutions for the problems of shock-wave structure, and Couette flow with heat transfer.

REFERENCES

Chapman, S. & Cowling, T. G. 1939 *Mathematical Theory of Non-uniform Gases.* Cambridge University Press.

Bhatnagar, P. L., Gross, E. P. & Krook, M. 1954 *Phys. Rev.* **94**, 511.

Grad, H. 1949 *Communs. Pure Appl. Math.* **2**, 331.

Gross, E. P., Jackson, E. A. & Ziering, S. 1957 *Ann. Phys.* **1**, 141.

Krook, M. 1955*a* *Ap. J.* **122**, 488.

Krook, M. 1955*b* *Phys. Rev.* **99**, 1896.

Mott-Smith, H. 1951 *Phys. Rev.* **82**, 885.

Rosenbluth, M. N., MacDonald, W. M. & Judd, D. L. 1957 *Phys. Rev.* **170**, 1.

Pressure drop due to viscous flow through cylinders

By HOWARD BRENNER
Department of Chemical Engineering, New York University

(Received 24 March 1959)

A general formula is developed which permits a calculation of the pressure drop arising from the slow steady flow of a viscous fluid through a circular cylinder for arbitrarily assigned conditions of velocity on the bounding surfaces of the cylinder. In particular, the diminution in pressure can be calculated *directly* from the prescribed boundary velocities without requiring a detailed solution of the equations of motion. Hence it is possible to compute, in comparatively simple fashion, the magnitude of this macroscopic parameter for a large variety of complex motions which would normally present great analytical difficulties.

By way of illustration the additional pressure drop arising from the presence of a point force situated along the axis of a cylinder is calculated. The additional force required to maintain the motion in the presence of the obstacle is exactly twice the magnitude of the point force itself.

One of the objectives of theoretical hydrodynamics is the calculation of various *macroscopic* parameters such as drag, lift, moment, pressure drop and the like from a knowledge of the stress field. In many instances one is less interested in the actual details of the fluid motion than in the numerical value of the parameters characterizing the flow. The adoption of this point of view is often imposed through purely mathematical difficulties occasioned by the complex structure of the fields. Accordingly, formulae which permit calculation of the macroscopic properties of the fluid motion *directly* from the boundary and initial conditions, without recourse to a detailed solution of the equations of motion, have much to commend them.

As a specific contribution in this general area we propose to develop an expression for the pressure drop associated with slow, steady viscous flows inside circular cylinders in terms of arbitrarily prescribed conditions of velocity over the bounding surfaces of the cylinder. This formula, coupled with a perturbation scheme known as the method of 'reflexions' (see, for instance, Brenner & Happel 1958), provides a useful tool for the study of the additional pressure drop caused by disturbances to a Poiseuille field of flow. These results, in turn, find application in the flow through dilute beds of particles such as in fluidized beds, pneumatic conveying, and similar processes (Happel & Brenner 1957).

Consider a time-independent viscous motion occurring within a circular cylinder of radius ρ_0 and length $2h$. It is presumed that the velocity and pressure fields $(\mathbf{v}, p)$ are well behaved at all points within the cylinder and that they there

satisfy the creeping motion equation (in the absence of external forces)

$$\nabla^2 \mathbf{v} = \frac{1}{\mu} \nabla p \tag{1}$$

and the continuity equation $$\nabla . \mathbf{v} = 0 \tag{2}$$

for incompressible fluids. In cylindrical co-ordinates (ρ, ϕ, z) the component velocities will be denoted by (v_ρ, v_ϕ, v_z).

The pressure drop in the positive z-direction, ΔP, is defined as the difference in pressure between the two planes, $z = -h$ and $z = h$, respectively, situated at either end of the cylinder; that is,

$$\Delta P = [p]_{z=-h} - [p]_{z=h}. \tag{3}$$

These planes are to be selected in such a way that the pressure across each is constant. Otherwise, our definition of pressure drop is ambiguous. In a majority of circumstances this requires that these planes be situated at $z = \pm\infty$.

In the absence of inertial and external forces the surface forces acting upon any fluid volume constitute a system of forces in equilibrium. Upon applying this argument to a cylinder of fluid of radius ρ bounded by the planes $z = \pm h$, and considering only the z-component of this force, we are led to the relation

$$\int_0^\rho \int_0^{2\pi} \{[P_{zz}]_{z=h} - [P_{zz}]_{z=-h}\} \rho \, d\phi \, d\rho + \int_{-h}^{h} \int_0^{2\pi} P_{\rho z} \rho \, d\phi \, dz = 0, \tag{4}$$

in which P_{zz} and $P_{\rho z}$ are the components of stress in the z-direction acting on the surfaces $z =$ constant and $\rho =$ constant, respectively.

For an incompressible viscous fluid these stresses can be written in the form

$$P_{zz} = -p + 2\mu \frac{\partial v_z}{\partial z}, \qquad P_{\rho z} = \mu \left(\frac{\partial v_z}{\partial \rho} + \frac{\partial v_\rho}{\partial z} \right).$$

However, according to the equation of continuity,

$$\frac{\partial v_z}{\partial z} = -\frac{\partial}{\rho \partial \rho}(\rho v_\rho) - \frac{\partial v_\phi}{\rho \partial \phi}$$

from which we eventually obtain

$$\int_0^\rho \int_0^{2\pi} \frac{\partial v_z}{\partial z} \rho \, d\phi \, d\rho = -\rho \int_0^{2\pi} v_\rho \, d\phi. \tag{5}$$

With the aid of these results and a simple partial integration, equation (4) can be put in the form

$$\Delta P \pi \rho^2 + \mu \rho \frac{\partial}{\partial \rho} \int_{-h}^{h} \int_0^{2\pi} v_z \, d\phi \, dz - \mu \rho \int_0^{2\pi} [v_\rho(\rho, \phi, h) - v_0(\rho, \phi, -h)] \, d\phi = 0.$$

If this relation is multiplied by $\rho \, d\rho$ and the resulting expression integrated from $\rho = 0$ to ρ_0 it takes the form

$$\frac{\Delta P \pi \rho_0^4}{4\mu} = -\rho_0^2 \int_{-h}^{h} \int_0^{2\pi} v_z(\rho_0, \phi, z) \, d\phi \, dz + 2 \int_{-h}^{h} \int_0^{\rho_0} \int_0^{2\pi} v_z \rho \, d\phi \, d\rho \, dz$$
$$+ \int_0^{\rho_0} \int_0^{2\pi} v_\rho(\rho, \phi, h) \rho^2 \, d\phi \, d\rho - \int_0^{\rho_0} \int_0^{2\pi} v_\rho(\rho, \phi, -h) \rho^2 \, d\phi \, d\rho.$$

Lastly, we can rid ourselves of the second integral in the above expression by setting $\rho = \rho_0$ in equation (5), multiplying both sides by dz and integrating the result from $z = -h$ to $z = z$. Upon doing this we finally obtain the desired formula,

$$\frac{\Delta P \pi \rho_0^4}{4\mu} = -\rho_0^2 \int_{-h}^{h} \int_0^{2\pi} v_z(\rho_0, \phi, z)\, d\phi\, dz + 4h \int_0^{\rho_0} \int_0^{2\pi} v_z(\rho, \phi, -h)\, \rho\, d\phi\, d\rho$$
$$- 2\rho_0 \int_{z=-h}^{z=h} \int_{z'=-h}^{z'=z} \int_0^{2\pi} v_\rho(\rho_0, \phi, z')\, d\phi\, dz'\, dz + \int_0^{\rho_0} \int_0^{2\pi} v_\rho(\rho, \phi, h)\, \rho^2\, d\phi\, d\rho$$
$$- \int_0^{\rho_0} \int_0^{2\pi} v_\rho(\rho, \phi, -h)\, \rho^2\, d\phi\, d\rho. \tag{6}$$

This relation enables us to compute the pressure drop directly from the prescribed values of v_z on the walls and bottom of the container, $v_z(\rho_0, \phi, z)$ and $v_z(\rho, \phi, -h)$, respectively, and from the prescribed radial component on the cylinder walls, top and bottom, $v_\rho(\rho_0, \phi, z)$, $v_\rho(\rho, \phi, h)$ and $v_\rho(\rho, \phi, -h)$, respectively. In those applications where it is necessary to choose the constant pressure planes at $z = \pm\infty$ the velocity at infinity is zero and the second, fourth and fifth integrals in the foregoing expression vanish.

As a trivial illustration of the use of this formula we shall deduce Poiseuille's law for the diminution in pressure accompanying the laminar flow of a viscous fluid in a circular pipe. In this application we are, of course, making use of the fact that in the rectilinear flow of an incompressible fluid the creeping motion and Stokes–Navier equations are identical. The boundary conditions to be satisfied are:

(i) on the cylinder walls, $\rho = \rho_0$, $\quad v_z(\rho_0, \phi, z) = v_\rho(\rho_0, \phi, z) = 0$;

(ii) at the top of the cylinder, $z = h$, $\quad v_\rho(\rho, \phi, h) = 0$;

(iii) at the bottom of the cylinder, $z = -h$, $\quad v_\rho(\rho, \phi, -h) = 0$;

and

$$\int_0^{\rho_0} \int_0^{2\pi} v_z(\rho, \phi, -h)\, \rho\, d\phi\, d\rho = Q;$$

where Q is the volumetric flow rate through the cylinder and is independent of z. If $L = 2h$ is the length of pipe through which the fluid passes, we have from (6)

$$\frac{\Delta P \pi \rho_0^4}{4\mu} = 4(\tfrac{1}{2}L)\, Q. \qquad \text{or} \quad \Delta P = \frac{8\mu Q L}{\pi \rho_0^4}, \tag{7}$$

which is Poiseuille's law.

As a somewhat more instructive example, we consider the problem of an external force localized at a point ($\rho = 0, z = 0$), situated at the longitudinal axis of the cylinder. This force, whose magnitude is F, acts in the direction of the negative z axis. The pressure drop associated with this disturbance can be calculated from (6).

In the absence of the cylinder walls, when the fluid extends to infinity in all directions, the unperturbed motion, $(\mathbf{v}^{(0)}, p^{(0)})$, given by Lamb (1932) can be expressed in the form

$$\mathbf{v}^{(0)} = \frac{F}{4\pi\mu} \left[\tfrac{1}{2} \nabla \left(\frac{z}{r} \right) - \mathbf{i}_z \frac{1}{r} \right], \tag{8}$$

and

$$p^{(0)} = -\frac{F}{4\pi} \frac{z}{r^3}. \tag{9}$$

As a result of the presence of a boundary encircling the fluid, the original field of flow is perturbed by an amount $(\mathbf{v}^{(1)}, p^{(1)})$ and the entire motion $(\mathbf{v}, p)$ is

$$\mathbf{v} = \mathbf{v}^{(0)} + \mathbf{v}^{(1)}, \tag{10}$$

$$p = p^{(0)} + p^{(1)}. \tag{11}$$

The validity of this method of treatment depends upon the linearity of the equations of motion.

On the hypothesis of no slip at the cylinder walls we have the boundary condition

$$\mathbf{v} = 0 \quad \text{at} \quad \rho = \rho_0, \tag{12}$$

which is equivalent to

$$\mathbf{v}^{(1)} = -\mathbf{v}^{(0)} \quad \text{at} \quad \rho = \rho_0. \tag{13}$$

There are no further restrictions imposed on the field $\mathbf{v}^{(1)}$ except that it be free from singularities in the interior of the cylinder. As such, it cannot alter the force acting at the isolated point, $r = 0$, and the force is thus passed along unaltered to become a property of the field $\mathbf{v}$.

The planes across which the pressure, p, is constant occur at $z = \pm\infty$. On the basis of (11), the pressure drop due to the entire motion can be calculated from the relation

$$\Delta P = \Delta P^{(0)} + \Delta P^{(1)}. \tag{14}$$

But, equation (9) shows that the pressure drop due to the unperturbed motion is

$$\Delta P^{(0)} = [p^{(0)}]_{z=-\infty} - [p^{(0)}]_{z=\infty} = 0, \tag{15}$$

and hence

$$\Delta P = \Delta P^{(1)}. \tag{16}$$

Now $\Delta P^{(1)}$ can be computed from (6) by putting $h = \infty$. Since $\mathbf{v}^{(0)} \to 0$ as $z \to \pm\infty$ and since $\mathbf{v}^{(0)}$ and $\mathbf{v}^{(1)}$ are related by (13) then $v_z^{(1)}$ and $v_\rho^{(1)}$ vanish at the top and bottom of the cylinder, whence

$$\frac{\Delta P^{(1)} \pi \rho_0^4}{4\mu} = -\rho_0^2 \int_{-\infty}^{\infty} \int_0^{2\pi} v_z^{(1)}(\rho_0, z)\, d\phi\, dz - 2\rho_0 \int_{z=-\infty}^{z=\infty} \int_{z'=-\infty}^{z'=z} \int_0^{2\pi} v_\rho^{(1)}(\rho_0, z')\, d\phi\, dz'\, dz. \tag{17}$$

In view of equations (13) and (14) and the lack of dependence of the velocity field on the angle ϕ, the above equation becomes

$$\frac{\Delta P \pi \rho_0^4}{4\mu} = 2\pi\rho_0^2 \int_{-\infty}^{\infty} v_z^{(0)}(\rho_0, z)\, dz + 4\pi\rho_0 \int_{z=-\infty}^{z=\infty} \int_{z'=-\infty}^{z'=z} v_\rho^{(0)}(\rho_0, z')\, dz'\, dz. \tag{18}$$

From (8)

$$v_z^{(0)}(\rho_0, z) = \frac{F}{4\pi\mu}\left[\frac{1}{2}\frac{\partial}{\partial z}\left(\frac{z}{\sqrt{(\rho_0^2 + z^2)}}\right) - \frac{1}{\sqrt{(\rho_0^2 + z^2)}}\right],$$

and

$$v_\rho^{(0)}(\rho_0, z') = \frac{F}{8\pi\mu} z' \left[\frac{\partial}{\partial \rho}\left(\frac{1}{\sqrt{(\rho^2 + (z')^2)}}\right)\right]_{\rho=\rho_0}$$

$$= \frac{F}{8\pi\mu}\rho_0 \frac{\partial}{\partial z'}\left(\frac{1}{\sqrt{(\rho_0^2 + (z')^2)}}\right),$$

which easily yields

$$\int_{z'=-\infty}^{z'=z} v_\rho^{(0)}(\rho_0, z')\,dz' = \frac{F}{8\pi\mu}\frac{\rho_0}{\sqrt{(\rho_0^2+z^2)}}.$$

Inserting these values in (18) it becomes

$$\frac{\Delta P\pi\rho_0^4}{4\mu} = \frac{F\rho_0^2}{4\mu}\int_{-\infty}^{\infty}\frac{\partial}{\partial z}\left(\frac{z}{\sqrt{(\rho_0^2+z^2)}}\right)dz, \tag{19}$$

from which we find $\Delta P = 2F/\pi\rho_0^2$. The pressure drop force, $\Delta P\pi\rho_0^2$, is thus exactly twice the external force which gives rise to it.

If the external force arises from the action of a viscous fluid impinging on a small spherical particle situated at the cylinder axis, then F is equal to and oppositely directed from the drag, D, experienced by the particle while ΔP is the *additional** pressure drop caused by its presence. Without further calculation, Faxén's (1927) law shows that for a small particle

$$D = -F = -6\pi\mu a(U_0 - U), \tag{20}$$

where $\frac{1}{2}U_0$ is the superficial velocity of the fluid, U is the velocity of the particle in the z-direction and a is the particle radius. Under these circumstances

$$\Delta P = \frac{12\mu a(U_0-U)}{\rho_0^2}. \tag{21}$$

For small values of a/ρ_0, this result agrees identically with that of Happel & Byrne (1954) obtained by a much more complex procedure requiring a detailed calculation of the field $\mathbf{v}^{(1)}$.

This work was carried out under a grant sponsored in part by the Research Corporation of America and in part by the National Science Foundation [Contract No. NSF (G) 1710]. The author would also like to thank John Happel of New York University for suggesting the research which culminated in this paper.

REFERENCES

Brenner, H. & Happel, J. 1958 *J. Fluid Mech.* **4**, 195.
Faxén, H. 1927 *Ark. Mat. Astr. Fys.* **20**, no. 8.
Happel, J. & Brenner, H. 1957 *J. A.I.Ch.E.* **3**, 506.
Happel, J. & Byrne, B. J. 1954 *Industr. Engng Chem.* **46**, 1181.
Lamb, H. 1932 *Hydrodynamics*, 6th ed., p. 606. *Cambridge University Press.*

* The fluid experiences a pressure drop even in the absence of the obstacle. The difference between the total pressure drop in the presence of the particle and the Poiseuillian pressure drop in the absence of the particle is the *additional* pressure drop. It is an experimentally measurable quantity.

Experiments on the flow past a circular cylinder at low Reynolds numbers

By D. J. TRITTON
Cavendish Laboratory, Cambridge

(Received 25 February 1959)

Part I describes measurements of the drag on circular cylinders, made by observing the bending of quartz fibres, in a stream with the Reynolds number range 0·5–100. Comparisons are made with other experimental values (which cover only the upper part of this range) and with the various theoretical calculations.

Part II advances experimental evidence for there being a transition in the mode of the vortex street in the wake of a cylinder at a Reynolds number around 90. Investigations of the nature of this transition and the differences between the flows on either side of it are described. The interpretation that the change is between a vortex street originating in the wake and one originating in the immediate vicinity of the cylinder is suggested.

Introduction

This paper is concerned with two-dimensional flow past a circular cylinder. The Reynolds number, R, is defined throughout on the diameter of the cylinder and the velocity, U, far from it. Directions are referred to in terms of the Cartesian co-ordinates, x, y and z, which are respectively in the direction of flow far from the cylinder, perpendicular to both this and the cylinder, and parallel to the cylinder.

It is well known that as R is increased from low values for which approximate solutions of the Navier–Stokes equations can be found, a complex sequence of events takes place. At a Reynolds number estimated at 3·2 by Nisi & Porter (1923), 5 by Taneda (1956), and 6 by Homann (1936), the flow separates from the cylinder before reaching the rear generator and a pair of attached eddies forms behind the cylinder.

The Reynolds number of the first appearance of a vortex street behind the cylinder is also rather variably estimated. It is common to take it as 40, though Taneda (1956), puts it as low as 30. It is often supposed (e.g. Goldstein 1938, § 183) that the street is produced by the attached eddies stretching farther and farther downstream, becoming distorted, and then being shed alternately from the sides of the cylinder. However, an inspection of the flow (as photographed for instance by Homann (1936)) suggests that at Reynolds numbers only a little above 40 the street develops out of an instability in the wake. The wind-tunnel experiments of Kovasznay (1949) lend support to this view. Further the work of Hollingdale (1940) and Taneda (1958) on the wake of a flat plate at zero

incidence has shown conclusively that a vortex street can develop independently of attached eddies.

According to Roshko (1954), the mode of flow first appearing at $R \sim 40$ continues until $R \sim 150$ when the motion of the vortices becomes less regular and turbulence is produced downstream.

Part I of this paper describes experiments that give values for the drag on a cylinder in the range $0{\cdot}5 < R < 100$—a range of some interest in view of the sequence of changes that occurs within it. Part II gives experimental evidence for there being a further change at $R \sim 90$, and suggests a qualitative explanation of this.

Part I. The Drag on Circular Cylinders for $0{\cdot}5 < R < 100$

The approximate solutions of the Navier–Stokes equations give theoretical values for the drag coefficient when the Reynolds number is rather less than 1. The previous lowest R at which an experimental value was obtained was 4·22 and good agreement between different experimental investigations did not begin until about $R = 20$. It has been, however, common practice to interpolate values in the intermediate range. The range is too long for this to be accurate and the interpolation would seem particularly subject to error in view of the fact that the first appearance of attached eddies occurs within it. Hence, when I was doing some experiments that provided some information on the drag coefficient in this low R region, it seemed worthwhile extending them to fill in this gap in the R–C_D curve.

The experiments concerned were a series of calibrations of quartz-fibre anemometers for measuring the low air speeds of free convective flows. This instrument was developed by Schmidt (1934) (see also, Schmidt & Beckmann (1930)), but has not previously been used as an absolute measure. An advantage of so using it is that it enables the measurements to be extended to speeds lower than those available for calibration.

In the author's arrangement of the instrument the quartz-fibre is cemented into the end of a piece of hypodermic tubing. The free end of the fibre is viewed through a tele-microscope with an eyepiece scale previously calibrated against a stage graticule. The objective has a working distance of about 4 cm, which is large enough for the tele-microscope not to affect the flow round the fibre.

If simple bending moment theory is supposed to apply, the deflexion of the end of the fibre produced by a force F per unit length normal to its axis is

$$h = \frac{8Fl^4}{\pi E d^4},$$

where l, d, and E are the length, diameter and Young's modulus of the fibre. If F is taken as the drag produced by a stream of air with velocity U flowing past an infinite circular cylinder, then the drag coefficient, defined as

$$C_D = \frac{F}{\frac{1}{2}\rho U^2 d}$$

(ρ is the density of air), is given by

$$C_D = \frac{\pi E d^3 h}{4\rho U^2 l^4}.$$

There are a number of requirements on the quantities involved for this result to be useful. (i) Simple bending moment theory must apply. It was calculated that, for errors to be less than 1 %, this requires $l/h > 15$. (ii) The cylinder must be long enough for it to be regarded as effectively infinite. The smallest value of l/d for the author's fibres was 150; judging by the results of Wieselsberger (1922) for finite cylinders this is perhaps not really large enough, but the results obtained with this fibre could be fitted in with those from fibres of much larger l/d. (iii) h must be an order of magnitude larger than d or it is not accurately measurable.

All these conditions could be satisfied with a set of fibres with diameters in the range 20–100 μ and lengths in the range 1–3 cm, which then fulfils the dual purpose of determining C_D in the range $0{\cdot}5 < R < 100$ (some overlap with the already established range was thought desirable as a check on the accuracy of the technique) and measuring air velocities down to 10 cm/sec.

Of the quantities that are needed for calculating R and C_D from observed values of U and h, the fibre diameter is the most difficult to measure and this is the limiting factor on the accuracy of the experiments. The diameters of the larger fibres were measured with a travelling microscope. For the smaller ones this was not sufficiently accurate and a wedge fringe optical interference method with reflected sodium light was used instead. It was also found necessary to measure the Young's modulus for each fibre diameter. This was done by determining the resonant frequencies of a mounted fibre. This work has already been described elsewhere (Tritton 1959) as it indicated that the modulus varies with diameter. In terms on the nth resonant frequency, ν_n, the Young's modulus is

$$E = \frac{64\pi^2 l^4 \rho_Q}{d^2}\left(\frac{\nu_n}{\phi_n^2}\right)^2,$$

where ρ_Q is the density of fused quartz and ϕ_n is the nth root of

$$\cos\phi \cosh\phi = -1$$

(Tritton 1959). Hence,

$$C_D = \frac{16\pi^3 d\rho_Q h}{\rho U^2}\left(\frac{\nu_n}{\phi_n^2}\right)^2.$$

The diameter dependence is thus reduced from third order to first, giving a fortunate increase in accuracy.

The resonance measurements also indicated rather better than the diameter measurements when the fibre was not truly circular; in this case each resonance became a doublet. Departures from circular cross-sections (calculated assuming elliptical ones) were in the worst cases around 3 % and usually rather less than this.

The measurements of the deflexions produced by the air flow were carried out in one of the Cavendish Laboratory's wind-tunnels. This is fitted with a manometer that measures speeds down to 250 cm sec^{-1}. The tunnel will, however, run

Fibre and method of velocity measurement	Pressure and temperature	Velocity, U (cm sec^{-1})	Deflexion, h (cm)	Reynolds no., R (Absolute measurements)	Drag coefficient C_D (Absolute measurements)
Fibre 1					
$l = 1{\cdot}70$ cm; $d = 0{\cdot}00194$ cm;	765 mm Hg,	31·9	0·0413	0·416	18·6
$\nu_n/\phi_n^2 = 16{\cdot}2$ sec^{-1}.	20·8° C	38·2	0·0501	0·494	15·8
Eddy frequency with $50 < R < 150$		39·7	0·0556	0·518	16·2
		41·15	0·0577	0·532	15·7
		44·5	0·0643	0·576	15·0
		48·7	0·0721	0·634	14·0
		50·7	0·0765	0·661	13·7
		56·85	0·0883	0·741	12·6
		60·5	0·0961	0·783	12·1
		63·4	0·1036	0·820	11·9
		64·95	0·1063	0·845	11·6
	752 mm Hg, 20·3° C	30·2	0·0375	0·387	19·2
Fibre 2					
$l = 1{\cdot}27$ cm; $d = 0{\cdot}00197$ cm;	760 mm Hg,	49·2	0·0226	0·650	14·8
$\nu_n/\phi_n^2 = 29{\cdot}45$ sec^{-1}.	19·1° C	54·3	0·0254	0·719	13·6
Combination of heat-pulse tracing and eddy frequency with $50 < R < 150$		73·3	0·0356	0·968	10·5
		87·8	0·0460	1·16	9·49
		97·2	0·0530	1·29	8·85
		99·5	0·0544	1·32	8·69
		112·7	0·0646	1·50	8·05
		129·6	0·0788	1·72	7·41
Fibre 3					
$l = 3{\cdot}12$ cm; $d = 0{\cdot}00442$ cm;	744 mm Hg,	36·7	0·0362	1·06	11·7
$\nu_n/\phi_n^2 = 10{\cdot}07$ sec^{-1}.	20·6° C	44·4	0·0462	1·28	10·2
Combination of heat-pulse tracing and eddy frequency with $50 < R < 150$		50·4	0·0554	1·45	9·07
		58·3	0·0668	1·68	8·13
	769 mm Hg, 22·2° C	55·8	0·0626	1·64	8·19
		57·8	0·0666	1·70	8·13
		69·35	0·0858	2·04	7·26
		76·4	0·0982	2·25	6·86
		81·35	0·1070	2·40	6·56
		91·2	0·1248	2·69	6·11
		103·6	0·1485	3·05	5·64
		109·8	0·1628	3·24	5·50
		119·2	0·1817	3·51	5·20
Fibre 6*					
$l = 2{\cdot}07$ cm; $d = 0{\cdot}00753$ cm;	768 mm Hg,	297	0·0224	15·3	2·20
$\nu_n/\phi_n^2 = 36{\cdot}4$ sec^{-1}.	16·5° C	335	0·0292	17·3	2·25
Manometer (calibrated by heat-pulse tracing and by Pitot tube + Chattock manometer)		429	0·0466	22·1	2·20
		454	0·0446	23·4	1·87
		530	0·0596	27·4	1·83
		553	0·0686	28·5	1·94
		586	0·0732	30·2	1·85
		660	0·0896	34·0	1·78
		738	0·1068	38·1	1·69
		808	0·1218	41·7	1·62

* Fibre 6 showed slight hysteresis, giving rather more scatter than other fibres.

TABLE 1

Fibre and method of velocity measurement	Pressure and temperature	Velocity, U (cm sec^{-1})	Deflexion, h (cm)	Reynolds no., R (Absolute measurements)	Drag coefficient C_D (Absolute measurements)
Fibre 7					
$l = 1{\cdot}12$ cm; $d = 0{\cdot}00745$ cm;	769 mm Hg,	620	0·0062	31·4	1·58
$E = 5{\cdot}95 \times 10^{11}$ dyne cm^{-2}.	18·0° C	759	0·0086	38·5	1·46
Manometer		918	0·0134	46·6	1·56
		967	0·0138	49·0	1·45
		1042	0·0162	52·8	1·46
		1194	0·0214	60·5	1·47
		1221	0·0214	61·9	1·41
		1275	0·0244	64·6	1·47
Fibre 8					
$l = 2{\cdot}11$ cm; $d = 0{\cdot}01125$ cm;	771 mm Hg,	587	0·0188	44·9	1·46
$E = 5{\cdot}95 \times 10^{11}$ dyne cm^{-2}.	18·2° C	597	0·0184	45·7	1·38
Manometer		730	0·0276	55·8	1·39
		836	0·0350	64·0	1·34
		844	0·0358	64·6	1·34
		900	0·0398	68·9	1·31
		990	0·0464	75·8	1·27
		1016	0·0510	77·8	1·32
		1082	0·0554	82·8	1·26
		1182	0·0660	90·5	1·26
		1237	0·0712	94·7	1·24
		1272	0·0764	97·3	1·26
		1377	0·0878	105	1·24
		1442	0·0962	110	1·24
		1508	0·1052	115	1·24
				('Fitted' values)	
Fibre 4					
$l = 2{\cdot}28$ cm; $d \sim 0{\cdot}0047$ cm.	751 mm Hg,	77·8	0·0228	2·44	6·47
Eddy frequency with $50 < R < 150$	16·8° C	91·0	0·0276	2·86	5·77
		121·5	0·0418	3·82	4·91
		155	0·0580	4·86	4·20
		174	0·0706	5·51	3·99
		208	0·0900	6·52	3·62
		237	0·1088	7·45	3·37
		257	0·1270	8·09	3·33
	747 mm Hg,	49·2	0·0130	1·54	9·38
	16·9° C	67·0	0·0190	2·09	7·40
		75·3	0·0216	2·36	6·67
		116	0·0390	3·61	5·08
Fibre 5					
$l = 1{\cdot}33$ cm; $d \sim 0{\cdot}0043$ cm.	749 mm Hg,	165	0·0102	4·81	4·45
Eddy frequency with $R > 300$	16·9° C	243	0·0180	7·10	3·61
(formula given by Roshko (1954))		324	0·0270	9·44	3·06
		342	0·0298	9·95	3·07
		391	0·0344	11·4	2·67
		449	0·0422	13·1	2·51
		539	0·0566	15·7	2·30
		646	0·0734	18·8	2·09
		756	0·0922	22·0	1·91

TABLE 1 (*cont.*)

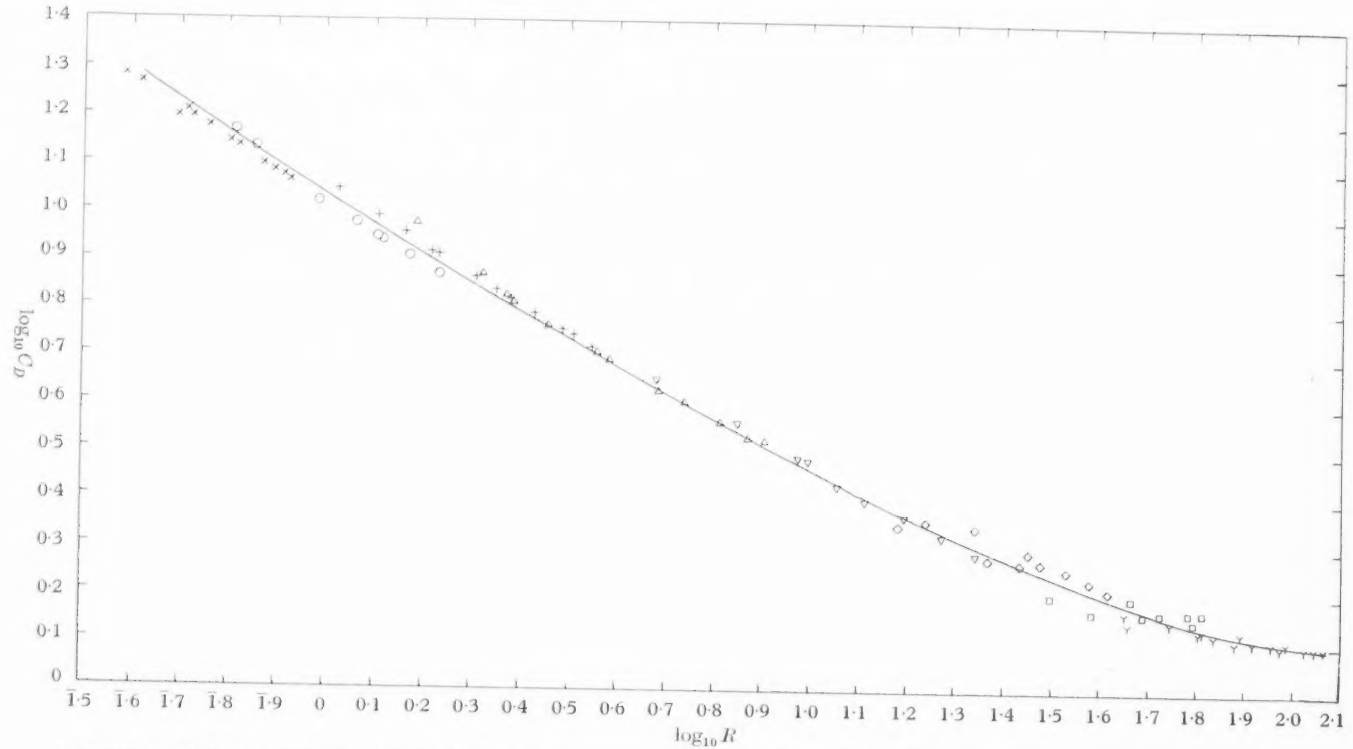

FIGURE 1. Plot of $\log C_D$ against $\log R$ showing all the observations listed in table 1. The line is an estimated mean curve, bearing in mind that the slope of the line for each fibre is known with greater accuracy than its position. This line is used for comparison purposes in figures 2 and 3. Absolute measurements: ×, fibre 1; ○, fibre 2; +, fibre 3; ◇, fibre 6; □, fibre 7; Y, fibre 8. 'Fitted' points: △, fibre 4; ▽, fibre 5.

as slowly as 30 cm sec^{-1}, so that other methods had to be developed for the lower speed runs. That first adopted was the measurement of the frequency of vortices in the street behind a second (thicker) cylinder (Roshko 1954). It was during this work that the frequency discontinuity that is to be described in Part II was discovered and the experimental methods will be recounted in more detail there. As a result of the existence of this discontinuity the formula given by Roshko for the velocity producing an observed frequency is less reliable than previously thought. Hence, some of the quartz fibres were also calibrated by tracing heat pulses down the wind-tunnel. The pulses were produced by a 50 c/s alternating current (giving 100 c/s temperature variations) in a 25 μ diameter wire stretched across the tunnel. The voltage supply to this was put across the X-plates of an oscilloscope, on the Y-plates of which was the amplified output of a hot-wire detector in the heat-wake. The velocity could then be measured by observing the variations in the resulting Lissajous figure as the detector was moved down the tunnel. At very low speeds the temperature variations are destroyed by diffusion too quickly for this technique to work. It was, therefore, necessary to use the eddy frequency method incorporating a correction, obtained from the results of the other runs, for the deviations from Roshko's result. This 'mixing' of velocity measuring method undoubtedly resulted in a small loss of accuracy.

The results are presented in table 1 and plotted on a log-log scale in figure 1. For two of the fibres the points are termed 'fitted'; this means that full measurements of the fibre diameter and Young's modulus were not made, but the results were adjusted to fit in with those of other fibres. Fibres were sometimes broken during the diameter measurements which could then not be completed. Since the U *vs* h measurements give the slope of the $\log R$ *vs* $\log C_D$ curve, independently of the constants of the fibre, the adjustment consisted of moving all the points for one fibre without changing their relative position.

The overall accuracy of the figures given for the drag coefficient is estimated at around 6 %. The internal accuracy of the points for a single fibre is, however, much better and is estimated at around 2 %.

Figure 2 compares the results for the drag coefficient with those of Relf (1913) and of Wieselsberger (1921).* (The former made direct measurements of the force on a frame of wires; the latter observed the deflexion of a weight suspended on a wire in the air-stream.) The agreement is good at the centre of the range of overlap. Probably the lowest R points of the other workers were stretching their techniques a little beyond their limits. The disagreement of about 10 % around $R = 100$ is more puzzling. Four comments may be made about my results in this region of R:

(i) The length–diameter ratio tends to be lower for the fibres used at the higher Reynolds numbers, which might slightly accentuate the decrease in C_D.

(ii) A similar effect might arise for the points of each individual fibre, from the fact that at the higher speeds it is more bent and so less exactly perpendicular to the flow.

* Though Wieselsberger describes his experiments in this paper, his actual figures are given in Prandtl (1923).

(iii) There was a rather large scatter in the diameter measurements of fibre 8 which was probably due to variations along its length (of maybe 2 %).

(iv) It is possible that there was some interaction between fibre 8 and the vortex street behind it. The street frequency was typically around the fifth fibre resonance, which is a sufficiently high order for it not to be easily stimulated. However, the possession of resonant frequencies by the fibre could lead to a modification of the street frequency and so of the drag. For *a few* of the points the fibre was vibrating slightly (though this is thought to be due to resonance of the wind-tunnel motor), but there is good agreement between these and points for which the fibre appeared quite stationary.

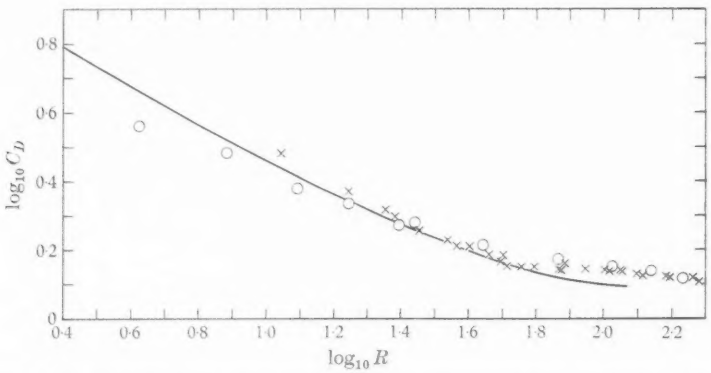

FIGURE 2. Comparison with other experimental measurements of the drag coefficient. ×, Relf; ○, Wieselsberger; —, Tritton.

Points such as these were taken into account in the above estimate of 6 % accuracy, but they do perhaps suggest that the error may be rather larger at the high R end of the curve. It seems unlikely, however, that this is sufficient to fully explain the difference from Relf and Wieselsberger, and I think that, despite their good mutual agreement, their measurements must be on the high side. Since neither author gives any discussion of systematic errors, it is difficult to tell how likely this is.

Figure 3 compares the present experimental results with the various theoretical calculations:

(i) The low Reynolds number solution of the Oseen equation, due to Lamb (1911).

(ii) Both Bairstow, Cave & Lang (1923) and Tomotika & Aoi (1950) have extended the solution of the Oseen equation to higher Reynolds number. Their results for the drag coefficient are in close agreement and are given as a single line in figure 3. This approach to the problem has been criticized by Proudman & Pearson (1957) on the grounds that the approximation involved in Lamb's solution is no worse than that already involved in the Oseen equation.

(iii) Southwell & Squire (1934) give a solution for Reynolds number 2, by a method similar to Oseen's, but supposing the convection to be conditioned by the irrotational velocities instead of the undisturbed velocity.

(iv) Kaplun (1957) gives a solution obtained by matching an Oseen solution far from the cylinder with a Stokes solution close to it. The effect is to give a third term in the low Reynolds number expansion, of which Lamb's solution gives the first two.

(v) Relaxational solutions of the Navier–Stokes equations: at $R = 1$ and 10 due to Allen & Southwell (1955); a rough solution at $R = 10$ (Thom 1929) and a detailed one at $R = 20$ (Thom 1933); and at $R = 40$ by Kawaguti (1953) and Apelt (1959), independently.

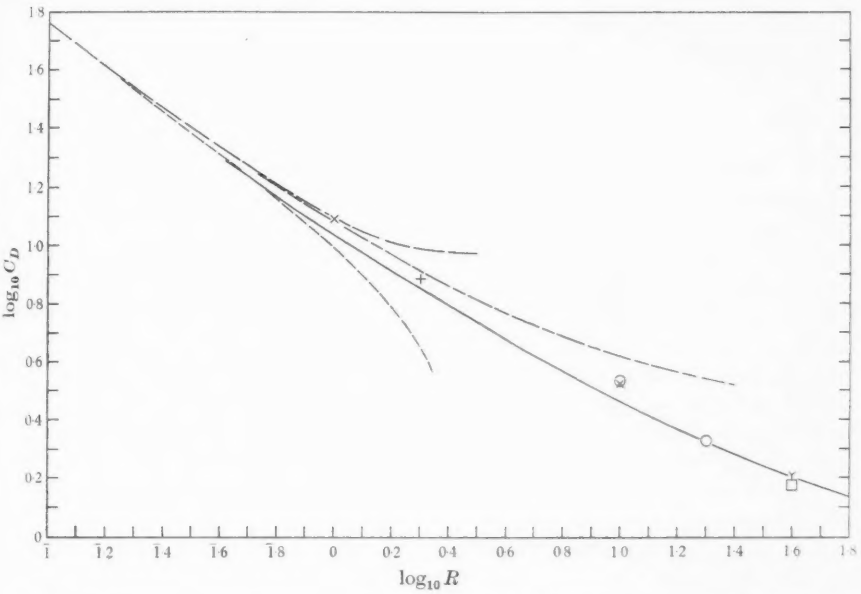

FIGURE 3. Comparison of the experimental curve with the various theoretical evaluations of the drag coefficient. —, Experimental (Tritton); — — —, Lamb; –·–·–, Bairstow, Cave & Lang; also Tomotika & Aoi; ----, Kaplun; +, Southwell & Squire; ×, Allen & Southwell; ○, Thom; Y, Kawaguti; □, Apelt.

The experimental points fit in satisfactorily with the overall picture given by these various theories. There is good agreement with the relaxation calculations particularly with Thom's at $R = 20$ and Kawaguti's at $R = 40$, which are thought to be particularly reliable calculations. At low Reynolds numbers, the experimental curve does not join on quite smoothly to the common curve of the theories, but the disagreement is within the limits of experimental error and there can be little doubt that the two curves should coincide for R less than about 0·6. The agreement with Kaplun's solution at rather higher Reynolds numbers than the others is satisfactory since this is a higher-order approximation.

The Reynolds number range covered by the present measurements includes the first appearance both of attached eddies and of the vortex street; the results should thus show what effects these changes have on the drag coefficient. Since the relative accuracy of points obtained from the same fibre is greater than

those from different fibres, the individual U *vs* h curves of the various fibres have been inspected. These show that there is no sharp discontinuity in the drag in either of the ranges $3 < R < 6$ and $30 < R < 45$. There is, however, some indication of a discontinuity around $R = 80$; this is presumably related to the phenomenon described in Part II and will be discussed there.

Part II. A Transition in Flow Past a Cylinder at $R \sim 90$

1. The discontinuity in frequency and amplitude

Roshko (1954) gives the relationship between the Reynolds number and the Strouhal number S (non-dimensional eddy frequency) as

$$\frac{nd}{U} = 0{\cdot}212 - \frac{4{\cdot}5}{R}$$

in the range $50 < R < 150$. (Here n is the frequency in the vortex street as given by a detector fixed relative to the cylinder.) In this range the street just dies out slowly as it is traced downstream; there is no turbulence.

Whilst I was using this result for measuring velocities (as described in Part I), it became apparent that it is not quite correct; there is a small discontinuity in the velocity-frequency curve. This is shown in figure 4, where frequency is plotted against velocity for three runs. The frequency was measured by putting the amplified output of a hot-wire anemometer placed in the wake onto the Y-plates of an oscilloscope and adjusting the frequency of an electronic oscillator on X-plates until a Lissajous figure was obtained. The velocity was obtained by recalibrating the quartz-fibre as described in Part I.

In each diagram of figure 4 the points fall on two separate lines; the transition between the two involves a sudden decrease of around 5 % in frequency as the velocity is increased. The broken line on each plot is the velocity-frequency dependence given by Roshko's formula. This does not come in just the same position relative to the points each time. The reason is that the internal accuracy of a single run is again markedly better than its absolute accuracy; if all the runs were shown on a single Reynolds number *vs* Strouhal number plot, the discontinuity would probably not be apparent. This is, incidentally, probably why it has not been noticed by other workers.

As a result of a detailed consideration of the runs shown in figure 4 together with a number of similar runs, it is suggested that Roshko's formula be replaced by two sections of the form $SR = a + bR + cR^2$,

with a, b and c taking the following values:

	a	b	c
$50 < R < 105$	$-2{\cdot}1 \pm 0{\cdot}3$	$0{\cdot}144 \pm 0{\cdot}010$	$0{\cdot}00041 \pm 0{\cdot}00010$
$80 < R < 150$	$-6{\cdot}7 \pm 0{\cdot}2$	$0{\cdot}224 \pm 0{\cdot}006$	0 ($\lvert c \rvert < 0{\cdot}00025$)

The errors are a combination of standard errors of the mean and small estimated systematic ones. Those on a, b and c may be regarded as indicating how well the equation gives, respectively, the position, slope, and curvature of the varia-

tion. The uncertainty in a is thus the principal guide to how well the formulae determine the Strouhal number for a given Reynolds number. The errors on the two limbs are, of course, interdependent; the frequency difference between the two modes in the transition region may be given as

$$\Delta(SR) = 0{\cdot}7 \pm 0{\cdot}1.$$

The equation for the low-speed mode is likely to be biased in favour of the upper end of the range, since in many runs the speed at $R \sim 50$ was too low to be measured by tracing heat pulses.

At a speed in the range $80 < R < 105$, the frequency is likely to be found on one of the two lines rather than between them. The behaviour of the flow in this

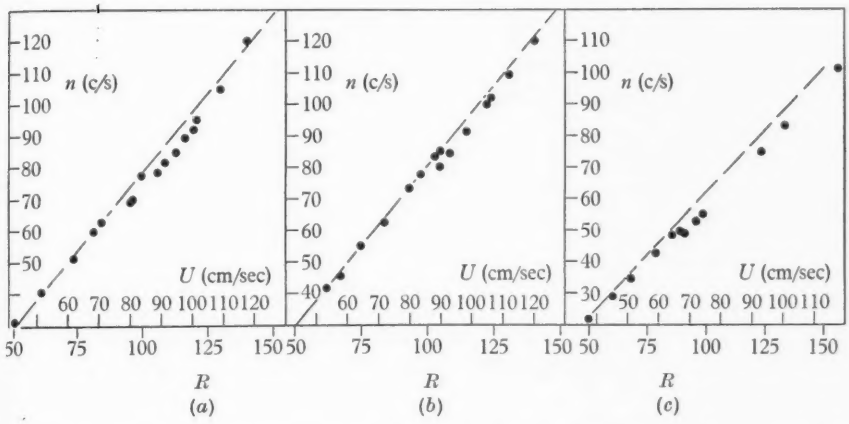

FIGURE 4. Three velocity-frequency plots showing the discontinuity. (*a*) Cylinder of diameter 0·178 cm, producing a long overlap between modes. (*b*) Same cylinder remounted, producing a sharp transition between modes, both frequencies being measurable at $U \sim 90$ cm/sec. (*c*) Cylinder of diameter 0·203 cm, with one point of intermediate frequency in transition region. The broken line in each plot is given by Roshko's formula.

transition region will be described more fully shortly, but, in connexion with the Reynolds number ranges for the two modes, it should be noted that when the low-speed mode occurred with $R > 95$, it almost always had irregularities. At lower speeds than this, irregularities could occur but did not necessarily do so.

All the above conclusions are based on wind-tunnel experiments. Water-channel investigations sometimes showed the transition beginning at speeds as low as $R = 70$.

Associated with the sudden decrease in frequency is a decrease in the intensity of the velocity fluctuations. (This probably means that the vortices are weaker, but could be due to the same amount of vorticity being more diffusely distributed.) This is shown in figure 5. At each speed a constant-current hot-wire anemometer 14·2 diameters downstream of the cylinder was traversed at right angles to the wake until the amplitude of its output was a maximum. This amplitude was then measured in arbitrary units (the scale on an oscilloscope screen) and plotted as

the ordinates of figure 5.* There is considerable scatter at the lowest speeds; apart from this, the graph shows an upward trend of amplitude with increasing speed on either side of a sharp drop. Simultaneous frequency measurements (figure 4*b*) showed that the flow changed from the low-speed mode to the high at the sharp drop; there was some unsteadiness in the frequency at 83·7 and 88·0 cm sec^{-1}, and at 90·1 cm sec^{-1} both frequencies were present, though it was possible to measure the amplitude of only the low-speed mode. That of the high-speed mode was clearly smaller.

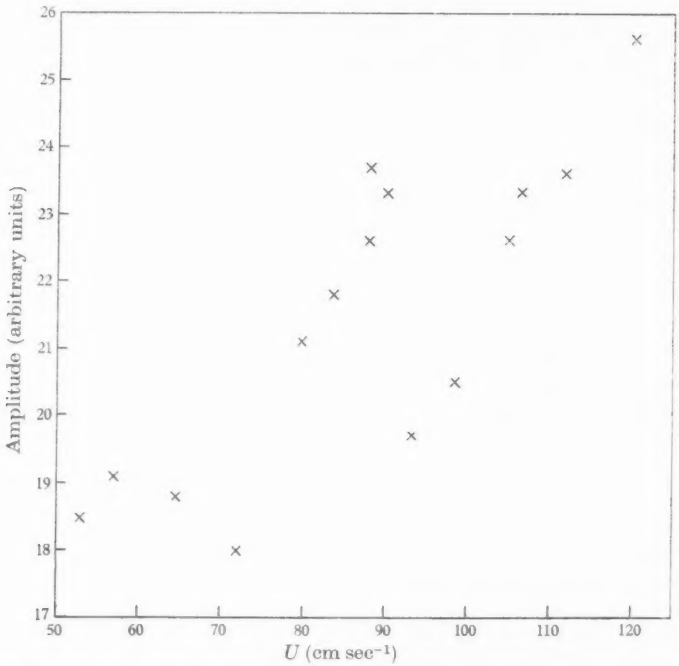

FIGURE 5. Plot of amplitude of output of constant-current hot-wire anemometer at amplitude maximum (with respect to y) against velocity for run shown in figure 4*b*.

The value of y (distance from the centre of the wake) was noted for each observation, but the maxima were too broad for any change in this at the transition to be detected.

2. Experimental arrangements

An investigation was carried out in the range of speeds between the two modes, where a more complex behaviour than either occurs. It shows a number of interesting features and, by indicating how each mode behaves when affected by the other, throws some light on the difference between the two. The observations

* Since the current through the hot-wire was held constant throughout the observations, the relationship between the velocity fluctuations and the observed amplitude depends in a complex way on the mean velocity (which is in any case an unknown quantity) at the position of the maximum. Only the discontinuity is significant in figure 5, not the form of the variation on either side of it. The constant-current method was chosen for experimental simplicity.

to be described suggest that the low-speed mode arises from an instability of the wake, whereas in the high-speed mode the vortex street is directly affected by the walls of the cylinder. The two modes have themselves been examined, as well as the transition between them, and some of the experiments show their contrasting features.

Experiments were carried out in both the wind-tunnel and a water-channel. The flow in the former was studied by making photo-traces of hot-wire outputs (with a drum-camera photographing an oscilloscope). The hot-wire probes used were of Wollaston wire with long unetched portions. This allowed the support to be outside the wake where it does not affect the street; it has been noted (see, for example, Kovasznay 1949) that distortion can be produced by having the support directly downstream of the wire, and I found that such an arrangement could even produce a change in the frequency when the wire was close to the cylinder. When only one wire was placed in the wake a time-scale could also be put on the photo-trace, but in a number of experiments both oscilloscope beams were used to indicate hot-wire outputs so that correlations between different positions in the wake could be studied.

The results could not be fully interpreted without visualization of the flow; the water-channel experiments, which I did not attempt to make quantitative, served this purpose. The channel used is open-topped, the water having a free surface. It enters through a 'honeycomb' which is followed by a short contraction before the working section. This does not give entirely uniform flow, but a cylinder of about 0·3 cm diameter placed vertically at the centre of the channel was clear of the velocity variations. The depth was about 14 cm, giving a length of about 30 diameters in which there were no wall or surface effects. The working section extended for about 20 cm beyond the cylinder before the flow was affected by the weir at the downstream end. Dye (potassium permanganate solution) was put into the flow through a small hole in the back of the cylinder producing the wake; this arrangement is better than putting the dye in upstream as it concentrates it close to the centre of rotation of each vortex and so gives a good picture of the motion of the vortices. (The dye comes away from the cylinder at the two separation points and thus gets into the regions of high vorticity.) This technique does not, of course, give any indication of three-dimensional effects. These were studied by using a cylinder coated with metallic tellurium; making this the cathode of an electrolytic cell (6 to 9 V between the cylinder and the walls of the channel proved satisfactory) produces marker all along the cylinder. The arrangement was similar to that in the dye experiments; because of the need to have the cylinder vertical, the vortex lines had to be viewed and photographed through a mirror.

In the water experiments, the approximate Reynolds number was determined from the eddy frequency.

3. Observations of the subcritical, critical and supercritical flows

Figure 6 (plate 1) shows the subcritical, critical, and supercritical flows (the term 'critical' being applied to the $R \sim 90$ transition). Photos 6*a* and *e* are of the low- and high-speed modes; both exhibit quite regular vortex streets. There is some

suggestion that in the high-speed mode the dye is less diffusely distributed, but this may be due to the fact that the same amount of dye was going into a faster flow. During the course of the experiment, I was unable to tell whether the flow was sub- or supercritical by looking at the vortices. A difference was apparent, however, when dye was put into the attached eddies (this was easily done by allowing the potassium permanganate to come out of the hole as a jet for a short while). Then in the low-speed mode the dye remained in the attached eddies (though there were oscillations of the vortex street frequency in this region), whilst in the high-speed mode it was removed by the fluctuations in a few cycles.

Photos 6*b*, *c* and *d* illustrate the critical flow. Irregularities of the type shown in 6*b* and *d* are a common feature of this flow. The pictures do *not* show a steady state. The irregularity first appears only a few diameters behind the cylinder (though only if dye is injected into the attached eddies can it be seen to affect these) and produces strongest lining-up (small or zero lateral separation of the vortices associated with increased longitudinal separation) at typically 20 diameters. The irregularity then travels further downstream with some reduction in the lining-up. The eddies upstream of this sometimes increase their lateral separation up to about 3/2 its normal value; this does not occur, however until typically 30 diameters behind the cylinder when the main part of the irregularity is still farther downstream. Photo 6*c* shows the same flow as 6*b* but between irregularities; one irregularity has just gone out of the picture downstream and another is just forming close to the cylinder.

Figure 7 (plate 2) shows the development of the irregularities as revealed by the wind-tunnel photo-traces. Even when the vortices have been largely dissipated by viscosity, the irregularities persist, thus producing some weak long time-scale turbulence.

Dye injected into the attached eddies in the transition flow stayed for some while and was then all removed very quickly. This could be regarded as the start of an irregularity. The dye removed in this manner went into the street a few eddies downstream of the ones that showed maximum lining-up.

The water-channel observations gave some indication that the irregularities travel upstream relative to the vortices. This is confirmed by wind-tunnel experiments with two hot-wires at different distances downstream (and separated slightly parallel to the cylinder so that one was not in the wake of the other); figure 8 (plate 2) shows a trace so produced. On average the irregularities had a velocity of about $0{\cdot}5U$ relative to the cylinder, though it varied considerably, occasionally going as low as $0{\cdot}3U$ and occasionally being very little less than U. There is some disagreement as to how fast the vortices themselves move—to take extreme examples, Tyler (1931) observed velocities mostly between $0{\cdot}7U$ and $0{\cdot}8U$, whilst Kovasznay's (1949) results imply a velocity of about $0{\cdot}98U$—but it is certainly faster than the irregularities.

Some two-wire experiments were also carried out with the separation in the y-direction. They showed, as the water-channel observations would lead one to expect, complete correlation of the irregularities across the wake.

It should be stressed that the behaviour being described here occurs not only

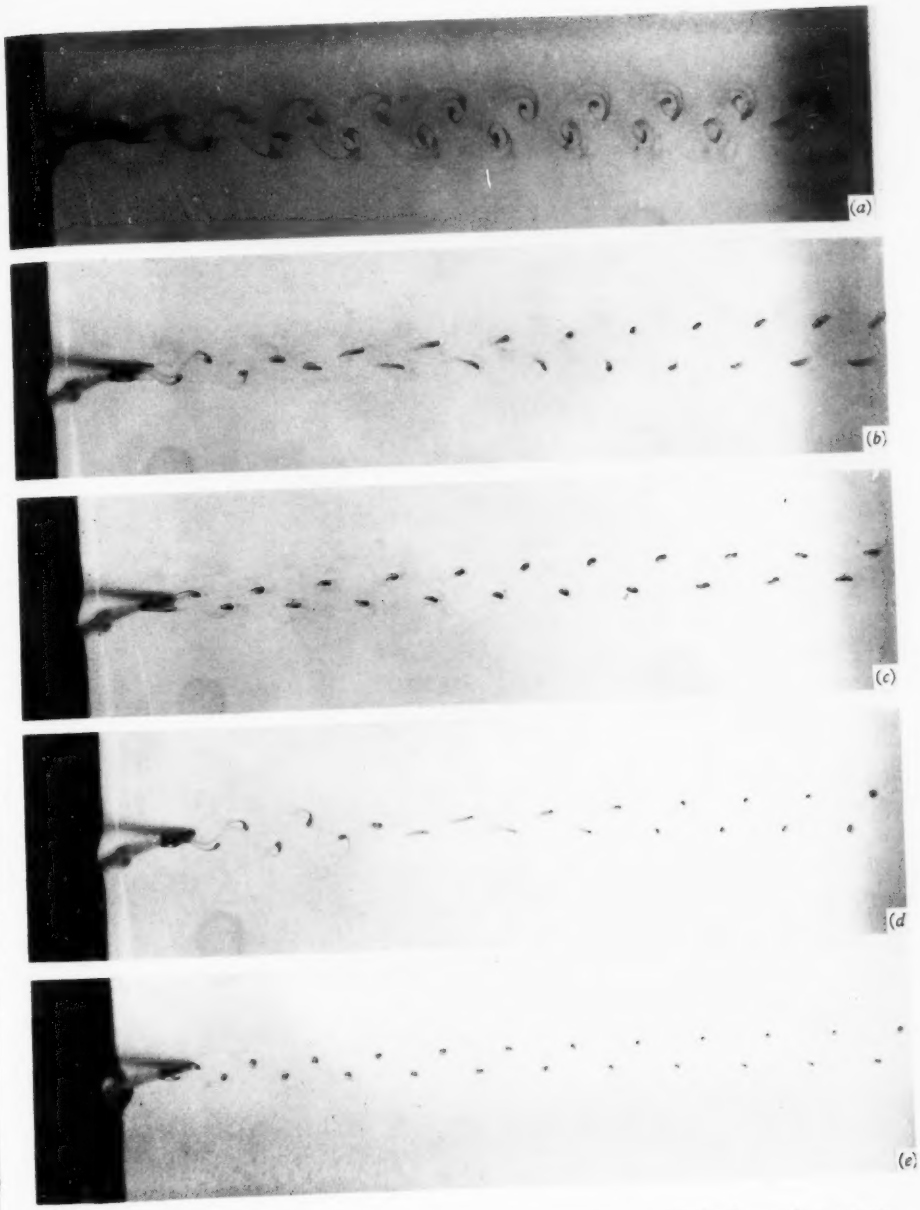

FIGURE 6. Water-channel photographs of the vortex streets (the cylinder is seen in perspective). (*a*) $R = 60$; low-speed mode. (*b*) $R = 75$; one of a sequence of randomly spaced irregularities. (*c*) $R = 75$; between irregularities. (*d*) $R = 79$; one of a periodic sequence of irregularities. (*e*) $R = 89$; high-speed mode.

(*Facing p.* 560)

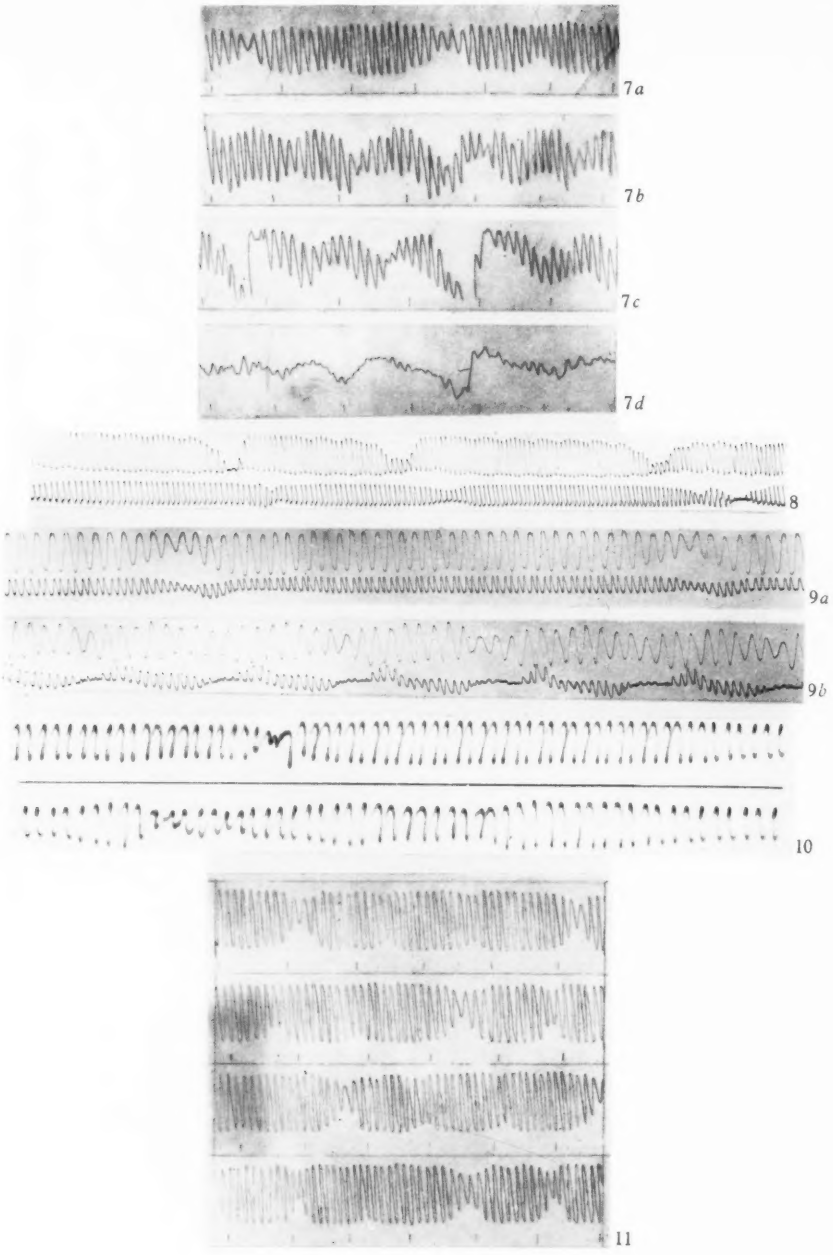

FIGURES 7 TO 11

DESCRIPTION OF PLATE 2

In all the photo-traces, time goes from left to right and, except where otherwise stated, the top corresponds to maximum velocity.

FIGURE 7. Photo-traces showing the development of randomly spaced irregularities as they travel downstream behind a cylinder of 0·178 cm diameter. The short lines on each trace mark 0·1 sec intervals. (*a*) $R = 102$; $x/d \sim 1{\cdot}5$; $y/d = 1{\cdot}0$. (*b*) $R = 101$; $x/d = 28{\cdot}5$; $y/d = 1{\cdot}8$. (*c*) $R = 104$; $x/d = 57$; $y/d \sim 2{\cdot}5$. (*d*) $R = 102$; $x/d = 104$; $y/d \sim 4$.

FIGURE 8. Simultaneous traces at different distances downstream behind a cylinder of diameter 0·178 cm, showing randomly spaced irregularities at $R = 105$. Upper trace—$x_1/d = 1{\cdot}5$; $y_1/d = 0{\cdot}7$. Lower trace—$x_2/d = 15{\cdot}7$; $y_2/d = 1{\cdot}0$ (the bottom corresponds to the maximum velocity). The separation of the irregularities on the two traces indicates the speed at which they travel downstream.

FIGURE 9. Photo-traces showing (*a*) randomly spaced irregularities and (*b*) periodically spaces ones, off-centre and at the centre of the wake. (*a*) $R = 98$; $x_1/d = x_2/d = 1{\cdot}5$; $y_1/d = 2{\cdot}5$; $y_2/d = 0$. (*b*) $R = 101$; $x_1/d = x_2/d = 14{\cdot}2$; $y_1/d = 2{\cdot}7$; $y_2/d = 0$. Note that in the two traces at the centre of the wake, the bottom corresponds to the maximum velocity.

FIGURE 10. Photo-trace showing intermittent jumps between the two modes. The two parts join straight onto one another. $R = 107$; $x/d = 15{\cdot}7$; $y/d = 1{\cdot}0$.

FIGURE 11. Photo-trace showing repetition of a complex pattern in the irregularities. The sequence of a large amplitude diminution followed after 10 wavelengths by a smaller one, then after another 11 wavelengths by an even smaller one, and then after 13 wavelengths by a large one, is repeated five times over. $R = 106$; $x/d \sim 1{\cdot}5$; $y/d = 1{\cdot}1$.

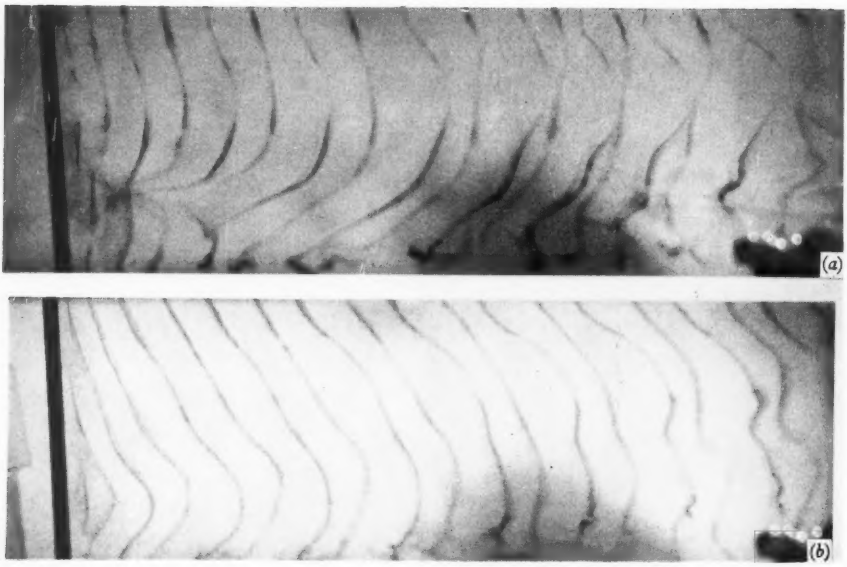

FIGURE 12. Tellurium experiments showing behaviour of the vortices parallel to the cylinder. (*a*) The occurrence of irregularities; $R = 78$. (*b*) High-speed mode, showing tendency for vortex lines to become wavy; $R = 88$.

when the flow changes from one mode to the other as a result of a speed change, but also as a repeated phenomenon when the Reynolds number is held in the short critical range between the two modes. A sequence of irregularities, usually similar to one another, with steady vortex streets between them, is then to be observed. The spacing can be either random or periodic. The flows shown in photos 6*b* and *d* differ in that in the former the irregularities were not evenly spaced, whereas in the latter they always had approximately 14 wavelengths between them. Figure 9 (plate 2) makes the same contrast for the wind-tunnel observations; photos 9*a* and *b* show the traces produced by a pair of hot-wires at the centre and a little off the centre of the wake for, respectively, random and periodic irregularities. Traces with a time-scale suggest that when the irregularities are randomly spaced the carrier frequency is that of the low-speed mode, and when they are periodic it is that of the high. In the latter case, considerable variation of the periodicity has been observed; the limits are about 6 and 14 wavelengths between consecutive irregularities. The frequency thus averages about twice the beat frequency of the two modes. I have not managed to relate the variations to any other feature of the flow.

The photo-traces revealed a wider variety of behaviour than the water-channel observations. Sometimes the amplitude modulation of a single carrier-frequency as described above did not occur at all; the transition region was then marked by a flow that would make sudden jumps from one mode to the other. These usually occurred too often for the frequencies between them to be measured on the photo-traces, but the modes could be identified by their different amplitudes (as in figure 10 (plate 2)); also the presence of the two frequencies could be detected by Lissajous figure observations on an oscilloscope. When this behaviour occurred the transition range was short, covering typically a difference of about 4 in Reynolds number (though there was considerable variation from one run to another of the position of this range).

More usually the transition flow occurred over a larger Reynolds number range of extent up to 10. The photo-traces then showed the more complex behaviour already discussed. Increasing the speed in small stages through the transition region could then produce in turn the low-speed mode modulated by random irregularities and the high-speed mode modulated by periodic ones. The former occasionally showed a striking repetition of a complex pattern in the irregularities, as illustrated by figure 11 (plate 2). This sort of odd behaviour is characteristic of the flow when it is in the low-speed mode at a speed at which it is normally in the high.

The photo-traces of figure 9 both show that at the centre of the wake the irregularities produce not only an amplitude modulation but also some variation in the mean velocity. This contrasts with the behaviour sufficiently far from the centre for the first harmonic to dominate; here the irregularities produce only amplitude modulation (together, of course, with the change in the spacing of the peaks corresponding to the increase in longitudinal spacing of the vortices). When the irregularities are periodic the mean velocity variation is almost sinusoidal. When they are random there is a peak shortly after each minimum in the amplitude (which is regarded as the main part of the irregularity); the

mean velocity does not change during the diminution. It thus appears that the irregularities have a flow into them from behind, a feature not apparent from the water-channel visualization. An alternative way of looking at this is to say that after the passage of an irregularity the flow is in a mode with a slightly different velocity profile at the centre of the wake from before and during its passage.

It is difficult to give a full interpretation of the photo-traces in terms of the observed motion of the vortex centres, as it is not clear how diffusely the vorticity is distributed; there is considerable difference between the velocity field of an ideal Karman street and one plotted out from experimental data (see, for example, Kovasznay (1949)). However, it seems satisfactory to associate the type of motion usually observed in the water-channel with the more complex of the transition features observed in the wind-tunnel. A different behaviour that also occurred in the water experiment, but only rarely, may then be associated with the sudden jumps between the modes. This different behaviour showed short transitions between the normal flow and a flow in which the eddies were very diffuse close to the cylinder, and in which some of the dye went into an amplified sinusoidal motion down the centre of the wake. This change did, of course, produce irregularities but they did not show the characteristics of the usual ones.

Presumably the exact behaviour in the transition region that occurs on any particular occasion is governed by small unobserved deviations from the theoretical arrangement. If the cylinder was slightly bent, a fairly complex motion always occurred. On the other hand, it was not always possible to produce a simple behaviour by taking care to make the cylinder straight.

The water-channel experiments on three-dimensional effects show that the irregularities are localized in the z-direction (parallel to the cylinder). This is shown in figure 12*a* (plate 3) in which one irregularity is just appearing close to the cylinder and another, at a different z, has travelled some distance downstream. An irregularity affects the flow for a distance of about six or eight diameters in the z-direction; outside this the vortex lines continue as normal.

The three-dimensional visualization was also examined to see whether it revealed any differences between the low- and high-speed modes. The differences are not so striking that they immediately revealed which mode the flow was in. There is, however, a general tendency for the vortex lines (identifying these with the observed lines of marker) to be straighter in the low-speed mode. This does not necessarily imply that the vortex lines are parallel to the cylinder in this mode; it requires only that the phase variation of the eddy production is proportional to z. In both modes angles of up to 30° or so between the vortex lines and the cylinder have been observed. However, vortex lines parallel or nearly parallel (at say $< 10°$) to the cylinder are more common in the low-speed mode than in the high. This tendency for the phase to be the same at different z for $R <$ about 90 but not for $R > 90$ has already been noted by Phillips (1956). In the high-speed mode any kinks in the vortex lines produced by the initial conditions are able to persist. Also, with increasing R there is a stronger tendency for bends to develop spontaneously (as illustrated by figure 12*b*); this is a trend towards the transition occurring at $R \sim 150$, when a three-

dimensional instability sets in producing both bends in the vortex lines and irregular motions of the vortices in the two-dimensional visualization.

The effect of a slight bend in the cylinder was investigated. The tendency for the bend to be reflected by a kink in the vortex lines is more marked in the high-speed mode than in the low.

The difference between the two modes was investigated with one further arrangement. The cylinder emitting dye through a small hole was used again, but with the hole at 90° to the front stagnation point. This was intended primarily to test the suggestion that the high-speed mode differs from the low in not possessing attached eddies; there would then be a single rear stagnation point of oscillating position. This is not the case, since the dye all left the cylinder wall at a single point some way in front of the rear generator in both modes; there were no oscillations of this point and no dye was carried across to the corresponding point on the other side. However, this arrangement did reveal a difference between the two modes further downstream. In the high-speed mode, the dye leaving the cylinder on one side of the wake went only into the vortices on that side. In the low-speed mode, on the other hand, there was a transfer of dye across the centre of the wake and it went almost equally into the two sides of the vortex street, though it was more diffusely distributed on the far side. It was thus clear that there was further development of the street downstream of the oscillating attached eddies, the street eddies being linked by an amplified sinusoid of dye. This feature was not shown by the high-speed mode.

With the hole between one of the separation points and the rear generator, most of the dye left the cylinder at the separation point on that side. A small amount was, however, transferred across to the other one, presumably by diffusion in the low-speed mode (dye can then accumulate in the attached eddies) and by the oscillations in the high-speed mode.

4. Effect of the transition on drag

The results of the experiments described in Part I have been examined to see whether the $R \sim 90$ transition affects the drag. As stated there, the U *vs* h curve for an individual fibre is more likely to reveal a change than the overall R *vs* C_D curve. The U *vs* h curve covering this Reynolds number is shown in figure 13. A glance along the points suggests that there might be a discontinuity in slope between $U = 1000$ and 1100 cm sec^{-1}, which correspond respectively to $R = 76{\cdot}5$ and $84{\cdot}0$. Since, however, the evidence for the discontinuity is not wholly convincing, the points have been analysed statistically, by making least squares fits of the points on either side of the suspected discontinuity to quadratics,* and comparing the differences in the coefficients with their standard errors. No significant discontinuity in slope was indicated, but the results did indicate a discontinuity, significant at the 5% level, in the actual value of h. The change was upwards with increasing U. This suggests that the transition does have some effect on the drag, but it is not evident just what. The point at $U = 1016$

* The origin, which is, of course, necessarily a point, was *not* included, as it would clearly have strongly influenced the fit and the logarithmic nature of the low Reynolds number solutions indicates that it would not fit in with any quadratic approximation.

cm sec^{-1}, which has a particularly high h, is obviously strongly influencing the result, and it may be that this point is in the transition region and should not be included in either fit (the analysis indicating the discontinuity includes it in the high velocity one). Clearly, further experiments are required, and the author hopes to be able to do these in due course.

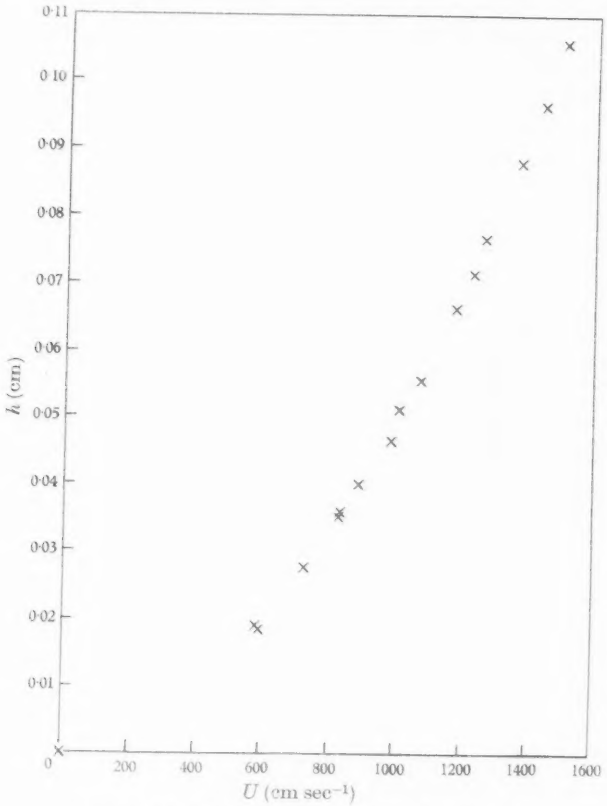

FIGURE 13. Velocity-deflexion curve for fibre 8.

5. Discussion

The most satisfactory explanation of the $R \sim 90$ transition seems to be the following. The first appearance of the vortex street at $R \sim 40$ is the result of an instability of the wake; the only role of the cylinder is to produce the velocity profile. The reason that the instability gives rise to a persisting periodic motion rather than turbulence is probably that the Reynolds number (based on the wake itself—not the cylinder producing it) is independent of the distance downstream; this contrasts with a two-dimensional jet in which the Reynolds number increases with x. For the same reason, it is to be expected that the beginning of instability will be close to the cylinder.

As the speed is increased, the development from this first appearance to a full vortex street is compressed more and more into a region just behind the cylinder

until the formation of the street is directly affected by its walls. The attached eddies might also have an effect, but since the velocity profiles in this region are similar to those further downstream except for their crossing the zero line (Kovasznay 1949; Kawaguti 1953) this is unlikely.

In the transition region the effect of the walls is only partial, but, when the flow is in the high-speed mode the origin of the vortex street is in the immediate vicinity of the cylinder. It no longer grows from an instability of a given velocity profile, so that the factors governing its parameters (frequency, spacing of eddies, etc.) are different. Frequency and amplitude discontinuities at the transition are thus plausible.

On either side of the critical Reynolds number, there are oscillations with the vortex street frequency of the attached eddies. The distinction is that, in the low-speed mode, these oscillations are produced by the beginnings of an instability which develops further as it goes downstream, whereas, in the high, a fully developed vortex street exists right from its start close to the cylinder. In the low-speed mode the same fluid remains in the attached eddies throughout, whilst in the high the fluid there is continually moving into the vortex street; only then is the common way of speaking of the vortex street being produced by shedding of the attached eddies strictly correct.

These conclusions imply that attempts to provide a theoretical derivation of the parameters of the vortex street must be differently based for the two modes. The well-known treatment by von Kármán (see Lamb 1932, § 156) of an infinite double row of equal point vortices provides primarily an explanation of why the street, once formed, should be stable; the reasons for the formation with a spacing-ratio fairly close to the theoretical stability requirement must lie in the mechanism of the formation. For the low-speed mode a stability theory of the wake seems likely to be appropriate. Hollingdale (1940) has developed such a theory for a parallel wake with $R \to \infty$ and attempted a comparison with experiments on wakes of flat plates at zero incidence and aerofoils. The comparison is difficult because of changes in the wake with distance downstream and this difficulty is likely to be even more marked for the cylinder. However, the partial success of Hollingdale's comparison, together with Taneda's (1958) observation that the wakes of plates and cylinders behave similarly, once they are clear of the direct influence of the walls, does suggest that an instability of the wake could give the observed value of the longitudinal spacing. For the high-speed mode, on the other hand, the above interpretation suggests that the eddy frequency is governed by the oscillations in the immediate vicinity of the cylinder; this, together with the speed with which the eddies travel downstream, then determines the longitudinal spacing. Birkhoff's (1953) rough derivation of the Strouhal number by considering the wake swinging from side to side as a solid simple harmonic oscillator might apply here, though it should be remembered that the attached eddies now consist of continually changing fluid.

There is one quantity that can be crudely estimated for either of these ideas about the origin of the street, namely the lateral spacing. Eddies produced by a wake instability are likely to have their centres close to the points of inflexion in the velocity profile (more specifically, the laminar profile at the origin of the

instability); the experimental profiles given by Kovasznay (1949) indicate that these are between 0·9 and 1·5 diameters from the centre line. On the other hand, eddies produced close to the cylinder are likely to be at about the same y as the maximum vorticity there; Kawaguti's (1953) numerical solution suggests that this is in the range 0·4–0·8 diameters. Observed lateral separations in the two modes (as in photos 6*a*, *e*, and other similar ones) are consistent with these interpretations; so too are wind-tunnel observations of the position of maximum amplitude (though it is not clear just how this position is related to the centre of rotation). In each mode, however, there is a continuous decrease of lateral separation with increasing Reynolds number, so that the observations may not be specifically a feature of the two modes; there was too much scatter for any discontinuity in the lateral separation at the transition to be detected.

Although there is no direct evidence on this point, the data seem to require a discontinuity in the longitudinal separation. For a von Kármán ideal vortex street the frequency is related to the longitudinal and lateral spacings s_1 and s_2, the strength of each vortex κ, and the free stream velocity U by

$$n = \frac{U}{s_1} - \frac{\kappa}{2s_1^2} \tanh \frac{\pi s_2}{s_1}.$$

It is known that n decreases at the transition, and the indications are that κ and s_2 both decrease. Since the second term is always small compared with the first, s_1 must increase. This contrasts with its general trend, which, like that of s_2, is downwards with increasing Reynolds number.

This change in longitudinal spacing is thought to be the root of the behaviour of the transition flow. If the speed is such that the high-speed mode is just beginning to produce vortices but their motion downstream is governed by the wake instability, then they will take up a longitudinal spacing that is too small for the rate at which they are being produced. This can continue only for a short while; there will then be a compensating region of increased longitudinal spacing, which could well produce the sort of irregularity shown in figures 6*b* and *d*. In all the photographs, such as these two, the vortices in an irregularity line up with those downstream of it more smoothly than with those upstream. This suggests that the street is forced into the large spacing of an irregularity by the rate at which vortices are formed, and then breaks off and starts anew in the mode with the small spacing.

Since, when the irregularities are randomly spaced, the carrier frequency is the low-speed mode, the flow is then presumably only intermittently inclined to produce vortices at the supercritical frequency. At slightly higher speeds they are continuously produced at this frequency, but still pulled into the subcritical spacing; the irregularities are then periodic. It is plausible that, in these circumstances, each one should take about the same time to develop, but attempts to produce a full theory of the periodicity have been unsuccessful.

The above remarks have, for the sake of simplicity, treated the behaviour as two-dimensional. It should be remembered that, in fact, the irregularities are localized in the third dimension. The return to regular street after an irregularity is probably brought about by the undistorted vortex lines on either side.

An alternative interpretation of the transition as the first onset of three-dimensional instability has been rejected, because it seems unlikely that this would produce supercritical streets as regular as the subcritical ones (compare photos 6*a* and *e*). The three-dimensional differences between the two modes, described earlier, are thought to be due to the high-speed mode being more directly affected by conditions at the cylinder than the low. The behaviour at $R \sim 150$ suggests that the beginning of three-dimensional instability occurs there.

My gratitude is expressed to all the members of the fluid mechanics group in the Cavendish Laboratory who have contributed in discussions to my understanding of the problem; I must mention by name Dr A. A. Townsend. I am also grateful to Mr A. M. Walker of the Cambridge University Statistical Laboratory who suggested the significance tests in § 4 of Part II and carried out the computations involved, and to Mr W. E. Thompson for his help in making apparatus. The water-channel used is in the hydraulics department of the Cambridge University Engineering Laboratories and my thanks go to all there for their co-operation. I also wish to acknowledge receipt of a maintenance grant from the Department of Scientific and Industrial Research.

REFERENCES

Allen, D. N. de G. & Southwell, R. V. 1955 *Quart. J. Mech. Appl. Math.* **8**, 129.
Apelt, C. J. 1959 *Rep. and Memo., Aero. Res. Counc., Lond.* (To be published.)
Bairstow, L., Cave, B. M. & Lang, E. D. 1923 *Phil. Trans.* A, **223**, 383.
Birkhoff, G. 1953 *J. Appl. Phys.* **24**, 98.
Goldstein, S. (ed.) 1938 *Modern Developments in Fluid Dynamics.* Oxford University Press.
Hollingdale, S. H. 1940 *Phil. Mag.* (7), **29**, 209.
Homann, F. 1936 *Forsch. Geb. IngWes.* **7**, 1.
Kaplun, S. 1957 *J. Math. Mech.* **6**, 595.
Kawaguti, M. 1953 *J. Phys. Soc. Japan*, **8**, 747.
Kovasznay, L. S. G. 1949 *Proc. Roy. Soc.* A, **198**, 174.
Lamb, H. 1911 *Phil. Mag.* (6), **21**, 112.
Lamb, H. 1932 *Hydrodynamics*, 6th edn. Cambridge University Press.
Nisi, H. & Porter, A. W. 1923 *Phil. Mag.* (6), **46**, 754.
Phillips, O. M. 1956 *J. Fluid Mech.* **1**, 607.
Prandtl, L. (ed.) 1923 *Ergebn. Aerodyn. VersAnst. Göttingen*, **2**, 23.
Proudman, I. & Pearson, J. R. A. 1957 *J. Fluid Mech.* **2**, 237.
Relf, E. F. 1913 *Tech. Rep. and Memo., Adv. Comm. Aero.* (*A.R.C.*), *Lond.*, no. 102.
Roshko, A. 1954 *Rep. Nat. Adv. Comm. Aero., Wash.*, no. 1191.
Schmidt, E. 1934 *Proc. 4th Int. Congr. App. Mech.* (*Camb.*), p. 92.
Schmidt, E. & Beckmann, W. 1930 *Tech. Mech. Thermodynam.* **1**, 341, 391.
Southwell, R. V. & Squire, H. B. 1934 *Phil. Trans.* A, **232**, 27.
Taneda, S. 1956 *J. Phys. Soc. Japan*, **11**, 302.
Taneda, S. 1958 *J. Phys. Soc. Japan*, **13**, 418.
Thom, A. 1929 *Rep. and Memo., Aero. Res. Coun., Lond.*, no. 1194.
Thom, A. 1933 *Proc. Roy. Soc.* A, **141**, 651.
Tomotika, S. & Aoi, T. 1950 *Quart. J. Mech. Appl. Math.* **3**, 140.
Tritton, D. J. 1959 *Phil. Mag.* (in the Press).
Tyler, E. 1931 *Phil. Mag.* (7), **11**, 849.
Wieselsberger, C. 1921 *Phys. Z.* **22**, 321.
Wieselsberger, C. 1922 *Phys. Z.* **23**, 219.

On the generation of surface waves by shear flows. Part 2

By JOHN W. MILES
Department of Engineering, University of California, Los Angeles

(Received 19 February 1959)

A previous analysis for the generation of surface waves by a parallel shear flow (Miles 1957*a*) is extended by: (*a*) presenting results based on a more accurate solution of the differential equation; (*b*) imposing the boundary condition at the surface wave, rather than at the mean surface; and (*c*) including the dominant viscous term in the complete Orr–Sommerfeld equation. The modification (*a*) yields an energy transfer somewhat smaller than that predicted previously but of the same order of magnitude as, and in rather better agreement with, observation, while (*b*) has no effect and (*c*) only a small effect for gravity waves. The analysis is based on the equations of motion in intrinsic co-ordinates (rather than the usual Orr–Sommerfeld equation) and may be of interest in other problems of hydrodynamic stability.

1. Introduction

This paper is a sequel to an earlier paper of the same title (Miles 1957*a*, hereinafter denoted by I). The principal result obtained there was that the mean rate at which energy is transferred from a parallel shear flow $U(y)$ to a surface wave of wavelength $2\pi/k$ and wave-speed c is given by

$$\overline{\dot{E}} = -\rho_a c(\pi U_c''/kU_c')\overline{v_c^2}, \tag{1.1}$$

where ρ_a denotes the density of the upper fluid (typically air), U_c'' and U_c' the curvature and slope of the wind profile at the point where $U = c$, and $\overline{v_c^2}$ the mean-square value of the vertical velocity there.†

The ultimate boundary-value problem posed in I was the solution of the inviscid Orr–Sommerfeld equation subject to boundary conditions at infinity and at the mean (undisturbed) position of the surface; this boundary-value problem was not actually solved, however, only an integral approximation for the energy-transfer coefficient having been obtained. The purpose of the following analysis is to: (*a*) present results based on an accurate integration of the differential equation (Miles & Conte 1959); (*b*) impose the boundary condition at the surface wave,

† In the notation of I, $\dot{E} = \zeta kc\bar{E}$, where $\bar{E}$ denotes the mean energy and $-\pi\zeta$ denotes the logarithmic decrement. The results then were presented in terms of a coefficient β, such that $\zeta = \sigma\beta(U_1/c)^2$, where $\sigma = \rho_a/\rho_w$ (air-water density ratio) and $U_1 = U_*/\kappa$ for a logarithmic profile. Prof. Lin has pointed out in a private communication that the energy transfer may be expressed as $\dot{E} = \tau c$, where $\tau = -\rho_a\overline{uv}$ is a Reynolds stress and u and v are the Cartesian components of velocity. Evaluating τ according to Lin (1954) then yields (1.1).

rather than at the mean surface; (*c*) include the dominant viscous term in the complete Orr–Sommerfeld equation. We shall find that: (*a*) yields an energy-transfer coefficient that is smaller than, but of the same order of magnitude as, that previously estimated; (*b*) has no effect on the end-results; and (*c*) shows that the viscous effects in the air just above the surface wave are small compared with those in the water (or other liquid), being of relative order $\sigma R_a^{-\frac{1}{2}} R_w$, where

$$R = c/k\nu, \tag{1.2a}$$

or, for a gravity wave,

$$R = c^3/g\nu \tag{1.2b}$$

denotes a Reynolds number based on wave-speed, wave-number, and the viscosity of either fluid (*a*: air or upper fluid; *w*: water or lower fluid).†

The model to be developed in § 2 resembles that of I in that it neglects perturbation Reynolds stresses (associated with the interaction between turbulent fluctuations in the original and perturbed flows; see I, Appendix); it differs in that it includes perturbation viscous stresses and is based on the intrinsic equations of motion (in which the streamlines appear as co-ordinate lines).‡ We shall include only a boundary-layer approximation to the perturbation viscous stresses, however, anticipating that (for large R) these stresses can be significant only in the small neighbourhoods of the surface wave (*outer viscous layer*) and of $U = c$ (*inner viscous layer*).

It might be objected that the neglect of the perturbation Reynolds stresses relative to perturbation viscous stresses is far more questionable than their neglect in the inviscid model of I, but to this objection one may reply that the primary purpose of including the viscous stresses is to show that they are indeed negligible compared with the terms included in I. We also remark that the outer viscous layer, which might have been suspected to be especially important in virtue of the interaction of viscous stresses in air and water, is likely to be confined within the laminar sublayer of the undisturbed flow.§ It is expedient, in this connexion, to introduce the dimensionless shear parameter

$$S_a = U'(0+)/kc = U_*^2/kc\nu_a = R_a(U_*/c)^2, \tag{1.3a,b,c}$$

where (1.3*b*) follows from (1.3*a*) through the equality of the shearing stresses $\rho_a U_*^2$ (U_* = Prandtl's friction velocity) and $\rho_a \nu_a U'(0+)$, while (1.3*c*) follows from (1.3*b*) through (1.2*a*). We find that the outer viscous layer will be confined within the laminar sublayer if (roughly) $S_a < 10$ and that this inequality will be satisfied for those combinations of parameters for which viscous dissipation in the

† The results of (*b*) and (*c*) were anticipated in I. See also Brooke Benjamin (1959).

‡ Following the completion of the present paper, the author spent a brief period at Cambridge University and learned of a very similar analysis by Brooke Benjamin (1959). His formulation, based on orthogonal curvilinear co-ordinates, is essentially equivalent to that given in § 2 below; his applications are more general, but there is very little overlap with the results obtained herein.

§ There is now a considerable body of evidence (see Takahashi 1958) that the flow *near* the water is aerodynamically smooth for wind-speeds as high as 800 cm/sec (at 400 cm above the water). This evidence does not include direct measurements in a laminar sublayer, but the measured profiles do imply the existence of a laminar sublayer having a thickness of the order of $3{\cdot}3\nu_a/U_*$.

air might have been expected to be significant (see § 5). We emphasize, on the other hand, that S_a may be rather large at higher wind-speeds.†

We shall develop the equations of motion for the water in § 3 on the assumption $S_w \ll 1$, where [based on $\rho_a U_*^2 = \rho_w \nu_w U'(0-)$]

$$S_w = U'(0-)/kc = \sigma U_*^2/kc\nu_w \tag{1.4a,b}$$

and

$$\sigma = \rho_a/\rho_w. \tag{1.5}$$

This permits the neglect of the shear flow in the water and the derivation of our results almost directly from Lamb (1945, § 349).

Having developed the equations of motion in §§ 2 and 3, we shall impose the boundary conditions of continuity of velocity and stress in § 4 to obtain a first approximation to the complex wave-speed. We assume, as in I, that the magnitude of the wave-speed is closely approximated by its unperturbed, inviscid value ($c^2 = g/k$ for gravity waves) and that this value may be used in the determination of the perturbation flows.

Numerical results based on our revised analysis are presented and discussed in § 5.

Concluding this introduction, we remark that the energy-transfer considered here augments that proposed by Phillips (1957), which considers the direct action of turbulent fluctuations in aerodynamic pressure on the water but neglects interaction between surface wave and air flow.‡ We hope to consider the simultaneous operation of these two complementary mechanisms in a subsequent paper.

2. Equations of motion for the air

We choose, as independent variables, the co-ordinates s and n measured along and normal to the streamlines (see figure 1) in a frame of reference moving with the wave-speed c and, as dependent variables, $q(s,n)$ and $\theta(s,n)$, the velocity along a streamline and the inclination of the streamline. (In accordance with the procedure outlined in § 1, c may be approximated as real throughout the following analysis except in (4.5c) and (4.6).) Starting from the intrinsic equations of motion (Milne-Thomson 1950, § 19.82)

$$qq_s + \rho^{-1}p_s = \nu q_{nn}, \tag{2.1a}$$

$$q^2\theta_s + \rho^{-1}p_n = 0, \tag{2.1b}$$

$$q_s + \theta_n q = 0, \tag{2.1c}$$

where ρ denotes density, p hydrodynamic pressure, ν kinematic viscosity (all parameters in this section referring to the upper fluid), subscripts partial differen-

† Brooke Benjamin (1959) has given an analysis for arbitrary values of S_a on the assumption that $U(y)$ is exactly linear, while Longuet-Higgins (1952) has treated a fixed wave ($c = 0$ or $S_a = \infty$) on the same assumption. Both find that the phase shifts associated with the viscous stresses can lead to a positive energy-transfer to the disturbance [cf. also Lin (1954)].

‡ It also seems likely that the energy-transfer associated with viscous phase shifts (see preceding footnote) could be of considerable significance for waves moving with speeds c corresponding to critical points ($c = U$) of small profile curvature. Such waves might not be important for the total energy-transfer (calculated in § 5 below), but could be important for the mean-square slope of the surface.

tiation and νq_{nn} the dominant shear term in a boundary-layer-type approximation, we seek the perturbation flow coupled with the displacement

$$\eta(s) = a\,e^{iks} \quad (k\,|a| \ll 1) \tag{2.2}$$

of the streamline $n = 0$ in a uniform, parallel shear flow $q^{(0)} = U(n) - c$. (Following the usual convention, the imaginary parts of complex quantities proportional to $\exp(iks)$ are to be discarded in the final interpretation.) The final motion will be unstable if $\mathscr{I}\{c\} > 0$, exhibiting the time-growth factor $\exp(k\mathscr{I}\{c\}t)$.

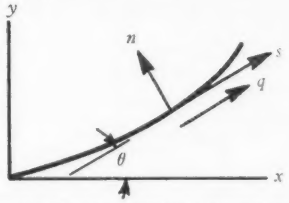

FIGURE 1. The co-ordinates for the intrinsic equations of motion (2.1*a*, *b*, *c*).

We first observe that the unperturbed solution to (2.1*a*, *b*, *c*) implied by our assumption of a strictly parallel shear flow is

$$q = q^{(0)}(n), \quad p = p^{(0)}(s), \quad \theta \equiv 0. \tag{2.3a,b,c}$$

In fact, we shall use (2.1*a*, *b*, *c*) to describe perturbations with respect to a turbulent flow for which $U(n)$ is the mean flow and in which the viscous stress $\rho\nu U'$ actually is balanced by a Reynolds stress; the model provided by (2.1*a*, *b*, *c*) then neglects perturbation Reynolds stresses (see I, Appendix).

We may linearize (2.1*a*, *b*, *c*) in the independent variable $\theta(s, n)$ by differentiating (2.1*a*) with respect to both s and n and (2.1*b*) twice with respect to s, taking the difference between the results to eliminate p, and eliminating q_s through (2.1*c*) whence

$$[(q^2\theta_n)_n + (q^2\theta_s)_s]_s = \nu(q\theta_n)_{nnn}. \tag{2.4}$$

Now, to first order in θ, we may approximate q by its undisturbed value $U(n) - c$ and assume θ to exhibit the harmonic s-dependence of (2.2), whence we obtain

$$[(U-c)^2\theta_n]_n - k^2(U-c)^2\theta = (\nu/ik)[(U-c)\theta_n]_{nnn} \tag{2.5}$$

as the linearized equation of motion. We remark that (2.5) differs from a boundary-layer approximation to the Orr–Sommerfeld equation (governing the perturbation stream function in Cartesian co-ordinates) in that it has a singularity at $U = c$; this implies that the linearized approximation to θ cannot be uniformly valid in the neighbourhood of $U = c$.† We shall find that this singularity introduces no essential difficulty (in so far as we require only the perturbation stresses at the interface $n = 0$), but it should be distinguished from the singularity that occurs at $U = c$ for the inviscid Orr–Sommerfeld equation of (2.9*a*) below; the latter singularity is a consequence of neglecting the viscous forces in a neighbourhood where the inertial forces tend to zero.

† Brooke Benjamin's (1959) formulation in orthogonal curvilinear co-ordinates avoids this difficulty but leads to an inhomogeneous form of the Orr–Sommerfeld equation unless terms in U^{iv} and U''' are neglected.

We shall delay consideration of the full complement of boundary conditions until § 4 below, but we note here that

$$\theta = \eta'(s) \quad (n = 0) \quad \text{and} \quad \theta \to 0 \quad (n \to \infty). \tag{2.6a,b}$$

We emphasize that these boundary conditions are imposed at the displaced, rather than the mean, position of the interface, thereby avoiding the assumption that the surface-wave displacement η must be small compared with a characteristic length (say c/U') for the shear profile; thus, we have only to assume $k|\eta| \ll 1$, rather than $U'(0+)|\eta|/c\,[= S_a k|\eta|] \ll 1$. It is for this reason that we choose a formulation in terms of $\theta(s,n)$, the streamline inclination in non-Cartesian co-ordinates, rather than the more conventional formulation in terms of a stream function in Cartesian co-ordinates.†

We shall seek asymptotic solutions to (2.5) as $R = c/k\nu \to \infty$. The formal procedure is essentially that for the Orr–Sommerfeld equation (Lin 1955, §§ 3.4 and 3.6) and yields two solutions that satisfy (2.6*b*). The first of these, the *inviscid solution*, may be obtained by setting $\nu = 0$ in (2.5); the second or *viscous solution* may be obtained by neglecting the second term on the left-hand side of (2.5) or, equivalently, omitting the pressure gradient in (2.1*a*) and disregarding (2.1*b*). We find it convenient to solve for $(U-c)\theta$ and $(U-c)\theta_n$ (which are proportional to vertical velocity and perturbation shearing stress) in these two cases and to separate the s-dependence by introducing the factor $\eta'(s)$; defining the dimensionless variables

$$\xi = kn, \quad f(\xi) = [U(n)-c]/c, \tag{2.7a,b}$$

we then write

$$f(\xi)\,\theta_1(s,n) = -ik\eta(s)\,\phi(\xi), \quad f(\xi)\,(\partial\theta_2/\partial n) = -ik^2\eta(s)\,\chi(R^{\frac{1}{3}}\xi), \tag{2.8a,b}$$

$$\theta = \theta_1 + \theta_2 = -ik\eta(s)\left[\frac{\phi(\xi)}{f(\xi)} + \int_\infty^\xi \frac{\chi(R^{\frac{1}{3}}\xi)\,d\xi}{f(\xi)}\right], \tag{2.8c}$$

where

$$f\phi'' - (f''+f)\,\phi = 0 \tag{2.9a}$$

and

$$(d^2\chi/d\xi^2) - iRf\chi = 0 \quad \text{or} \quad \chi'' - if\chi = 0 \tag{2.9b,c}$$

as may be confirmed either by substituting (2.8*c*) in (2.5) and allowing R to tend to infinity or through the approximations described in the preceding sentence.

The inviscid equation (2.9) is identical with the inviscid Orr–Sommerfeld equation considered in I, so that our introduction of intrinsic co-ordinates and imposition of the boundary condition (2.6*a*) at the displaced position of the interface have not altered the inviscid problem. The viscous equation (2.9*b*), on the other hand, differs from its counterpart in the asymptotic solution of the Orr–Sommerfeld equation in consequence of our choice of variables. The available

† We may compare our introduction of $\theta(s,n)$ with the von Mises transformation suggested (but not used) in I to allow the imposition of the boundary conditions at the displaced interface. We also note that if Cartesian co-ordinates x_1 and x_2 are introduced according to $x_1 = x$ and $x_2 = y + \int_{-\infty}^{x} \theta\,dx$, where y denotes the vertical distance of a given streamline above the interface in the undisturbed flow, then partial differentiations with respect to s and n are equivalent to partial differentiations with respect to x and y. Cf. also Brooke Benjamin (1959).

methods of asymptotic solution remain the same, nevertheless, and we may use the *WKB* approximation to obtain†

$$\chi \sim f^{-\frac{1}{4}} \exp\left\{-\int_{\xi_c}^{\xi} \sqrt{(iRf)}\, d\xi\right\} [1 + O(R^{-\frac{1}{2}})], \tag{2.10}$$

where $f(\xi_c) = 0$ and the phase of the radical is $\pm \frac{1}{4}\pi$ as $\xi \gtrless \xi_c$, the path of integration being indented under the branch point at $\xi = \xi_c$ (Lin 1955, § 3.4).

We remark that (2.10) is not uniformly valid near $\xi = \xi_c$, but that it suffices for our purpose in so far as $S \ll R^{\frac{1}{2}}$ (the condition that the inner and outer viscous layers be well separated),‡ a condition that will be satisfied for those combinations of parameters for which viscous dissipation in the air is most significant (albeit still small). Formally superior solutions may be constructed (cf. Lin, §§ 3.6 and 8.5), but they serve only to substantiate this conclusion.

It remains to express the perturbation stresses on the interface in terms of ϕ and χ. Neglecting terms of $O(R^{-1})$, in keeping with our boundary-layer approximation, we may calculate the normal stress from (2.1*a*, *c*), (2.3*a*, *b*), (2.8), and (2.9*b*) according to

$$p_{22} = -(p - p_0) \tag{2.11a}$$

$$= -(ik)^{-1} \rho[q^2\theta_n + \nu(q_{nn} - U'')] \tag{2.11b}$$

$$= -(ik)^{-1} \rho[q^2\theta_n - (\nu/ik)(q\theta_n)_{nn}] \tag{2.11c}$$

$$= \rho c^2 (f\phi' - f'\phi)\, k\eta. \tag{2.11d}$$

Evaluating (2.11*d*) at $n = 0$, where $f = -1$ and $f' = S$ [see (1.3)], we write

$$(p_{22})_{n=0+} = -\varpi \rho c^2 k \eta \phi_0, \tag{2.12}$$

where

$$\varpi = (\phi_0'/\phi_0) + S = (\alpha + i\beta)(U_1/c)^2; \tag{2.13a, b}$$

the parameters α and β are defined as in I (where $\phi_0 \equiv 1$), and the subscript zero implies evaluation at $\xi = 0+$.

The tangential stress is given by (within the boundary-layer approximation)

$$p_{12} = \rho\nu(q_n - U') \tag{2.14a}$$

$$= -(ik)^{-1} \rho\nu(q\theta_n)_n \tag{2.14b}$$

$$= \rho c^2 R^{-\frac{1}{2}} \chi'(R^{\frac{1}{2}}\xi)\, k\eta. \tag{2.14c}$$

Substituting χ from (2.10) and setting $\xi = 0+$, we obtain

$$(p_{12})_{n=0+} = -e^{-\frac{1}{4}i\pi} \rho c^2 k\eta\, R^{-\frac{1}{2}} \chi_0. \tag{2.15}$$

We remark that the viscous solution enters the calculation of the normal stress and the inviscid solution that of the tangential stress only through the boundary conditions, which relate ϕ_0 and χ_0.

3. Equations of motion for the water

We shall proceed on the assumption that the shear flow in the water (induced by the traction of the shear flow in the air) may be neglected. As stated in § 1, this will be a good approximation if $S_w \ll 1$, where S_w is defined by (1.4). (This has

† The error factor in (2.10) is referred to the exact solution of (2.5), not (2.9*b*).

‡ The parameter $R^{\frac{1}{2}} S^{-1}$ is similar to the parameter $Z^{\frac{1}{2}}$ (Lin 1955, § 3.5) in the plane Poiseuille stability problem.

been confirmed by an analysis similar to that of the preceding section.) We emphasize that this assumption does not preclude the existence of a surface current, since our velocities are defined relative to such a current; all that $S_w \ll 1$ does imply is that the water moves approximately uniformly with the surface current to a depth of the order of $1/k$ ($= \lambda/2\pi$). We add that the small shear flow that is present must be oppositely directed to the airflow—i.e. $U_w < 0$ if $U_a > 0$; it follows that $U - c$ could not vanish in $n < 0$ for a wave travelling downwind, whence the shear flow in the water could not transfer energy to the surface wave through the mechanism of I.†

Assuming small perturbations with respect to a uniform flow $-c$ (in our moving frame of reference), we may take over Lamb's (1945, § 349) solution for a surface wave of the form (2.2) moving over a viscous liquid. Converting Lamb's notation to that introduced in § 2 above (in particular $v = -c\theta$; also, we omit the hydrostatic pressure from p_{22}), we may pose the streamline inclination and perturbation stresses in the forms

$$\theta = (a\, e^{\xi} + b\, e^{\kappa\xi})\, ik\eta, \tag{3.1}$$

$$p_{22} = -\rho c^2[(1 + 2iR^{-1})\, a\, e^{\xi} + 2i\kappa R^{-1}\, b\, e^{\kappa\xi}]\, k\eta, \tag{3.2}$$

$$p_{12} = \rho c^2[2R^{-1} a\, e^{\xi} + (2R^{-1} - i)\, b\, e^{\kappa\xi}]\, k\eta, \tag{3.3}$$

$$\kappa = (1 - iR)^{\frac{1}{2}}, \quad \mathscr{R}\{\kappa\} > 0, \tag{3.4a, b}$$

where a and b are constants to be determined ($A = iac$ and $C = -bc$ are the corresponding constants in Lamb's solution) by the boundary conditions at the interface, and ρ, ν, and R are to be evaluated for the water. We emphasize that the boundary-layer approximation is not applicable to the water (since the interface is approximately free for the heavy fluid below the interface) and that (3.1)–(3.4) are based on the full, linearized equations of viscous flow; subsequently, we shall assume R_w to be large, but this approximation has yet to be invoked.

4. Determination of wave-speed

We may infer the boundary conditions at the interface from the considerations that both θ_a and θ_w must be equal to the slope of the surface wave, that the velocity (or θ_n) be continuous, that the shear stress be continuous, and that the discontinuity in normal stress be prescribed—viz.

$$\theta_a = ik\eta, \quad \theta_w = ik\eta, \quad \Delta\theta_n = 0, \tag{4.1a, b, c}$$

$$\Delta p_{12} = 0, \quad \Delta p_{22} = L\eta, \tag{4.1d, e}$$

where Δ denotes a jump operator according to

$$\Delta(\quad) = (\quad)_{n=0+} - (\quad)_{n=0-} \tag{4.2}$$

and $L\eta$ the (static) restoring stress of the interface. We may relate the operator L to the inviscid wave-speed in the absence of the upper fluid according to (see I)

$$L\eta = \rho_w c_w^2 k\eta; \tag{4.3}$$

† Such an energy transfer would be predicted for a wave travelling upwind, but it generally would be much smaller than the energy absorbed by viscous dissipation, primarily because U_w'' almost certainly would be very small at that depth where $U_w - c = 0$.

for gravity waves, we have simply

$$c_w^2 = g/k. \tag{4.4}$$

We need not pose the boundary conditions at infinity, assuming them to be satisfied implicitly.

Substituting (2.8*c*), (2.12), (2.15), (3.1)–(3.3), and (4.3) in (4.1*a–e*), setting $f(0) = -1$ and $f'(0) = S_a$, and cancelling common factors, we may place the results in the form

$$\phi_0 - e^{\frac{1}{4}i\pi} R_a^{-\frac{1}{2}} \chi_0 = 1, \tag{4.5a}$$

$$a + b = 1, \tag{4.5b}$$

$$\phi_0' + S_a \phi_0 + \chi_0 = a + \kappa b, \tag{4.5c}$$

$$-e^{-\frac{1}{4}i\pi} \sigma R_a^{-\frac{1}{2}} \chi_0 = 2R_w^{-1}(a+b) - ib, \tag{4.5d}$$

$$c_w^2 = c^2[(1 + 2iR_w^{-1})\, a + 2i\kappa R_w^{-1} b - \sigma\varpi\phi_0]. \tag{4.5e}$$

Solving (4.5*a–d*) for ϕ_0, χ_0, a, and b, and substituting the results in (4.5*e*), we obtain

$$c^2 = c_w^2\{1 - 4iR_w^{-1} + \sigma\varpi - \sigma(1-\varpi)^2 e^{\frac{1}{4}i\pi} R_a^{-\frac{1}{2}} + O[R_w^{-\frac{3}{2}},\ \sigma R_a^{-\frac{1}{2}} R_w^{-\frac{1}{2}},\ \sigma S_a R_a^{-1},\ \sigma^2]\}. \tag{4.6}$$

Substituting ϖ from (2.13*b*) and R_w and R_a from (1.2*b*) in (4.6) and neglecting higher-order terms, we obtain the damping ratio (see first footnote in § 1 above)

$$\zeta = \frac{2\mathscr{I}\{c\}}{\mathscr{R}\{c\}} = \sigma\beta\left(\frac{U_1}{c}\right)^2 - \frac{4g\nu_w}{c^3} - \sigma\left(\frac{g\nu_a}{2c^3}\right)^{\frac{1}{2}}\left[1 - 2(\alpha+\beta)\left(\frac{U_1}{c}\right)^2 + (\alpha^2 - \beta^2 + 2\alpha\beta)\left(\frac{U_1}{c}\right)^4\right], \tag{4.7}$$

where the three terms on the right-hand side represent the positive energy-transfer from the shear flow, the viscous dissipation in the water, and the viscous dissipation in the air. Approximating the bracketed terms by 1 (they will be only slightly in excess of 1 for typical c/U_1), we find that the viscous dissipation in the air will be less than 10 % of that in the water for $c < 52$ cm/sec ($\lambda = 17$ cm) and will exceed it only for $c > 240$ cm/sec ($\lambda = 360$ cm). We also observe that neither of the dissipation terms is numerically significant for $c > 100$ cm/sec ($\lambda > 64$ cm) and wind speeds sufficiently high ($U_* \sim 10$ cm/sec) to permit the achievement of near-maximum values of β.

5. Numerical results

It remains to determine the parameter ϖ, as defined by (2.13*a, b*). This requires the determination of the ratio ϕ_0'/ϕ_0 through the integration of (2.9*a*) subject to (2.6*b*)—or, better, $\phi' + \phi \to 0$, $\xi \to \infty$. Only an integral approximation to the parameter β was attempted in I, but (2.9*a*) has since been integrated numerically (Conte & Miles 1959) for the logarithmic profile (I, equation (5.3*b*))

$$U(n) = U_1 \log(n/z_0), \quad U_1 = U_*/\kappa, \tag{5.1a, b}$$

with $\kappa = 0{\cdot}4$. The results for α and β, defined as in I and (2.13*b*) above, are plotted *vs* ξ_c and c/U_1 in figures 2 to 6 for three values of the parameter Ω, where (I, equation (6.2))

$$\xi_c = \Omega(U_1/c)^2 e^{c/U_1}, \quad \Omega = gz_0/U_1^2, \tag{5.2a, b}$$

with $c^2 = g/k$ (in zero'th approximation). Figure 6 has been included to illustrate the phase shift between the perturbation pressures outside the critical layer and at the surface wave. We add that the independent variable actually used in the integration was f, rather than ξ, and the logarithmic profile was assumed to be

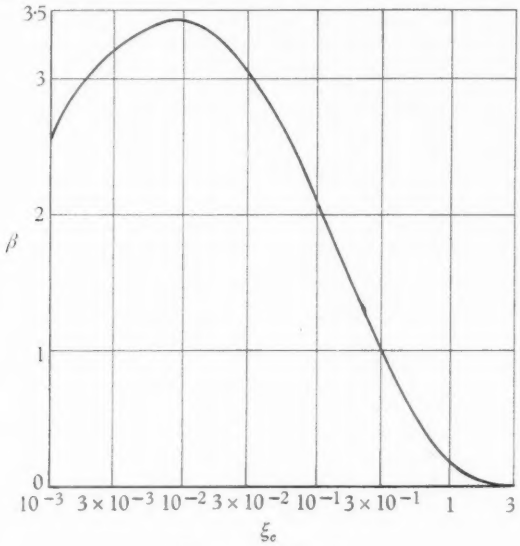

FIGURE 2. β *vs* ξ_c.

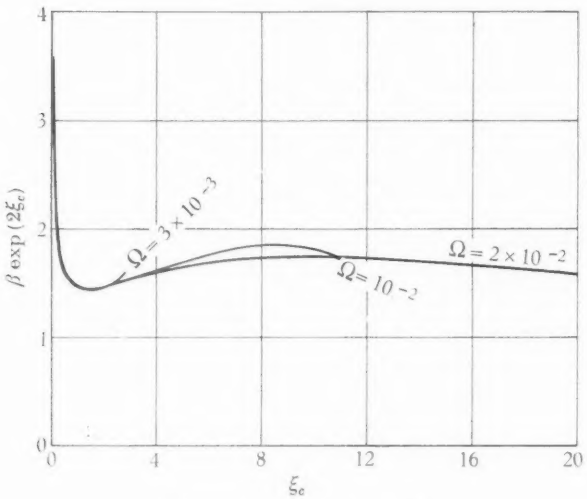

FIGURE 3. $\beta \exp(2\xi_c)$ *vs* ξ_c.

valid down to $f = -1$ (where $\xi = kz_0$). The correction required for the departure of the actual profile from the logarithmic profile in (say) $\xi < \xi_1$ is found in Appendix A to be $O(\xi_1)$ and therefore negligible for the range of the numerical integration.

Comparing the results of figures 2 and 3 with those of I (figure 1), we find that, as previously concluded, β *vs* ξ_c is essentially independent of Ω for $\xi_c < 2$ and is $O(e^{-2\xi_c})$ as $\xi_c \to \infty$; on the other hand, the numerical values of β are generally smaller than those estimated in I. We also find that α *vs* ξ_c is independent of Ω for

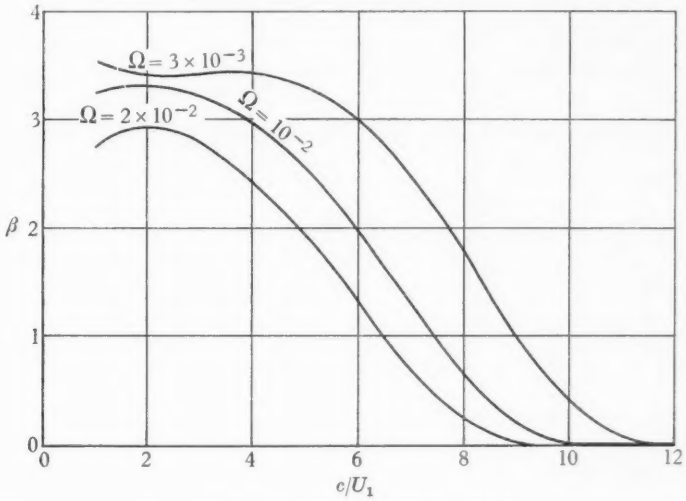

FIGURE 4. β *vs* c/U_1; $\Omega = gz_0/U_1^2$.

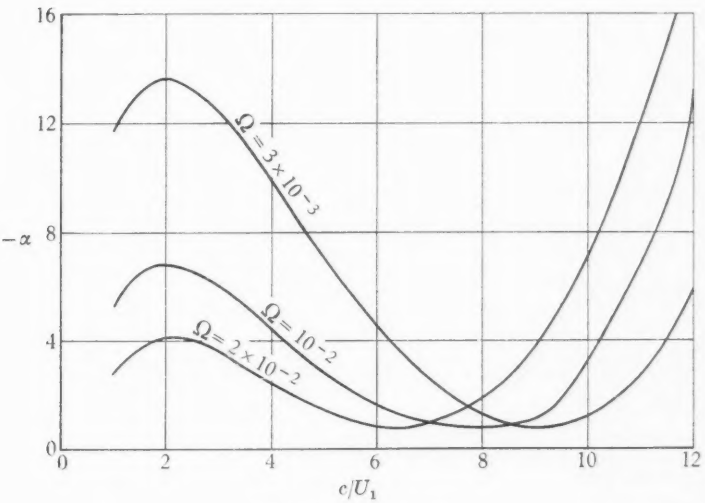

FIGURE 5. $-\alpha$ *vs* c/U_1.

sufficiently small ξ_c, since α then may be expressed in terms of β (see Appendix B). Assuming aerodynamically smooth flow ($z_0 = \nu_a/9U_*$), we find that the critical wind-speed at which the energy-transfer from the shear flow is just balanced by laminar dissipation in the water [see I, equations (6.5) to (6.7)] is given by

$U_1 = 14$–15 cm/sec for waves of length 20–30 cm. The availability of energy from the direct action of the turbulent fluctuations of the wind (as described by Phillips)† renders this critical wind-speed of only secondary significance, however, and there is now little reason to compare it directly with the minimum wind-speed ($U_1 = 9$–10 cm) at which water waves are first observed.

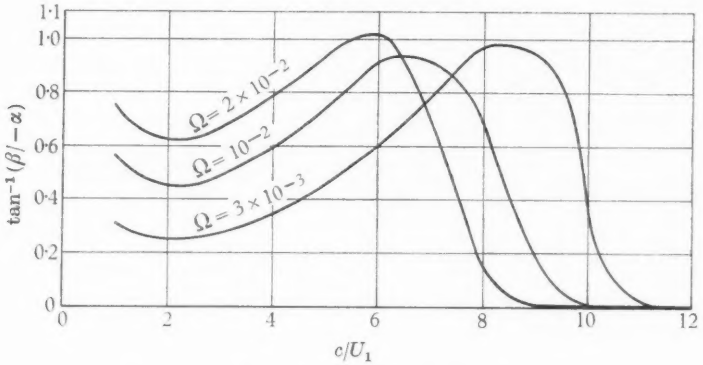

FIGURE 6. The phase shift $\tan^{-1}(\beta/-\alpha)$ *vs* c/U_1.

We conclude by calculating mean values of β, say β_E and β_τ, on the basis of mean energy-transfer and mean Reynolds stress. The rate at which energy is transferred from the shear flow to surface waves by normal pressures is given by

$$\bar{E} = \overline{\mathscr{R}\{p_{22}(-ikc\eta)^*\}} \tag{5.3a}$$

$$= \rho_a U_1^2 (c\beta k^2 \overline{|\eta|^2 \cos^2\theta}) \tag{5.3b}$$

$$= \rho_a U_1^2 \int_0^\infty \int_{-\frac{1}{2}\theta_0}^{\frac{1}{2}\theta_0} c\beta\left(\frac{c}{U_1\cos\theta}\right) k^2 S(k,\theta)\cos^2\theta\, k\, dk\, d\theta, \tag{5.3c}$$

where θ now denotes the angle between the wind and the direction of propagation of a given wave, θ_0 the total beam width of the wave spectrum, and S the power spectral density of the surface displacement; we have substituted p_{22} from (2.12) with $\phi_0 = 1$ (corresponding to the neglect of the viscous solution), assumed that the effective wind-speed for an obliquely moving wave is reduced by $\cos\theta$, and posed β as a function of the ratio of wave-speed to effective wind-speed.‡ It follows from (5.3*c*) that we may define β_E, the mean value of β for energy transfer, according to

$$\int_0^\infty \int_{-\frac{1}{2}\theta_0}^{\frac{1}{2}\theta_0} c\left[\beta\left(\frac{c}{U_1\cos\theta}\right) - \beta_E\right] k^2 S(k,\theta)\cos^2\theta\, k\, dk\, d\theta = 0. \tag{5.4}$$

We shall assume the Neumann spectrum (I, equation (8.4))

$$k^2 S k\, dk\, d\theta = C\, e^{-2(c/U_a)^2}\, dc\, d\theta, \tag{5.5}$$

† And perhaps also from the viscous phase shifts predicted by Longuet-Higgins and Brooke Benjamin (see last two footnotes in § 1 above).

‡ More precisely, $\beta = \beta(c/U_1\cos\theta, \Omega)$, where $\Omega = gz_0/U_1^2\cos^2\theta$. The subsequent calculations neglect the dependence of Ω on $\cos\theta$.

where C is a constant [irrelevant for (5.4)] and U_a the wind speed at the anemometer height. If we also introduce the change of variable $x = c/U_1 \cos\theta$, we may place the result for β_E in the form

$$\beta_E = 4\left(\frac{U_1}{U_a}\right)^2 \int_0^\infty x\beta(x) f_E\left[\left(\frac{U_1}{U_a}\right)^2 x^2, \theta_0\right] dx, \tag{5.6}$$

where

$$f_E(y, \theta_0) = \int_{-\frac{1}{2}\theta_0}^{\frac{1}{2}\theta_0} e^{-2y\cos^2\theta} \cos^4\theta \, d\theta \Big/ \int_{-\frac{1}{2}\theta_0}^{\frac{1}{2}\theta_0} \cos^2\theta \, d\theta. \tag{5.7}$$

We shall consider the two extremes $\theta_0 = 0$ and π, for which (5.7) yields

$$f_E(y, 0) = e^{-2y} \tag{5.8a}$$

and

$$f_E(y, \pi) = e^{-y}[I_0(y) - (1 + \tfrac{1}{2}y^{-1}) I_1(y)], \tag{5.8b}$$

where (5.8b) follows from (5.7) through the integral representation of I_n, the modified Bessel function of the first kind.

The mean Reynolds stress (cf. first footnote in § 1) in the direction of the wind is given by

$$\bar{\tau} = \overline{\mathscr{R}\{-p_{22}(ik\eta)^* \cos\theta\}}. \tag{5.9}$$

Following the development of (5.3) and (5.4), we then may define β_τ, the mean value of β for Reynolds stress, according to

$$\int_0^\infty \int_{-\frac{1}{2}\theta_0}^{\frac{1}{2}\theta_0} \left[\beta\left(\frac{c}{U_1 \cos\theta}\right) - \beta_\tau\right] k^2 S(k, \theta) \cos^3\theta \, k \, dk \, d\theta = 0. \tag{5.10}$$

Introducing S from (5.5), we obtain†

$$\beta_\tau = \sqrt{\left(\frac{8}{\pi}\right)} \left(\frac{U_1}{U_a}\right) \int_0^\infty \beta(x) f_\tau\left[\left(\frac{U_1}{U_a}\right)^2 x^2, \theta_0\right] dx, \tag{5.11}$$

where

$$f_\tau(y, \theta_0) = \tfrac{1}{4}[\sin(\theta_0/2) - \tfrac{1}{3}\sin^3(\theta_0/2)]^{-1} (\theta_0 + \sin\theta_0) f_E(y, \theta_0). \tag{5.12}$$

Numerical integrations of (5.6) and (5.11) have been carried out for $\Omega = 10^{-2}$, which is representative of fully developed rough flow [see I, equation (7.5a, b)], and $U_a/U_1 = 9$, which is appropriate for wind-speeds of the order of 10 m/sec at 10 m above the surface.‡ It also was assumed that $\beta(x) \equiv 0$ for $x \leqslant 3$, where the logarithmic profile presumably ceases to hold.§ The resulting values of β_E are 1·24 and 1·05 for $\theta_0 = 0$ and π; the values of β_τ are 0·90 and 0·75. The corresponding

† Comparing (5.9) and (5.11) $\times (U_1/U_a)^2$ with I (8.1) and (8.7), we note that the latter results are not entirely consistent in their treatment of $\cos\theta$-factors [see also Munk (1955) on this point]; accordingly, $\beta_\tau = (U_a/U_1)^2 \beta_M$ only for $\theta_0 = 0$, but the discrepancies are relatively unimportant compared with other uncertainties in the numerical calculations.

‡ The wind-speed of 10 m/sec at 10 m is representative (in order of magnitude) of wind-speeds for which the Neumann spectrum was measured; for a wind-speed of 3 m/sec at 10 m $U_a/U_1 = 12$ would be closer to the mark.

§ A rough correction factor for the fall-off of profile curvature as a laminar sublayer is approached was constructed on the basis of the approximation $\beta \sim (U_c''/U_c')$ and an interpolated profile (linear at boundary and asymptotically logarithmic, Miles 1957b). This factor was found to be 0·99, 0·86, and 0·19 for $c/U_1 = 4{\cdot}8$, 3·6, and 2·9, respectively, indicating a rather sharp cut-off of β as the critical layer approaches the laminar sublayer. It is by no means certain that the flow *close to the surface* is aerodynamically smooth, but Takahashi's measurements (1958) tend to support such an assumption.

values referred to U_a—viz. $(U_1/U_a)^2\beta_E$ and $(U_1/U_a)^2\beta_\tau$—are $1{\cdot}5\times10^{-2}$, $1{\cdot}3\times10^{-2}$, $1{\cdot}1\times10^{-2}$ and $0{\cdot}9\times10^{-2}$. The latter values are in order-of-magnitude agreement with the 'sheltering coefficient' of $1{\cdot}3\times10^{-2}$ estimated by Sverdrup & Munk (1947) from their data on wave-growth and with the incremental shearing stress inferred by Munk (1955) from measurements made by Van Dorn. We emphasize that any of these numbers might be modified by a factor as large as (but probably no larger than) two either by changes in the assumed values of U_a/U_1, Ω and the cut-off point for $\beta(x)$ or by changes in the treatment of the observational data.

The results of the preceding paragraph are summarized in table 1.

$U(y) = U_1 \log(y/z_0) = U_1 \log(100\,gy/U_1^2)$, $U_a \doteqdot 9U_1$

θ_0	β_E	β_τ
0	$1{\cdot}24\,(1{\cdot}5\times10^{-2})$	$0{\cdot}90\,(1{\cdot}1\times10^{-2})$
π	$1{\cdot}05\,(1{\cdot}3\times10^{-2})$	$0{\cdot}75\,(0{\cdot}9\times10^{-2})$

Sverdrup & Munk: $(U_1/U_a)^2\beta_E \doteqdot 1{\cdot}3\times10^{-2}$
Munk/Van Dorn: $(U_1/U_a)^2\beta_\tau \doteqdot 0{\cdot}6-1{\cdot}8\times10^{-2}$

TABLE 1. Comparison with observation.

6. Conclusions

We conclude that our model for energy-transfer from a parallel shear flow to deep-water gravity waves yields a total energy-transfer in order-of-magnitude agreement with observation. This suggests that such a mechanism may be a decisively important adjunct to initial excitations from other sources—in particular, turbulent fluctuations of wind pressure, as in the model proposed by Phillips (1957).

I am indebted to C. S. Cox, W. H. Munk and W. H. Van Dorn of the Scripps Institute of Oceanography for frequent discussions on the general subject of wave-generation, to M. S. Longuet-Higgins for making available to me his unpublished work, and to T. Brooke Benjamin for making available to me the page proof of his paper and for reading the manuscript of the present paper and offering several valuable suggestions for its improvement. I also take pleasure in acknowledging support, in the form of a fellowship, from the John Simon Guggenheim Memorial Foundation.

Appendix A

Suppose that the profile $f_l(\xi)$ agrees with the true profile $f(\xi)$ for $\xi > \xi_1$ but not for $\xi < \xi_1$ and that a value of ϖ, say ϖ_l, has been calculated by approximating f by f_l in $\xi < \xi_1$; then, given $f(\xi)$, $f_l(\xi)$ and ϖ_l we require the true value of ϖ on the assumption that ξ_1 is small.

Let ϕ_1 and ϕ_1' denote the true values of $\phi(\xi)$ and $\phi'(\xi)$ at $\xi = \xi_1$; then we may integrate (2.9a) inward from ξ_1 to obtain the approximate solution (cf. Lin 1955, § 3.4)

$$\phi(\xi) = (\phi_1/f_1)\,f(\xi) + (\phi_1' f_1 - \phi_1 f_1')\,f(\xi)\int_{\xi_1}^{\xi}\frac{d\xi}{f^2(\xi)}, \tag{A 1}$$

with an error factor $1+O(\xi_1^2)$. Substituting (A 1) in (2.13a), we may place the result for ϖ in the form

$$\frac{1}{\varpi} = \frac{1}{\varpi_1} - \int_0^{\xi_1} \frac{d\xi}{f^2(\xi)}, \tag{A 2}$$

where

$$\varpi_1 = \frac{f_1(\phi_1' f_1 - \phi_1 f_1')}{\phi_1}. \tag{A 3}$$

Similarly,

$$\frac{1}{\varpi_l} = \frac{1}{\varpi_1} - \int_{\xi_0}^{\xi_1} \frac{d\xi}{f_l^2(\xi)}, \tag{A 4}$$

where ξ_0 denotes the lower limit actually used in the calculation based on f_l.

Assuming

$$f_l(\xi) = (U_1/c)\log(\xi/\xi_c), \quad f_l(\xi_0) = -1, \tag{A 5a,b}$$

introducing the logarithm as the variable of integration in (A 4), and eliminating ϖ_1 between (A 2) and (A 4), we obtain

$$\frac{1}{\varpi} = \frac{1}{\varpi_l} + \left(\frac{c}{U_1}\right)^2 \xi_c \int_{-c/U_1}^{\log(\xi_1/\xi_c)} \frac{e^\eta\, d\eta}{\eta^2} - \int_0^{\xi_1} \frac{d\xi}{f^2(\xi)}. \tag{A 6}$$

The first integral may be reduced to the tabulated exponential integral; assuming $\xi_1 < \xi_c$ (as must be so if the logarithmic profile is valid through the critical layer) and that f decreases monotonically from 0 at $\xi = \xi_c$ to -1 at $\xi = 0$, we then find that both integrals are $O(\xi_1)$. Choosing the lower limit of validity for the logarithmic profile as $30z_0$, we have

$$\xi_1 = 30kz_0 = 30\Omega(U_1/c)^2, \tag{A 7}$$

which renders the difference between ϖ and ϖ_l negligible for the range of parameters covered in figures 2–6.

Appendix B

We seek to express α in terms of β for small ξ_c. Rewriting (2.9a) according to

$$(f\phi' - f'\phi)' = f\phi, \tag{B 1}$$

integrating both sides between $\xi = 0$ and $\xi = \xi_c$, setting $f(0) = -1$ and $f'(0) = S$, and evaluating ϖ from (2.13), we obtain

$$(\alpha + i\beta)(U_1/c)^2 = f_c'(\phi_c/\phi_0) + \phi_0^{-1} \int_0^{\xi_c} f\phi\, d\xi \tag{B 2a}$$

$$= f_c'(\phi_c/\phi_0)[1 + O(\xi_c^2)]. \tag{B 2b}$$

Taking the absolute value of both sides of (B 2b) yields

$$\alpha^2 + \beta^2 = (c/U_1)^2 f_c'^2 |\phi_c/\phi_0|^2; \tag{B 3}$$

eliminating $|\phi_c/\phi_0|^2$ through [I (4.3)]

$$\beta = -\pi(c/U_1)^2 (f_c''/f_c') |\phi_c/\phi_0|^2, \tag{B 4}$$

assuming $\alpha < 0$ [as may be proved from I, equation (4.1)], and evaluating f_c' and f_c'' for the logarithmic profile of (A 5a), we obtain

$$\alpha = -[(\beta/\pi\xi_c) - \beta^2]^{\frac{1}{2}}. \tag{B 5}$$

We have used this result to obtain an independent check on the numerical integration for small ξ_c.

REFERENCES

BENJAMIN, T. BROOKE 1959 *J. Fluid Mech.* **6**, 161.

CONTE, S. & MILES, J. W. 1959 *J.S.I.A.M.* (in the Press).

LAMB, H. 1945 *Hydrodynamics.* New York: Dover.

LIN, C. C. 1954 *Proc. Nat. Acad. Sci., Wash.*, **40**, 741.

LIN, C. C. 1955 *The Theory of Hydrodynamic Stability.* Cambridge University Press.

LONGUET-HIGGINS, M. S. 1952 (Unpublished manuscript.)

MILES, J. W. 1957*a* *J. Fluid Mech.* **3**, 185.

MILES, J. W. 1957*b* *J. Aero. Sci.* **24**, 704.

MILNE-THOMSON, L. M. 1950 *Theoretical Hydrodynamics.* New York: Macmillan.

MUNK, W. 1955 *Quart. J. R. Met. Soc.* **81**, 320.

PHILLIPS, O. M. 1957 *J. Fluid Mech.* **2**, 417.

SVERDRUP, H. U. & MUNK, W. 1947 *Wind, Sea and Swell. Theory of Relations for Forecasting. Publ. Hydrog. Off., Wash.*, no. 601.

TAKAHASHI, T. 1958 *Micrometerological Observations and Studies over the Sea.* Faculty of Fisheries, Kagoshima University, Japan.

CORRIGENDA FOR I (MILES 1957*a*)

(1) Equations (3.2a, b) should read: $u = -\psi_y$, $v = \psi_x$.

(2) Footnote, p. 193: replace $w_c'' w_c'$ by w_c''/w_c'.

(3) Caption, figure 4: replace $\zeta_a s$ by ζ_a/s.

(4) Equation (A 5b): replace $)\overline{u}_i''$ by $\overline{u}_i'')$.

On the generation of surface waves by shear flows

Part 3. Kelvin–Helmholtz instability

By JOHN W. MILES

Department of Engineering, University of California, Los Angeles

(Received 4 March 1959)

The Kelvin–Helmholtz model for the formation of surface waves at the interface between two fluids in relative motion is generalized for parallel shear flows. It is assumed that phase changes across the flow are negligible and hence that the aerodynamic pressure on the wave is in phase with its displacement (rather than its slope). A variational formulation is established and leads to the determination of appropriately weighted means for the velocity profiles. The principal application is to flow of a light inviscid fluid over a viscous liquid; it is shown that the principle of exchange of stabilities is applicable to such a configuration, and a critical wind speed in satisfactory agreement with observation is predicted for an air-oil interface. The results also are applied to an air-water interface and lead to the conclusion that Kelvin–Helmholtz instability of such an interface is unlikely at commonly observed wind speeds. A more general formulation of the Kelvin–Helmholtz boundary-value problem and variational principle, allowing for variations in both velocity and density, is given in two appendices.

1. Introduction

The primary problem to which we shall address the following analysis is the investigation of the static stability of the interface ($y = 0$) between a parallel shear flow $U(y)$ of a light inviscid incompressible fluid in $y > 0$ and a viscous liquid at rest in $y < 0$ when this interface is subjected to the small periodic displacement

$$y = \eta_0(x) = \sqrt{2}a \cos kx, \tag{1.1}$$

where a denotes the root-mean-square displacement and k the wave-number. The restriction implicit in our use of the adjective *light* is

$$s = \rho_+/\rho_- \ll 1, \tag{1.2}$$

where ρ_+ and ρ_- denote the densities of the upper and lower fluids, while by *inviscid* we imply (but cf. (4.5) below)

$$U(y)/k\nu_+ \gg 1 \quad \text{for} \quad y > y_0, \quad ky_0 \ll 1, \tag{1.3a,b}$$

where ν_+ denotes the kinematic viscosity of the upper fluid. The restriction (1.3a) permits the existence of a region ($0 < y < y_0$, say) in which $U(y)$ tends to zero, while (1.3b) implies that this region is of negligible significance in so far as it is sufficiently thin compared with the wavelength—i.e. in so far as a suitable y_0

can be chosen. We also observe that our assumption that the lower fluid is at rest can be satisfied only approximately for real fluids and implies $\mu_-/\mu_+ \gg 1$; however, this assumption does not rule out the existence of a surface current, since we may define $U(y)$ as the velocity relative to the surface.

We define *static instability* to be an instability that does not depend on phase changes across the flow; therefore, in the present context, it must be a consequence of an aerodynamic pressure that is in phase with the displacement η_0 and of the same order of magnitude as the gravitational and surface-tension forces resisting this displacement. We contrast this aerodynamic pressure with one in phase with the slope, which would have to be of the same order of magnitude as (and opposite to) the dissipative forces to produce instability. The latter type of instability was considered in Part 1 of this study (Miles 1957), where, on the other hand, the aerodynamic pressure in phase with the displacement was considered negligible compared with other forces of the same phase.

A rather simpler, but analogous, contrast is presented by a simple oscillator of natural (undamped) frequency ω_0 and damping ratio δ (damping ÷ critical damping) that is perturbed by a force having components in phase with both displacement and velocity and proportional to parameters α and 2β, respectively. For a displacement $x(t)$, we then may write the equation of motion in the form

$$\ddot{x} + 2(\delta\omega_0 - \beta)\dot{x} + (\omega_0^2 - \alpha)x = 0.$$

If $\alpha + (\delta\omega_0 - \beta)^2 < \omega_0^2$ the condition for instability is simply $\beta > \delta\omega_0$, but, independently of β, instability will occur if $\alpha > \omega_0^2$. It is customary to designate these two types of instability as *dynamic* and *static*, and we observe that static stability ($\alpha < \omega_0^2$) is a necessary but not sufficient condition for dynamic stability.

The simplest models for dynamic or static instability are defined respectively by $|\alpha/\omega_0^2|, |\beta/\omega_0|, \delta \ll 1$, or $|\beta| \ll \delta\omega_0$ and $\alpha = O(\omega_0^2)$, in analogy with the respective conditions posed in Parts 1 and 2 of this study. In the latter instance—i.e. for the model assumed here—we say that the *principle of exchange of stabilities* holds and that the transition from stable to unstable motion is a transition from a steady flow to a disturbed flow that exhibits an exponential time-growth (at least in the immediate vicinity of the critical condition).† Both of these simplified models of fluid flow constitute idealizations, to be sure, but they do throw light on two distinctly different mechanisms, the simultaneous treatment of which would present a far less tractable problem.

The Kelvin–Helmholtz (hereinafter abbreviated K–H) model for the problem posed in the opening paragraph assumes U to be independent of y in $y > 0$. It predicts instability, within the approximation (1.2), if (Kelvin 1871; Lamb 1945, §268)

$$c_0^2 = gk^{-1} + (T/\rho_-)k < sU^2. \tag{1.4a}$$

† We note that this conclusion depends on the neglect of the shear flow in the lower fluid, so that this fluid is at rest at the transition from stable to unstable motion and no work need be done against viscosity to produce instability. The situation would be quite different for a shallow (compared with the wavelength) liquid; for then the shear no longer would be negligible, even though the flow rate were small, and work would have to be done against viscosity to produce instability. We conclude (perhaps belabouring the obvious) that a lower wall should act as a stabilizing constraint.

We also may pose this criterion in the alternative and physically more significant forms

$$(\rho_- g + Tk^2)\,\eta_0(x) < -p_a = \rho_+ kU^2\eta_0(x), \tag{1.4b}$$

and

$$\tfrac{1}{2}(\rho_- g + Tk^2)\,a^2 < \overline{W}_a = \tfrac{1}{2}\rho_+ kU^2a^2. \tag{1.4c}$$

The left-hand side of (1.4*b*) gives the restoring force (per unit area) of gravity and surface tension (T) associated with the displacement $\eta_0(x)$, while the right-hand side gives the aerodynamic suction ($-p_a$); (1.4*b*) then predicts instability if the aerodynamic suction exceeds the restoring force. Similarly, the left-hand side of (1.4*c*) gives the mean potential energy per unit area, while the right-hand side gives the mean aerodynamic work per unit area ($\overline{W}_a$); (1.4*c*) then predicts instability if the aerodynamic work exceeds the potential energy.

We have identified the wave speed appropriate to the prescribed wave-number k by c_0 in (1.4*a*), but we emphasize that this wave speed has no direct physical significance for the question of static stability. The fact that the minimum wind speed for K–H instability and the minimum wave speed correspond to the same value of k merely reflects the fact that the aerodynamic suction (or work) and the inertia force (or kinetic energy) for the wave motion at fixed wave speed both must be proportional to k in consequence of the fact that both are associated with a velocity potential of the form $C\eta_0(x)\exp(-k|y|)$.

Assuming air over water, each of (1.4*a*, *b*, *c*) predicts that the minimum value of U for instability is 660 cm/sec, corresponding to a wavelength of 1·73 cm. This instability sometimes has been invoked as an explanation for the generation of water waves by wind, although Kelvin (1871) stated only that 'water with a plane level surface is unstable if the velocity of the wind exceeds [660 cm/sec], and that 'the wind would blow into spin-drift' those waves for which (1.4*a*) is not satisfied.† Observation generally has indicated much lower wind speeds than 660 cm/sec for water-wave formation, however, and more recent theoretical models (Phillips 1957; Miles 1957) have offered explanations as to why this should be so; nevertheless, it seems that the K–H mechanism of instability still should be physically significant, albeit not responsible for the initial formation of water waves. Thus, Munk (1947) has conjectured that certain changes in the appearance of the surface of the sea at wind speeds in the neighbourhood of 660 cm/sec might be indicative of K–H instability, while Francis (1954, 1956) has observed *initial* wave formation at an air-oil interface for air speeds roughly approximating that predicted by Kelvin's model.

We shall find (in § 4) that allowance for the y-dependence of U in the calculation of the aerodynamic suction ($-p_a$) or work ($\overline{W}_a$) yields a critical wind speed for an air-oil interface in close agreement with observation but renders the actual manifestation of K–H instability for an air-water interface rather unlikely (§ 5). We remark that these conclusions are in accord with the qualitative picture sketched in the second paragraph of this section. That component of aerodynamic pressure in phase with the slope of the wave is much more effective for a relatively inviscid fluid like water than for a very viscous fluid like oil, whereas static

† Kelvin also emphasized the probable importance of viscosity and went on to offer a qualitative explanation of wave generation on the basis of the sheltering hypothesis that was considered later but more quantitatively by Jeffreys (1924, 1925).

instability appears as the more efficient mechanism for the viscous fluid and takes precedence in accord with the principle of least work.

We shall develop in §§2 and 3 a rather brief analysis that is adequate for the problem posed in the opening paragraph and for the specific applications in §§4 and 5. Kelvin–Helmholtz instability may be of interest in problems for which the restrictions of the first paragraph are not satisfied,† however, and we also shall develop (in Appendices A and B) a more general analysis for the problem in which velocity and density have the arbitrary distributions $U(y)$ and $\rho(y)$—although, in general, we contemplate a discontinuity in $\rho(y)$ at $y = 0$—and in which the interfacial displacement is given by

$$y = \sqrt{2}a\mathscr{R}[e^{ik(x'-ct)}] \tag{1.5}$$

in Cartesian co-ordinates x' and y. Neglecting phase changes across the flow (thereby neglecting viscosity in $y < 0$ as well as $y > 0$), we may assume c to be real up to the critical condition of instability and reduce (1.5) to (1.1) through the Gallilean transformation

$$x = x' - ct, \tag{1.6}$$

thereby rendering the disturbed flow steady to an observer in an (x, y)-co-ordinate system.

The K–H model for this more general problem assumes ρ and U to be discontinuous across $y = 0$ (from ρ_- to ρ_+ and U_- to U_+) but otherwise neglects their y-dependence. These assumptions lead to a solution for the wave speed in the form (Kelvin 1871; Lamb 1945, §§232, 268)

$$c = \bar{U} \pm [c_0^2 - (\widetilde{U^2} - \bar{U}^2)]^{\frac{1}{2}}, \tag{1.7}$$

where

$$\widetilde{U^n} = \frac{\rho_+ U_+^n + \rho_- U_-^n}{\rho_+ + \rho_-}, \quad (n = 1, 2) \tag{1.8}$$

denotes an appropriately weighted, mean value of the steady flow, and (cf. (1.4a))

$$c_0^2 = \frac{(\rho_+ - \rho_-)g + Tk^2}{(\rho_+ + \rho_-)k} \tag{1.9}$$

denotes the square of the wave speed in the absence of the steady flow ($U_+ = U_- = 0$). Equation (1.7) predicts instability if

$$c_0 < (\widetilde{U^2} - \bar{U}^2)^{\frac{1}{2}} = (\rho_+ + \rho_-)^{-1}(\rho_+\rho_-)^{\frac{1}{2}}|U_+ - U_-|. \tag{1.10}$$

We observe that the unstable motion then exhibits an exponential time-dependence only in a reference frame moving with the mean speed $\bar{U}$ (but $\bar{U}$ is independent of k).

We shall find (in Appendix B) that the result for y-dependent ρ and U still may be cast in the form (1.7), with appropriate generalizations of (1.8) and (1.9).

† The K–H stability problem for $s = 1$ has been treated by Carrier (1954) and, for a slightly viscous fluid, by Lessen (1950) and Esch (1957). See also Taylor (1931) and Goldstein (1931) for earlier studies on stratified fluids, with particular reference to meteorological problems.

2. Equations of motion

We consider small perturbations with respect to a two-dimensional steady parallel shear flow in an inviscid incompressible homogeneous fluid of density ρ. Let the disturbed velocity vector be

$$v = \{U(y) - \psi_x, \psi_y\}, \tag{2.1}$$

where $\psi(x, y)$ denotes the perturbation stream function. Assuming the x-dependence $\eta_0(x)$ of (1.1), posing the 'separation-of-variables' solution

$$\psi(x, y) = \eta_0(x)\, U(y) f(y), \tag{2.2}$$

and referring to Lighthill's (1957) study of shear flows (see also Appendix A), we find that $f(y)$ must satisfy

$$(U^2 f')' - k^2 U^2 f = 0, \tag{2.3}$$

where the primes imply differentiation with respect to y. Alternatively, we could have deduced (2.3) from the inviscid Orr–Sommerfeld equation, which must be satisfied by ψ.

The boundary conditions corresponding to the requirement that the flow must be tangential to $y = \eta_0(x)$ as $y \to 0+$ and that it must tend to $U(y)$ as $y \to \infty$ are

$$\left[\frac{\psi(x, y)}{U(y)}\right]_{y=0+} = \eta_0(x), \quad \psi(x, \infty) = 0, \tag{2.4a, b}$$

or

$$f(0+) = 1, \quad f(\infty) = 0. \tag{2.5a, b}$$

We may calculate the aerodynamic perturbation pressure from the Euler equation, viz.

$$\rho \frac{D\mathbf{q}}{Dt} = -\nabla p. \tag{2.6}$$

Substituting (2.1) in (2.6) and integrating the x-component of the result, we obtain

$$p = \rho(U\psi_y - U_y\psi) = \rho U^2(y) f'(y)\, \eta_0(x), \tag{2.7a, b}$$

where (2.7b) follows from (2.7a) in consequence of (2.2).

3. Variational formulation

We may identify (2.3) as a Sturm–Liouville differential equation and hence may infer the existence of a variational integral for p_a. Multiplying both sides of (2.3) by $f(y)$, integrating from $0+$ to ∞, integrating the term $(U^2 f')' f$ by parts, imposing (2.5a, b), and evaluating p_a from the resulting expression for $f'(0+)$, we obtain

$$-p_a(x) = -p(x, 0+) = \rho\eta_0(x) \int_{0+}^{\infty} U^2(y)\,[f'^2(y) + k^2 f^2(y)]\, dy. \tag{3.1}$$

We may show, by the usual procedures, that the integral on the right-hand side of (3.1) is an absolute minimum with respect to variations of $f(y)$ about the exact solution to (2.3), provided that the variational approximation to $f(y)$ satisfies the boundary conditions (2.5a, b). A more general derivation of this variational principle, based on the principle of least work, is given in Appendix B.

Substituting (3.1) in (1.4*b*) and dividing the result through by $\rho k\eta_0(x)$, we may place the critical condition for K–H instability in the form

$$c_0^2 = \frac{s}{k}\int_{0+}^{\infty} U^2(y)\,[f'^2(y) + k^2 f^2(y)]\,dy. \tag{3.2}$$

It follows from the foregoing variational principle that the substitution of an approximate $f(y)$ in (3.2) for a wind profile of prescribed shape will *underestimate* the magnitude of the critical wind speed (at some prescribed level) for K–H instability.

4. Air-oil interface

Francis (1954), blowing air over an oil having the properties $\rho = 0{\cdot}875$, $T = 34$, and $\nu = 2{\cdot}5$ c.g.s. units, observed an initial formation of surface waves of $\lambda \doteqdot 2$ cm and $c \doteqdot 1$ cm/sec with $U = 967$ cm/sec at $y = 8$ cm.† Extrapolating his profile data to $y = 0{\cdot}05$ cm, the estimated amplitude of the observed waves, he obtained a value of U between 500 and 560 cm/sec, which he compared with the value of 516 cm/sec predicted by Kelvin's formula. The agreement is close enough to suggest the validity of the K–H effect, but (aside from the fact that the observation of amplitude may have been subject to appreciable error) the selection of the wind speed at the elevation of the crests appears rather arbitrary; moreover, Ursell (1956) has questioned whether Kelvin's theory may be applied to such a viscous fluid.

We shall attempt to provide a more rational model for an air-oil interface by allowing for the y-dependence of U and by admitting viscosity in the oil. We shall neglect the mean flow of the oil, on the other hand, assuming it to move uniformly with the surface current to a depth of the order of $1/k$; a rough calculation, assuming laminar flow in the oil, yields $|U_-| < 1$ cm/sec (relative to the surface) in the first centimetre below the surface.

Surface waves on a viscous liquid have been considered by Lamb (1945, §349): assuming the displacement (1.5) and adding aerodynamic pressure p_a to his results, we obtain (where the subscript $-$ now refers to the oil)

$$\mathscr{R}\{\rho_- k[c^2 + 4ik\nu c + 4k^2\nu^2(\sqrt{[1-(ic/k\nu)]} - 1)] - (\rho_- g + Tk^2)\}\sqrt{2}\,a\,e^{ik(x'-ct)} = p_a, \tag{4.1}$$

where ν denotes the kinematic viscosity of the oil. Now, by hypothesis, p_a must be in phase with the surface wave displacement, whence the quantity in braces in (4.1) must be real; moreover, the transition from stable to unstable motion must be through a neutrally stable motion, corresponding to a real value of c, say, c_n. Imposing both of these conditions yields

$$4ik\nu c_n + 4ik^2\nu^2\mathscr{I}\{\sqrt{[1-(ic_n/k\nu)]}\} = 0, \tag{4.2}$$

† The wavelengths were originally estimated by Francis at 1·0 cm (1954) and 1·5 cm (1956), but improvements in photographic technique have since permitted more accurate measurements (Francis 1959; see figure 1 of the present paper), and the wavelength for initial instability of the same oil now appears to be approximately 2 cm. Francis also found (1956) that increasing the viscosity of the oil by a factor of 11·5 increased the observed, critical wind speed by only 4%.

and a little algebra confirms the anticipated result that the only admissible root to (4.2) is $c_n = 0$. We conclude that the principle of exchange of stabilities holds for K–H instability of a light, inviscid fluid over a viscous liquid and that viscous forces in the liquid have no effect on the critical wind speed; we emphasize, however, that this result is contingent upon the neglect of the mean flow (relative to the surface) in the liquid to a depth of the order of $1/k$.†

We shall calculate the critical wind speed on the assumption of the logarithmic profile (implying turbulent flow‡)

$$U(y) = U_1 \log (y/z_0), \quad U_1 = U_*/\kappa, \tag{4.3a, b}$$

where U_* denotes Prandtl's friction velocity, $\kappa \doteq 0{\cdot}4$ (Kármán's turbulence constant), and z_0 is the effective roughness parameter. This profile cannot be valid down to $y = 0$, but if it is valid down to $y = y_0$ (where $ky_0 \ll 1$, but y_0 need not be identical with y_0 in (1.3a, b)) we may show that the error in the following calculations is $O(ky_0)$ relative to unity. Assuming (provisionally) that the flow over the surface of the oil resembles that over a smooth wall, we find (Prandtl (1952), p. 128) that (4.3) provides a reasonably good estimate of $U(y)$ down to $y_0 = 30z_0$, and that

$$z_0 = \frac{\nu_a}{3{\cdot}6U_1}, \tag{4.4}$$

where $\nu_a\,(\equiv \nu_+)$ denotes the kinematic viscosity of the air. The restriction $ky_0 \ll 1$ then implies

$$\frac{U_1}{8k\nu_a} = \frac{U_1\lambda}{50\nu_a} \gg 1. \tag{4.5}$$

This is much more severe than (1.3a) if y_0 is taken as $30z_0$ there, but it still is satisfied in the subsequent calculations of this section.

Substituting (4.3a) in (3.2), and introducing $\xi = ky$ as the variable of integration, we obtain

$$c_0^2 = sU_1^2 \int_{0+}^{\infty} \left[\left(\frac{df}{d\xi}\right)^2 + f^2\right] \log^2\left(\frac{\xi}{kz_0}\right) d\xi \tag{4.6}$$

for the determination of the critical value of U_1. We recall that the right-hand side of (4.6) is an absolute minimum with respect to variations of f about the true solution to (2.3) provided that the boundary conditions (2.5a, b) are satisfied.

An especially simple approximation to f, which not only satisfies (2.5a, b) but also tends to the true solution as $|U'/Uk|$ tends to zero, is provided by

$$f(y) = e^{-ky} = e^{-\xi}. \tag{4.7}$$

Substituting (4.7) in (4.6) and evaluating the integral as a Laplace transform, we obtain

$$c_0^2 = sU_1^2[\tfrac{1}{6}\pi^2 + \log^2(2\gamma kz_0)] \tag{4.8a}$$

$$= s[\tfrac{1}{6}\pi^2 U_1^2 + U^2(0{\cdot}045\lambda)], \tag{4.8b}$$

where $\log \gamma$ denotes Euler's constant ($\gamma = 1{\cdot}78\ldots$) and λ the wavelength.

† Including the shear flow in $y < 0$ according to (B. 16) and approximating f by $\exp(ky)$ in $y < 0$, we find that this shear flow could be important only where $\exp(2ky)$—which decreases to 0·04 at $y = -\frac{1}{4}\lambda$—is not small.

‡ See Appendix, Part 1, for a discussion of the assumptions implicit in approximating a turbulent flow by a parallel shear flow for the study of small perturbations. The rather good agreement between theory and experiment obtained in this section appears to lend additional support to such a model.

We require the minimum value of U_1 for instability. Substituting c_0^2 from (1.4a) and z_0 from (4.4) in (4.8a), differentiating the resulting equation with respect to k, equating $\partial U_1^2/\partial k$ to zero, and solving for k in so far as it occurs explicitly (i.e. holding the argument of the logarithm constant), we obtain

$$k = \left(\frac{\rho_- g}{T}\right)^{\frac{1}{2}} \left[\frac{L^2 - 2L + \frac{1}{6}\pi^2}{L^2 + 2L + \frac{1}{6}\pi^2}\right]^{\frac{1}{2}}, \tag{4.9}$$

where

$$L = \log(U_1/k\nu_a). \tag{4.10}$$

Substituting (4.9) in (4.8a) then yields

$$sU_1^2 = 2\left(\frac{Tg}{\rho_-}\right)^{\frac{1}{2}} [(L^2 + \tfrac{1}{6}\pi^2)^2 - 4L^2]^{-\frac{1}{2}}, \tag{4.11}$$

which we must solve simultaneously with (4.9) to obtain the minimum value of U_1 and the corresponding wavelength.

Substituting $\rho_- = 0{\cdot}875$, $T = 34$, $s = 1{\cdot}41 \times 10^{-3}$, and $\nu_a = 0{\cdot}154$ c.g.s. units and solving (4.9) and (4.11) by iteration, we obtain $U_1 = 104$ cm/sec at $\lambda = 1{\cdot}8$ cm ($k = 3{\cdot}44\,\text{cm}^{-1}$). Using the profile data measured by Francis in the first three centimetres above the surface (our weighting factor $\exp(-2ky)$ being less than 10^{-8} for $\lambda = 1{\cdot}8$ and $y = 3$), we deduce $U_1 = 97$ cm/sec and $z_0 = 2{\cdot}3 \times 10^{-4}$ cm. This value of z_0 is approximately half that given by (4.4) for the same value of U_1; allowing for this discrepancy by doubling the argument of L in (4.9) and (4.11), we obtain the modified, theoretical value $U_1 = 91$ cm/sec.†

We can improve this last figure by assuming

$$f = e^{-\xi}\left(1 + \sum_{n=1}^{N} b_n \xi^n\right) \tag{4.12}$$

in (4.6) and, in accordance with the variational principle, minimizing the right-hand side thereof with respect to each of the b_n. Including only the first term ($b_1\xi$) in the series, evaluating the resulting integrals as Laplace transforms, and minimizing with respect to b_1, we obtain

$$c_0^2 = sU_1^2\{[\tfrac{1}{6}\pi^2 + l^2] - 2l^2[\tfrac{1}{6}\pi^2 + 1 + l + l^2]^{-1}\}, \tag{4.13a}$$

$$l = -\log(2\gamma k z_0), \tag{4.13b}$$

in place of (4.8a). The resulting change in (4.9) is negligible (for the numerical data considered), while the revised value of U_1 (based on the revised value of z_0—i.e. on $l = \log(2U_1/k\nu_a)$) is 93 cm/sec. We infer, from the proximity of this result to that based on the original approximation, that the exact theoretical result is not likely to be appreciably larger than 93 cm/sec. (That it must be larger follows from the variational principle.)

The agreement between our theoretical value of 93 cm/sec and the experimental value of 97 cm/sec is almost certainly within experimental error (especially

† It should be understood that the problem we have posed assumes the profile to be prescribed; taking z_0 from experiment then serves only to rectify the provisional assumption (4.4).

for the profile measurements); moreover, we should expect the experimental value for waves of observable amplitude to exceed the theoretical value for neutral stability. The theoretical value of 1·8 cm for the critical wavelength also appears to be in excellent agreement with experiment (see figure 1, plate 1).

There remains a discrepancy between the observed (1 cm/sec) and theoretical (zero relative to surface current) values of c, but it appears that the observed value of c may be charged to surface current within the accuracy of observation. Francis writes (1959): 'I have also just done an experiment to see if your assumption about the surface velocity of the oil is correct. I sprinkled aluminium dust on the oil when the instability was just occurring. The speed of dust particles came out at very nearly 0·40 cm/sec (average of 5 tests). Thus your assumption appears to be a good one....'

5. Air-water interface

We now apply (3.2) to an air-water interface. We emphasize at the outset, however, that the known effectiveness of the component of aerodynamic pressure in phase with the slope in producing surface waves renders static stability of at most secondary interest, and we seek to determine only its qualitative significance.

Assuming the logarithmic profile of (4.3), we may take over the results (4.6) to (4.8); we do not assume (4.4), however, since the flow at speeds for which K–H instability might occur almost certainly would be aerodynamically rough (but see last paragraph in this section).

We consider first the critical wind speed calculated for $\lambda = 1.73$ cm (the critical wavelength for Kelvin's model), $s = 1{\cdot}2 \times 10^{-3}$, and $z_0 = 5 \times 10^{-3}$ cm; this value of z_0 was suggested by Ursell (1956), on the basis of Roll's (1948) results, as being representative for moderate wind speeds. Substituting these numbers in (4.8a) yields $U_1 = 200$ cm/sec, corresponding to a wind speed of roughly 24 m/sec at 10 m above the surface; the assumed value of z_0 then is much too low, however, and the actual critical wind speed (if any) would be even higher.

We may obtain a more realistic appraisal of the K–H effect by introducing the measured pair of values $U_1 = 140$ cm/sec and $z_0 = 0{\cdot}26$ cm (Hay 1955). Substituting these data in the right-hand side of (4·8a) and assuming $\lambda = 10$ cm (and even this does not render the argument of the logarithm large as, by hypothesis, it must be) yields 84 compared with a left-hand side (c_0^2) of 1560.

It does not appear that the minimum critical wind speed for our model could be calculated without severely violating the restriction $kz_0 \ll 1$ (although available information on z_0 is perhaps too unreliable for certainty on this point), but we conclude from the foregoing examples that K–H instability of an air-water interface is unlikely at wind speeds for which reliable observations are available.†

† It might be thought that the shear flow in the water, being of order $s^{\frac{1}{2}}|U_+|$ for turbulent flow (continuity of shear stress demanding $\rho_- U_{*-}^2 = \rho_+ U_{*+}^2$) could be important. We have investigated this possibility on the basis of (1.7), (B.16), and (B.17), with the end result that the shear flow in the water leads to $\tilde{U} = U_-(-0{\cdot}045\lambda)$ and adds an increment $\frac{1}{8}\pi^2 s U_1^2$ to $(\widetilde{U^2} - \tilde{U}^2)$ in (1.7). This implies that $\frac{1}{8}\pi^2$ should be replaced by $\frac{1}{3}\pi^2$ in applying (4.8) to an air-water interface, but the resulting differences in the numerical values given above are trivial.

We add that if z_0 had been evaluated from (4·4), the air-oil calculations would have applied also to an air-water interface except for the changes in T and ρ_-. Introducing the air-water parameters in (4.9) to (4.11), we obtain a critical value of $U_1 = 130\,\text{cm/sec}$ (corresponding to a wind speed of roughly 17 m/sec at 2 m above the surface). We offer the *conjecture* that such a critical speed might be significant for wind blowing over a water surface that has been contaminated in such a way as to inhibit the formation of ripples, thereby rendering the air flow aerodynamically smooth. Both Keulegan (1951) and Van Dorn (1953) have produced such surfaces through the addition of a detergent, but in neither case were wind speeds as high as $U_1 = 130\,\text{cm/sec}$ recorded.

6. Conclusions

We conclude that the modified Kelvin–Helmholtz model developed herein appears adequate to explain the instability of the interface between a fairly viscous liquid and an approximately parallel shear flow in air and that the dominance of the K–H mechanism then is a consequence of its intrinsically static nature, in virtue of which viscous forces cannot inhibit the initial deformation of the interface. It appears unlikely, on the other hand, that the K–H mechanism could be significant for liquids of small viscosity—in particular, for wind over water.

Appendix A

Equations of motion for shear flow in an inhomogeneous fluid

Turning now to the general problem of small perturbations with respect to a two-dimensional parallel shear flow $U(y)-c$ in an inviscid, incompressible fluid of density $\rho_0(y)$, we first write the equations of motion in their so-called intrinsic form, using distance measured along (s) and normal (n) to a streamline (figure 2) as independent variables. The equations of continuity and momentum then read (Milne-Thomson 1950, §§4.20–4.25, 19.82)

$$\rho_s = 0, \quad v_s + \theta_n v = 0, \tag{A.1a,b}$$

$$\rho v v_s = -p_s - \rho g \sin\theta, \quad \rho v^2 \theta_s = -p_n - \rho g \cos\theta, \tag{A.2a,b}$$

where v denotes the velocity (along the streamline by definition), θ the angle between the streamline and the horizontal, ρ the perturbed density, and p the perturbed pressure. We shall linearize these equations in $\eta(x,y)$, the vertical displacement of a given streamline from its initially horizontal position.

We first eliminate v_s from (A.2a) through (A.1b), after which we may invoke the approximations

$$\theta = \eta_x, \quad v = U(y) - c. \tag{A.3a,b}$$

Converting differentiation with respect to s and n to differentiation with respect to x and y, we then may linearize (A.1a) and (A.2a,b) to obtain

$$\rho_x + \rho_0'(y)\,\eta_x = 0, \tag{A.4}$$

$$q\eta_{xy} = p_x + [p_0'(y) + \rho_0(y)\,g]\,\eta_x, \quad q\eta_{xx} = -p_y - \rho g, \tag{A.5a,b}$$

where

$$q = q(y) = \rho_0(y)\,[U(y) - c]^2, \tag{A.6}$$

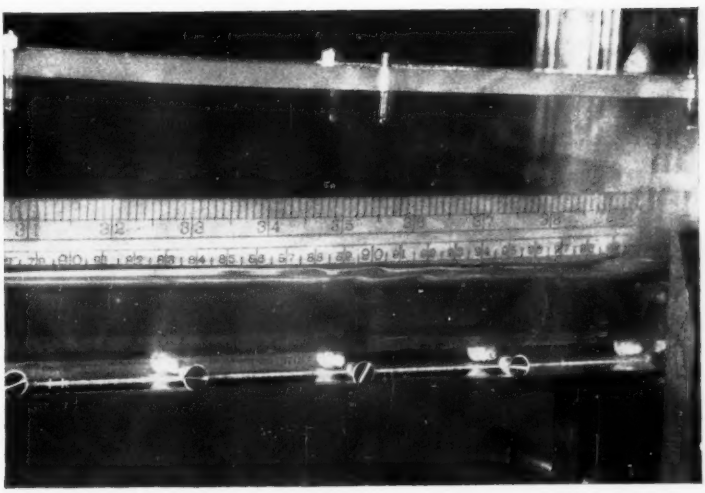

FIGURE 1 (plate 1). Photograph of incipient wave-formation at critical wind speed for oil described in text (Francis 1959).

(*Facing p. 592*)

and $p_0(y)$ and $\rho_0(y)$ denote the unperturbed pressure and density. The condition of static equilibrium is

$$p_0'(y)+\rho_0(y)g = 0, \tag{A.7}$$

whence we may integrate (A. 4) and (A. 5a) to obtain

$$\rho(x,y) = \rho_0(y)-\rho_0'(y)\,\eta(x,y) \tag{A.8}$$

and

$$p(x,y) = p_0(y)+q(y)\,\eta_y(x,y) \tag{A.9}$$

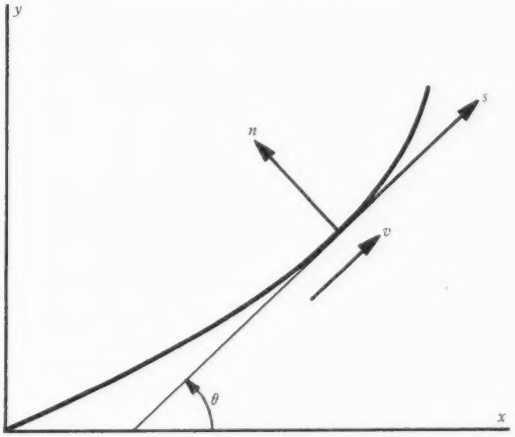

FIGURE 2. The geometry for the intrinsic equations of motion, (A. 1a, b) and (A. 2a, b).

as the linear approximations to the density and pressure. Finally, substituting (A. 7) to (A. 9) in (A. 5b), we obtain the linear, self-adjoint partial differential equation

$$L\{\eta\} = \nabla\cdot[q(y)\,\nabla\eta(x,y)]-w'(y)\,\eta(x,y) = 0. \tag{A.10}$$

where ∇ denotes the conventional nabla operator and

$$w(y) = \rho_0(y)\,g \tag{A.11}$$

the specific weight.† We have tacitly assumed, in writing (A. 8) to (A. 10), that $w(y)$ is continuous; if it is discontinuous $q\eta_y$ could be calculated by direct integration of (A. 10) through the discontinuity.

We shall find it convenient to separate variables by writing

$$\eta(x,y) = \eta_0(x)f(y), \tag{A.12}$$

where $\eta_0(x)$ is given by (1.1). Substituting (A. 12) in (A. 10), we obtain the Sturm–Liouville equation

$$(qf')'-(k^2q+w')f = 0. \tag{A.13}$$

The corresponding boundary conditions, as dictated by the requirements $\eta = \eta_0$ at $y = 0$ and $\eta \to 0$ as $|y| \to \infty$, are

$$f(0) = 1, \quad f(\pm\infty) = 0. \tag{A.14a, b}$$

† The result (A. 10) was obtained by Lighthill (1957) for three-dimensional perturbations in the absence of buoyancy force, i.e. $w' = 0$. Special cases also were given by Taylor (1931) and Goldstein (1931).

We observe that if $U(y)-c=0$ at, say, $y=y_c$, the differential equation (A.13) has a regular singularity there (in which case the description *Sturm–Liouville* is not strictly applicable), reflecting the fact that viscous and/or non-linear effects are not negligible in that neighbourhood. Applying the method of Frobenius to (A.13) in this neighbourhood, we find that *sufficient* conditions for $y=y_c$ not to be a branch point for the solution are

$$\rho_c'=0, \quad U_c'\neq 0, \quad \rho_c''g+\rho_c U_c' U_c''=0, \tag{A.15a,b,c}$$

where the subscript c implies evaluation at $U=c$. We shall assume that these conditions are satisfied in the subsequent development with sufficient accuracy to justify our neglect of phase changes across the flow; in the special case of constant density this will be so if

$$|U_c''/kU_c'|\ll 1. \tag{A.16}$$

Assuming the (approximate) satisfaction of (A.15a,b,c), $f(y)$ still will exhibit a simple pole at $y=y_c$, but *this* singularity is simply a consequence of approximating v by $U-c$ near $y=y_c$ (rather than a consequence of the neglect of viscous forces) and appears only in the streamline displacement, the perturbation velocity remaining finite there.

Appendix B

Variational formulation

Let $W_\pm$ denote the work by the fluid in $y\gtrless 0$ on the interfacial wave at $y=0$, and V_0 the potential energy of this wave. We shall first show that

$$W_\pm=\frac{1}{2}\iint_{y\gtrless 0}[q(\nabla\eta)^2+w'\eta^2]\,dx\,dy, \tag{B.1}$$

where the y-intervals of integration for W_+ and W_- are $(0+,\infty)$ and $(-\infty,0-)$, and the x-interval for both W_+ and W_- is either any integral number of wavelengths if η is periodic in x or $(-\infty,+\infty)$ if $\eta\to 0$ as $|x|\to\infty$. We then shall deduce the principle of virtual work in the form

$$\delta W_\pm=0 \quad \text{for} \quad \delta\eta(x,0\pm)=0, \tag{B.2a,b}$$

thereby establishing that (B.1) is a variational integral for the differential equation (A.10).†

A more complete statement of the principle of virtual work (the statement (B.2) refers only to the boundary-value problem for the fluid motion in a half-space ($y\gtrless 0$) with prescribed boundary conditions at $y=0$) is

$$\delta(W_++W_--V_0)=0. \tag{B.3a}$$

We could invoke (B.3a) to obtain a direct formulation for the entire motion, without singling out the motion of the interface in any special way. However, such a procedure is not advantageous (herein at least) in establishing approximate solutions, and we shall use it only to deduce the equation of motion of the interfacial wave for a virtual displacement $\delta\eta_0(x)$. Even this is unnecessary for the

† We also could reverse the argument and deduce (A.10) from (B.2), but our chief interest in the variational principle is as a vehicle for the approximation of $W_\pm$.

determination of the wave speed, which we may infer directly from the requirement of conservation of energy, namely†

$$W_+ + W_- - V_0 = 0. \tag{B.3b}$$

To prove (B. 1), we first transform the integral of $q(\nabla\eta)^2$ through Kelvin's generalization of Green's theorem (Courant & Hilbert 1931, vol. 1, p. 239) to obtain

$$W_\pm = -\frac{1}{2}\iint_{y\gtrless 0} L\{\eta\}\,\eta\,dx\,dy \mp \frac{1}{2}\int_{y=0\pm} q\eta_y\eta\,dx. \tag{B.4a}$$

Invoking (A. 10) and identifying $q\eta_y$ with $p-p_0$ through (A. 9) then yields

$$W_\pm = \mp\frac{1}{2}\int_{y=0\pm}(p-p_0)\,\eta\,dx, \tag{B.4b}$$

which we may identify with the work done on the interface in virtue of the (presumed) linearity of $p-p_0$ in η.

To prove (B. 2), we take the variation of (B. 1) to obtain (*ibid.*, p. 181)

$$\delta W_\pm = -\iint_{y\gtrless 0} L\{\eta\}\,\delta\eta\,dx\,dy \mp \int_{y=0\pm} q\eta_y\,\delta\eta\,dx \tag{B.5a}$$

$$= \mp\int_{y=0\pm}(p-p_0)\,\delta\eta\,dx. \tag{B.5b}$$

Invoking (B. 2*b*) in (B. 5*b*) then yields (B. 2*a*).

Turning to (B. 3*a*, *b*), we have

$$V_0 = \frac{1}{2}\int_{y=0}[T\eta_x^2 + (\Delta w)\,\eta^2]\,dx \tag{B.6}$$

for the potential energy associated with surface tension and the buoyancy force, where Δ denotes a jump-operator according to

$$\Delta(\ ) = (\ )_{y=0-} - (\ )_{y=0+}, \tag{B.7}$$

and the x-intervals of integration correspond to those for $W_\pm$. Taking the variation of (B. 6) and combining the result with (B. 5*b*), we obtain

$$\delta(W_+ + W_- - V_0) = \int_{y=0}[\Delta p + T\eta_{xx} - (\Delta w)\,\eta]\,\delta\eta\,dx. \tag{B.8}$$

Invoking (B. 3*a*) for arbitrary $\delta\eta$ then yields

$$\Delta p + T\eta_{xx} - (\Delta w)\,\eta = 0, \quad y = 0, \tag{B.9}$$

as otherwise follows directly from the equilibrium of the forces acting on the interface.

We may simplify the foregoing results by separating variables according to (1.1) and (A. 12) and replacing the x-integrations by mean values (denoted by bars) over a wavelength. We also find it convenient to separate the work done by

† Equations (B.1)–(B.3*a*) may be generalized for an arbitrary number of interfaces, but (B.3*b*) provides a direct determination of the wave speed only for a single interface.

the hydrodynamic pressure, say $W_{a\pm}$, from that done by the buoyancy pressure and include the negative of the latter with the potential energy. We then write

$$\overline{W_{a\pm}} = \frac{1}{2}\int_{y\gtrless 0} q\overline{(\nabla\eta)^2}\,dy \tag{B.10a}$$

$$= \tfrac{1}{2}a^2\int_{y\gtrless 0}\rho_0(U-c)^2(f'^2+k^2f^2)\,dy \tag{B.10b}$$

and

$$\overline{V} = -\frac{1}{2}\left(\int_{-\infty}^{0-}+\int_{0+}^{\infty}\right)w'\overline{\eta^2}\,dy+\tfrac{1}{2}T\overline{\eta_{0x}^2}+\tfrac{1}{2}(\nabla w)\,\overline{\eta_0^2} \tag{B.11a}$$

$$= \tfrac{1}{2}a^2\left[g\int_{\rho_0(\infty)}^{\rho_0(-\infty)}f^2\,d\rho_0+Tk^2\right], \tag{B.11b}$$

where the integral in (B. 11*b*) includes the jump in ρ_0 at $y = 0$.

In the important, special case of constant densities, ρ_+ for $y > 0$ and ρ_- for $y < 0$, $\overline{W}_{a\pm}$ constitutes a variational integral for the reduced differential equation ($\rho_0' = 0$ in (A. 13))

$$[(U-c)^2f']'-k^2(U-c)^2f = 0, \quad y\gtrless 0, \tag{B.12}$$

subject to the boundary conditions (A. 14*a*, *b*); moreover, $\overline{W}_{a\pm}$ then not only is stationary with respect to first-order variations of $f(y)$ about the true solution to (B. 12) but also is positive definite and therefore an absolute minimum with respect to variations ($\delta f(y)$) of arbitrary magnitude provided only that the approximate $f(y)$ satisfies (A. 14*a*, *b*). We also note that (B. 11*b*) reduces to

$$\overline{V} = \tfrac{1}{2}a^2[(\rho_- -\rho_+)\,g+Tk^2] \tag{B.13}$$

in this special case.

In the restricted problem posed in the opening paragraph of §1, we not only assume constant densities but also neglect ρ_+ compared with ρ_- and $\overline{W}_{a-}$ compared with $\overline{W}_{a+}(U_- \doteqdot 0)$ and set $c = 0$. The results of this and the preceding appendix then are equivalent to those of §§2 and 3. If, in place of $c = 0$, we neglect c compared with U_+ and neglect U_- compared with c in the calculation of $\overline{W}_{a+}$ and $\overline{W}_{a-}$, we obtain

$$f = e^{ky} \text{ in } y < 0 \quad \text{and} \quad \overline{W}_{a-} = \tfrac{1}{2}\rho_- c^2ka^2, \tag{B.14a, b}$$

whence (B. 3*b*) yields the slightly more general result (in place of (3.2))

$$c^2 = c_0^2-\frac{s}{k}\int_0^\infty U^2(f'^2+k^2f^2)\,dy. \tag{B.15}$$

where c_0^2 is given by the left-hand side of (1.4*a*). The variational principle predicts that the substitution of an approximate $f(y)$ in (B. 15) will overestimate the integral, thereby underestimating both the wave speed $|c|$ and the magnitude of the critical wind speed at any prescribed level for a profile of prescribed shape. We note, however, that the predicted values of c^2 near the critical wind speed (at which $c^2 = 0$) may be appreciably in error in consequence of its calculation as a difference between nearly equal quantities.

We turn now to the more general problem posed in the closing paragraphs of §1. Substituting (B. 10*b*) and (B. 11*b*) in (B. 3*b*) and solving for c in so far as it appears

explicitly (it also occurs implicitly through f), we may place the result in the form (1.7), replacing (1.8) and (1.9) by

$$\widetilde{U^n} = \int_{-\infty}^{\infty} \rho_0 U^n (f'^2 + k^2 f^2)\, dy \Big/ \int_{-\infty}^{\infty} \rho_0 (f'^2 + k^2 f^2)\, dy \tag{B.16}$$

and

$$c_0^2 = \left[g \int_{\rho_0(\infty)}^{\rho_0(-\infty)} f^2 d\rho_0 + Tk^2 \right] \Big/ \int_{-\infty}^{\infty} \rho_0 (f'^2 + k^2 f^2)\, dy. \tag{B.17}$$

If we assume ρ_0 and U to be independent of y except for discontinuities across $y = 0$, (A. 13) and (A. 14a, b) are satisfied by $f = \exp(-k|y|)$, and we may reduce (B. 16) and (B. 17) to (1.8) and (1.9).

The foregoing development, in so far as it appeals to classical Sturm–Liouville theory (through our references to Courant & Hilbert), requires additional justification if $q = 0$ at (say) $y = y_c$ in the range of integration. We may extend the results by excluding the singular region from the area integrals, thereby obtaining additional line integrals over $y = y_c \pm$. The end-result of such a procedure is that the results (B. 10) and (B. 11) may be interpreted formally by deforming the path of integration around the singular point $y = y_c$; in so far as the conditions (A. 15a, b, c) are satisfied (at least approximately), this procedure then leads to finite, *real* values of $\overline{W}$ (at least approximately). Unfortunately, however, the characterization *positive definite* no longer is appropriate to the integrand over the deformed path, and we then may not assert that $\overline{W}_{a+}$ and $\overline{W}_{a-}$ are absolute minima with respect to variations of f about the true solution to (B. 12).

We may circumvent this last difficulty by assuming (in addition to either (A. 15a, b, c) or (A. 16))

$$k|y_c| \ll 1, \tag{B.18}$$

noting that this restriction usually must be satisfied if phase variations across the flow are to be negligible and the aerodynamic force in phase with the interfacial displacement is to be of the same order of magnitude as the restoring forces. We then may calculate the work done on a virtual interface at, say, $|y| = \delta$ through (B. 10b), after which the energy transferred from shear flow to surface wave in $0 < |y| < \delta$ could be calculated through a direct integration of (A. 13) or (B. 12) for small $k|y|$ (as in obtaining the inviscid solutions to the Orr–Sommerfeld equation). We find, however, that the latter energy is to the former as $k\delta$ to 1 and hence, by hypothesis, negligible. In fact, we have used (in §§ 4 and 5) only non-singular approximations to f, and may regard the procedure outlined in this paragraph primarily as a justification for such approximations within the framework of the variational principle.

I am indebted to T. Brooke Benjamin (Cambridge University), C. S. Cox (Scripps Institute of Oceanography) and J. R. D. Francis (Imperial College) for valuable discussions and suggestions during the course of the foregoing research, and particularly to Mr Francis for providing the photograph in figure 1. I also take pleasure in acknowledging support, in the form of a fellowship, from the John Simon Guggenheim Memorial Foundation.

REFERENCES

Carrier, G. F. 1954 Interface stability of the Helmholtz type. *Los Alamos Internal Report.*

Courant, R. & Hilbert, D. 1931 *Methoden der Mathematischen Physik.* Berlin: Julius Springer.

Esch, R. E. 1957 *J. Fluid Mech.* **3**, 289.

Francis, J. R. D. 1954 *Phil. Mag.* (7), **45**, 695.

Francis, J. R. D. 1956 *Phil. Mag.* (8), **1**, 685.

Francis, J. R. D. 1959 Private communication.

Goldstein, S. 1931 *Proc. Roy. Soc.* A, **132**, 524.

Hay, J. S. 1955 *Quart. J. Roy. Met. Soc.* **81**, 307.

Jeffreys, H. 1924 *Proc. Roy. Soc.* A, **107**, 189.

Jeffreys, H. 1925 *Proc. Roy. Soc.* A, **110**, 341.

Lord Kelvin 1871 *Mathematical and Physical Papers*, vol. iv, pp. 76–85. Cambridge University Press (1910).

Keulegan, G. H. 1951 *J. Res. Nat. Bur. Stand.* **46**, 358.

Lamb, H. 1945 *Hydrodynamics*, 6th ed. New York: Dover.

Lessen, M. 1950 NACA Tech. Report 979, Washington, D.C.

Lighthill, M. J. 1957 *J. Fluid Mech.* **3**, 113.

Miles, J. W. 1957 *J. Fluid Mech.* **3**, 185.

Milne-Thomson, L. M. 1950 *Theoretical Hydrodynamics.* New York: Macmillan.

Munk, W. 1947 *J. Mar. Res.* **6**, 203.

Phillips, O. M. 1957 *J. Fluid Mech.* **2**, 417.

Prandtl, L. 1952 *The Essentials of Fluid Dynamics.* New York: Hafner.

Roll, H. 1948 *Ann. Met., Hamburg*, **1**, 139.

Taylor, G. I. 1931 *Proc. Roy. Soc.* A, **132**, 499.

Ursell, F. 1956 Article in *Surveys in Mechanics.* Cambridge University Press.

Van Dorn, W. 1953 *J. Mar. Res.* **12**, 249.

The symmetric state of a rotating fluid differentially heated in the horizontal

By ALLAN R. ROBINSON*
Pierce Hall, Harvard University

(Received 16 March 1959)

The motion of a fluid inside a rotating annulus of square cross-section, whose dimensions are small compared with the distance from the axis of rotation, is considered. The rigid side walls are held at different constant temperatures, and the fluid motions that occur are strongly influenced by Coriolis accelerations. A detailed study is made of the azimuthally independent state, a Hadley cell, in the limit of small thermal Rossby number. It is convenient to employ a boundary layer type analysis, essentially with respect to the Taylor number, and all the imposed boundary conditions are rigorously satisfied.

An entirely geostrophic thermal wind is found to obtain over the main body of the fluid. The circulation in the plane of the annular cross-section is entirely confined within narrow boundary layers and consists of a superposition of three cellular motions: a cell occupying the cross-section and two additional cells confined to the side-wall boundary layers. These motions are intimately related to the rotational constraint. The temperature distribution and its relation to the conductive and convective processes are determined.

1. The Hadley cell

1.1. *Introduction*

When a fluid is differentially heated in a horizontal direction, motions immediately occur, even if the imposed horizontal temperature difference is infinitesimal, since there is no pressure distribution capable of balancing the thermally induced gravitational body force. The simplest steady state attainable for a fluid of finite vertical extent with heating independent of one horizontal co-ordinate is that of a single cellular motion. The fluid ascends in the region of maximum heating, moves horizontally towards the region of maximum cooling, descends, and returns to its place of origin.

When the fluid is observed in a co-ordinate frame which is rotating relative to an inertial system, Coriolis acceleration produces a component of horizontal velocity perpendicular to the direction of the imposed thermal gradient. This component of velocity may be called the thermal wind. If rotation and heating rates are such that the Coriolis acceleration and the thermal body force are of the same order of magnitude, the thermal wind will be the largest component of velocity over the main body of the fluid.

The simple cellular motion of a horizontally heated rotating fluid bears the

* Present address, Cavendish Laboratory, Cambridge.

name of George Hadley (1735), who first made the above remarks in a discussion of the general circulation of the atmosphere.

1.2. *Hadley's original work*

The large-scale atmospheric motions have long been known to be driven by the latitudinal variation of the heating of the earth by the sun. However, the predominant feature of the resulting circulation is its longitudinal component. Hadley first related this phenomenon to the constraint of the earth's rotation in the paper referred to above, entitled 'Concerning the Cause of the General Trade-Winds'. In his words,

> 'I Think the Causes of the General Trade-Winds have not been fully explained by any of those who have wrote on that Subject, for want of more particularly and distinctly considering the Share the diurnal Motion of the Earth has in the Production of them. . . .'†

Hadley considered the atmosphere to be thermally driven away from the state of solid rotation:

> 'For, let us suppose the Air in every Part to keep an equal Pace with the Earth in its diurnal Motion. . .then by the Action of the Sun on the Parts about the Equator, and the Rarefaction of the Air proceding therefrom, let the Air be drawn down thither from the N. and S. Parts.'‡

He then showed that easterlies would occur near the equator because

> '. . .the Air, as it moves from the Tropicks toward the Equator, having a less velocity than the Parts of the Earth it arrives at, will have a relative Motion contrary to that of the diurnal Motion of the Earth in these Parts. . .'§

Westerlies at mid-latitudes were similarly explained.

Hadley then made quantitative calculations of the magnitude of the winds assuming the air to keep the longitudinal velocity of the earth at the point of the airs origin. Finding the values thus calculated to be too large, he called upon surface friction:

> '. . .before the Air from the Tropicks can arrive at the Equator, it must have gained some Motion Eastward from the Surface of the Earth or Sea, whereby its relative Motion will be diminished, and in several successive Circulations, may be supposed to be reduced to the Strength it is found to be of.'‖

Hadley concluded

> 'That without the Assistance of the diurnal Motion of the Earth, Navigation, especially Easterly and Westerly, would be very tedious, and to make the whole Circuit of the Earth perhaps impracticable.'††

1.3. *Modelling in geophysical fluid dynamics*

The general circulation of the real atmosphere is of course much more complicated than a simple Hadley cell. Furthermore, theoretical studies are hampered not only because of the complexity of the governing mathematics, but also because meaningful quantitative data on real geophysical flows are very difficult to

† Hadley (1735), p. 58. ‡ *Ibid.* p. 60. § *Idem.* ‖ *Ibid.* p. 61. †† *Ibid.* p. 62.

obtain, especially on the large scale. Detailed theory could give information not obtainable observationally, but such theory is not useful unless it has first undergone a careful and detailed comparison with nature in some instances.

Recently, theoretical geophysical fluid dynamics has been stimulated by the initiation of controlled laboratory experiments in rotating tanks (Long 1953). These experiments, of interest in themselves, are also capable in some sense of modelling the larger scale, but the precise validity of the modelling remains an open question of great interest.

A class of experiments has been performed with a rotating fluid differentially heated in the horizontal. The initial motivation for these experiments lay in the possibility of their relation to the origin of the earth's magnetic field by convection in the liquid core (Hide 1958); and the meteorological interest aroused by early experimental results has led to extensive further work (Fultz 1956). The results are certainly a fascinating example of the physics of natural convection in the presence of rotation.

The annular space between two coaxial cylinders mounted on a rotating platform is filled with water. A horizontal temperature gradient is imposed on the boundaries. Three distinct types of steady states appear. First, a Hadley cell, or symmetric régime, in which the velocity and temperature fields are independent of the azimuthal angle about the axis of the cylinders is found. Secondly, a wave régime is found, i.e. a laminar flow in which the streamlines viewed from the top form a wave pattern, and various wave numbers appear. Thirdly, a turbulent régime is found with various numbers of well-defined eddies.

The régime and wave number selected by the fluid depends upon the imposed horizontal temperature difference and the rotation rate of the apparatus. For a given moderately strong rotation rate ($\Omega > 0{\cdot}1\,\mathrm{sec}^{-1}$), the symmetric régime occurs both for sufficiently small ($\Delta T < 0{\cdot}3\,^{\circ}\mathrm{C}$), and sufficiently large temperature differences. (These will be designated the lower and upper symmetric régimes.) At intermediate temperature differences the wave régime occurs. The transitions from régime to régime and from one wave number to another occur at definite critical values of the parameters. For large enough rotation rates, where the transition to the upper symmetric régime occurs at large temperature differences, the turbulent régime occurs between two wave régimes. A diagram of the various régimes is presented in figure 1. Since a full range of experiments has not as yet been performed on a given fluid in a given annular geometry, figure 1 is qualitatively inferred from several experiments.

To date, experiments, especially in the symmetric régime, have been mostly qualitative with some quantitative results for critical values of parameters governing the instabilities. Some ambiguity exists in the results because of lack of control of the boundary conditions, e.g. surface evaporation, wind stress, and uneven heating.

Meteorological interest in these experiments lies in the apparent relation of the wave and eddy régimes to the general circulation patterns in the atmosphere. However, to gain understanding of these complicated régimes by existing theoretical techniques, it is necessary first to have a complete theory of the symmetric state. Then by study of the stability of the symmetric state, the

criterion for the initial onset of the wave régime can be found. Finally, it would be possible to attempt to determine the conditions which govern the preference of one particular wave number over another, a highly non-linear problem.

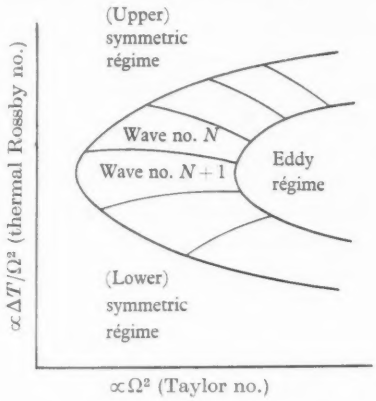

FIGURE 1. Qualitative picture of the various régimes.

Each step in this theoretical approach depends upon the preceding one and becomes succeedingly more difficult. Thus the theory of the Hadley cell, of interest *per se*, also provides the necessary firm foundation for a study of the more complicated states of a horizontally heated rotating fluid.

1.4. *The present problem*

In formulating a theoretical approach to a general class of phenomena, it is of course invaluable to study the simplest physical situation possible. We want the important aspects of the physics to be retained within the simplest framework in which their full implications can be realized, and also the situation considered must be simultaneously capable of precise experimental study and quantitative theoretical analysis.

In order for a fluid to exhibit a Hadley cell and the subsequent instabilities, it is important only that the fluid be heated from the sides and experience Coriolis accelerations. Therefore, it is of interest to consider a fluid confined to a rotating annular region of square cross-section, the dimension of which is small compared to the distance from the centre of rotation so that curvature and centrifugal effects will be minimized. The side walls are to be held at different constant temperatures, and the top and bottom walls are to be thermally insulating. Four rigid walls allow the elimination of extraneous boundary effects. In addition, the symmetry simplifies the physical situation and thereby reduces the mathematical complexity of its description. This model will be formalized in the next section.

Previous theoretical studies (e.g. Davies 1956; Kuo 1956) relevant to the general experimental situation described above differ from that indicated here. The situations discussed have been more complicated. Moreover, because these studies were primarily concerned with the stability problem, simplifying mathematical assumptions were made about the symmetric régime, and the assumptions

used failed to bring boundary condition information into the final description. Aspects of the symmetric régime, such as internal temperature gradients, which are in fact determined by the boundary conditions, have been treated as free parameters in the stability problem.

2. The mathematical model

2.1. *Definitions and assumptions*

Consider a fluid contained between two coaxial cylinders and two parallel planes, the distance between the cylinders being equal to the distance between the planes. Let the container rotate with respect to an inertial system. The rotation vector, anti-parallel to gravity, coincides with the axis of the cylinders, both being normal to the planes (see figure 2).

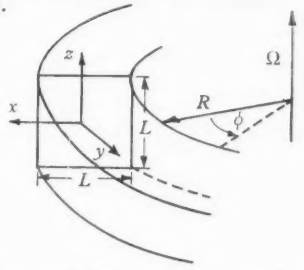

FIGURE 2. The co-ordinate system.

The fluid is thermally driven away from the state of solid rotation by an imposed horizontal temperature gradient, i.e. the inner and outer cylinders are held at different constant temperatures. The horizontal surfaces are thermally insulating.

We use the following nomenclature:

$\mathbf{r}$	Co-ordinate vector with components (x, y, z). With respect to the cylinders, x is radial, y is azimuthal, z is vertical. x and y are also referred to as meridional and zonal
$\mathbf{v}$	Velocity with components (u, v, w)
p	Deviation from hydrostatic pressure
T	Temperature. N.B. The above symbols primed have dimensions, unprimed they are dimensionless
Ψ	Stream function for the velocity components in the x-z plane. N.B. v, T, Ψ are also used with superscripts as coefficients in perturbation expansions
$(\hat{\mathbf{i}}, \hat{\mathbf{j}}, \hat{\mathbf{k}})$	Unit vectors in the (x, y, z) directions
g	Acceleration due to gravity
α	Coefficient of thermal expansion
ρ	Fluid density
ν	Kinematic viscosity
κ	Thermometric conductivity
Ω	Angular velocity of solid rotation
ΔT	Total horizontal temperature difference
R	Radius of inner cylinder
L	Side of square cross-section of annulus

The explicit assumptions defining the mathematical model applied to the fluid system are:

(*a*) A linear dependence of density on temperature alone as the equation of state:

$$\rho = \rho_0[1-\alpha(T'-T_0)]. \tag{2.1}$$

(*b*) The coefficient of thermal expansion, α, of the fluid is taken to be zero except when coupled with the gravitational constant. This allows for the thermally induced gravitational force, but neglects all other effects of density variation. In particular the assumption is made of local incompressibility,

$$\nabla' . \mathbf{v}' = 0. \tag{2.2}$$

Assumptions (*a*) and (*b*) are frequently used in similar problems and are known as the Boussinesq Approximation.

(*c*) Viscosity and thermal conductivity are constant.

(*d*) Frictional dissipation is neglected in the energy equation, which becomes, using also (*b*) and (*c*),

$$\kappa\nabla'^2 T' - \mathbf{v}' . \nabla' T' = 0. \tag{2.3}$$

(*e*) The distance between the bounding cylinders is small compared to the radius of the inner cylinder, i.e. $L/R \ll 1$. This serves to eliminate curvature effects in the equations and implies a constant centrifugal term.

(*f*) The centrifugal acceleration is much smaller than the gravitational acceleration, i.e. $\Omega^2 R/g \ll 1$. This is consistent with assumption (*b*) above.

Under these assumptions, the Navier–Stokes equations describing the symmetric ($\partial/\partial y' \equiv 0$) steady ($\partial/\partial t \equiv 0$) state take the form

$$-\nu\nabla'^2\mathbf{v}' + \mathbf{v}' . \nabla'\mathbf{v}' + 2\boldsymbol{\Omega}\times\mathbf{v}' - \alpha g T'\mathbf{k} + \rho_0^{-1}\nabla' p' = 0. \tag{2.4}$$

Here p' is the difference between the actual pressure and a pressure which balances the constant terms $\rho_0(g\hat{\mathbf{k}} - \Omega^2 R\hat{\mathbf{i}})$. The symbolic operators, of course, are only two-dimensional.

Equations (2.2), (2.3) and (2.4) provide five equations for the three components of velocity, the temperature and the pressure. Specifying the necessary boundary conditions completes the exposition of the formal mathematical problem. On the four rigid walls, all velocity components must vanish, i.e. $\mathbf{v}' = 0$ at $x' = \pm\frac{1}{2}L$, $z' = \pm\frac{1}{2}L$. The condition of constant temperature on the vertical walls is taken as $T' = \pm\frac{1}{2}(\Delta T)$ at $x' = \pm\frac{1}{2}L$; and no transfer of heat across the horizontal walls implies $\partial T'/\partial z' = 0$ at $z' = \pm\frac{1}{2}L$.

2.2. *The method of approximation*

Although in §1 the simplest physical problem for the symmetric circulation of a horizontally heated rotating fluid has been formally posed, it is still too difficult mathematically for direct solution. The equations are coupled, high order, non-linear partial differential equations. In order to proceed, some approximate procedure must be adopted.

Since any approximation will consist of arguments concerning relative orders of magnitude, it will be convenient to introduce non-dimensional variables and parameters at this point. Let $\mathbf{r}' = L\mathbf{r}$, $T' = (\Delta T)\,T$, $\mathbf{v}' = c\mathbf{v}$, and $p' = c^2\rho_0 p$,

where c is an as yet undetermined velocity. When these variables are substituted into (2.4), it can be seen that the choice of $c = \alpha g(\Delta T)(2\Omega)^{-1}$ will transform the terms $2\boldsymbol{\Omega}\times\mathbf{v}' - \alpha g T'\hat{\mathbf{k}}$ into $\hat{\mathbf{k}}\times\mathbf{v} - T\hat{\mathbf{k}}$, i.e. into terms which are (non-dimensionally) of order unity. This is appropriate because $T\hat{\mathbf{k}}$ represents the driving force, and also because interest lies in the case where the constraint of rotation, $\hat{\mathbf{k}}\times\mathbf{v}$, is of the same order of magnitude.

It is also convenient now to make use of the azimuthal symmetry in the continuity equation (2.2), which becomes $\partial u/\partial x + \partial w/\partial z = 0$. Thus it is possible to introduce a stream function for the velocity components in the x-z plane defined by $u \equiv \Psi_z$, $w \equiv -\Psi_x$, subscripts denoting partial differentiation. The boundary conditions on the velocity now require that Ψ and its normal derivative be zero on all boundaries.

Introducing the non-dimensional variables and the stream function, and subtracting after cross-differentiating the first and third components of (2.4) to eliminate the pressure, we obtain the remaining equations:

$$-\epsilon\nabla^4\Psi + \beta[\Psi_z\Psi_{xzz} + \Psi_z\Psi_{xxx} - \Psi_x\Psi_{zzz} - \Psi_x\Psi_{xxz}] - v_z + T_x = 0, \quad (2.5)$$

$$-\epsilon\nabla^2 v + \beta[\Psi_z v_x - \Psi_x v_z] + \Psi_z = 0, \quad (2.6)$$

$$-\epsilon\nabla^2 T + \beta\sigma[\Psi_z T_x - \Psi_x T_z] = 0, \quad (2.7)$$

where $\epsilon = \nu(2\Omega)^{-1}L^{-2}$ is the reciprocal square-root of a Taylor number, $\beta = \alpha g(\Delta T)(2\Omega)^{-2}L^{-1}$ is a thermal Rossby number, and $\sigma = \nu\kappa^{-1}$ is the Prandtl number.

The lower symmetric régime is characterized by small total temperature difference and, in the range of interest where instabilities are known to occur in related experiments, by moderately strong rotation rates; thus this régime is associated with small values of β and ϵ. We now assume that $\beta < 1$, $\epsilon < 1$, and $\sigma = O(1)$, but since these properties of the parameters are used to develop approximate solutions, more explicit limitations on their magnitudes will be found later.

Ordinary perturbation expansions in β of all the variables can now be made, i.e.

$$\Psi = \sum_{n=0}^{\infty}\beta^n\Psi^{(n)}, \quad v = \sum_{n=0}^{\infty}\beta^n v^{(n)}, \quad T = \sum_{n=0}^{\infty}\beta^n T^{(n)}.$$

A single superscript (n) denotes the nth order β-expansion coefficient for the variable on which it appears. The expansions are inserted into equations (2.5), (2.6) and (2.7), and terms of order β^n are collected.

The terms of zero order give:

$$-\epsilon\nabla^4\Psi^{(0)} - v_z^{(0)} + T_x^{(0)} = 0, \quad (2.8)$$

$$-\epsilon\nabla^2 v^{(0)} + \Psi_z^{(0)} = 0, \quad (2.9)$$

$$\nabla^2 T^{(0)} = 0. \quad (2.10)$$

The terms of first order give:

$$-\epsilon\nabla^4\Psi^{(1)} - v_z^{(1)} + T_x^{(1)} + [\Psi_z^{(0)}\Psi_{xzz}^{(0)} + \Psi_z^{(0)}\Psi_{xxx}^{(0)} - \Psi_x^{(0)}\Psi_{zzz}^{(0)} - \Psi_x^{(0)}\Psi_{xxz}^{(0)}] = 0, \quad (2.11)$$

$$-\epsilon\nabla^2 v^{(1)} + \Psi_z^{(1)} + [\Psi_z^{(0)}v_x^{(0)} - \Psi_x^{(0)}v_z^{(0)}] = 0, \quad (2.12)$$

$$-\epsilon\nabla^2 T^{(1)} + \sigma[\Psi_z^{(0)}T_x^{(0)} - \Psi_x^{(0)}T_z^{(0)}] = 0, \quad (2.13)$$

and so on. Each $\Psi^{(n)}$ separately satisfies the boundary conditions on Ψ. $T^{(0)}$ satisfies the non-dimensional condition $T^{(0)} = \pm\frac{1}{2}$ at $x = \frac{1}{2}$, $T^{(n)} = 0$ at $x = \pm\frac{1}{2}$ for $n > 0$. At $z = \pm\frac{1}{2}$, $T_z^{(n)} = 0$ for all n.

From the form of these equations, the role of β in the heat equation, as a measure of the relative importance of conduction and convection in determining the temperature distribution, is made clear. Small β means that conduction effects are important. The zero-order temperature is in fact determined entirely by conduction, and thus is not coupled to the zero-order velocity. This temperature distribution then acts as the forcing term for the coupled zero-order velocity equations (2.8) and (2.9). Next, the first-order temperature is determined by conduction balancing advection of the zero-order temperature field by the zero-order velocities. Similarly, to any order in β, the temperature is first determined, by conduction, from a Poisson equation in which the inhomogeneity consists of advections of lower-order temperatures by lower-order velocities. The known temperature then appears as an inhomogeneity in the coupled velocity equations of the same order, which are also forced by lower-order momentum advections. The latter will be found to be relatively unimportant.

The mathematical difficulties have now been considerably lessened. All the equations have been linearized, and the heat equation has been reduced to a simple standard form. However, the coupled velocity equations are not simple, and it will be worthwhile to exploit the fact that ϵ is small in their solution. Since ϵ multiplies the highest order differentiated terms in each equation, a direct expansion in this parameter is not permissible. If this were done, the order of the equations would be lowered and the boundary conditions could not be satisfied. Singular perturbation theory or boundary-layer analysis must be used (see Carrier, 1953).†

The highest-order differentiated terms can contribute only when they are large enough to overcome the small factor ϵ. Extreme changes of the velocity functions and their derivatives are not expected over the main body of the fluid, but can occur near the boundaries, where viscous effects are important. Therefore solutions of approximate equations of low order will be tolerated in the interior of the fluid only. Near each boundary additional contributions to the solutions will appear; these additional contributions will satisfy approximate equations of higher order, and together with the interior solutions will satisfy all boundary conditions.

Since the zero-order velocities are expected to have a boundary-layer character, and these velocities force the first-order temperature, it is expected that first- and higher-order temperatures will also exhibit boundary-layer effects. It is pertinent to notice that in equation (2.13) the same small parameter ϵ also couples the highest-order differentiated terms in the temperature.

In the next section, solutions for the lower symmetric régime will be obtained by the double perturbation procedure outlined above.

† This reference should be consulted for any questions in standard boundary-layer techniques which are employed in the following analysis.

3. Analysis and results

3.1. *The zero order*

The zero-order temperature may be trivially obtained from equation (2.10) because of the particularly simple boundary conditions imposed. Thus

$$T^{(0)}(x,z) = x, \tag{3.1}$$

and $T_x^{(0)} = 1$ is to be inserted into (2.8).

Treating (2.8) and (2.9) as a boundary-layer problem, we must first determine the boundary-layer widths and the amplitudes as functions of ϵ. Since the equations are linear, the boundary-layer widths, or more precisely the characteristic lengths normal to the boundaries in which the highly differentiated terms contribute, can be determined independently of amplitude considerations. This is done most simply by considering the single equation satisfied by either $\Psi^{(0)}$ or $v^{(0)}$ alone, e.g.

$$\epsilon^2 \nabla^6 \Psi^{(0)} + \Psi^{(0)}_{zz} = 0, \tag{3.2}$$

which is obtained by cross-differentiation.

Scaled normal co-ordinates are defined near each of the boundaries by $\xi = \epsilon^a(x+\frac{1}{2})$ near $x = -\frac{1}{2}$ and $\zeta = \epsilon^b(z+\frac{1}{2})$ near $z = -\frac{1}{2}$. The exponents a and b will be determined by deriving appropriate approximate equations for the contributions near each wall from (3.2). Negative values are anticipated so that ξ and ζ will be stretched co-ordinates, i.e. a large change in ξ will be equivalent to a small change in x. Equation (3.2) is now rewritten in terms of ξ and z, and x and ζ as independent variables. The derivatives $\partial/\partial x$ and $\partial/\partial z$ are expressed as $\epsilon^{-a}(\partial/\partial\xi)$ and $\epsilon^{-b}(\partial/\partial\zeta)$ respectively. The assumption that $\Psi^{(0)}$ is smooth, i.e. the function itself and all its derivatives are bounded above by order unity, is made. The equations can then be ordered with respect to ϵ as a small quantity. To perform the ordering, the highest term of ∇^6 is required in each case to balance the rotational constraint, the last term in (3.2). This procedure yields $a = -\frac{1}{3}$, $b = -\frac{1}{2}$, and the approximate equations

$$\Psi^{(0)}_{\xi\xi\xi\xi\xi\xi} + \Psi^{(0)}_{zz} = 0, \quad \text{near } x = -\tfrac{1}{2}, \tag{3.3}$$

$$\Psi^{(0)}_{\zeta\zeta\zeta\zeta\zeta\zeta} + \Psi^{(0)}_{\zeta\zeta} = 0, \quad \text{near } z = -\tfrac{1}{2}. \tag{3.4}$$

The first neglected terms in (3.3) are $O(\epsilon^{\frac{2}{3}})$, and in (3.4) are $O(\epsilon)$.

The same equations in similarly defined stretched co-ordinates will pertain near $x = \frac{1}{2}$, $z = \frac{1}{2}$. It will be noticed that the side-wall boundary layers, of width $O(\epsilon^{\frac{1}{3}})$, are broader than the top and bottom boundary layers, of width $O(\epsilon^{\frac{1}{2}})$. The approach adopted here will, of course, break down in the corner regions where none of the approximations are valid. However, these regions are small and relatively unimportant. The vertical and horizontal boundary layers will be mutually consistent because they will uniquely satisfy, when added to the same interior solution, boundary conditions along their respective walls.

To determine the amplitudes of the contributions to the fields in the separate regions, it is necessary to return to the coupled equations which also contain the forcing inhomogeneity. It is convenient to transfer the inhomogeneity into the boundary conditions. This is readily done by extracting the particular solution with the substitution $v^{(0)} = z + v_h^{(0)}$. The boundary conditions change to $v_h^{(0)} = -z$

at $x = \pm\frac{1}{2}$; $v_h^{(0)} = \mp\frac{1}{2}$ at $z = \pm\frac{1}{2}$. The particular solution is recognized as the geostrophic thermal wind, well known in meteorology. To isolate the dependence of the amplitudes on ϵ, let

$$\Psi^{(0)} = A(\epsilon)\,\psi^{(0)}, \quad v_h^{(0)} = B(\epsilon)\,v^{(0)}, \quad \text{in the interior;}$$
$$_{(1)}\Psi^{(0)} = A_1(\epsilon)\,{}_{(1)}\psi^{(0)}, \quad {}_{(1)}v_h^{(0)} = B_1(\epsilon)\,{}_{(1)}v^{(0)}, \quad \text{near the vertical wall;}$$
$$_{(2)}\Psi^{(0)} = A_2(\epsilon)\,{}_{(2)}\psi^{(0)}, \quad {}_{(2)}v^{(0)} = B_2(\epsilon)\,{}_{(2)}v^{(0)}, \quad \text{near the horizontal wall.}$$

For convenience the boundary-layer region near the vertical wall will hereafter be referred to as region 1, and that near the horizontal wall as region 2. A lower left-hand subscript on a variable refers to the region. ${}_{(i)}\psi^{(0)}$ and ${}_{(i)}v^{(0)}$ are assumed to be independent of ϵ, and to be smooth in their arguments. The above expressions are now substituted into the approximate forms of (2.8) and (2.9), using the scaling information obtained above, yielding:

In the interior:
$$Bv_z^{(0)} = 0, \tag{3.5}$$
$$A\psi_z^{(0)} = 0. \tag{3.6}$$

In region 1:
$$\epsilon^{-\frac{1}{3}}A_1\,{}_{(1)}\psi_{\xi\xi\xi\xi}^{(0)} + B_1\,{}_{(1)}v_z^{(0)} = 0, \tag{3.7}$$
$$\epsilon^{\frac{1}{3}}B_1\,{}_{(1)}v_{\xi\xi}^{(0)} - A_1\,{}_{(1)}\psi_z^{(0)} = 0. \tag{3.8}$$

In region 2:
$$\epsilon^{-1}A_2\,{}_{(2)}\psi_{\zeta\zeta\zeta\zeta}^{(0)} + \epsilon^{-\frac{1}{2}}B_2\,{}_{(2)}v_\zeta^{(0)} = 0, \tag{3.9}$$
$$B_2\,{}_{(2)}v_{\zeta\zeta}^{(0)} - A_2\epsilon^{-\frac{1}{2}}\,{}_{(2)}\psi_\zeta^{(0)} = 0. \tag{3.10}$$

These homogeneous equations† yield relationships between the amplitudes of $\Psi^{(0)}$ and $v_h^{(0)}$, which are required to make all terms in a given equation consistently the same order in ϵ.

The interior equations contain no amplitude information. However, the boundary-layer equations (3.7) and (3.8) give, consistently,

$$A_1 = \epsilon^{\frac{1}{3}}B_1, \tag{3.11}$$

and, (3.9) and (3.10),
$$A_2 = \epsilon^{\frac{1}{2}}B_2. \tag{3.12}$$

The boundary conditions further require that at least part of $v_h^{(0)}$ be of order unity near each wall; thus
$$B_1 = 1 \quad (A_1 = \epsilon^{\frac{1}{3}}), \tag{3.13}$$
$$B_2 = 1 \quad (A_2 = \epsilon^{\frac{1}{2}}), \tag{3.14}$$

in the appropriate regions. If relationships (3.13) and (3.14) had happened to be identical, it would have been relatively simple to proceed from this point. Since they are not, further argument is necessary.

The only factor affecting amplitudes not contained in the above general statements is the requirement that the boundary conditions be satisfied by the boundary-layer contributions near each wall added to the same interior solution. In the formal expansion which is being evolved here, boundary conditions must of course be separately satisfied by all orders in ϵ. Thus amplitudes in one region strongly influence amplitudes in another region. In considering the effect of the

† The homogeneous equations are definitely correct for the contributions, of lowest order in ϵ, to $\psi^{(0)}$ and $v^{(0)}$ in each region. The equations for higher-order terms may be modified by the appearance of inhomogeneities in the form of the neglected parts of ∇^4 and ∇^2 operating on the lower-order fields.

application of both vertical and horizontal wall boundary conditions on the amplitude problem, certain particular properties of the solutions to the governing equations (3.5–3.10) are necessary and will now be derived. These equations are taken as independent of ϵ and solved under the auxiliary restrictions (3.11, 3.12).

The interior equations (3.5, 3.6) integrate immediately to

$$v^{(0)} = f(x), \tag{3.15}$$

$$\psi^{(0)} = g(x). \tag{3.16}$$

The boundary-layer equations in region 2, (3.9, 3.10),† can be treated as ordinary equations (with constant coefficients) in ζ with x-dependent integration constants. Rejecting solutions which do not approach zero asymptotically in ζ, and requiring the normal derivative of ${}_{(2)}\psi^{(0)}$ to vanish on the wall, we find the solutions to be

$${}_{(2)}\psi^{(0)} = G(x)\, e^{-\zeta/\sqrt{2}}(\sin\zeta/\sqrt{2} + \cos\zeta/\sqrt{2}), \tag{3.17}$$

and

$${}_{(2)}v^{(0)} = -\sqrt{2}\, G(x)\, e^{-\zeta/\sqrt{2}}\cos\zeta/\sqrt{2}. \tag{3.18}$$

Thus at $\zeta = 0$,

$${}_{(2)}\psi^{(0)} = G(x), \tag{3.19}$$

and

$${}_{(2)}v^{(0)} = -\sqrt{2}\, G(x). \tag{3.20}$$

Near the top boundary, let $\zeta^* = \epsilon^{-\frac{1}{2}}(z - \frac{1}{2})$; then the form of equations (3.9, 3.10) is reproduced in ζ^* under the transformation

$$\zeta \to -\zeta^*, \quad {}_{(2)}\psi^{(0)} \to {}_{(2)}\psi^{(0)}, \quad {}_{(2)}v^{(0)} \to -{}_{(2)}v^{(0)}.$$

Thus along the top wall,

$${}_{(2)}\psi^{(0)} = G^*(x), \tag{3.21}$$

and

$${}_{(2)}v^{(0)} = \sqrt{2}\, G^*(x). \tag{3.22}$$

Those properties of the solutions which have been obtained now enable the amplitude argument to be concluded. The boundary conditions require that values of $v_h^{(0)}$ of order unity exist in both regions 1 and 2, i.e. the existence of $B_1 = 1$ and $B_2 = 1$. In turn, the amplitude consistency relations (3.15, 3.16) then require $A_1 = \epsilon^{\frac{1}{3}}$ and $A_2 = \epsilon^{\frac{1}{2}}$ in their respective regions. A boundary-layer contribution to $\Psi^{(0)}$ which will add to an interior contribution to give a zero stream function on the walls forces the amplitude of the interior stream function, i.e. requires definite values of A. Since the amplitudes of $\Psi^{(0)}$ required in the different boundary layers by the above arguments are not of the same order in ϵ, they cannot simply add together with the same interior solution.

To proceed, it would seem necessary to require contributions to the interior $\Psi^{(0)}$ of both amplitudes, i.e. to have in the interior $\Psi^{(0)} = \epsilon^{\frac{1}{3}}\psi^{(0,\frac{1}{3})} + \epsilon^{\frac{1}{2}}\psi^{(0,\frac{1}{2})} + \ldots$. (Hereafter when two superscripts are used the first will refer to the order in β and the second to the order in ϵ. A single superscript will continue to refer to the order in β.) However, the appearance of an amplitude of $\Psi^{(0)}$ in the interior further requires the same amplitude in the boundary layer other than whence it originated. E.g. $A_1 = \epsilon^{\frac{1}{3}}$ implies $A = \epsilon^{\frac{1}{3}}$ which in turn implies $A_2 = \epsilon^{\frac{1}{3}}$, etc.

Invoking again the amplitude consistency relationships (3.11, 3.12), we see that $A_2 = \epsilon^{\frac{1}{3}}$ requires a contribution to ${}_{(2)}v_h^{(0)}$ of $B_2 = \epsilon^{-\frac{1}{6}}$. This in turn would carry a

† These equations are controlled by the rotational constraint in a manner first noticed by Ekman (1905) while considering the effect of the wind stress on the ocean.

$v_h^{(0)}$ of order $\epsilon^{-\frac{1}{6}}$ through the interior and into the side-wall boundary layer. Thus the fact that (3.11) and (3.12) differ would generate, indefinitely, further amplitudes of both $\Psi^{(0)}$ and $v_h^{(0)}$ in all three regions.

The possibility of simplification arises only if one of the originally required contributions to $\Psi^{(0)}$ satisfies the boundary conditions by itself at the wall of the boundary-layer region in which it necessarily exists. Note that this is physically interpreted as allowing for the possibility of a boundary-layer counter-current. If either ${}_{(1)}\psi^{(0,\frac{1}{3})} = 0$ at $\xi = 0$ or ${}_{(2)}\psi^{(0,\frac{1}{2})} = 0$ at $\zeta = 0$, a contribution of the same amplitude from the interior, etc., is not required. Finally, the properties of ${}_{(2)}\psi^{(0,\frac{1}{2})}$ revealed in (3.17, 3.19) show that ${}_{(2)}\psi^{(0,\frac{1}{2})}$ cannot be zero at $\zeta = 0$. Such a requirement would force ${}_{(2)}\psi^{(0,\frac{1}{2})}$ to be identically zero everywhere in region 2, which is impossible.

However, it will be seen that ${}_{(1)}\psi^{(0,\frac{1}{3})}$ can meet this requirement in region 1. Therefore, the following problem is formulated as being the simplest consistent with the full amplitude and scaling requirements. The unique and unambiguous results obtained below indicate that it is the correct boundary-layer problem associated with equations (2.8, 2.9), and therefore provides formal approximate solutions to these equations.

In the interior and in region 2, near the horizontal wall, the stream function is $O(\epsilon^{\frac{1}{2}})$ and the zonal velocity is $O(1)$, $A = A_2 = \epsilon^{\frac{1}{2}}$, and $B = B_2 = 1$. The boundary conditions at $z = -\frac{1}{2}$ are applied to $\Psi^{(0)} = \epsilon^{\frac{1}{2}}(\psi^{(0,\frac{1}{2})} + {}_{(2)}\psi^{(0,\frac{1}{2})})$ and $v_h^{(0)} = v^{(0,0)} + {}_{(2)}v^{(0,0)}$, and similarly at $z = +\frac{1}{2}$. Near the vertical wall in region 1, two amplitudes of the stream function and two amplitudes of the zonal velocity are required, $A_1 = \epsilon^{\frac{1}{3}}$ and $\epsilon^{\frac{1}{2}}$, and $B_1 = 1$ and $\epsilon^{\frac{1}{6}}$, i.e. ${}_{(1)}\psi^{(0)} = \epsilon^{\frac{1}{3}}\,{}_{(1)}\psi^{(0,\frac{1}{3})} + \epsilon^{\frac{1}{2}}\,{}_{(1)}\psi^{(0,\frac{1}{2})}$, ${}_{(1)}v_h^{(0)} = {}_{(1)}v^{(0,0)} + \epsilon^{\frac{1}{6}}\,{}_{(1)}v^{(0,\frac{1}{6})}$. Each set ${}_{(1)}\psi^{(0,\frac{1}{3})}$, ${}_{(1)}v^{(0,0)}$ and ${}_{(1)}\psi^{(0,\frac{1}{2})}$, ${}_{(1)}v^{(0,\frac{1}{6})}$ separately satisfies equations (3.7, 3.8). The boundary conditions at $x = -\frac{1}{2}$ are $\psi^{(0,\frac{1}{2})} + {}_{(1)}\psi^{(0,\frac{1}{2})} = 0$, ${}_{(1)}\psi^{(0,\frac{1}{3})} = 0$, $v^{(0,0)} + {}_{(1)}v^{(0,0)} = -z$, ${}_{(1)}v^{(0,\frac{1}{6})} = 0$. These boundary conditions are symmetrical in x, and introducing near $x = +\frac{1}{2}$ the variable $\xi^* = \epsilon^{-\frac{1}{3}}(x - \frac{1}{2})$, the form of (3.7, 3.8) is reproduced in ξ^* under the transformation $\xi \to -\xi^*$. Thus solutions near $x = \frac{1}{2}$ are immediately available from those at $x = -\frac{1}{2}$.

Applying the boundary conditions at the top and bottom walls to the solution (3.15, 3.16, 3.19–3.22), we obtain

$$\begin{aligned} G(x) + g(x) &= 0, \\ G^*(x) + g(x) &= 0, \\ -\sqrt{2}\,G(x) + f(x) &= -\tfrac{1}{2}, \\ \sqrt{2}\,G^*(x) + f(x) &= +\tfrac{1}{2}, \end{aligned}$$

which have the solutions

$$g(x) = -G(x) = -G^*(x) = \frac{1}{2\sqrt{2}}, \tag{3.23}$$

and

$$f(x) = 0. \tag{3.24}$$

Thus the total zero order interior velocity is purely the geostrophic thermal wind. The velocity in the x-z plane, the vertical and meridional flow, is identically zero to this order in ϵ and β.

It remains to find the solutions near the side walls. The boundary conditions are now further specified in terms of equations (3.23, 3.24) as ${}_{(1)}\psi^{(0,\frac{1}{2})} = -1/(2\sqrt{2})$,

${}_{(1)}v^{(0,0)} = -z$. With the conditions imposed, the solutions are most readily obtained in terms of Fourier series in the vertical co-ordinate, the Fourier coefficients being explicit functions of the boundary-layer co-ordinate. Separated solutions of the constant coefficient equations (3.7, 3.8) exist of the form $\exp\{(k^2)^{\frac{1}{6}}\xi\}\begin{matrix}\sin\\ \cos\end{matrix} kz$, and the boundary conditions can be applied in terms of well-known square wave and sawtooth Fourier series. The solutions are

$$
\begin{aligned}
{}_{(1)}\psi^{(0,\frac{1}{2})} = \frac{1}{2\sqrt{2}}\left(\frac{16\sqrt{2}}{3\sqrt{3}\,\pi^{\frac{7}{3}}}\right)\sum_{n=0}^{\infty}(2n+1)^{-\frac{7}{3}}\Big\{&\sqrt{3}\exp\{-[(2n+1)\pi]^{\frac{1}{3}}\xi\}\\
&+\exp\{-[(2n+1)\pi]^{\frac{1}{3}}\}\frac{\xi}{2}\left(-\sqrt{3}\cos[(2n+1)\pi]^{\frac{1}{3}}\frac{\sqrt{3}}{2}\xi+\sin[(2n+1)\pi]^{\frac{1}{3}}\frac{\sqrt{3}}{2}\xi\right)\Big\}\\
&\times(-)^n\cos(2n+1)\pi z, \qquad (3.25)
\end{aligned}
$$

$$
\begin{aligned}
{}_{(1)}v^{(0,0)} = \left(\frac{8}{3\sqrt{3}\,\pi^2}\right)\sum_{n=0}^{\infty}(2n+1)^{-2}\Big\{&\sqrt{3}\exp\{-[(2n+1)\pi]^{\frac{1}{3}}\xi\}\\
&+\tfrac{1}{2}\exp\{-[(2n+1)\pi]^{\frac{1}{3}}\}\frac{\xi}{2}\left(\sqrt{3}\cos[(2n+1)\pi]^{\frac{1}{3}}\frac{\sqrt{3}}{2}\xi+\sin[(2n+1)\pi]^{\frac{1}{3}}\frac{\sqrt{3}}{2}\xi\right)\Big\}\\
&\times(-)^{n+1}\sin(2n+1)\pi z, \qquad (3.26)
\end{aligned}
$$

and

$$
\begin{aligned}
{}_{(1)}\psi^{(0,\frac{1}{6})} = \frac{1}{2\sqrt{2}}\left(\frac{-4}{\sqrt{3}\,\pi}\right)\sum_{n=0}^{\infty}(2n+1)^{-1}\exp\{-[(2n+1)\pi]^{\frac{1}{3}}\}\frac{\xi}{2}\\
\times\left(\sqrt{3}\cos[(2n+1)\pi]^{\frac{1}{3}}\frac{\sqrt{3}}{2}\xi+\sin[(2n+1)\pi]^{\frac{1}{3}}\frac{\sqrt{3}}{2}\xi\right)(-)^n\cos(2n+1)\pi z, \qquad (3.27)
\end{aligned}
$$

$$
\begin{aligned}
{}_{(1)}v^{(0,\frac{1}{6})} = \left(\frac{\sqrt{2}}{\sqrt{3}\,\pi^{\frac{2}{3}}}\right)\sum_{n=0}^{\infty}(2n+1)^{-\frac{2}{3}}\\
\times\exp\{-[(2n+1)\pi]^{\frac{1}{3}}\}\frac{\xi}{2}\left(\sin[(2n+1)\pi]^{\frac{1}{3}}\frac{\sqrt{3}}{2}\xi\right)(-)^{n+1}\sin(2n+1)\pi z. \qquad (3.28)
\end{aligned}
$$

These results are plotted and discussed more fully in § 3.4 below. ${}_{(1)}\psi^{(0,\frac{1}{2})}$ represents a flow up the hot wall and down the cold wall, the streamlines of the flow are bowed out from the wall, the maximum bowing occurring at the mid-point of the wall. All the mass transport in the side boundary layers is associated with ${}_{(1)}\psi^{(0,\frac{1}{2})}$. ${}_{(1)}\psi^{(0,\frac{1}{6})}$ represents a narrow circulating cell of velocity confined to the vertical wall boundary layers.† This is an interesting unanticipated result directly related to the rotational constraint.

3.2. *The first order*

The first-order temperature calculation is of particular interest because it contains the first modifications of the temperature from that governed purely by conduction. In physical situations where the perturbation calculations evolved here are expected to be useful, the observable temperature will be the temperature through first order in β. Thus the vertical temperature gradient of importance to the anticipated stability problem will be a result of this calculation.

† *Note added in proof.* From a consideration of the asymptotic form of the exact solution to equation (3.2), a single contribution to this cell of width $\epsilon^{\frac{1}{3}}$ is found. Thus ${}_{(1)}\psi^{(0,\frac{1}{6})}$ is partly spurious. This failure of boundary-layer analysis is discussed more fully elsewhere (Carrier & Robinson, to be published). It corresponds solely to a modification of the non-mass-transporting cell confined to the side-wall boundary layer. No other results are affected. For an example of the appearance of an $\epsilon^{\frac{1}{3}}$ contribution in a similar problem, see Stewartson (1957).

The zero-order convection terms in (2.13) forcing the first-order temperature can be evaluated from the results of the preceding section. Since $T_z^{(0)} = 0$ and $T_x^{(0)} = 1$ everywhere, the last term of (2.13) is identically zero and $T^{(1)}$ is determined by the equation

$$-\epsilon\nabla^2(\sigma^{-1}T^{(1)}) + \Psi_z^{(0)} = 0. \tag{3.29}$$

On comparison with equation (2.9) for the zero-order zonal velocity, $v^{(0)}$, (3.29) is seen to be identical with $\sigma^{-1}T^{(1)}$ replacing $v^{(0)}$. Therefore a particular solution of (3.29) is $T_p^{(1)} = \sigma v^{(0)}$. As anticipated, this contribution to the temperature forms strong boundary layers. With respect to ϵ, $T_p^{(1)}$ is $O(1)$ everywhere with an additional contribution $O(\epsilon^{\frac{1}{4}})$ near the constant temperature side walls, region 1.

To preserve the physical conditions on the total temperature, the first-order temperature at the walls must obey the conditions $T^{(1)} = 0$ at $x = \pm\frac{1}{2}$; $\partial T^{(1)}/\partial z = 0$ at $z = \pm\frac{1}{2}$. Since $v^{(0)}$ is zero on all walls, the first condition is obeyed by $T_p^{(1)}$, but the second condition is not. From (3.18) and (3.23),

$$\frac{\partial}{\partial z}T_p^{(1)}|_{z=-\frac{1}{2}} = \epsilon^{-\frac{1}{2}}\frac{\sigma}{z}\frac{\partial}{\partial\zeta}(\exp\{-\zeta/\sqrt{2}\}\cos\zeta/\sqrt{2}|_{\zeta=0} + O(1) = -\frac{\epsilon^{-\frac{1}{2}}\sigma}{2\sqrt{2}} \tag{3.30}$$

to the lowest order in ϵ. $T_p^{(1)}$ is antisymmetric in z; therefore

$$\frac{\partial}{\partial z}T_p^{(1)}|_{z=+\frac{1}{2}} = -\frac{\epsilon^{-\frac{1}{2}}\sigma}{2\sqrt{2}}$$

also. Thus homogeneous solutions to (3.29) must contribute to $T^{(1)}$, and must satisfy the boundary conditions

$$T_h^{(1)} = 0 \quad \text{at} \quad x = \pm\tfrac{1}{2}; \quad \frac{\partial}{\partial z}T_h^{(1)} = +\frac{\epsilon^{-\frac{1}{2}}\sigma}{2\sqrt{2}} \quad \text{at} \quad z = \pm\tfrac{1}{2}.$$

Since $T_h^{(1)}$ satisfies the homogeneous Laplace equation, it cannot form boundary layers, i.e. have extremely sharp gradients near the walls. Therefore the condition in ϵ on the gradient of $T_h^{(1)}$ on the top and bottom walls must be taken as a condition on the amplitude of $T_h^{(1)}$ everywhere. Thus $T_h^{(1)}(x, z) = \epsilon^{-\frac{1}{2}}T^{(1,-\frac{1}{2})}(x, z)$, where $\nabla^2 T^{(1,-\frac{1}{2})} = 0$. Since the temperature $T^{(1,-\frac{1}{2})}$ is $\epsilon^{-\frac{1}{2}}$ larger than the directly convected temperature $T_p^{(1)} = T^{(1,0)}$, then $T^{(1,-\frac{1}{2})}$ will be the observed temperature. Thus in this case, the vertical temperature distribution is primarily set directly by conduction, but is, nevertheless, implicitly controlled by convective processes. Conduction acts to maintain the physical boundary conditions disturbed by convection.

Anticipating the first-order velocity calculation to be forced by this temperature distribution, it is most convenient to obtain $T^{(1,-\frac{1}{2})}$ as a Fourier series in the vertical co-ordinate. This is readily done by applying a finite Fourier transform. The result is

$$T^{(1,-\frac{1}{2})} = \frac{\sigma}{2\sqrt{2}}\left\{\left(\frac{4}{\pi^2}\right)\sum_{n=0}^{\infty}\left[\frac{(-)^{n+1}\cosh(2n+1)\pi x\sin(2n+1)\pi z}{(2n+1)^2\cosh(2n+1)\frac{1}{2}\pi}\right] + z\right\}. \tag{3.31}$$

The isotherms of this temperature distribution plotted in §3.4 are seen to be almost horizontal over the main body of the fluid. Thus the isotherms of the total temperature, to first order, will be tilted away from the vertical zero-order conduction isotherms. The shape of the tilted isotherms is given by the purely numerical function $\sigma^{-1}T^{(1,-\frac{1}{2})}$. The magnitude of the deviation from the pure conduction temperature is conveniently expressed by the multiplicative factor $\beta\epsilon^{-\frac{1}{2}}\sigma$.

To obtain the first-order velocities, equations (2.12, 2.13) are employed. A boundary-layer analysis entirely similar to that used in solving the zero-order equations (2.8, 2.9) can be used, even in the presence of the more complicated inhomogeneous terms now present. The inhomogeneous forcing terms consist of zero-order inertial terms and the first-order horizontal temperature gradient. From the zero-order solutions, the inertial terms in (2.11, 2.12) are found to be identically zero except near the side walls. In region 1, the inertial terms in (2.11) are at most $O(\epsilon^{-\frac{1}{4}})$, and in (2.12) at most $O(1)$. The contributions to $\Psi^{(1)}$ and $v^{(1)}$ forced by these terms will be of lower order in ϵ than the contributions forced by $T_x^{(1)}$ considered below, and may therefore be formally neglected.

Since the equations are linear, the contributions to the velocities from $T^{(1,-\frac{1}{2})}$ and $T_p^{(1)}$ may be dealt with separately. Considering first $T^{(1,-\frac{1}{2})}$, from (3.31) the corresponding particular solution to (2.11, 2.12) is obtained,

$$v^{(1,-\frac{1}{2})} = \frac{\sigma\sqrt{2}}{\pi^2} \sum_{n=0}^{\infty} \frac{(-)^n \sinh(2n+1)\pi x \cos(2n+1)\pi z}{(2n+1)^2 \cosh(2n+1)\tfrac{1}{2}\pi}. \tag{3.32}$$

Since $\cos(\pm(2n+1)\frac{1}{2}\pi) = 0$, $v^{(1,-\frac{1}{2})}$ satisfies boundary conditions at $z = \pm\frac{1}{2}$, no additional boundary layer contributions being necessary. However, boundary layers are necessary at the side walls, since $v^{(1,-\frac{1}{2})}$ given by (3.32) does not satisfy the boundary conditions at $x = \pm\frac{1}{2}$. A boundary-layer contribution to the zonal velocity implies a related contribution to the stream function. By (3.11), ${}_{(1)}\psi^{(1,-\frac{1}{6})}$ is found to be required by ${}_{(1)}v^{(1,-\frac{1}{2})}$. These fields together must satisfy (3.7, 3.8). The appropriate boundary conditions at $\xi = 0$ are

$${}_{(1)}\psi^{(1,-\frac{1}{6})} = 0, \quad {}_{(1)}v^{(1,-\frac{1}{2})} = -\frac{\sigma\sqrt{2}}{\pi^2} \sum_{n=0}^{\infty} a_n \cos(2n+1)\pi z,$$

where, by (3.32),

$$a_n = (-)^n \sinh(2n+1)(-\tfrac{1}{2}\pi)\cosh(2n+1)\tfrac{1}{2}\pi\,(2n+1)^{-2}. \tag{3.33}$$

The solutions are

$${}_{(1)}v^{(1,-\frac{1}{2})} = \left(\frac{2\sigma}{3\sqrt{3}}\right) \sum_{n=0}^{\infty} a_n \left\{\sqrt{3}\exp\{-[(2n+1)\pi]^{\frac{1}{3}}\xi\} + \tfrac{1}{2}\exp\{-[(2n+1)\pi]^{\frac{1}{3}}\xi\}\frac{\xi}{2}\right.$$
$$\left. \times\left(\sqrt{3}\cos[(2n+1)\pi]^{\frac{1}{3}}\frac{\sqrt{3}}{2}\xi + \sin[(2n+1)\pi]^{\frac{1}{3}}\frac{\sqrt{3}}{2}\xi\right)\right\}\cos(2n+1)\pi z, \tag{3.34}$$

$${}_{(1)}\psi^{(1,-\frac{1}{6})} = \left(\frac{2\sigma}{3\sqrt{3}\,\pi^{\frac{1}{3}}}\right) \sum_{n=0}^{\infty} a_n (2n+1)^{-\frac{1}{3}} \left\{\sqrt{3}\exp\{-[(2n+1)\pi]^{\frac{1}{3}}\xi\}\right.$$
$$+\tfrac{1}{2}\exp\{-[(2n+1)\pi]^{\frac{1}{3}}\xi\}\frac{\xi}{2}\left(-\sqrt{3}\cos[(2n+1)\pi]^{\frac{1}{3}}\frac{\sqrt{3}}{2}\xi\right.$$
$$\left.\left.+\sin[(2n+1)\pi]^{\frac{1}{3}}\frac{\sqrt{3}}{2}\xi\right)\right\}\sin(2n+1)\pi z. \tag{3.35}$$

The existence of these boundary-layer solutions indicates that the zonal velocity as given by (3.32) is the correct total $v^{(1)}$ for the interior of the fluid. Isolines of $v^{(1,-\frac{1}{2})}$ are seen in §3.4 to be essentially horizontal. Thus the zonal velocity v, to first order, will be tilted away from the purely horizontal zero-order thermal wind by $v^{(1,-\frac{1}{2})}$, much as the first-order temperature is tilted from the vertical by $T^{(1,-\frac{1}{2})}$.

The stream function ${}_{(1)}\psi^{(1,-\frac{1}{6})}$ given by (3.35) is associated with two narrow cells

of velocity confined to each side-wall boundary-layer region, one extending from $z = -\frac{1}{2}$ to $z = 0$, and the other from $z = 0$ to $z = +\frac{1}{2}$. $\psi^{(1,-\frac{1}{2})}$ exists only in region 1 and is consistently associated with no net mass transport. The additional contributions to the first-order velocities forced by $T_p^{(1)}$ can be seen also to exist only in region 1, and therefore not to affect net transports. In region 1, $T_{px}^{(1)} = O(\epsilon^{-\frac{1}{3}})$ and will only force amplitudes of $\Psi^{(1)}$ and $v^{(1)}$ smaller than those already calculated. However, these velocities are at best of interest only *per se*; and the involved calculations will not be performed. The results given by (3.34, 3.35) were obtained because they were necessary to establish the results for the first-order velocity in the interior.

3.3. *Range of validity of the theory*

It is of course impossible to prove and to define the range of the convergence of the double perturbation expansions for the solutions with mathematical rigour. It is, however, useful and necessary to place plausible restrictions on the applicability of the theory. This will be done in terms of the magnitude of the largest neglected terms. Therefore, although no detailed calculations of the complicated second-order fields will be made, an examination of the magnitude of the second-order temperature is given.

The equation for the second-order temperature is found to be

$$-\epsilon\nabla^2 T^{(2)} + \sigma(\Psi_z^{(0)} T_x^{(1)} - \Psi_x^{(0)} T_z^{(1)} + \Psi_z^{(1)} T_x^{(0)} - \Psi_x^{(1)} T_z^{(0)}) = 0. \tag{3.36}$$

The last term will be zero everywhere, since $T_z^{(0)} = 0$. The remaining convection terms are also zero in the interior, since the interior stream function, though first order, remains constant; conduction alone still determines the interior temperature through second-order terms. In each boundary layer, expanding the convection terms in ϵ yields many contributions to $T^{(2)}$ differing only by terms $O(\epsilon^{\frac{1}{3}})$. Note that convection terms involving the vertical gradient of the temperature, which were identically zero in the first-order temperature equation, appear in (3.36). However, all the amplitudes of $T^{(2)}$ required for the particular solution to (3.36) are found to be of higher order in ϵ than the homogeneous solution required to satisfy the insulating condition along the top and bottom walls. This is precisely similar to the first-order result.

The amplitude of $T^{(2)}$ thus required is $O(\epsilon^{-1})$, N.B. $\beta^2\epsilon^{-1} = (\beta\epsilon^{-\frac{1}{2}})^2$. The ϵ-independent amplitude of $T^{(2,-1)}$ is determined by the condition on the gradient at $z = -\frac{1}{2}$, which is

$$\frac{\partial}{\partial z} T^{(2,-1)}\big|_{z=-\frac{1}{2}} = -\sigma T_x^{(1,-\frac{1}{2})}(x, -\tfrac{1}{2}) \frac{\partial}{\partial \zeta} v^{(0,0)}\big|_{\zeta=0}. \tag{3.37}$$

The right-hand side of (3.37) is a known function of x. In order to obtain a numerical estimate of the amplitude of $T^{(2,-1)}$, the absolute value of (3.37) is averaged over x, yielding

$$\left(\left|\frac{\partial}{\partial z} T^{(2,-1)}\big|_{z=-\frac{1}{2}}\right|\right)_{\text{avg}} = \left(\frac{\sigma}{2\sqrt{2}}\right)^2 O(1). \tag{3.38}$$

The order unity quantity in (3.38) is found from (3.31), or from figure 6, to be approximately $\frac{3}{4}$.

This result indicates that the critical parameter for the double expansion procedure is actually

$$\lambda = (2\sqrt{2})^{-1}\sigma\beta\epsilon^{-\frac{1}{2}} = (2\sqrt{2})^{-1}\alpha g(\Delta T)\,\nu^{\frac{1}{2}}\kappa^{-1}(2\Omega)^{-\frac{3}{2}}. \tag{3.39}$$

Thus convergence is indicated for $\lambda < 1$. To make second-order terms less than 10 % of first-order terms, $\lambda^2 = (0{\cdot}36)^2(\sigma\beta\epsilon^{-\frac{1}{2}})^2 < 0{\cdot}1$, i.e. $\sigma\beta\epsilon^{-\frac{1}{2}}$ may be only slightly less than 1. A safe restriction to indicate that the first-order fields are correct to 10 % is $\sigma\beta\epsilon^{-\frac{1}{2}} < \frac{3}{4}$.

The original restriction $\beta < 1$, $\epsilon < 1$ must of course still be retained. Now that boundary-layer widths are known in terms of ϵ, further restrictions may be placed on this parameter. Requiring that the broad side-wall boundary layers be less than 15 % of the total non-dimensional distance, we must have $\epsilon^{\frac{1}{4}} < 0{\cdot}15$, i.e. $\epsilon < 3\times10^{-3}$.

In summary, the limitations are

$$\beta < 1, \quad \epsilon < 3\times10^{-3}, \quad \sigma\beta\epsilon^{-\frac{1}{2}} < \tfrac{3}{4}. \tag{3.40}$$

For a given fluid (ν), in a given geometrical situation (L), a minimum bound on ϵ (maximum bound on Ω), may be obtained to maintain the validity of the original assumption, (f), of negligible centrifugal effects. The range of parameters allowed by these considerations indicates that the first-order theory should be valid for the lower symmetric régime in most situations attainable in the laboratory (see Fultz 1956, p. B-84).

3.4. *Results*

The lower symmetric régime of a horizontally heated rotating fluid, confined to a square cross-section annulus whose dimensions are small compared to the distance from the centre of rotation, has been discussed. The solutions for the non-linearly coupled temperature and velocity fields have been obtained by first expanding in the thermal Rossby number, $\beta = \alpha g(\Delta T)\,(2\Omega)^{-2}L^{-1}$, and then, to each order in β, performing boundary-layer analysis with respect to the reciprocal of the Taylor number squared, $\epsilon = \nu(2\Omega)^{-1}L^{-2}$.

In the range of parameters appropriate to this procedure, it has been seen that the non-linear convective terms in the heat equation significantly control the development of the fields, while the non-linear momentum advections (the inertial terms in the Navier–Stokes equations) are negligible. Because of the perturbation analyses the parameters β and ϵ do not appear in the approximate equations, which contain only the Prandtl number, $\sigma = \nu\kappa^{-1}$. Since inertial terms are negligible, σ appears only as a factor in the amplitude of all fields of higher β-order than zero. The mathematical problem solved is the same as that which would have arisen had the assumptions been made that $\beta = 0$, $(\beta\sigma) \neq 0$, with an accompanying expansion in $\beta\sigma$. This would be a valid approach for $\sigma > 1$, as it is for laboratory experiments with water. However, the approach actually used is more revealing in that the effects of the inertial terms are examined and the modifications occurring from their inclusion can be estimated in terms of ϵ and σ.

The theory will be most useful when the conditions (3.40) are satisfied. We then have that the temperature and zonal velocity are described by terms up to first order in β. The boundary-layer velocities are adequately described by the

zero-order terms in β, first-order effects being entirely confined to internal modifications in the side-wall boundary regions. The meridional and vertical velocity components are identically zero in the interior up to the first order.

The dependence on β, ϵ and σ has been extracted so that these parameters determine only amplitudes and scaled co-ordinates. Thus, except for scaling, the results of any particular experiment are fully described in terms of functions devoid of physical dimensions. Figures 3–8 are graphs of the numerical functions most useful for comparison with experiment.

The zero-order side-wall boundary-layer vertical and meridional velocity streamlines, from the expressions (3.25, 3.27), are shown in figures 3 and 4. The streamline distortion associated with ${}_{(1)}\psi^{(0,\frac{1}{2})}$ is a result of Coriolis effects as well as the appearance of the additional cell implied by ${}_{(1)}\psi^{(0,\frac{1}{3})}$. The total zero-order streamlines are a linear superposition of these two contributions,

$$ {}_{(1)}\psi^{(0)} = \epsilon^{\frac{1}{3}}{}_{(1)}\psi^{(0,\frac{1}{3})} + \epsilon^{\frac{1}{2}}{}_{(1)}\psi^{(0,\frac{1}{2})}. $$

The cell velocity strengthens, the mass-transporting velocity near the wall and weakens it away from the wall. The extra factor of $\epsilon^{-\frac{1}{6}}$ tends to make ${}_{(1)}\psi^{(0,\frac{1}{3})}$ dominant, but from figures 3 and 4 the purely numerical amplitude of ${}_{(1)}\psi^{(0,\frac{1}{3})}$

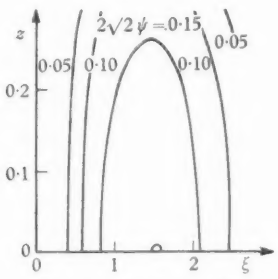

FIGURE 3. Streamlines of ${}_{(1)}\psi^{(0,\frac{1}{3})}$.

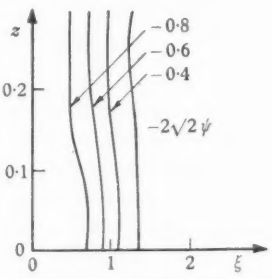

FIGURE 4. Streamlines of ${}_{(1)}\psi^{(0,\frac{1}{3})}$.

is seen to be less than that of ${}_{(1)}\psi^{(0,\frac{1}{2})}$. Thus for low rotation rates (large ϵ), the counter current associated with ${}_{(1)}\psi^{(0,\frac{1}{3})}$ may or may not be observable, but it definitely will be observable for large rotation rates. The boundary-layer streamlines along the top and bottom walls are straight lines given by (3.17) and (3.23).

The zonal velocity would of course vanish if there were no rotation. The relation of the zonal velocity to Coriolis effects is easily seen in the zero-order results. In the top and bottom boundary layers where the cross-rotation-lines meridional velocity is the largest, the velocity-dependent Coriolis accelerations are the largest and the zonal velocity attains its maximum and minimum values. In the interior, the pressure balances the Coriolis accelerations due to the zonal velocity together with the thermally induced gravitational body force. In order for the interior pressure to do this consistently, the vertical zonal velocity gradient must equal the horizontal temperature gradient; this is the thermal wind relationship. Consistent with the zero-order linear horizontal conduction temperature is a zero-order linear vertical zonal velocity distribution. The contributions to the zero-

order zonal velocity in the side-wall boundary layers, ${}_{(1)}v^{(0)} = {}_{(1)}v^{(0,0)} + \epsilon^{\frac{1}{2}}\,{}_{(1)}v^{(0,\frac{1}{2})}$, are given by (3.26, 3.28) and are shown in figures 5 and 6.

The observable first-order temperature has been found to be directly set by conduction, although it satisfies boundary conditions determined by the first effects of convection. This temperature, $T^{(1,-\frac{1}{2})}$, is given by (3.31) and shown in figure 7. $T^{(1,-\frac{1}{2})}$ predominantly governs the vertical temperature structure. Therefore the actual vertical temperature gradient of interest to the stability problem is seen to be proportional to $(\alpha g \nu^{\frac{1}{2}}\kappa^{-1})\,L^{-1}(\Delta T)^2\,\Omega^{-\frac{3}{2}}$ degrees Centigrade

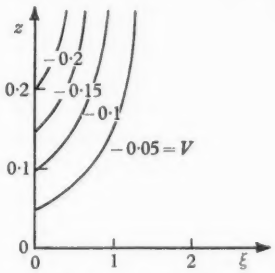

FIGURE 5. Isolines of ${}_{(1)}v^{(0,0)}$.

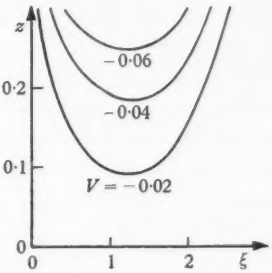

FIGURE 6. Isolines of ${}_{(1)}v^{(0,\frac{1}{2})}$.

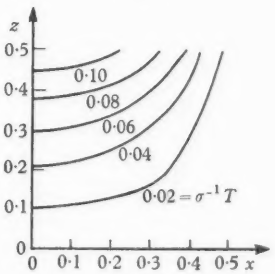

FIGURE 7. Isotherms of $\sigma^{-1}T^{(1,-\frac{1}{2})}$.

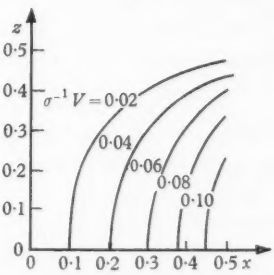

FIGURE 8. Isolines of $\sigma^{-1}v^{(1,-\frac{1}{2})}$.

per centimetre; this is a second-order effect in the temperature difference, and varies with the inverse three-halves power of the rotation rate. Figure 8 shows the first-order zonal velocity consistent with $T^{(1,-\frac{1}{2})}$ given by (3.32).

The macroscopic quantity of greatest physical interest which characterizes the system is the total heat transport. A measure of this quantity is the integrated normal temperature gradient along either of the constant temperature side walls. Internally, the fluid transports the heat injected at the hot wall both by conduction and by convection in the boundary-layered velocity cell. *A priori*, one would suppose that the fluid system would be a more efficient total heat transporter than a solid system of identical geometry and conductivity. However, to first order this is not so. Because of the vertical asymmetry of the first-order temperature [equations (3.26, 3.28, 3.31)], $\int_{-\frac{1}{2}}^{+\frac{1}{2}} \frac{\partial}{\partial x} T^{(1)}(\pm\tfrac{1}{2}, z)\,dz = 0$, and the macroscopic heat transfer does not differ from the purely conductive zero-order

transport. However, the first-order effects redistribute the gradient along the walls so that the effective heat source is lowered at the hot wall and the effective sink is raised at the cold wall. The second-order temperature will not possess the vertical asymmetry of the first order and will modify the heat transport, but for the range of parameters considered above, this will be a very small effect.

3.5. *Concluding remarks*

The relation to experiment. Unfortunately, at the present time there exist no experiments with which the theory can be quantitatively compared. However, such experiments are planned for the near future in the rotating tank laboratory at the Woods Hole Oceanographic Institution under the direction of Dr Alan Faller. An apparatus has been designed for experiments with horizontal heating of a rotating fluid. The design is such that precise and unambiguous descriptions of the various régimes and their instabilities can be obtained, and also such that comparison with the theory initiated here will be possible. An annulus of 8 cm square cross-section is mounted on a rotating platform approximately 1 m from the centre of rotation. The side walls of the annulus are copper, the bottom is plywood and the top is plexiglass. Horizontal temperature contrasts from $\frac{1}{10}$ °C upward can be maintained by constant-temperature baths; the rotation rate is continuously variable up to well over 1 rad/s. The working fluid is water.

In pilot experiments with this apparatus the lower symmetric régime has been found to exist for values of $\Delta T < 0{\cdot}2 \sim 0{\cdot}3$ °C. Thus a sample point conveniently attainable experimentally and well within the convergence of the theory is

$$\Delta T = 0{\cdot}10\,^{\circ}\mathrm{C}, \quad \Omega = 1{\cdot}0\,\mathrm{sec}^{-1}.$$

For water at 25 °C,

$$\alpha = 2{\cdot}62 \times 10^{-4}\,^{\circ}\mathrm{C}^{-1}, \quad \nu = 8{\cdot}96 \times 10^{-3}\,\mathrm{cm}^2.\mathrm{sec}^{-1} \quad \text{and} \quad \sigma = 6{\cdot}28.$$

For $L = 8$ cm. and $g = 980\,\mathrm{cm}.\mathrm{sec}^{-2}$, $\beta = 8{\cdot}0 \times 10^{-4}$, $\epsilon = 0{\cdot}70 \times 10^{-4}$, and $\beta\sigma\epsilon^{-\frac{1}{2}} = 0{\cdot}60$. In figures 9 and 10 the temperature distribution over the body of the fluid and the streamlines in the side-wall boundary layer are shown at these values of the parameters.

The boundary conditions. It is interesting to note the relative role played by the boundary conditions along the vertical and the horizontal surfaces in controlling the behaviour of the system. The imposed horizontal gradient does drive the system, but otherwise the details of the evolved fields are strongly controlled by the conditions along the top and bottom walls. More precisely, after the zero-order temperature calculation, a consideration of the side-wall boundary region was the last step in the calculation of any field, and was done consistently with the requirements from the interior and horizontal boundary-layer region. The fact that (in this range of Rossby and Taylor numbers) the details of the side-wall boundary layers do not affect the fields in the other regions is of vital interest to the philosophical question of the validity of modelling the atmosphere in a laboratory tank. The side walls, which cannot be eliminated or made non-rigid, are the most artificial aspect of the modelling.

On the other hand, the influence of the horizontal wall boundary conditions on the velocity and temperature throughout the fluid is strong. The counter-current

along the side walls has been traced to the rotational constraint manifest in the lack of freedom in the solutions of the horizontal boundary-layer equations after application of boundary conditions at the top and bottom walls. There may be other situations of geophysical interest where a counter current along one boundary, not at all associated with the mass-transporting flow, is intimately connected with the detailed conditions along another boundary.

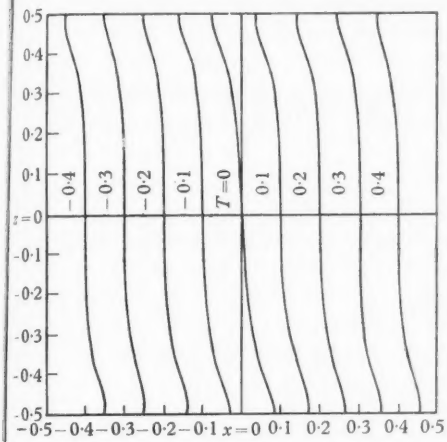

FIGURE 9. Isotherms, $\epsilon = 0{\cdot}7 \times 10^{-4}$, $\beta = 8 \times 10^{-4}$, $\sigma = 6{\cdot}3$.

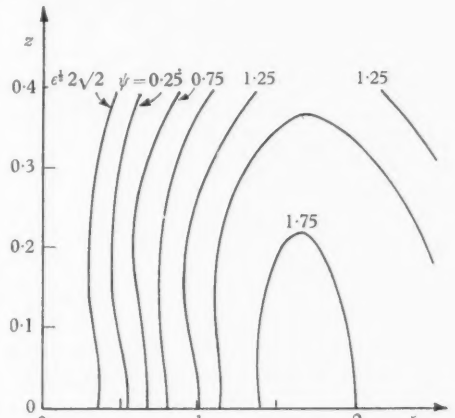

FIGURE 10. Side-wall boundary-layer streamlines, $\epsilon = 7 \times 10^{-4}$, $\beta = 8 \times 10^{-4}$, $\sigma = 6{\cdot}3$.

The temperature distribution to first and higher orders has been seen to be dominated by the insulating condition on the horizontal walls. A change of temperature boundary conditions along the top and bottom walls would therefore markedly alter all results, e.g. if the condition were placed on the temperature itself instead of on the temperature gradient, the amplitude of the first-order temperature and therefore of the interior vertical gradient would be $O(\beta)$, not $O(\beta\epsilon^{-\frac{1}{2}})$, as has been found. A detailed consideration of a change of boundary conditions (on the vertical walls as well) would be of interest. The resulting mathematical problems could be readily treated by the technique developed here. The problem resulting from changing the vertical surfaces from perfectly insulating to perfectly conducting is essentially included in the above work. The temperature along the top and bottom walls would then be a linear function of the horizontal co-ordinate between the hot and cold wall temperatures. The first-order temperature would be entirely given by the particular solution, $T_p^{(1)}$, of §2, which was entirely obscured in the homogeneous solution, $T^{(1,-\frac{1}{2})}$.

It is a pleasure to thank Professor George F. Carrier for his very valuable advice and criticism. I should also like to thank both Dr Willem V. R. Malkus, who suggested the problem, and Dr George Veronis for many interesting discussions. The material presented here is part of a doctoral thesis presented to the Department of Physics, Harvard University. I should like to thank the Woods Hole Oceanographic Institution for fellowships held during the time of this research.

REFERENCES

CARRIER, G. F. 1953 *Advanc. Appl. Mech.* **3**, 1.

DAVIES, T. V. 1956 *Phil. Trans.* A, **249**, 27.

EKMAN, V. W. 1905 *Arkiv. Mat. Astr. Fys.* v. 2, no. 11.

FULTZ, D. 1956 Studies in experimental hydrodynamics applied to large scale meteorological phenomena. *Final Report, Hydrodyn. Lab., University of Chicago.*

HADLEY, G. 1735 *Phil. Trans.* **39**, 58.

HIDE, R. 1958 *Phil. Trans.* A, **250**, 441.

KUO, H.-L. 1956 *J. Met.* **13**, 389.

LONG, R. R. (editor) 1953 *Proceedings of the First Symposium on the Use of Models in Geophysical Fluid Dynamics.* U.S. Government Printing Office.

STEWARTSON, K. 1957 *J. Fluid Mech.* **3**, 17.

CORRIGENDA

'Cellular convection with finite amplitude in a rotating system.'
(*J. Fluid Mech.* **5**, 1959, 401.)

In the discussion following equation (2.21) it is incorrectly stated that overstability cannot occur when the Prandtl number σ exceeds the value $\sqrt{\frac{2}{3}}$. As Prof. Chandrasekhar has pointed out to me, the Rayleigh number in the overstable case has no minimum for $\sigma > \sqrt{\frac{2}{3}}$, but it is certainly possible for equation (2.20) to be satisfied for this range of σ. As long as $\sigma < 1$ there always exist values of α^2 for which equation (2.20) can be satisfied.

I neglected to include in the bibliography the reference to:

CHANDRASEKHAR, S. & ELBERT, D. D. 1955 The instability of a layer of fluid heated below and subject to Coriolis forces. II. *Proc. Roy. Soc.* A, **231**, 198.

This investigation treated the stability problem with rigid boundaries for the overstable motions. Figure 5 of my paper is the same as figure 1 in Chandrasekhar & Elbert for the range $\sigma < 0{\cdot}677$.

G. VERONIS

'Energy content and ionization level in an argon gas jet heated by a high intensity arc.' (*J. Fluid Mech.* **4**, 1958, 529.)

The left-hand side of equation (4) should be replaced by its logarithm to base e.

G. L. CANN and A. C. DUCATI

REVIEWS

Introduction to the Theory of Compressible Flow. By SHIH-I PAI. Princeton: D. Van Nostrand Co., 1959. 385 pp. $9.75 or 73*s*.

In writing this book Prof. Pai has attempted what is probably the most ambitious scheme by a single author in the recent history of fluid mechanics. He has tried to provide a comprehensive introduction to compressible fluid dynamics in all ramifications—subsonic flow, supersonic flow, hypersonic flow, viscous flow, flames, condensation, dissociation, electromagnetic effects, gas mixtures, small disturbance theory, etc. Such a programme, it might be thought, must lead to a book of encyclopedic proportions, particularly as it should contain a good deal of basic mathematical theory and extensive reference to experimental work. However, Prof. Pai has managed to get it all into less than 400 pages.

He begins with a short introduction and then discusses those parts of thermodynamics which he considers are essential for the reader to know. In the following twelve chapters inviscid compressible flow is discussed, beginning with one-dimensional theory including shock waves and continuing with a chapter on the fundamental equations. Then in chapter VI the method of small perturbations, which effectively means linearized potential theory, is discussed and is followed by chapters on subsonic flow, the hodograph method, and on the well-known exact solutions of the steady flow equations. He continues with a discussion of transonic and hypersonic flows, concentrating on the similarity laws, and then introduces the method of characteristics. In the last three chapters on the theory of inviscid flow, three-dimensional and rotational flows are considered. (It should be noted that in the chapter on rotational flows the author regards, without justification, rotational flow as identical with non-homentropic flow or, in his notation, anisentropic flow.) In chapters XV and XVI the effects of viscosity are discussed, and in the final chapter magneto-gas-dynamics is analysed.

Apparently Prof. Pai has drawn everything into his net. In the opinion of the reviewer, however, in doing so he has made nonsense of the title and the principal claim in the preface. The prime purpose of a text-book deserving the title 'Introduction' is to introduce new readers to the subject. Accordingly, in a book of this sort it is necessary for a reader to be aware of how much he is expected to know and, from that starting point, the author should give a connected and so far as possible a self-contained account of the way in which the subject develops. Unfortunately, this book cannot be said to have been a success in these respects.

First, it is not clear how much mathematics and physics the student must know before reading the book. To give an example, he is supposed to have the theory of tensors at his fingertips but is not expected to know what a vector is. Moreover, the reader is expected to see that temperature gradient is clearly a vector from its directional property, even though a finite rotation, which also has a magnitude and direction, is not a vector. Secondly, the argument is far

from self-contained. On almost every page appeal is made to the references, or else the reader is expected to undertake difficult and laborious calculations. Even so, the book would be of value in the way intended by the author if, by taking the gaps in the argument for granted, the reader was able to discover the more important features of the behaviour of the fluid, but unfortunately he is frequently left at a loss. Consider for example chapter XVI, entitled 'Boundary layer flow of viscous compressible fluids'. At the start of this chapter the reader is assumed to know nothing at all about boundary layers, but within the space of twenty pages he has been brought right to the frontiers of knowledge in this field in the discussions of hypersonic boundary layers and improvements to boundary-layer theory. The meal offered is, however, so rich and concentrated that a reader new to the subject would find it completely indigestible, and even if he knew something about incompressible boundary layers he might still find this chapter unfathomable. What in general terms are the effects on the boundary layer of Mach number, heat transfer, pressure gradient and Prandtl number? Why is the interaction of the boundary layer with the main stream taken more seriously in hypersonic flow than when the fluid is incompressible? On these and other questions which are vital to an understanding of compressible boundary layers the author is practically silent, preferring to fill the space available with an avalanche of formulae and equations which must in the end bewilder all but the most experienced aerodynamicist. This chapter is perhaps an extreme example and the topic discussed in it is certainly not an easy one, but the tendency exhibited is present almost every chapter of the book.

Another unsatisfactory aspect of the book is that the author does not have a point of view. He is most reluctant to criticize, even though it is clearly of importance to the reader to have the defects and merits of methods put to him. One of the best written sections of the book is concerned with the Kármán–Tsien method, of use in the theory of subsonic steady flow. The account is clearly and simply presented and the reader should have no difficulty in understanding it. However, there is no appraisal of the method; the reader must look elsewhere for a discussion of its advantages and disadvantages and of its relation to the less sophisticated Rayleigh–Jantzen method.

The book is designed primarily to give a theoretical introduction to the dynamics of a compressible fluid and, as is probably already clear, I do not consider that it is a success in this respect and cannot recommend it to new students of the subject. However, a secondary object is to serve as a reference book for research workers in the field, and here the author has had more success. The active aerodynamicist may well find it useful to consult the book and the extensive list of references, many of which were new to me at least. Nevertheless, he will regret the uncritical approach and the lack of the contact with the experimental results which is essential if the theoretical worker's due sense of obligation is to be maintained.

K. Stewartson

INDEX

BENJAMIN, T. BROOKE Shearing flow over a wavy boundary, 161

BLACK, M. C. *See* WRIGHT and BLACK

BLOCK, M. J. *See* YOUNG, GOLDSTEIN and BLOCK

BRAY, K. N. C. Atomic recombination in a hypersonic wind-tunnel nozzle, 1

BREEZE, J. C. *See* EDWARDS, WILLIAMS and BREEZE

BRENNER, HOWARD Pressure drop due to viscous flow through cylinders, 542

BURNS, J. G., CHILDS, W. H. J., NICOL, A. A. and ROSS, M. A. S. Development and use of a vane device for boundary-layer measurements, 97

CARRIER, G. F. *See* GREENSPAN and CARRIER

CHILDS, J. G. *See* BURNS, CHILDS, NICOL and ROSS

CLARKE, JOSEPH H. Reverse flow and supersonic interference, 272

COLLIS, D. C. and WILLIAMS, M. J. Two-dimensional convection from heated wires at low Reynolds numbers, 357

CRAPPER, G. D. A three-dimensional solution for waves in the lee of mountains, 51

CROSSLEY, A. F. *See* DURST, CROSSLEY and DAVIS

DAVIS, N. E. *See* DURST, CROSSLEY and DAVIS

DIPRIMA, R. C. The stability of viscous flow between rotating concentric cylinders with a pressure gradient acting round the cylinders, 462

DURST, C. S., CROSSLEY, A. F. and DAVIS, N. E. Horizontal diffusion in the atmosphere as determined by geostrophic trajectories, 401

EDWARDS, D. H., WILLIAMS, G. T. and BREEZE, J. C. Pressure and velocity measurements on detonation waves in hydrogen-oxygen mixtures, 497

ELLISON, T. H. and TURNER, J. S. Turbulent entrainment in stratified flows, 423

ESKINAZI, SALAMON *See* SCHAEFER and ESKINAZI

FELDMAN, SAUL On the instability theory of the melted surface of an ablating body when entering the atmosphere, 131

GOLDSTEIN, J. S. *See* YOUNG, GOLDSTEIN and BLOCK

GREENSPAN, H. P. and CARRIER, G. F. The magnetohydrodynamic flow past a flat plate, 77

KEULEGAN, GARBIS H. Energy dissipation in standing waves in rectangular basins, 33

KROOK, MAX Continuum equations in the dynamics of rarefied gases, 523

LAPWORTH, K. C. An experimental investigation of the stability of plane shock waves, 469

LARISCH, E. Interactions of detonation waves, 392

LEVEY, H. C. Heat transfer in slip flow at low Reynolds number, 385

LOW, W. *See* MANHEIMER-TIMNAT and LOW

LU TING The pressure distribution on dihedral wings at supersonic speed, 302

MANHEIMER-TIMNAT, Y. and LOW, W. Electron density and ionization rate in thermally ionized gases produced by medium strength shock waves, 449

MENKES, J. On the stability of a shear layer, 518

MILES, JOHN W. On the generation of surface waves by shear flows. Part 2, 568

MILES, JOHN W. On the generation of surface waves by shear flows. Part 3. Kelvin–Helmholtz instability, 583

MOORE, D. W. The rise of a gas bubble in a viscous liquid, 113

NICOL, A. A. *See* BURNS, CHILDS, NICOL and ROSS

ROBINSON, ALLAN R. The symmetric state of a rotating fluid differentially heated in the horizontal, 599

ROSENBLAT, S. Torsional oscillations of a plane in a viscous fluid, 206

ROSS, M. A. S. *See* BURNS, CHILDS, NICOL and ROSS

SAFFMAN, P. G. A theory of dispersion in a porous medium, 321

SANDBORN, V. A. Measurements of intermittency of turbulent motion in a boundary layer, 221

SCHAEFER, JOHN W. and ESKINAZI, SALAMON. An analysis of the vortex street generated in a viscous fluid, 241

TOWNSEND, A. A. The analysis of temperature fluctuations by pulse-counting techniques, 261

TRITTON, D. J. Experiments on the flow past a circular cylinder at low Reynolds numbers, 547

TURNER, J. S. *See* ELLISON and TURNER

VINCENTI, WALTER G. Non-equilibrium flow over a wavy wall, 481

WILLIAMS, G. T. *See* EDWARDS, WILLIAMS and BREEZE

WILLIAMS, M. J. *See* COLLIS and WILLIAMS

WRIGHT, J. K. and BLACK, M. C. The theory of electromagnetically driven shock waves, 289

YOUNG, N. O., GOLDSTEIN, J. S. and BLOCK, M. J. The motion of bubbles in a vertical temperature gradient, 350

REVIEWS

Proceedings of the Symposium on Naval Hydrodynamics, edited by F. S. SHERMAN, 156

Festschrift Jakob Ackeret, 159

Fluid Mechanics for Engineers, by P. S. BARNA, 313

A Textbook of Fluid Mechanics, by J. R. D. FRANCIS, 316

Fluid Mechanics, by V. L. STREETER, 318

Introduction to the Theory of Compressible Flow, by SHIH-I PAI, 621

TENTH INTERNATIONAL CONGRESS OF APPLIED MECHANICS

The *Tenth International Congress of Applied Mechanics* will be held in the Congress Building at Stresa (Italy) from *Wednesday*, 31 *August through Wednesday*, 7 *September* 1960.

Apart from a number of invited general lectures the technical sessions of the Congress will be held in two sections, viz.:

SECTION 1: Fluid dynamics (hydrodynamics and aerodynamics).

SECTION 2: Mechanics of solids (rigid body dynamics, vibrations, elasticity, plasticity and theory of structures).

It should be noted that thermodynamics and computational methods as such are not included, although specific applications of computational methods to pertinent problems of one of the two sections mentioned above are acceptable subjects for papers to be read at the Tenth Congress.

Previous Congresses have demonstrated the desirability of an adequate period of time for the presentation and discussion of individual papers. In order to allow a period of 45 minutes for each paper (30 min. for presentation and 15 min. for discussion) a Programme Committee will make a selection from papers submitted for presentation. Abstracts of papers should be submitted *in four copies to the Secretary of the International Committee* (*W. T. Koiter*) *before* 1 *January* 1960. Preferably they should not exceed two type-written pages (doubly-spaced) and in no case should they exceed four pages. In order to facilitate the work of the Programme Committee it is recommended that abstracts be in *two* of the official Congress languages (English, French, German and Italian). Authors are urged to make their abstracts as clear as possible, since selection of papers has to be based upon them. *Decisions of the Programme Committee are final*, and it will be understood that it is impossible to enter into correspondence about them with authors of papers. They will be informed promptly of the decision on each paper.

Day-to-day organization of the Congress is in the hands of the Italian Organizing Committee (President: Prof. G. Colonnetti; Secretary: Dr F. Rolla, Consiglio Nazionale delle Ricerche, Ufficio relazioni internazionali, Piazza delle Scienza 7, Roma). All correspondence (apart from submission of papers) should be addressed to the Italian Organizing Committee. Information on accommodation, also registration forms, will be obtainable from Dr Rolla after 1 September 1959.

The Executive Committee of the International Committee for the Congresses of Applied Mechanics

C. B. BIEZENO, *President*; RICHARD V. SOUTHWELL; W. T. KOITER, *Secretary*; (Prof. Mekelweg 2, Delft, Netherlands).

JOURNAL OF FLUID MECHANICS

Volume 6, Part 4 November 1959

CONTENTS

Non-equilibrium flow over a wavy wall
by WALTER G. VINCENTI *page* 481

Pressure and velocity measurements on detonation waves in hydrogen-oxygen mixtures
by D. H. EDWARDS, G. T. WILLIAMS and J. C. BREEZE 497

On the stability of a shear layer
by J. MENKES 518

Continuum equations in the dynamics of rarefied gases
by MAX KROOK 523

Pressure drop due to viscous flow through cylinders
by HOWARD BRENNER 542

Experiments on the flow past a circular cylinder at low Reynolds numbers
by D. J. TRITTON 547

On the generation of surface waves by shear flows. Part 2
by JOHN W. MILES 568

On the generation of surface waves by shear flows. Part 3. Kelvin–Helmholtz instability
by JOHN W. MILES 583

The symmetric state of a rotating fluid differentially heated in the horizontal
by ALLAN R. ROBINSON 599

REVIEWS

Introduction to the Theory of Compressible Flow 621

INDEX TO VOLUME 6 623

Printed in Great Britain at the University Press, Cambridge
(Brooke Crutchley, University Printer)

9363